MARMARA UNIVERSITY
INSTITUTE FOR GRADUATE STUDIES IN
PURE AND APPLIED SCIENCES

EXPERIMENTAL INVESTIGATION AND MULTIDIMENSIONAL MODELING OF BIOGAS EFFECTS ON THE DIESEL ENGINE COMBUSTION CHARACTERISTICS

HASAN KÖTEN

Ph.D. THESIS

Department of Mechanical Engineering

ADVISOR

Prof. Dr. M. Zafer GÜL

ISTANBUL, 2014

MARMARA UNIVERSITY
INSTITUTE FOR GRADUATE STUDIES IN PURE AND APPLIED SCIENCES

EXPERIMENTAL INVESTIGATION AND MULTIDIMENSIONAL MODELING OF BIOGAS EFFECTS ON THE DIESEL ENGINE COMBUSTION CHARACTERISTICS

HASAN KÖTEN
(724609006)

Ph.D. THESIS
Department of Mechanical Engineering

ADVISOR
Prof. Dr. M. Zafer GÜL

ISTANBUL, 2014

MARMARA UNIVERSITY
INSTITUTE FOR GRADUATE STUDIES IN PURE AND APPLIED SCIENCES

Hasan KÖTEN, a Doctor of Philosophy student of Marmara University Institute for Graduate Studies in Pure and Applied Sciences, defended his thesis entitled "Experimental investigation and multidimensional modeling of biogas effects on the diesel engine combustion characteristics", on and has been found to be satisfactory by the jury members.

Jury Members

Prof.Dr. M. Zafer GÜL
Marmara University ....

Prof.Dr. A. Korhan BİNARK
Marmara University... ....

Prof.Dr. İhsan KARAMANGİL
Uludağ University ....

Assoc.Prof.Dr. H. Serhad SOYHAN
Sakarya University ....

Assist.Prof. Mustafa YILMAZ
Marmara University... ....

APPROVAL

Marmara University Institute for Graduate Studies in Pure and Applied Sciences Executive Committee approves that Hasan KÖTEN is granted the degree of Doctor of Philosophy in Department of Mechanical Engineering, Mechanical Engineering Program on . (Resolution no:).

Director of the Institute

Prof. Dr. Abdülkerim KAR

ACKNOWLEDGEMENT

Firstly, I would like to thank my advisor Prof. Dr. Mehmet Zafer GÜL, for his support and guidance during my PhD. The support from Professor GÜL keenly offered advice for my future.

I also would like thank to Marmara University BAPKO institution as an entitled of FEN-C-DRP-101012-0327 for support in experimental procedure and CFD analysis.

Many thanks to Dr. Mustafa YILMAZ who supported and gave valuable advice.

I am sincerely grateful for the conversations with all my colleagues at the Mechanical Engineering Department.

A special thanks to Associated Prof. Dr. Metin GÜMÜŞ for helping, discussions and answering all my questions I had about the dual fuel diesel gas engine and injection system in his laboratory. I would also like to thank İlker Turgut YILMAZ for support on experimental instrumentations.

Finally, I also give my special thanks to my family who never made me feel the deficiency of their support throughout my education.

April 2014 **Hasan KÖTEN**

TABLE OF CONTENTS

PAGE

ÖZET

BİR DİZEL MOTORUN YANMA KARAKTERİSTİKLERİNE BİYOGAZ ETKİSİNİN DENEYSEL VE NÜMERİK İNCELENMESİ

Buji ateşlemeli LPG ve CNG yakıtlı motorlara alternatif olarak, bu projede, on binlerce model çalışmasından sonra sıkıştırma ile ateşlemeli biyogaz yakıtlı dizel motor tasarımı elde edilmiştir. Biyogaz yakıtı, CNG ve LPG gaz yakıtlara göre ülkemizde üretilmesinden dolayı çok ekonomiktir. Ayrıca biyogaz yüksek oktan sayısı nedeniyle dizel motorlarda kullanılmaya oldukça elverişlidir. Bu çalışmada, Türkiye'de üretilen sıkıştırılmış biyogaz (CBG) yakıtını kullanan, yakıt sarfiyatı azaltılmış, çevreci yeni bir çift yakıtlı dizel motor tasarlanmıştır. Optimizasyon çalışması esnasında 1B ve emme ve egzoz manifoldları dahil 3B HAD simülasyonları kullanılmıştır. Bu projede tasarlanan çift yakıtlı dizel motor ile özellikle motor silindirlerinde hiçbir yapısal değişiklik yapmadan CBG yakıtının kullanılması maliyetleri oldukça düşürmektedir. Tasarım aşamasında bir boyutlu (1B), üç boyutlu (3B) hesaplamalı akışkanlar dinamiği (HAD) yazılımları ve çok amaçlı optimizasyon yazılımı eş zamanlı olarak kullanılmıştır. Çift yakıtlı dizel motor modellemesinde biyogaz ve dizel yakıtı ayrıca bir kod yazılarak sürükleyici yakıt olarak tanımlanmıştır. Optimizasyon çalışmasında uygun motor çalışma parametrelerini elde etmek amacıyla, CBG ve pilot dizel yakıt oranları, motor hızı, ateşleme zamanı, sıkıştırma oranı ve subap zamanlamaları farklı motor yüklerinde değişken olarak tanımlanarak yaklaşık 20000 model elde edilmiştir. HAD ile elde edilen sonuçlar test sisteminde doğrulanmıştır. Yeni tasarım sıkıştırılmış CBG dizel motor ile, tüm motor yüklerinde tek yakıtlı dizel motorlara göre oldukça düşük NOx emisyon değerleri elde edilmiştir. Ayrıca NOx ve SOOT emisyonlarının azaltılmasında CBG dizel motor en iyi performansı sağlamıştır.

Bu çalışma, Marmara Üniversitesi BAPKO Birimi tarafından FEN-C-DRP-101012-0327 proje kapsamında desteklenmiştir.

ABSTRACT

EXPERIMENTAL INVESTIGATION AND MULTIDIMENSIONAL MODELING OF BIOGAS EFFECTS ON THE DIESEL ENGINE COMBUSTION CHARACTERISTICS

As an alternative to LPG and CNG fueled SI engines, in this study, CBG fueled CI engine design was obtained after thousands model study. Biogas fuel is considerably economic due to the home product fuel compared to that of CNG and LPG fuels. In addition, due to the higher-octane rate, biogas is considerably adaptable for diesel engines. In this study, a new ecological dual fuel diesel engine with low fuel consumption and Compressed Bio Gas (CBG) produced in Turkey has been designed. 1D and full geometry 3D computational fluid dynamics (CFD) simulations including intake and exhaust ports were used in optimization process. Usage of CBG fuel in new designed CBG engine without any constructive change in cylinder will considerably decrease the cost. During the engine design, one dimensional (1D), three dimensional (3D) CFD codes and multi-objective optimization code were employed by coupling codes. CBG and diesel fuels were defined as leading reactants using user defined code in dual fuel diesel engine modeling. In optimization study, CBG and diesel mass flow rates, start of pilot diesel fuel injection, compression ratio, valve timing and engine speed were defined as input variables in different engine loads and evaluated about 20000 cases to define the proper operating conditions. Obtained CFD results were validated on engine test system. With this new design CBG diesel engine, significantly lower NOx emissions were emitted under dual-fuel operation for all cases compared to single-fuel mode at all engine load conditions. Moreover, CBG diesel engine provided superior performance in reductions of NOx and SOOT emissions. This project has been supported by Marmara University BAPKO institution as an entitled of FEN-C-DRP-101012-0327.

CLAIM FOR ORIGINALITY

EXPERIMENTAL INVESTIGATION AND MULTIDIMENSIONAL MODELING OF BIOGAS EFFECTS ON THE DIESEL ENGINE COMBUSTION CHARACTERISTICS

Automotive industry focused on new engine concepts in order to provide the stringent emissions legislation. Since possibility of consuming of petroleum, tendency to the alternative clean energy sources has been increased. Generally, diesel engines are used to get power as one of the most effective types of internal combustion engine with regard to transforming fuel energy to work. However, particulates matter (PM) and nitrogen oxides (NOx) emissions are disadvantages of the diesel engine. In this study, to reduce both NOx and PM new ecologic CBG engine design awarded by Turkish Economy Ministry with pilot diesel fuel was designed. A user defined code has been written and implemented to CFD solver for dual fuel combustion modeling. In addition, fuel consumption was decreased by using CFD code and optimization codes. In this study, CFD tools were coupled with multi-objective optimization code including latest models and they have been used to design thousands of CI engine. CFD codes were used to define proper boundary conditions of dual fuel diesel engine and designed continuous improvements:

- Proper premixed ratio for CBG fuel and pilot diesel fuel at different engine loads.
- Definition of proper valve overlap.
- Piston bowl design and optimal fluid motion for dual fuel CBG engine.
- Mixture formation and combustion for dual fuel CBG engine concept.
- Optimum compression ratio for dual fuel CBG engine and fuel injection timing.

The cost of engines has been increased due to the studies on the after-treatment system to decrease emissions. However, this new designed CBG engine showed superior performance on NOx and HC exhaust emissions in-cylinder before after-treatment system.

LIST OF SYMBOLS

a	: Thermal diffusivity
$\boldsymbol{A_s}$	: Droplet surface area and
cd	: Nozzle's discharge coefficient
$\mathbf{c}_\mathrm{f}$	: Friction coefficient,
$\boldsymbol{c_p}$	: Specific heat
$\boldsymbol{c_\mu}$	: Coefficient of $k-\varepsilon$ model
D	: Diameter of the cylinder (m)
$\boldsymbol{D_{d,stable}}$	: Stable droplet diameter,
$\boldsymbol{D_d}$	: Instantaneous droplet diameter
e	: Dissipation rate of turbulence (m^2/s^3)
$\boldsymbol{F_m}$	: Dass transfer rate per unit surface area
$\boldsymbol{F_{dr}}$	: Drag force
$\boldsymbol{F_p}$	: Pressure force
$\boldsymbol{F_{am}}$	: Virtual mass force
$\boldsymbol{F_b}$	: Body forces (gravity, magnetic forces, etc.)
H	: Total enthalpy
h	: Roughness height
$\boldsymbol{h_{fg}}$	: Latent heat of phase change
$\mathbf{h}_\mathrm{g}$	: Heat transfer coefficient
$\boldsymbol{k}, \boldsymbol{k_a}$	: Turbulent kinetic energy (m^2/s^2)
$\boldsymbol{K_c}$	: Hole length and form loss coefficient,
$\boldsymbol{K_\varepsilon}$	: Empirical coefficient and
L	: Characteristic length

$\dot{m}_i$	: Inlet mass
$\dot{m}_e$	: Exit mass
$\dot{m}_{sub}$	: Rate of change in mass within a subsystem
N	: Engine speed (rpm)
Pr	: Prandtl number
$\dot{q}''$	: Heat transfer rate per unit surface area of the droplet
SR	: Swirl ratio (non-dimensional)
$\mathbf{T}_{gas}$	: Temperature of the gas
$\mathbf{T}_{wall}$	: Temperature of the wall
U	: Radial velocity (m/s)
$\mathbf{U}_{eff}$	: Effective speed outside boundary layer
$\mathbf{U}_c$	: Characteristic speed
v	: Tangential velocity (m/s)
$\mathbf{Y}_\alpha$	: Species mass fraction
z	: Axial coordinate (m)
$\boldsymbol{\rho}$	: Density (kg/m^3)
$\boldsymbol{\eta}$	: Dynamic viscosity
$\boldsymbol{\lambda}$	: Heat conduction coefficient,
$\boldsymbol{\nu}$	: Kinematic viscosity and
σ_d	: Surface tension coefficient

ABBREVIATIONS

2D	: Two-Dimensional
3D	: Three-Dimensional
aBDC	: after bottom dead center
aTDC	: after top dead center
A/F	: Air-fuel ratio
BDC	: Bottom Dead Center
BMEP	: Brake Mean Effective Pressure
Bsfc	: Brake specific fuel consumption (g/kWh)
BSN	: Bosch Smoke Number
BSU	: Bosch Smoke Unit
CA	: Crank Angle
CAI	: Controlled Auto Ignition
CAD	: Crank Angle Degree
CBG	: Compressed Bio Gas
CDC	: Clean Diesel Concept
CFD	: Computational Fluid Dynamics
CI	: Compression Ignition
CN	: Cetane Numbers
CO	: Carbon monOxide
CR	: Compression Ratio
DCCS	: Dilution Controlled Combustion Strategy
DI	: Direct Injection
EGR	: Exhaust Gas Recycling
EOI	: End of Injection

Eq. : Equation

Fig. : Figure

GIMEP : Gross IMEP

HC : the exhaust emission level of unburned HC (kg/kg-fuel)

HCCI : Homogeneous Charge Compression Ignition

HCLI : Homogeneous Charge Late Injection

HPLI : Highly Premixed Late Injection

HR : Heat Release

IC : Internal Combustion

IT : Injection Timing

IMEP : Indicated Mean Effective Pressure

NOx : oxides of nitrogen

MCDM : Multi-Criteria Decision Making

MULDIC : MULtiple training course DIesel Combustion

MK : Modulated Kinetics concept (Nissan origin).

NADI^{TM} : Narrow Angle Direct Injection (proceeded developed by the IFP).

PCCI : Premixed Charge Compression Ignition (Mitsubishi origin)

PFI : Port-Fuel Injected

PISO : Pressure Implicit by Splitting of Operators

PM : Particulate Matter

PPCI : Partially Premixed-Charge Compression Ignition

PREDIC : PREmixed lean DIesel Combustion.

ROHR : Rate Of Heat Release

RON : Research Octane Numbers

SIMPLE : Semi-Implicit Method for Pressure-Linked Equations

SI : Spark Ignition

SOC **:** Start of Combustion (cad)

SOI : Start of Injection (cad)

SOR : Start of Reaction

TDC : Top Dead Center

UHC : Unburned HydroCarbon

UNIBUS : UNIform BUlky combustion System (Toyota origin).

LIST OF FIGURES

PAGE

LIST OF TABLES

PAGE

1 INTRODUCTION AND OBJECTIVE

1.1 Introduction

This chapter is intended to give an overview of the work, such as aim and background of this PhD thesis. A motivation for IC engine research is presented and the combustion process for the SI and CI engine was shortly overviewed. In addition that, new alternative combustion concepts for CI engines were discussed. Finally, the research background and objective of the present work was presented.

1.2 IC Engine Research

In recent century, the IC engine has been a reliable power source for industry and humankind. With increasing economic development in the former developing countries, rate of oil consumption are steadily increasing with rapidly increasing the usage of automotive and heavy-duty vehicles.

At the same time, increasing fossil fuel consumption increases a negative effect on human health and atmosphere. These harmful emissions have an immediate impact on lively life. The most common emissions which spread from ICE engines are listed below (Garrett et al., 2001):

- Major precursors to both ground level ozone and acid rain, and may affect the whole ecosystem are NOx emissions.

- CO is very harmful to humans in small amounts, especially indoors such as parking lots and garages.

- PM is created during incomplete combustion. Increased levels of PM have a negative influence on the human respiratory system.

- Unburned HC are an exhaust and evaporative pollutant of hydrogen and carbon atoms resulting from unburned or partially burned fuel. HC participates in the formation of ground level ozone (Strålin, P., 2007).

Emissions affects environment in the long term effects and damages especially to atmosphere. Recent investigations which are related with Climate Change conclude that global atmospheric concentrations of CO2, CO and NOx have increased significantly because of human activities since 18th century. CO_2 increases primarily in the atmosphere due to fossil fuel consumption. In consequence of the increment in CO_2, global warming increases and the climate system changes around the world. The effects of a rise in global temperature include a change in the amount and pattern of rains and a rise in sea levels, also a probable expansion of deserts. In the Arctic region, climate warming is expected to be strongest and would be related with the continuing retreat of icecaps, sea ice and permafrost.

In addition emission problems around the world, the presently known fossil fuel sources are finite. Researches indicate that within a half century present fossil fuel sources will not be able to fuel supply industry with the current demands of oil.

Decreasing reserve of fossil fuel known and the emission problems of IC engines is not really a new problem and for the past century, there has been an increasing interest in the IC engines and on how to obtain ultra-low exhaust emission levels and to decrease fuel consumption.

Fulfilling the emission standards and reduction of fuel consumption without losing the performance that customer desires are future challenges for the both SI and especially CI engines. Besides the system costs of vehicle engines, for CI engines PM and NO_x which caused by the negative regimes of spray combustion are dominant exhaust gas emissions. One of the strategies for a solution is alternative diesel combustion systems that avoid the above mentioned disadvantages by using alternative fuels in diesel cycle and combustion process.

Generally, diesel engines are operated on liquid diesel petroleum fuels. On the other hand, recently diesel engines operating on gaseous fossil fuels have gained much interest because of the recent increase in oil prices and the availability of cheaper gaseous fuels such as biogas and natural gas. Todays, CI engines can be converted to operate on gaseous fuels efficiently in what is known as dual fuel diesel engine via relatively basic conversion processes and modification. In dual fuel diesel engine, a homogenous mixture of gaseous fuel and air is compressed and ignited through the injection of a smaller amount of pilot diesel fuel contrary to known diesel operation by only fresh air is induced to the cylinder. Generally, combustion process being similar to that of diesel engine cycle, dual fuel diesel engine tends to keep most of the positive trades of diesel cycle operation like high thermal efficiency and power output (Badr et al., 1999). Papagiannakis et al. (2007) suggested two operating modes, conventional dual fuel operation and pilot ignited dual fuel operation.

PPCI combustion engines constitute alternative or complementary answers to the sophisticated and complex after treatments strategy, which helps to reduce of engine exhaust emissions. Principle of PPCI engine consist a compromise between achieving the control of CIDI combustion but with the exhaust gas emissions of dual fuel diesel engine, specifically soot emissions in preparing a highly diluted by burned gases air/fuel mixture. CBG fuel air mixture is compressed in a PPCI mode in achieving its simultaneous ignition by pilot diesel fuel in the whole space of the combustion chamber and in precisely controlling such combustion for the best performance in terms of efficiency and pollutant emissions. As the combustion takes place in a more homogeneous way throughout the bulk of the mixture, the thermal NOx formation and the soot production are known to be much lower than the conventional diesel combustion diffusion flame.

At part load, especially direct injection systems used to perform partially premixed charge allow for optimized fuel consumption and a low level of emissions. During like this process, the engine has quite more homogeneous air fuel mixture and low in-cylinder temperature which caused lower NOx emissions. Also, the use of a pilot injection has become an effective way for reducing combustion noise.

In PPCI combustion concepts have been recently developed with the purpose to strive the problem of the high emission levels of conventional direct injection Diesel engines. A good example is the PPCI combustion, a strategy in which early fuel injections are used, causing a burning process in which more air fuel is burned in premixed conditions, which affects combustion performance and exhaust emissions.

Experimental studies due to the extreme conditions inside a typical IC engine such as high combustion temperatures and pressures, precipitation of soot and other combustion products, etc. are sometimes limited in approaching exhaust emission problem. However, CFD software offers the opportunity to carry out and optimize repetitive parameter studies with clearly defined boundary conditions in order to investigate various configurations.

In this study, effects of dual fuel combustion characteristics were investigated on the combustion performance and the reduction of exhaust emissions for a CI engine fueled with CBG–Diesel dual-fuel experimentally and numerically. Different approaches for alternative diesels combustion systems are also investigated by CFD and optimization software. This combustion system is investigated in homogenous CBG fuel air mixture with early and late pilot diesel injection strategy.

1.3 Objective

The intention of this study is to find out the effects of dual fuel combustion characteristics for the decrease in exhaust emissions and the combustion performance in the CI engine fueled with CBG-Diesel dual-fuel. For this reason, in-cylinder combustion pressure and the rate of heat release (ROHR) were evaluated under different operating conditions to find out the combustion characteristics of the diesel engine for single-fuel and dual-fuel combustions. Moreover, combustion performance and indicated mean effective pressure (IMEP), exhaust gas temperature, and also the concentrations of soot, NOx, HC, CO and CO2 exhaust emissions were also investigated under various engine operating conditions to compare the exhaust emission and engine performance of single-fuel and CBG-Diesel fuel modes experimentally and numerically. Within this framework, the combustion processes and performance of a commercial four-cylinder, turbocharged compression ignition engine is analyzed and improved the exhaust emission values of the engine by proposing some modifications for advance mode of combustion system by using CFD and multi-objective optimization codes.

In accordance with this purpose, first;

- Overall thermodynamic cycle simulation for one cylinder,
- In-cylinder fluid motion,
- Including inlet, exhaust manifold and valves are analyzed in 3D.

Therefore,

- To perform a detailed analysis in-cylinder cold flow,
- Fuel spray atomization,

- The combustion and emissions are investigated numerically and experimentally.

Second part of this work included optimization for an advance combustion mode need to the following parameters;

- Valve timing,
- Compression ratio,
- Pilot diesel fuel injection timing were optimized.

Lastly, selected cases which were optimized by CFD and multi-objective optimization code analyzed and compared with existing experimental single fuel and CBG-diesel dual fuel diesel engine combustion performance and exhaust emissions.

1.4 Methodology

In this project, methodology was designed to accomplish the objectives described in objective parameters.

In literature review: The first task was to carry out a overall and critical research of available literature in the dual fuel diesel engine field. This review was done to fully understand the progress of dual fuel combustion process in this particular field of research also this is aided with the identification of issues/areas of further research.

The survey considered published books, journals, papers. It was broadened to consider information published on the Ohio state University database and on the Center for automotive research laboratories.

Full geometry model: After the study of the commercial CFD software documentation, some applications were carried out to aid with the meshing of the geometry.

Simulation: A preliminary simulation in commercial CFD software was carried out in order to build confidence levels, since combustion of spray droplets involves complex models both of pilot diesel fuel and CBG fuel injectors. The main simulations were divided into four main configurations as follows:

- Cold flow (no liquid fuel)
- Air/liquid spray mixture
- Combustion simulation using Turbulence-controlled eddy break-up

• Dual fuel combustion simulation using non-premixed and partially premixed model

For each model, these five turbulence models were investigated (k-ε/High Reynolds, k-ε/RNG, k-ε/Chen, k-ε/Speziale/High Reynolds and k-ε/Standart/High Reynolds models). The method adopted for this simulation generally follows the steps outlined in commercial CFD software studies.

Analysis: The analysis of the results was based on the post processed data from all analyzes carried out. In combustion modeling, two leading reactants CBG and diesel fuel are defined by using user defined code. The predicted results by commercial CFD code were compared with each other.

Experimental study: existing engine and modified dual fuel engine are modeled in 3D and tested on experimental setup and compared each other.

Conclusion: Conclusions were shoed based on the analysis of the results.

1.4.1 Structure of report

Relevant detailed literature review was carried out in Chapter 2. Chapter 3 explains the experimental technique. In Chapter 4 the information needed to understand mathematical background used in the simulations are described and description of the CFD set-ups including the simulation geometry, numerical mesh and the boundary conditions are defined. Chapter 5 deals with the discussion experimental and numerical analysis of all the post process results obtained from the simulation. Conclusions and recommendations are given in Chapter 6.

2 GENERAL BACKGROUND

2.1 Engine Exhaust Emissions Legislations

Exhaust emission related issues can be discussed globally and locally. Since the industrial revolution, the worldwide fuel consumption has been growing steadily. According to the Energy Information Administration (EIA), world fuel and energy consumption is expected to rise by 50 percent over the next years. The increase in fuel consumption and the share of different fuels from 1980 to 2030 is given in Figure 2.1 (Kaiadi, M. 2011). Fossil fuels such as liquid petroleum fuels, coal and natural gas are expected to dominate the energy consumption in the next years. Petroleum fossil fuels are of great importance since their combustion produces significant amounts of energy; however they have a damage impact on the environment. A greenhouse gas is CO that contributes to the climate change which is an issue of growing international concern. CO2 emission increases as fuel consumption increases as shown in Figure 2.2 (Kaiadi, M. 2011).

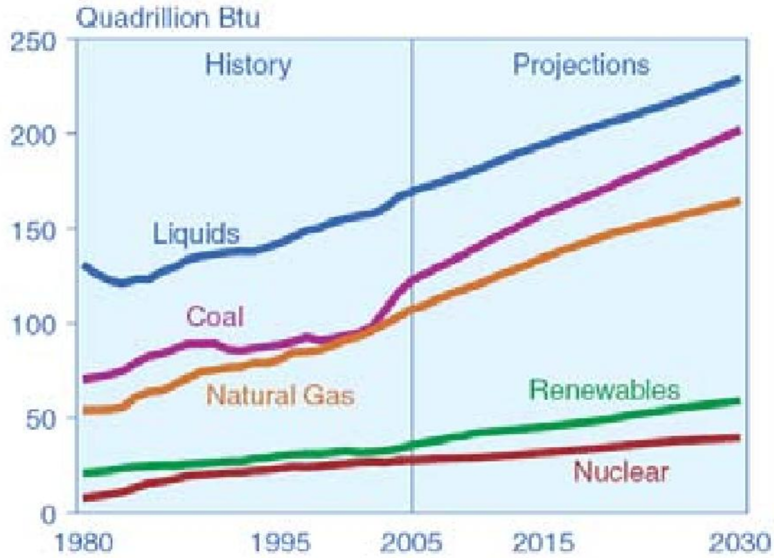

Figure 2.1. Fuel use around the world 1980-2030.

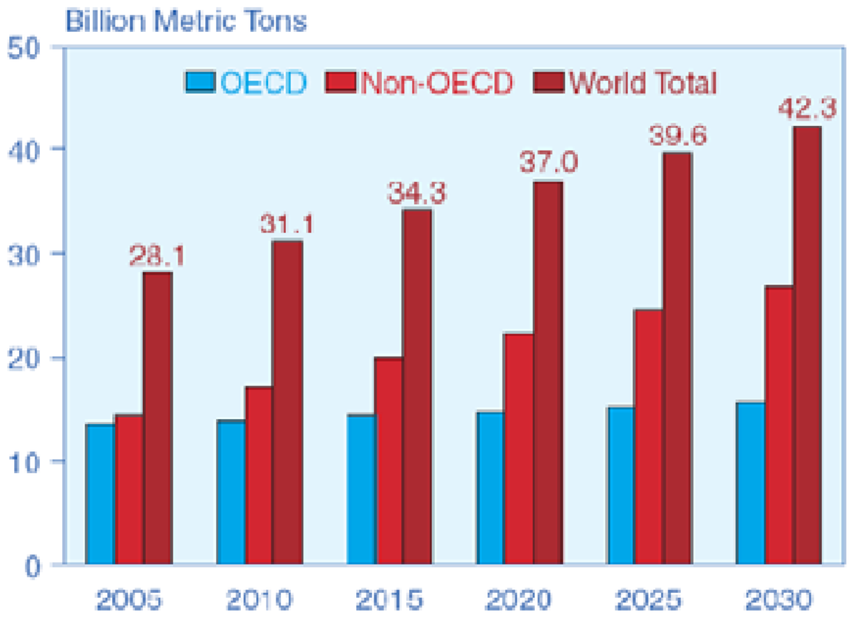

Figure 2.2. Expectation of CO2 emission between 2005 and 2030.

The automotive industry is the biggest sector in liquid fuel consumption as shown in Figure 2.3 (Kaiadi, M. 2011). Road transportation is the main part in the automotive industry. The fuels generally used in Internal Combustion Engines (ICE) are oil products i.e. diesel and gasoline. Fuel resources are gathered only in a few countries, mainly in the Middle East, which is recognized as a politically unstable region as shown in Figure 2.4. This means unsustainability in fuel supply and price for developing countries (Kaiadi, M. 2011).

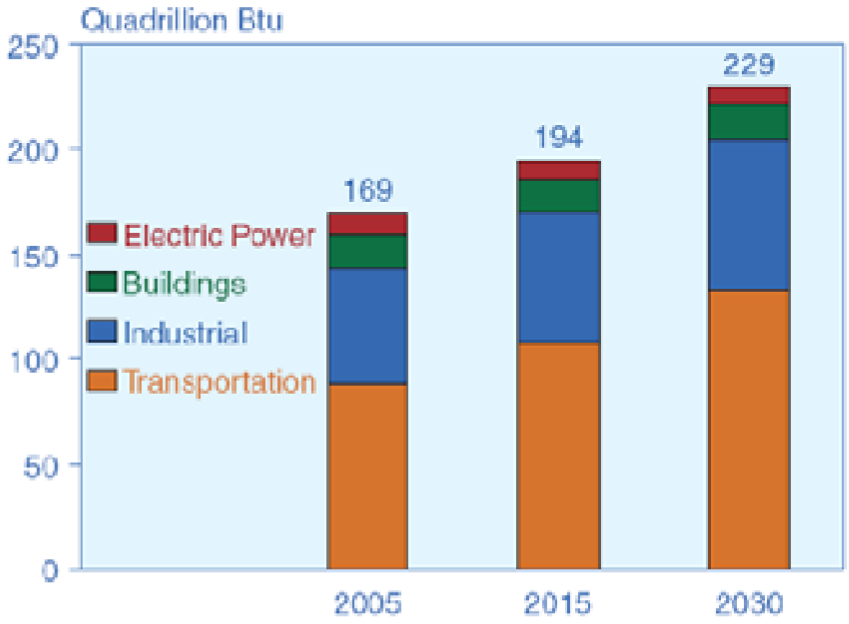

Figure 2.3. liquid fuel consumption in sectors 2005 and 2030.

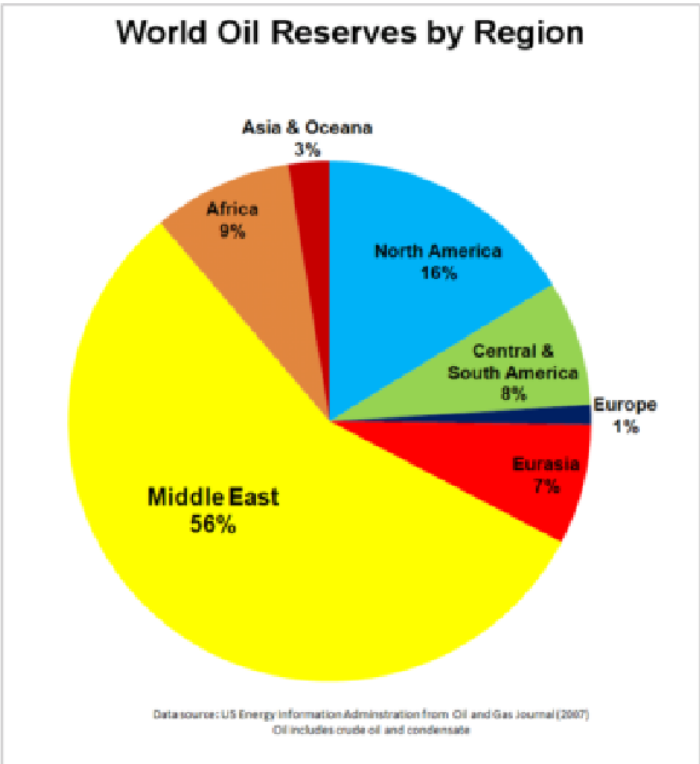

Figure 2.4. Oil resources.

Unsustainably in fuel supply, oil prices and global concerns about global warming have been recognized as the major global energy issues. Also the share of the transport sector for energy consumption is identified as significant. In ICEs, combustion is not always ideal and apart from carbon dioxide and water vapor damage products due to several factors can be released to the environment. These harmful exhaust emissions are mainly CO, unburned Hydro Carbons (HC), Nitrogen Oxides (NO) and Particulate Matter (PM) or soot. These harmful emissions have generally local impacts on environment and public live life health. Emission standards were regulated by different governments to limit the amount of these harmful pollutants. European emission standards from 2000 to 2013 for heavy-duty diesel, gas engines and it is clear that the standards become more stringent with time as shown in Table 2.1. NOX and PM are the main emissions for diesel engines which are the most dominating heavy-duty engines in the market. The most significant limitations are on NOx and PM emissions around the world as shown in Table 2.1. In addition, Diesel engines need more complex and costly emission control technology to achieve the emission requirements. In the future, increasing diesel engine cost will make them less attractive.

Table 2.1. Emission Standards for Diesel and Gas Engines, ETC Test, g/kWh.

EU Emission Standards for Heavy-Duty Diesel and Gas Engines: Transient Testing

Stage	Date	Test	CO	NMHC	CH_4 [a]	NOx	PM [b]	PN [e]
					g/kWh			1/kWh
Euro III	*1999.10 EEV only*	ETC	*3.0*	*0.40*	*0.65*	*2.0*	*0.02*	
	2000.10		5.45	0.78	1.6	5.0	0.16 [c]	
Euro IV	2005.10		4.0	0.55	1.1	3.5	0.03	
Euro V	2008.10		4.0	0.55	1.1	2.0	0.03	
Euro VI	2013.01	WHTC	4.0	0.16 [d]	0.5	0.46	0.01	6.0×10^{11}

a - for gas engines only (Euro III-V: NG only; Euro VI: NG + LPG)
b - not applicable for gas fueled engines at the Euro III-IV stages
c - PM = 0.21 g/kWh for engines < 0.75 dm^3 swept volume per cylinder and a rated power speed > 3000 min^{-1}
d - THC for diesel engines
e - for diesel engines; PN limit for positive ignition engines TBD

Demand for cheaper engines that meet emission standards together with increased concern for climate change force automotive developers to investigate more efficient alternative engine exhaust emission management. Using alternative fuels such as natural gas and CBG instead of conventional fuels is a better way to reduce the energy-related and exhaust emission problems. CBG fuel has very attractive fuel properties which makes it a suitable fuel for ICE application. High octane number, low carbon content, low fuel price, availability and sustainability of fuel resources are some of the attractive properties of CBG. Furthermore CBG is a natural bridge to the "hydrogen society" and future vision of transportation systems.

2.2 Gas Engines

Recently, SI engine operation has been determined as a proper engine technology for gas fuel operation due to the high octane number of natural gas which has nearly 120 octane number. In these gas engines, combustion concept is the same as for gasoline engines however the higher octane number of gas fuels give an advantage over gasoline. Because of the low knock resistance the compression ratio is limited in gasoline engines. The compression ratio can be increased fairly in natural gas engines without knocking combustion which affects on peak power and increased efficiency. In Figure 2.5 the effects of compression ratio on efficiency and power are shown. Increased compression ratio, enhances the expansion ratio which results in higher efficiency, however there is a limit when the compression ratio reaches 16:1 in spark ignited engines. These gas fuels also proper for CI engines due to their octane number and can be used in diesel engine by pilot diesel fuel with some optimization processes.

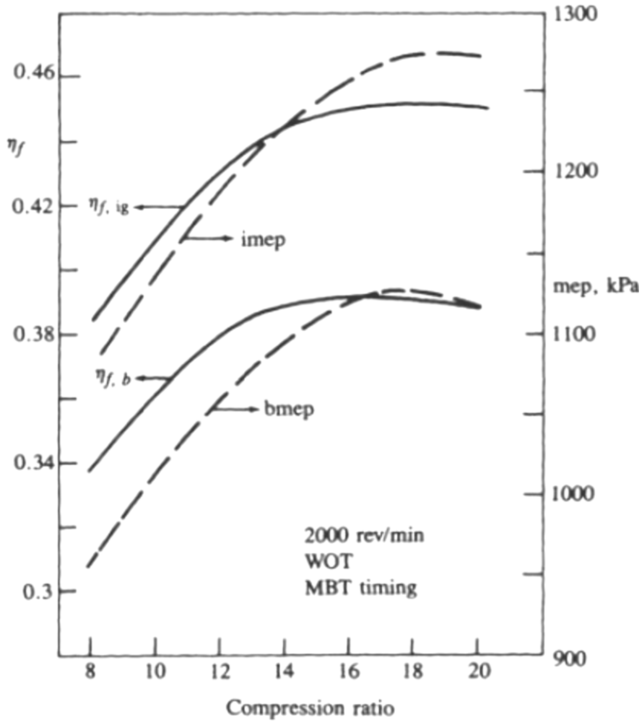

Figure 2.5. Effect of compression ratio.

Gas fuels such as natural gas can be operated either stoichiometric or lean. Lean operation means operating the engine with excess air in this operations lambda is greater than 1 and stoichiometric operation means that lambda is equal to 1. λ is defined

$$\lambda = \frac{\frac{fuel}{air}\ stoichiometric}{\frac{fuel}{air}\ actual} \tag{1.1}$$

Lean operation of a gas fuel engines increases the total efficiency since the engine operates with more open throttle like in some situations without any throttle at all resulting in less friction losses. In these cases, the combustion will be very high fuel to heat conversion efficiency and combustion efficiency and more complete due to the excess of air can be achieved. Higher λ increases specific heat ratio during expansion resulting in higher efficiency.

In addition that lean operation retains the exhaust gas temperatures low and there will not be hard limitations on construction structures. The main deficit with lean combustion natural gas engines is NOx emissions since a three-way catalyst cannot be used and a separate more complex and expensive NOx reduction catalyst must be used.

However, this challenge is resolved by using CBG fuel instead of natural gas in diesel gas engines due to the low combustion temperature of CBG pilot diesel dual fuel diesel engine.

Three-way catalyst can be used for stoichiometric operating and in this case all emissions are reduced meanwhile. When compared with lean operation lower efficiency will be reached, primarily due to more throttling and heat losses. Throttling losses can to a great extent be recoup for by using the proper amount of Exhaust Gas Recirculation (EGR) in gas fuel engines such as natural gas excluding CBG fuel. CBG fuel provides EGR effect inside cylinder due to the CO2 content and decreases throttling loses for engines. Stoichiometric operation of the engine in some operating conditions, results in increased exhaust gas temperature which can also be used with CBG fuel instead of other gas fuels like natural gas. Usage of CBG fuel in diesel engine by pilot diesel fuel, decreases exhaust gas temperature and also NOx emissions. In addition, in this thesis new operating engine parameters are designed by using CFD code and multi-objective optimization code for CBG diesel dual fuel engine and the best exhaust emissions and engine performance results are obtained.

For heavy-duty engines fuel economy and emissions take an important place as engine parameters. Highest efficiency is obtained with lean operation whereas stoichiometric operation with a three-way catalyst provides lowest emissions at lowest cost. However, highest efficiency and lowest emission are possible in CBG diesel dual fuel engine concept and resolved this trade-off.

Although most heavy-duty engines are diesel engines, it has been established that gas fuels like CBG and CNG gas is an important and suitable fuel for engine applications. Therefore, a lot of the heavy-duty CNG gas engines are diesel engines converted for SI operation sharing a main of the components with the original diesel engine. Engine equipments such as block, cylinder liners, pistons, cooling and lubrication systems are the same as for the diesel engine in CNG engines. Converting diesel engines for CNG operation involves changing the compression ratio, intake geometry that means more swirl, combustion chamber, fuel delivery and ignition system. However CBG engines don’t need any majority converting of the engine components. In CBG dual fuel diesel gas engine, end of the compression stroke the air fuel gas mixture is ignited by pilot diesel fuel. Although most of heavy duty converted gas engines from CI engines, CBG diesel dual fuel gas engine operates using diesel cycle. In CBG dual fuel gas engines, engine block cylinders, pistons, cooling, lubricating systems, ignition systems, compression ratio and combustion chamber are the same for diesel engines. For CBG dual fuel system, intake ports of the engine are modified to convert into CBG dual fuel engine. In this study CBG gas injector was defined on the intake port and CBG fuel was injected during the intake process both of CFD study and experimental work. The overall efficiency and power density of natural gas engines are lower than for diesel engines for many reasons.

Generally, gas fuel engines use a throttle to regulate demanded power. Use of a throttle causes pumping losses which are especially significant at low loads. In diesel engines there are no a throttle and pumping losses are very low also at low loads.

The high octane number and high auto-ignition temperature of CBG and CBG fuels makes them appropriate for CI engines. Normally SI cycle engine is used which results in use of lower compression ratio compared to CI engines. Lower compression ratio means lower engine efficiency as shown in Figure 2.5. When CBG and CNG fuels use in CI cycle higher engine efficiency can be obtained.

Also, the exhaust gas temperature of diesel engine is low due to the diesel engines operate lean, and the construction materials do not endure high exhaust gas temperatures. The converted engines have more stringent limitations in terms of high exhaust gas temperatures than dedicated SI engines. In this way CBG fuel more proper for CI engines than CNG fuel due to its lower operating temperatures.

Normally, the main parameters which results in lower heavy-duty natural gas engine performance compared to diesel engines are throttle losses, lower compression ratio, sensitivity to high exhaust gas temperature and lower fuel density. In this thesis CBG fuel have been used with higher compression ratio instead of CNG fuel and valve timing, start of pilot diesel fuel injection and other engine parameters are optimized by using multi-objective optimization code and coupled CFD solver. According to results, using CBG fuel instead of CNG fuel in optimized and modified dual fuel diesel engine more suitable for exhaust emissions particularly NOx emissions and engine performance.

Heavy-duty gas fuel engines are mostly used in power plants and also in relatively small numbers for public transport system. In compare with diesel engine research, CNG engines are relatively getting ignored because of the small market demand and lack of necessary infrastructure for CNG fuel vehicles. Today the trend is changing, however, and the demand and interest in CNG and CBG fuel vehicles start to increase and more research for more efficient technologies is needed. In this direction CFD simulations and optimization process gained more importance in this research field. Now there are about 13 million CNG fuel vehicles worldwide and in Europe, Italy, Russia and Germany have the largest fleets and in Sweden the fleet is developing rapidly. Also in Sweden, CBG fuel have been started to use in transport vehicles by using SI engines. The European Union has set a target of replacing petroleum fuel use in the transport sector with 20% alternative fuels by the year 2020 and will issue a Directive on the use of alternative fuels. This could mean 10% of the market for natural gas by 2020 (Kaiadi, M. 2011).

There are great potential for optimization of the existing technologies because of the lack of focus on natural gas engine research. In this study through these information's full engine geometry including intake ports, exhaust ports, intake valves, exhaust valves and combustion chamber modeled within a multi-dimensional framework also CFD solver is coupled via multi-objective optimization code. In optimization process, engine parameters such as start of pilot diesel fuel injection, compression ratio, equivalence ratio, engine speed, valve timing and amount of pilot diesel fuel are defined variable and optimized. At the end of this optimization process, about 20000 cases are obtained and selected proper cases with respect to exhaust emissions and engine performance. Moreover selected cases are validated on experimental setup.

2.3 Conventional Diesel

2.3.1 Gas fuels

As a gas fuel, CNG is a fossil fuel consisting mainly about 90% methane (CH_4) depending on origin and including small quantities of ethane, other gases and inert gas. CNG and CBG has lower carbon content which results in lower CO_2 production compared to the other conventional fuels. CNG and CBG are colorless and odorless in its pure form.

CNG fuel can be stored in a different form; CNG is a form of natural gas storage that is stored at a high pressure around 250 bar. On the other hand Liquid Natural Gas (LNG) is liquefied under pressure of 10-20 bar at -170 ^{o}C. The density of LNG is roughly 500 kg/m3 which give it a volume that is approximately 1/600 of the gaseous volume at atmospheric conditions or one third of the volume of CNG (Kaiadi, M. 2011). This property is very advantageous because of the possible travel distance is much greater than with CNG, but the liquefaction process and the tanks are very energy expensive and also consuming.

Adsorbed Natural Gas (ANG) is another process to store CNG and ANG applies adhesion of molecules of natural gas, to the surface of a solid. The ability of a solid to adsorb depends on the chemical makeup of the solid and its physical structure (Kaiadi, M. 2011). Although CNG and LNG are commercially available but ANG has only been used in some research centers until now. CNG and CBG is the most dominating fuel storage method for CNG vehicles.

Besides all these fossil fuels, Compressed Bio Gas as an alternative renewable fuel is a very important gas fuel which has very similar properties to CNG. this fuel manufactured from organic material through biochemical reaction is called biogas. These organic materials can be various crops such as sugar cane, corn or residuals from food, wood, plant or manure. At the proper temperature and in an oxygen-free environment, bacteria break down the organic material to methane and carbon dioxide which consequently can be purified to pure methane.

Compared to the conventional gasoline or diesel fuels, CBG significantly reduces greenhouse gases. A life-cycle impact assessment has been performed by the energy and environment group to evaluate the greenhouse reduction with CBG produced from different ways. Depending on the source of the CBG the greenhouse gas reduction is different as shown in Table 2.2 (Heywood, J. B., 1988). The highest reduction can be obtained from organic materials. The main reason for the table values over 100% is the indirect calculations effects (Kaiadi, M. 2011). Organic materials are potentially pure methane which is an important greenhouse gas with a global warming potential of compared to CO_2. As organic materials are collected, greenhouse gas reduced and converted to bio methane which hereby is burned and CO_2 and H_2O vapor are resulted.

Table 2.2. Greenhouse gas reduction according to CBG sources.

CBG sources	Greenhouse gas reduction
Manure	148%
Food Waste	119%
Sugar	85%
Corn	75%

CBG fuel reduces greenhouse gases dramatically in comparison with conventional other fuels. This reduction can be very varied based on the source of CBG production. In addition required engine technology is essentially the same because of the very similar fuel properties of CNG fuel and CBG fuel. Moreover CBG fuel promisingly, is also to be abundantly available as fuel for CI engines and is regarded as an alternative clean energy resource in view of its friendly environmental nature due to it has lower effect on pollution compared to fossil liquid fuels. In general, it is produced by the anaerobic fermentation of organic waste in landfills and the anaerobic digestion of sludge, crops, and agro-industrial byproducts and animal organic waste (Rahmouni, C., 2002). Also CH_4 is the main component about over 70% by vol. of the biogas and exhibits greater resistance to the knock phenomenon due to its higher octane rating and auto-ignition temperature, making it appropriate for CI engines with high compression ratios (Tricase, C., 2009, Sahoo, B., 2009). In addition, the carbon content of methane is also relatively very low compared to that of conventional diesel fuel, resulting in a significant decrease in pollutant exhaust emissions (Kaiadi, M. 2011, Yoon and Lee, 2011).

2.3.2 Conventional diesel combustion

To provide for the desired power output, the basic operating principle of an IC engine is to convert the chemical bond energy of the supplied fuel from either in liquid form or in gaseous form into thermal energy through the some combustion operations. Diesel engines work by using the heat energy generated through the compression of air to initiate the ignition of the diesel fuel inside a combustion chamber of the engine. In comparison SI engines, the higher compression ratios generally from 12 to 24 and the ability to operate in lean fuel mixture combustion together with the absence of throttling have led to higher engine efficiencies in diesel combustion.

Diesel engines operate generally on four-stroke cycle, meaning two revolutions of crankshaft are required to get one power per stroke. To illustrate the combustion characteristics of diesel engines, the rate of heat release graph which derived from the in-cylinder pressure data is used for explaining each part that occurs during the combustion process. The combustion of fuel takes place in a very short period of time near the top dead center which is, at the end of the compression stroke and at the early stage of the expansion stroke for a typical four stroke diesel engine. The combustion process of diesel engine is divided into four main phases, as showed in Figure 2.6.

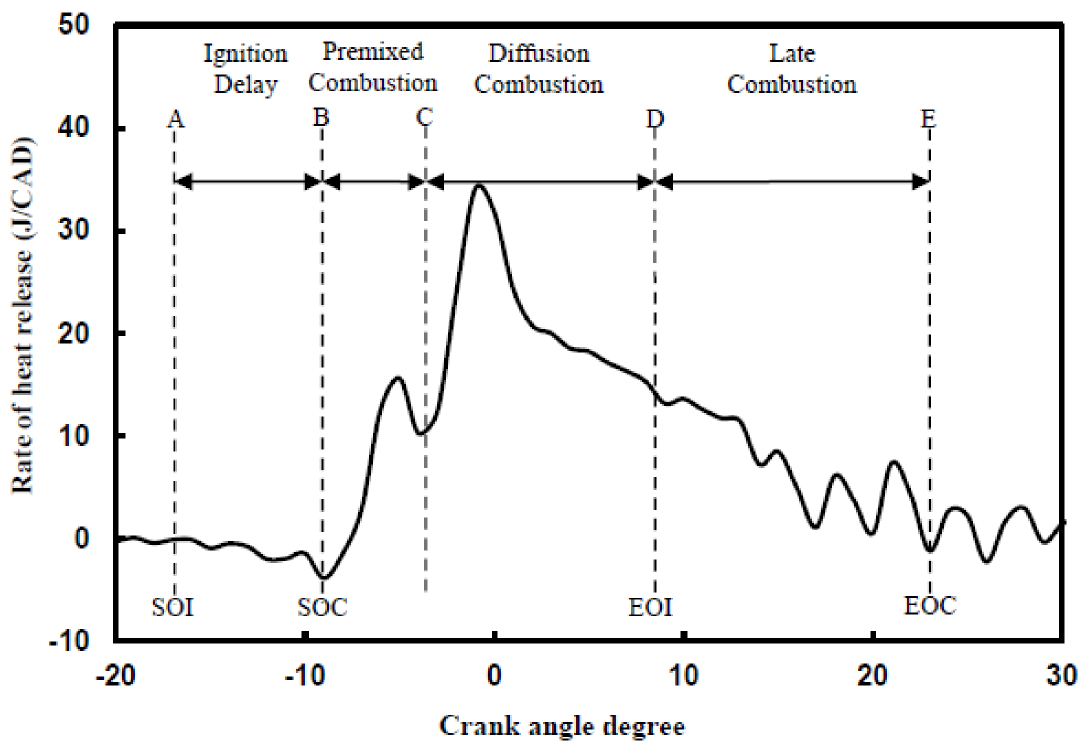

Figure 2.6. Typical ROHR diagram for a direct-injected diesel fuelled CI engine.

A-B: Ignition delay is defined as the period between the start of injection (SOI) to the start of combustion (SOC) in which the injected fuel undergoes the vaporization process and mixes with the intake air, resulting in the negative value of ROHR.

B-C: Premixed combustion, whereby the premixed air-fuel mixture has reached the flammability limit and combusts within a very short period of time. This gives rise to the sudden sharp peak in the ROHR diagram.

C-D: Diffusion combustion commences once the premixed combustion stopped and it ends at the end of injection (EOI). In this phase, the main combustion process of the injected fuel occurs and the heat release rates are mainly controlled by the availability of the air-fuel mixture for the combustion reaction.

D-E: Late combustion is the final combustion phase which extends into the expansion stroke. The heat release during this phase is due to the combustion of small fractions of unburned fuel with very low heat release rate (primarily due to the decreasing cylinder temperatures during the expansion stroke) and this phase completes at the end of combustion (EOC).

The whole cyclic process is then repeated again, starting with the induction of air in the intake stroke for the new engine cycle (Launder, O., 2002).

During the thermo-chemical energy of fuel and air transformation to power, combustion products are inevitable. Combustion products and the efficiency of the process are highly dependent upon, firstly, the intake-air, its pressure, temperature, motion and ingredients, secondly, the combustible fuel, its type, injection, atomization, evaporation, and finally, their states and interaction, leading to the auto-ignition and combustion of the charge. In current DI diesel engines, combustion is usually composed of a premixed-combustion phase, followed by a diffusion-combustion phase (Heywood, a, 1988).

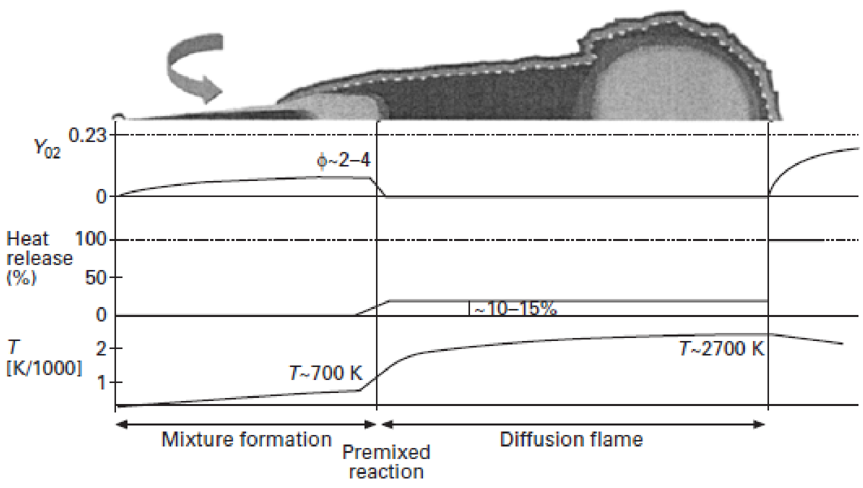

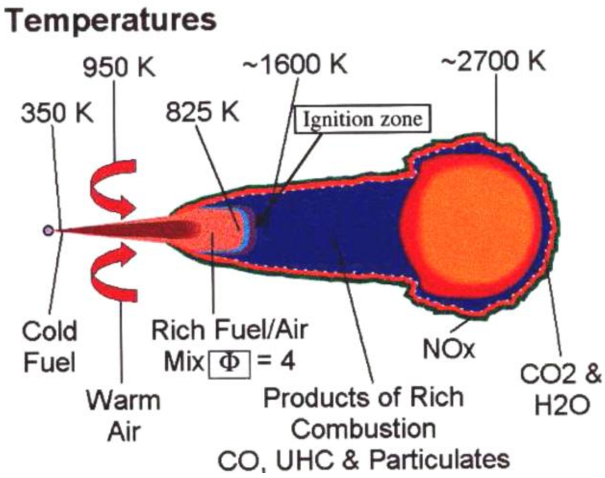

Figure 2.7.Direct injection (DI) diesel spray. Adapted from Dec (1997).

Premixed combustion is characterized by a high Rate Of Heat Release (ROHR) or pressure change, which is a consequence of the combustion of the fuel injected during the auto-ignition delay. Figure 2.7 represents a schematic of the conventional diesel combustion and the in-cylinder rate of heat release. This demonstrates the existence of the two phases during the combustion. The profile of the rate of heat release vary when the totality of the fuel is injected, evaporated and mixed with the air before auto-ignition, leading to fully-premixed charge combustion. Even when all the fuel has been injected before auto-ignition occurs, it does not guarantee that the combustion is of a fully-premixed nature. Once the fuel is injected, all is needed to evaporate and mix with the air to ensure there will be no diffusion combustion.

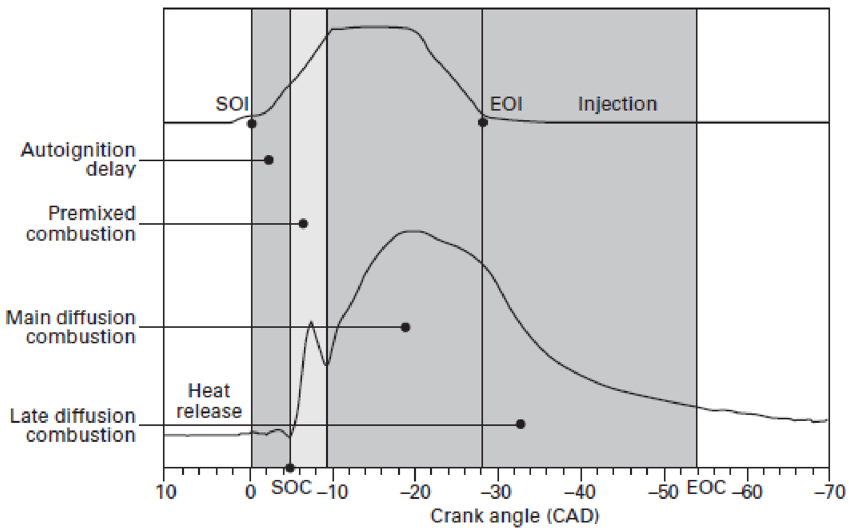

Figure 2.8. Evolution of diesel combustion.

2.3.3 Conventional diesel emissions

NOx, CO, HC and PM emissions shown in Table 2.3 represent the regulated emissions. The main mechanisms for their formation are described by Heywood (b) (1988) and are related to the mixing and flame temperature characteristics described in Figure 2.9. There are two possible ways to form HC emissions in a conventional diesel engine. The first is when the local fuel-air mixture is too lean to ignite or to support a propagating flame (over-leaning) and the second is when the fuel-air mixture is too rich to ignite or support a flame (under-mixing). In SI engines where homogeneous mixtures are prevalent, HC emissions have several additional sources, ranging from colder temperatures near the cylinder walls quenching the flame, to crevices trapping the mixture, oil absorbing and desorbing the mixture during the compression and expansion strokes. This explains the higher HC emissions observed with more recent developments of diesel combustion. CO emissions are formed in areas of the combustion where the AFR is close to stoichiometric or below, reflecting the lack of oxygen. This has rarely been a problem with conventional diesel engines since even in the worst cases; the flame is stabilized at a mixture with an AFR above stoichiometric.

PM emissions are formed in the fuel-rich regions in the liquid core of the diesel fuel spray, within the flame region at temperatures between 1000 and 2800 K. The pyrolysis of fuel by surrounding hot burned gases forms PM. A large portion of the PM is then burned with oxygen giving a yellow color to the flame, however, a smaller portion grows and accumulates to form PM emissions, which exit the engine as visible smoke. The diffusion-combustion phase is the main supplier to PM emissions since premixed combustion is characterized by high levels of mixing making it too lean to form PM. On the other hand, if the diffusion-combustion phase temperature is high enough, it will promote PM oxidation and reduce the total emissions

NOx emissions (NO2 and NO) the latter being predominant, are formed during the combustion when high temperatures are reached. These conditions are accomplished during the combustion of a close-to-stoichiometric mixture in a high pressure and temperature environment. A direct correlation has been established between the NOx formation rates and the flame temperatures in the combustion above 700 K. These conditions are realized during diffusion combustion, once the flame temperatures have been elevated by the premixed-combustion phase and when the flame is stabilized in a fuel-air mixture zone just lean of stoichiometric. Premixed combustion will not contribute much to NOx emissions since the temperatures are too low and the mixture is well mixed.

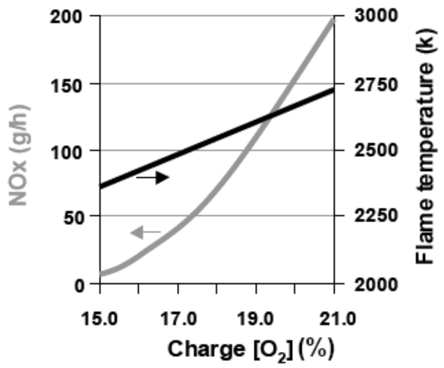

Figure 2.9. Temperature effect on NOx emissions using the Zeldovich mechanism.

Heywood (1988) describes the extended Zeldovich mechanism that widely used in computational fluid dynamics to model NOx emissions. Nakayama et al. (2003) used it to show the impact of oxygen concentration on the calculation of adiabatic flame temperature and the associated calculated NOx emissions, as shown in Figure 2.9. Sstrong dependence between NOx emissions and flame temperature is highlighted.

To date, there are two approaches to tackling tailpipe NOx and PM emissions, one using after-treatment for NOx, and the other using particulate filters for PM, as described by Knecht (2000), Lejeune et al. (2002), Wuensche et al. (2003) or Henein et al. (2003). The potential for a particular engine to be optimized for low PM or low NOx in conjunction with the appropriate after-treatment capabilities determine the approach, taking into consideration cost, technology development and durability. Figure 2.10 demonstrates the two options for meeting Euro 4 based on a typical PM versus NOx emissions trade-off curve of an engine meeting Euro 3 emissions regulations. Euro 5 and Tier 2 Bin 5 emissions targets are also showed in the Fig. 2.11.

The main approach of NOx after-treatment minimizes PM emissions, treating NOx engine-out emissions with a lean NOx trap or a selective catalytic reduction system. Advance the injection timing to obtain a large portion of diffusion combustion is one method of minimizing PM emissions. These remain in a hot in-cylinder environment in spite of representing ideal conditions for PM formation, promoting their oxidation. Increasing the injection pressure to elevate the mixing is another method. The increase in NOx formation in both cases is main drawback. This approach is fuel-efficient since advancing injection timing or increasing injection pressure both supply to a more rapid combustion, however, NOx after-treatment is still in its infancy. The diesel particulate filter approach minimizes NOx emissions by retarding the injection timing to reduce combustion flame temperatures, as detailed by Gill et al. (2002), Kidoguchi et al (2002), Shi et al. (2006), Payri et al. (2006), Fang et al. (2007) or Kim and Lee (2007). In these studies also obtained reductions in NOx emissions using EGR, which takes action as a heat sink, which limits the temperature raise during the combustion. Because of the lower in-cylinder temperatures limiting the oxidation process during and after the combustion process, engine-out PM emissions are increased. For trapping and burning PM emissions, a diesel particulate filter is inserted in the exhaust line. The diesel particulate filters are an efficient means of reducing PM emissions by means of the current state of development and production.

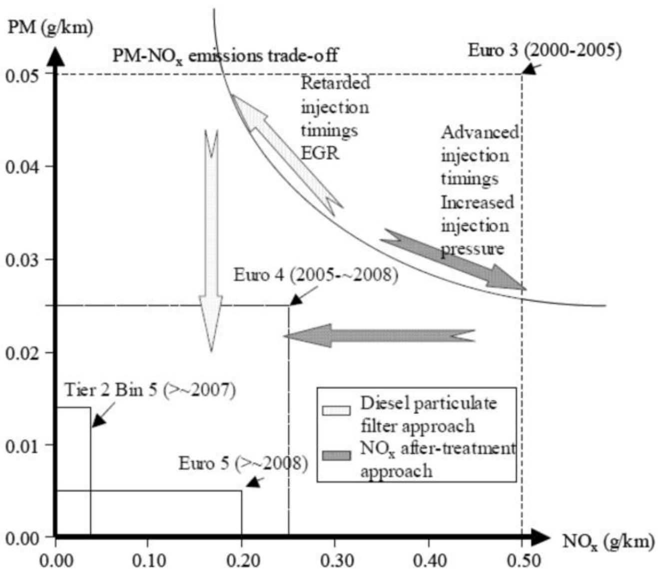

Figure 2.10. Approaches for achieving PM and NOx emissions targets.

Additional engine-out emissions reductions and after-treatment are required to meet future emissions targets, even in the case where mild-hybrid powertrain applications start making their appearance as seen in Fig. 2.10. Decreasing engine-out NOx and PM emissions has become the priority for CI engine and after-treatment developers, and especially the priority of the CI-engine developers in order to improve the cost of after-treatment and keep the diesel powertrain cost competitive.

2.3.4 Key parameters influence the combustion and emissions

The key developments to increase the efficiency, reduce emissions and further increase power have been in terms of compression ratio reductions permitted by the development of cold start technology. EGR rate increases and level of swirl reductions, both permitted by injection system strategies developed using the flexibility and capability of modern injection systems and engine controllers since Monaghan's 1995 future light-duty diesel engine specification. The starting points may vary when comparing results from different investigations. For example, in many cases, varying a parameter to understand its impact in the combustion process requires a re-optimization of another: when investigating the impact of injection pressure on emissions, the bowl shape and main-injection timing should be optimized for each injection pressure. Therefore, a study carried out with an optimized piston bowl and injection timing for 600 bar injection pressure will not give the same results as a study carried out with an optimized set-up for a 1600 bar injection pressure. Therefore, trends will always be valuable but may not always be comparable.

2.3.5 Compression ratio reduction studies

Recently the reduction of compression ratio is achieved by modifying the piston bowl shape and volume for CI engines is. Even though lower compression ratios leading to lower combustion efficiencies, the fact that compression is one of the largest providers to friction necessitates a compromise between thermal efficiency and friction, Heywood (1988). For the same maximum allowable in-cylinder pressure, i.e. structural strength, a compression ratio change from 20 to 14:1 only gives a small drop in efficiency, whereas the lower ratio considerably reduces engine friction, leakage and torque requirement for starting, as described by Taylor (1984). Jackson (2000) proposed a compression ratio of 15:1 as being the right balance between the two factors whilst pointing out that the current HSDI ratios of 18 to 20:1 is necessary to provide sufficient pressures and temperatures for cold starts. If compression ratio is decreased and the inlet-manifold pressure and temperature are maintained constant, the in-cylinder pressure and temperature at TDC reduce, thereby increasing auto-ignition delay, as described by Laguitton et al. (2002a). If compression ratio is reduced below 18:1, the auto-ignition delay becomes such that it does not ignite during the compression or expansion stroke and the engine fails to start. In reducing compression ratio further, the cold-start condition is currently the limiting factor. One of the main drawbacks of the compression ratio reduction is cold start and engine running stability. However, new technologies will be available in the near future as new glow plugs (made of ceramic, spark glow plug, flame glow plug), or electric air heater. Higher engine crank speed thanks to high-speed starter or integrated starters generators (ISG) could be also methods of great improvement. Moreover further reductions may be possible when considering flywheel mounted starter generators, capable of adjusting engine cranking speeds, or electrically assisted boost systems, capable of increasing the inlet-manifold pressure without relying on the turbine, or even variable valve timing, enabling a high compression ratio build to be used for starting and then capable of decreasing the effective compression ratio. An further benefit from lowering the compression ratio highlighted by Jackson (2000) is that higher specific ratings are attainable for the same maximum in-cylinder pressure (Pmax). At full load, higher levels of inlet-manifold pressure are possible for the same injection timing or more advanced injection timings are possible, both extending the full load torque capabilities. Reduction in compression ratio has been a key parameter for reducing engine friction. However, its reduction is now considered more and more for emissions purposes. Lower compression ratios lead to lower in-cylinder pressures and temperatures during the injection and combustion, which increase the auto-ignition delay and decrease the rates of combustion, as shown by Kawano et al. (2005), who reduced the effective compression ratio by retarding the intake valve opening. Kennaird et al. (2002) studies shows that the penetration of the fuel spray is also extended with lower in-cylinder pressures, and combined with the increased auto-ignition delay. These effects lead to improved fuel-air mixing. This is expected to reduce PM emissions and also peak combustion pressures and temperatures, and hence NOx formation as shown by Araki et al. (2005).

2.3.6 Pressure increasing by EGR and associated inlet-manifold:

A recent trend for diesel engines is the use of increasing EGR rates in order to control NOx formation in-cylinder. At speeds and loads at which the engine operates during an emissions drive cycle, EGR is mainly used. It proceeds in two ways on the combustion. At first, it enhances the auto-ignition delay, as visible in the results shown by Henein et al. (2001), which increase the premixed-combustion phase relative to the diffusion combustion. This limits the amount of close-to-stoichiometric. Secondly, EGR performs as a heat sink, thereby reducing the peak burned-gas temperatures, and hence NOx formation, Heywood (e) (1988). The drawback of EGR is its effect on soot emissions since at equal inlet-manifold pressure; it substitutes itself for part of the air. Developments in turbo-charging and injection systems as illustrated by Jackson (2000) and Payri et al. (2003a) who operated engines at higher inlet-manifold pressures and higher injection pressures compensate for this. In order to operate the engine at high EGR rates without increasing the inlet-manifold pressure requirements, it is necessary to cool the combustion product recirculation to increase their density and to introduce larger masses for the same volume. However, care must be taken to avoid issues with water condensation in the EGR and HC emissions for durability reasons (Gatellier and Walter, 2002). As well as for increased specific power outputs, the requirements for higher EGR rates have encouraged technology development in the field of turbo-charging. The goal has been to increase the inlet-manifold pressure in order to maintain AFR targets despite greatly increasing the EGR rate and to increase the air mass flow at higher loads, thereby reducing smoke emissions by supplying more oxygen, and increasing the load capabilities. This offers realistic engine downsizing opportunities that aim to maintain the same full load torque (Laguitton et al., 2002a), whilst reducing fuel consumption at part load due to reduced engine weight, pumping losses and friction as well as operating more efficiently at higher loads at similar speeds. The bigger turbochargers provide higher inlet-manifold pressures and full load torque capabilities, but the vehicle drivability then becomes a concern since the bigger turbines suffer from longer transient response times and poor low speed performance. Supercharging does not have this drawback since it is disconnected from the exhaust system but its impact on efficiency is negative. Turbo-charging can increase fuel consumption at lower loads even when used with a waste gate since it increases the backpressure, thus pumping losses, as detailed by Chi et al. (2002). They describe the benefits of technologies such as variable geometry turbines or variable nozzle turbines in terms of higher levels of inlet-manifold pressure realizable and lower pumping losses at lower loads. Other attractive solutions making their first appearance in vehicles or in development are twin turbocharger applications and electrically driven compressors. Thus negative effects of the turbine are reduced or eliminate.

2.3.7 Swirl levels

Swirl increases the fuel-air interactions and results in reduced PM emissions. As described by Kawashima et al. (1998) for applications; with variable levels of swirl, a high level is used at low loads and engine speeds, where the benefits of swirl are greater than the impact of throttling the engine. Lower level is used for higher loads to obtain the highest air mass flow possible. As described by Browne et al. (1986), the main effect of swirl is to increase the gaseous fuel and air interactions by increasing the portion of fuel burned in the premixed-combustion, without affecting the auto-ignition delay. Unfortunately, current engines have different levels of swirl requirements during their operation, yet they rarely have variable swirl capabilities. The current practice is to define a level of swirl giving the best compromise between full load and part load by means of soot emissions. At full load, the highest volumetric efficiency must be achieved for maximum ‘breathing’ of the engine, whereas at part load, the fuel-air mixing must be increased through air motion since the use of EGR causes higher soot emissions. The drawback of increasing swirl is that it degrades the volumetric efficiency and increases the pumping losses, and hence fuel consumption. Different mechanisms of swirl generation which from inlet-port configuration, helical or tangential (Kawashima et al., 1998) to port deactivation by throttling (Henein et al., 2001), or various levels of valve lift or flow guiding blades (Shenghua et al., 1999) are used. For increased levels of swirl requirements become less with conventional diesel combustion strategies but the injection systems take more importance in the mixing process, as demonstrated by Whelan (2001).

2.3.8 Developments on injection system

The most significant step in diesel engine evolution is perhaps the injection-system improvements. These improvements are a better injection in terms of atomization, evaporation and fuel-air mixing, leads to a more controlled combustion, reducing emissions and fuel consumption. The injector-nozzle hole diameters have been steadily reduced in order to increase the fuel-air interactions. Following the manufacturing and durability limitations, as smaller holes generate smaller droplets, which tend to evaporate and mix faster. The number of holes has increased leading to a compromise between hole size and number of holes in order to compensate for the flow restriction imposed by the diameter reduction. Injection pressure is also in constant increase since it acts in three ways. The first compensates for the smaller holes to maintain the fuel-injection rates. The second increases the level of fuelling before auto-ignition so fuel-air interactions are maximized leading to low soot emissions (NOx emissions increase but in a much smaller proportion than the soot emissions reduction, Chi et al., 2002). The third leads to much higher air entrainment and hence mixing, which reduces soot emissions. Conical-hole profiles with rounded inlets are used to counter the potential cavitation in injector nozzles associated with the higher injection pressures As described by Mahr (2002) and illustrated by Blessing et al. (2002). When comparing injector nozzles used in research work conducted by Bae and Kang (2000) before 2000 and injector nozzles used by the same team a few years later, these trends can be seen. Bae and Kang (2000) were investigating five-hole injector nozzles with hole diameters of 0.142 mm, whereas two years later they were studying six-hole injector nozzles with hole diameters down to 0.126 mm and with various conical hole profiles (Bae et al., 2002). Other emissions and fuel consumption reductions are to be expected with the appearance of faster responding injectors such as fast-acting solenoids, high-pressure unit injectors, piezo-electric injectors as illustrated by Takeuchi and Toyao (2002). These developments increase the ability to control the injection and allow the use of multiple injections to control the combustion. During one cycle, several combinations are now possible: pilot, early-pilot, main, split-main, post and far-post injections or simply several identical successive injections.

The control systems and their capabilities have been in constant progress in order to control the fuel injection system and other engine systems, such as the EGR and variable nozzle turbine. Most control systems are open loop that means the various systems around the engine are set based on predefined models, as functions of different requirements. Currently, some advanced controllers are closed-loop controlled means that the operating conditions are set and varied based on the response to the setting. Control of oxygen concentration and used it to control NOx emissions during engine transient responses is investigated by Nakayama et al. (2003).

Pilot injections are used to reduce combustion noise; however, they can lead to increased soot emissions as described by Lejeune et al. (2000). Injecting a small amount of fuel during the compression stroke suppress the combustion noise which burns before the main-injection, thereby increasing the in-cylinder pressure and temperature. This reduces the auto-ignition delay, and hence the premixed combustion. By burning the main-injection fuel as it enters the combustion chamber limits the rapid increase in rate of pressure change, hence noise. Apart from an increase in soot emissions, the pilot injection has limited adverse effects due to the small quantity of fuel it represents. An increase in HC emissions due to the over-leaning of the pilot injection observed Chi et al. (2002) but that this increase could be minimized by optimizing the pilot-injection timing. How the correct timing of the pilot and main injections were essential in creating the appropriate conditions for the main combustion described Trueba et al. (2002). The higher in-cylinder pressure and temperature lead to an instantaneous combustion of the fuel during the main injection, if the main injection occurs when the pilot-injection fuel has started burning or has fully burned. This suppresses the rapid pressure increase during premixed combustion and consequently reduces noise and NOx formation. It becomes too lean to burn and results in an increase in fuel consumption and HC emissions if the pilot injection occurs too early. The unburned fuel also increases the premixed-combustion phase and increases NOx emissions. With respect to to investigation of Badami et al. (2002) the impact of two pilot injections, which usually resulted in similar trends but more obviously. The second pilot injection assisted in the combustion of the earlier first pilot injection.

As detailed by Lejeune et al. (2000), Beatrice et al. (2002a) and Badami et al. (2002), post injections, occurring after the main injection, are used to reduce PM emissions, whilst having limited effects on NOx emissions. The main role of these late injections is to re-activate the combustion that proves beneficial for further oxidation of PM and for improved fuel consumption.

Relating with the main injection, Gill et al. (2002) confirmed that if main injection timing was retarded, NOx emissions and noise decreased whereas fuel consumption, PM and HC emissions increased. The lower in-cylinder temperature and pressure attained with retarded injections reduce NOx emissions, but limit the post-combustion PM oxidation processes. The improved premixed-combustion phase due to the lower in-cylinder temperature and pressure conditions also results in over-leaning of the outer-boundary of the fuel spray and an associated raise in HC emissions. The reduced PM emissions associated with the better premixed combustion were not sufficient to offset the reduced oxidation processes, therefore resulting in an overall increase. The rise in fuel consumption is related to the increased lost energy at exhaust valve opening. Beatrice et al. (2002b) evaluated comparison a combined pilot injection and main injection with a combined pilot injection and split-main injection. The split injection approach showed benefits in terms of NOx and PM emissions for no apparent raise in fuel consumption. Promoting soot oxidation and to enhance the utilization of air and delay part of the combustion acting in the same way as post injection was thought by using split injection. The separation between injections that referred to as dwell, was varied and showed that increased dwell led to increased soot and reduced NOx emissions. The larger dwell led to a more retarded second part of the main injection, which resulted in lower combustion temperatures hence reduced oxidation of PM. However, Brooks et al. (2004) found that a pilot injection and a split-main injection led to potential NOx and soot emissions reductions. However, these were attended by fuel consumption raise linked with the longer aspect of the injection and the later phasing relative to TDC of both the injection and the combustion. Chmela and Riediger (2000) showed higher average temperatures than for normal injection, which explained the increased soot oxidation. Ricaud and Lavoisier (2002) summarizes the effects of different strategies, i.e. pilot and main, pre injection (close pilot) and main, two pre injections and main, two pre injections, main and post injections. In this research the last strategy resulted in a slight reduction in noise and fuel consumption and a reduction of more than 50 % in soot, HC and CO emissions for fixed NOx emissions. The first multiple-injection results using successive identical injections to achieve HCCI published by Groenendijk and Müller (2002). The causes for multiple injections investigation were to enhance the fuel-air interactions and to reduce the wall wetting. This demonstrates the new approach to diesel engine combustion made possible by accurate control of the injection.

2.4 Diesel Combustion Concepts

2.4.1 Description and challenges

The goal of PCCI operation is to achieve the same lean and homogeneous mixture as that obtained and the associated NOx and soot emissions reductions. The main difference with HCCI operation is in the way the mixture is prepared. Late injections, rather than early, combined with high EGR rates enable the SOC to be delayed thus allowing all the fuel to be injected before auto-ignition (Soyhan H., et al., 2008). The increased fuel-air interactions form a fully premixed charge prior to combustion rather than the combined premixed and diffusion combustion, as can be seen by the rate of heat release in Fig. 2.10. Reduction in NOx and soot emissions is a function of the level of premix at the time of combustion, which is itself a function of the delay between the EOI and SOC. This type of combustion is also more flexible in operating AFR ranges and does not require precise control of the local AFR to control start of combustion since this is mainly achieved through injection timing. Typically, a single-stage combustion process occurs with PCCI combustion, which resembles more the conventional diesel premixed combustion, compared with the low and high temperature oxidation phases seen with HCCI combustion (Kimura et al., 1999).

The PCCI combustion does not offer the same levels of emissions reduction nor does it have the same challenges. It is an approach generally more adapted to diesel-fuelled applications as it does not rely on early injection timings and is therefore less level to wall wetting and high increases in HC and CO emissions. Furthermore, the combustion is not fully decoupled from the injection as in HCCI operation due to the late injections used, making the control of the SOC easier. PCCI operation can be used as a target across the engine speed and load, not meeting the target does not result in excessive cylinder head stresses and ultimately engine failure as would be the case with HCCI operation, but it results in higher NOx and soot emissions. As detailed by Kimura et al. (1999), EGR is used to delay the SOC. This reduces the constant-volume Otto cycle aspect but serves to give even further reductions in NOx emissions.

2.4.2 PCCI combustion application example

MK: In fact modern practical diesel engines use many other strategies to promote premixed combustion such as the Nissan Modulated Kinetics system. Kawashima et al. (1998) were one of the first teams to present an application of PCCI operation, which was achieved by employing high levels of swirl. The levels of swirl investigated were between 3.5 and 10 Rs, much higher than in conventional DI diesel engines. Kimura et al. (1999) conducted more detailed investigations on a single-cylinder engine with a swept volume of 488 cc and a compression ratio of 18:1, with EGR capabilities at light load and injection pressures up to 700 bar. This approach relies on the combustion phasing relative to the injection. Its essence is the completion of injection before auto-ignition. This increases the air entrainment in the spray before combustion and thereby reduces the amount of stoichiometric mixture and suppresses diffusion combustion. In contrast with HCCI operation, the injection is retarded as much as possible past TDC to inject into lower in-cylinder pressures and temperatures in order to delay auto-ignition and increase fuel-air interactions. The typical instantaneous heat release shows a single phase. Kimura et al. (1999) demonstrated low PM emissions backed-up by an indiscernible flame in an optical set-up and a tenfold reduction in NOx emissions at 2000 rev/min 5 bar BMEP. This may seem like a standard engine calibration process, but in reality, it is a step towards a new type of combustion. Furthermore, the authors explained the underlying processes, which prove very useful in understanding the engine optimization requirements.

The impact of the three measures used to suppress diffusion combustion is shown in Fig. 2.11 (Kimura et al., 2001). Lowering the oxygen concentration from 21 to 15 % was the first, which had as effect a drastic reduction in NOx emissions. This measure increased the auto-ignition delay and limited the hot and close-to-stoichiometric diffusion combustion, and hence NOx emissions. This also led to the over-leaning of the fuel-air mixture in the outer boundary of the spray, thereby increasing HC emissions. The lower oxygen concentration limited the PM oxidation processes and led to incomplete combustion, another source of HC emissions. The thermal efficiency was slightly improved from 40 to 41 %, which was close to the measurement accuracy, but may result from a faster combustion despite being retarded. Retarding the injection timing from 3 to -7 °CA aTDC was the second measure, which led to a further decrease in NOx emissions due to a further reduction, and maybe total suppression, of diffusion combustion. The increased fuel-air interactions, resulting from the lower in-cylinder pressures and temperatures during the injection and combustion, as well as the increased delay in auto-ignition, were also beneficial for PM emissions. A further over-leaning of the fuel-air mixture increased HC emissions. Despite the faster combustion, the impact of retarding the combustion relative to TDC reduced thermal efficiency. Finally, the third measure was an increase in level of swirl. This limited the over-leaning of the fuel spray by limiting radial penetration in favor of tangential motion. It also reduced smoke emissions by increasing the air entrainment. This was accompanied by an increase in the rate of combustion as demonstrated by the increases of both NOx emissions and thermal efficiency.

Further work (Kimura et al., 2001) was carried out on a four-cylinder engine with a swept volume of 2488 cc, mainly extending the range of PCCI operation. Injection pressure was increased to shorten the injection duration and the compression ratio was reduced to 16:1 in order to reduce the pressure and temperature in the cylinder during the compression, thereby delaying auto-ignition further. EGR used in the first instance was cooled in order to increase the rates achievable, thus retarding the auto-ignition further and serving as a thermal capacitance. Kawamoto et al. (2004) proposed the use of higher CN fuel, which went against other operating requirements, but was recommended to reduce HC emissions under cold-start conditions. The major advantage of PCCI combustion is illustrated here by its ease of implementation since it does not require additional or different hardware. Equally, its operation with conventional hardware did not affect the engine specific power output negatively.

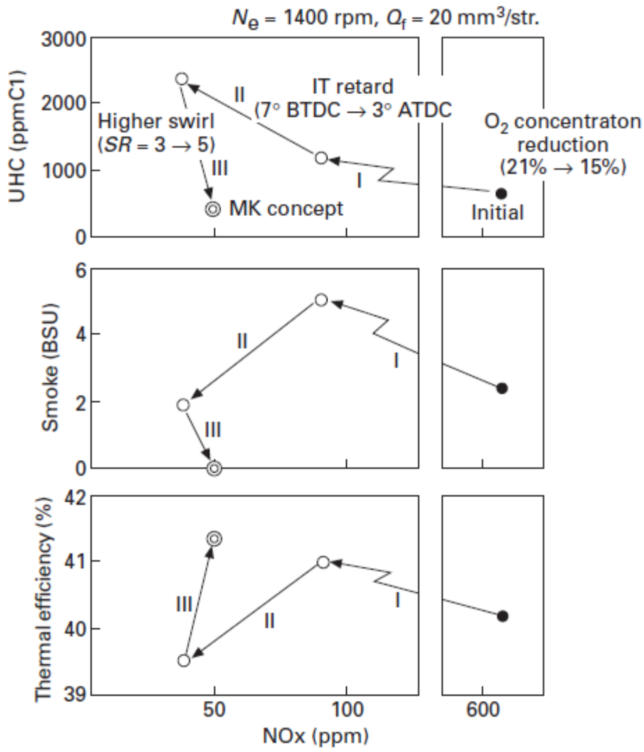

Figure 2.11. Effects of each combustion factor on exhaust emissions and thermal efficiency.

The research carried out to date has investigated means of realizing the full benefits of HCCI and PCCI combustion. There are many comparison elements amongst different operating conditions, including the heat release or instantaneous heat release, BMEP, IMEP and GIMEP, combustion efficiency, EGR rate, AFR, BSFC, auto-ignition delay and emissions characteristics. These are directly monitored or calculated from the inlet-manifold, exhaust and in-cylinder pressures and temperatures, torque, emissions (HC, NOx, PM, CO, CO2), air and fuel flows etc. These have been investigated for many operating conditions and a wide range of hardware, in order to understand their impact on combustion and to provide an understanding of the requirements to control the mixture, the start of combustion or start of reaction and the rate of reaction during HCCI or PCCI combustion. The main operating conditions varied to assess their impact are listed below:

Inlet: temperature, pressure, EGR rate

Mixture: motion, turbulence, AFR.

Injection system: injector and nozzle characteristics

Injection operation: timing, pressure, number of injections, quantity

Engine operation: speed and load range, valve timing

Engine hardware: piston-bowl geometry, compression ratio, port geometries

Fuel: pump, bio, single-component fuel, pure or blends or with additives

Table 2.3, 4 and 5 summarized key diesel-fuelled research and shows the main parameters investigated and the results.

Table 2.3. Comparison between HCCI concepts: emissions (Walter et al., 2002).

		NO_X	Smoke	HC/CO	BSFC
Port Injection	SWRI, Lund, UWM	Very low (/100)	Low (-27%)	High	Very high (+28%)
Early In-Cylinder Injection	HiMiCS	Low (1/3 or)	Low (1/3)	High (3000-8000 ppm)	Improved in a limited area
	UNIBUS PCI	Very low (1/100 and 90%)	Very low (near 0)	Acceptable (2000 ppm)	High (+10%)
	PREDIC MULDIC	Very low (<20 ppm)	Improved (1/2)	High	High (+15%)
Late In-Cylinder Injection	MK Concept	Very low (-90%)	Very low (<1 BSU)	Low (<1000 ppm)	No change/DI
Dual Fuel Introduction	HCDC	Very low (-75%)	Low (-40%)	High (6000 pmc)	No change/DI

Ryan (1997) investigated impact of fuel characteristics on compression ignition in a single-cylinder engine and six multi-cylinder prototype engines. Design parameters vary: for CN from 42 to 53, density from 830 to 869 kg/m3, mono-aromatics, from 10 to 25 % and poly-aromatics from 2.5 to 10 % respectively. They looked at the impact on weighted NOx emissions and on the impact of EGR. They found NOx emissions increased with fuel density and aromatic content, remained constant for varying CN and decreased for higher hydrogen contents. Fuel type did not affect the impact of EGR.

Kong et al. (2001) investigated impact of operating conditions on HCCI operation using experimental and modeling results in a diesel, 2440 cc, CR 16.1:1, single-cylinder engine (caterpillar 3400 series SCOTE). Design parameters vary: for injector type (injection pressure) from 500 to 900 bar, AFR from 50 to 60:1, injection timing (single or split injection) from 131 to 44 °CA bTDC, speed from 700 to 1500 rev/min. They looked at the impact on in-cylinder pressure, ROHR, combustion duration, ignition delay. ROHR showed two phases. Little impact was obtained from engine speed on combustion duration and ignition delay.

Table 2.4. Comparison between HCCI concepts: combustion control and HCCI (Walter et al., 2002).

		Control start of reaction	Knock at High Load	Range	Test speed (rpm)	BSFC
Port Injection	SWRI, Lund, UWM	No	High	Large (IMEP 16 bar)	1000-1500	High (65%)
Early In-Cylinder Injection	HiMiCS	Possible	No	Large	1000-1600	Low (15%)
	UNIBUS	Possible	High	Small (IMEP 3 bar)	1000	High (+10%)
	PCI	Possible	High	Large with supercharge	1000	Not but possible
	PREDIC MULDIC	Possible	High	Very limited (λ>2.5)	1000	Not but possible
Late In-Cylinder Injection	MK Concept	Possible	No	Limited (λ>1.3)	1200-2000	High (45%)
Dual Fuel Introduction	HCDC	Possible	No	Large	1500	Low (30%)

Iwabuchi et al. (1999) investigated impact of injector-nozzle hole configuration on spray and combustion characteristics for PCCI diesel engine. The engine has single-cylinder, 4-valve, CR 12:1, 2000 cc, equipped with 800 bar injection pressure-capable injection system, 80 ° cone angle injector-nozzle type and hole configuration, level of swirl 2.2 Rs. Design parameters vary: for EGR/AFR from 0 % / 59:1 to 58 % / 20:1, injection timing from 80 °CA bTDC to 10 °CA aTDC. BSFC, ROHR and NOx, HC and smoke emissions, flame luminescence, spray penetration; simulated cone angle effect and adhered fuel to wall were investigated. PCCI results with conventional injector nozzle worsened in most cases. An optimized injector nozzle reducing penetration and enhancing the mixing gave a tenfold reduction in NOx and smoke emissions below conventional levels. HC emissions improved but remained elevated for a BSFC penalty of circa 10 %. Impinged spray injector nozzle linked with lower CR led to lower ROHR. Combustion occurring earlier than TDC decreased the efficiency. If EGR increased, SOR retarded and ROHR decreased in amplitude and duration leading to an increase in efficiency.

Table 2.5. Comparison between HCCI concepts: design (Walter et al., 2002).

		Conception	Walls impingement	Compression ratio	Displacement (cc)
Port Injection	SWRI, Lund, UWM	Simple	Yes	Variable (10-28)	702 1600-2000
Early In-Cylinder Injection	HiMiCS	Simple	Yes	18	2147
	UNIBUS	Simple	Yes	Variable (12-21)	915
	PCI	Simple	Limited	12	2000
	PREDIC MULDIC	Very complicated	Yes	16.5	2004
Late In-Cylinder Injection	MK Concept	Simple	No	18 and 16	488 622
Dual Fuel Introduction	HCDC	Very complicated	Yes	20.4	522

Yokota et al. (1997) investigated impact of multiple injections on compression ignition in a diesel, CR 18:1, 2147 cc, single-cylinder engine equipped with 900 bar injection pressure capable injection system. Design parameters vary: for number of holes from 6 to 30, for cone angle from 55 to 155 °, for injection timing from 5 to -20 °CA bTDC with different strategies, looking at the impact on NOx and HC emissions, Bosch Smoke Unit (BSU). They investigated BSFC, ROHR and combustion flame. Multiple injections (Homogeneous Charge Intelligent Multiple Injection Combustion System) were worse than pilot and main injections with traditional injection timing. Multiple injections were better for NOx emissions, bsfc, BSU with worse HC and CO emissions at retarded ITs. Early multiple injections led to lower ROHR and benefited from the 30-hole injector nozzle.

Ryan III and Matheaus (2002) investigated impact of fuel type on compression ignition in a combustion bomb and in a 702 cc, Port-Fuel Injected (PFI), single-cylinder engine with CR from 14 to 16:1. Design parameters vary: for fuel from Fisher Tropsch Naphtha to diesel with up to 80 % gasoline content, for inlet-manifold temperature from 110 to 170 °C, for CN from 20 to 100, RON from -600 to 100. The impact on Bosch Smoke Number (BSN), SOR, HR, in-cylinder pressure, elevated pressure auto-ignition temperatures and ignition delay were investigated. For inlet-manifold temperatures up to 150 °C, both the lower temperatures and gasoline contents led to higher BSN. Higher CRs advanced SOR. Higher gasoline contents required higher inlet-manifold temperatures to react and led to higher ICPs and cumulative heat released. Higher CNs lowered the elevated pressure auto-ignition temperatures and the opposite was seen with higher RONs.

Shimazaki et al. (2003) investigatied impact of near-TDC injection for premixed diesel combustion using a 125 ° cone angle with a large bowl in a 4-valve, CR 16.5:1, diesel engine. the engine has 1298 cc, single-cylinder, equipped with 1200 bar injection pressure-capable injection system, level of swirl 1.1 Rs. Design parameters vary: for injection pressure from 30 to 1200 bar, injection timing from 40 to -5 °CA bTDC, for CN from 19 to 61. ROHR, in-cylinder pressure, BMEP, BSCO, BSFC, BSNOx, BSHC and smoke were investigated. With CN 19, BSNOx, BSCO, BSHC and smoke emissions were lowest at 25 °CA BTDC. Earlier injection timings led to a general increase in emissions for the same BSFC. When injection pressure was varied from 900 to 1200 bar, emissions decreased for a stable IMEP but friction losses from pump resulted in increased BSFC. With 60 % EGR and AFR of 58:1, CN 61 gave lower NOx emissions than with CN 19 but higher smoke emissions for ITs near TDC. Late injections at 4 °CA aTDC showed benefits for smoke and NOx emissions but large penalties in terms of BSFC.

Su et al. (2003) investigated impact of multiple injections and bump combustion chamber on premixed and lean diffusion combustion in a 2-valve, CR 15:1, 1620 cc single- cylinder diesel engine. The engine was equipped with 800 bar injection pressure-capable injection system, level of swirl 1.8 Rs. Design parameters vary: for piston bowl with or without inner ring, AFRs from 20 to 30:1 by increasing inlet-manifold pressure, number of injections from 1 to 4 early injections plus one main injection, for injection timing from 150 to -3 °CA bTDC. In-cylinder pressure, ROHR, PM, NOx and HC emissions were investigated. Early injections led to a two-phase heat release, the peak typically towards 20 °CA bTDC, and the second nearer TDC. The earlier the injections, the later the second phase of HR. Earlier injections led to lower NOx, higher HC and smoke emissions whereas when adding a main injection, NOx and smoke emissions trends inversed. The bump impact seemed to be beneficial also in conventional mode for smoke emissions by avoiding bowl impingement. When using 4+1 pulses, the first four seemed to work against the engine as the combustion occurred before TDC.

Simescu et al. (2003) investigated impact of simultaneous PFI and DI strategies on PCCI operation and emissions in a diesel, CR 16.6:1, 14.6 L, 6-cylinder engine equipped with electronic unit injectors. Design parameters vary: for a fixed load, for fuel injected in port from 0 to 70 %, for injection timing of PFI from 310 to 370 °CA ATDC, main injection timing from 10 to -5 °CA bTDC. Mass fraction burned and NOx, CO and smoke emissions. Varying PFI timing did not affect the combustion. With the main injection timing unchanged, the higher portions of PFI led to lower ROHR in main combustion, but higher in-cylinder pressures at low load. At low loads, PFI seemed beneficial for NOx emissions whereas at higher loads, DI seemed more appropriate. HC emissions and BSFC both increased with increasing portion of PFI. With main injection at TDC or later, a low and a high temperature, oxidation occurred and finished before the main injection started. This cancelled the increase in CO emissions previously obtained with the increases in BSFC and smoke emissions reduced. NOx emissions were reduced by up to 35 %. Large cylinder-to-cylinder variations were observed.

Gatellier and Walter (2002), Ranini et al. (2004) investigated narrow nozzle cone angle and adapted piston geometry operating conditions in a diesel, 416 cc, single-cylinder engine equipped with 1350 bar injection pressure capable injection system and multiple injections. Design parameters vary: for CR from 18.0 to 14.0:1,for speed 1500 and 2500 rev/min, load from 2 to 8 bar IMEP. EGR was not cooled below 90 °C to avoid condensation issues. At 1500 rev/min, high CR with advanced injection timings led to penalty in BSFC due to untimely ignition, hence negative work. Lower EGR rates were required to delay the combustion with lower CR. Lower CR led to lower NOx and PM emissions but also lower HC and CO emissions. Results at 2000 rev/min showed that the increased speed was beneficial for early injection timings because time to TDC was shorter reduced the auto-ignition delay in crank angle terms. The trends for HC and CO emissions were clearer. Concerns for diesel oxidation catalysts were increased due to the reduced exhaust temperatures. Electrically assisted boost, multiple injections, variable valve actuation were seen as extremely valuable for special operation.

Tanaka et al. (2001) investigated impact of in-cylinder conditions on HCCI combustion characteristics in a rapid compression machine with similarities to a small diesel engine at 1100 rev/min, n-heptane, 900 bar injection pressure-capable injection system. (Concept also demonstrated on diesel fuelled, CR 15:1, 4249 cc, 4-cylinder engine). Design parameters vary: for AFRs from 8 to 60:1, for oxygen concentration from 15 to 21 %, CR from 6 to 8:1. Despite injecting 5 minutes before the compression, results indicate that higher CRs and oxygen concentrations led to earlier ignition, faster combustion and higher pressures. The ignition delay increased slightly for increased AFRs.

The diesel-like n-heptane fuel is clearly much more attractive and has been extensively used since it offers the same auto-ignition properties as diesel fuel but has a much lower boiling temperature of about 100 °C (similar to gasoline). The main advantage is that it permits easy evaporation with very early injection timing, especially in HCCI combustion, without the usual wall-wetting issues. Its lower molecular weight, density and its higher calorific value must be kept in mind when making comparisons with diesel-fuel results. This allows an improved understanding of the mixing requirements, without needing to address the poor evaporation problems. It seems to be an acceptable approach when considering the great leaps forward being made in injection systems technology. Indeed, engine developers are now able to rely on multiple-injection capable injection systems with micro-hole injector nozzles and high injection pressures, thus leading to extremely rapid injection and evaporation, which explains the value of the diesel-like n-heptane based research.

Suzuki et al. (1997) investigated impact of in-cylinder conditions on HCCI diesel combustion characteristics in a 4-valve, PFI and DI, CR 20.4:1, 522 cc, single-cylinder engine equipped with 1800 bar injection pressure-capable injection system and with iso-octane and n-heptane for PFI-premixed and light oil for DI, running at 1500 rev/min and injection timing of 15 °CA bTDC. Design parameters vary: for port injected to total injected ratio from 0 to 1 (1 being all PFI), EGR from 0 to 30 %, for RON from 50 to 100, for AFRs from 30 to 80:1, for load from low to maximum acceptable in conventional mode (smoke limited). Varying premixed ratio had little impact on ISFC. NOx and smoke emissions decreased with increased ratios whereas HC and CO emissions increased. For loads between 50 and 75 % full load and RONs between 75 and 100, NOx emissions with the increased ratios reached the level of the lower loads and RONs tested. This was achieved with little impact on smoke emissions. Increasing EGR reduced NOx emissions to the detriment of smoke emissions.

Groenendijk and Müller (2002) investigated impact of homogeneity on compression ignition via simulation and experimental results using n-heptane (same CN as diesel), in a CR 14.7:1, 3+1-valve, 1800 cc, single-cylinder engine. Design parameters vary: for injection timing from 11 to 95 °CA bTDC, 8 injections of 5 mg or one injection of 40 mg of fuel, for EGR/AFR from 0 % / 45:1 to 50 % / 28:1, for injection pressures from 800 to 1400 bar. Higher EGR rates retarded auto-ignition and lowered HR and NOx emissions while increasing CO emissions. Advancing injection timing delayed auto-ignition, lowered HR, NOx, CO and smoke emissions and BSFC.

Christensen and Johansson (2002) Investigated impact of swirl and turbulence on combustion characteristics in a 2-valve, PFI, 50 % iso-octane, 50 % n-heptane (RON 50), CR 11.1:1, 1600 cc single-cylinder engine (Volvo TD100 HDD). Design parameters vary: for level of swirl from 2 to 2.8 Rs, combustion chamber from disc to square bowl. Square combustion chamber geometry required lower inlet-manifold temperatures since it got hotter. It also increased combustion duration and lowered ROHR. Swirl did not influence the combustion duration.

Peng et al. (2003) investigating impact of AFR and EGR rate on HCCI operation in an n-heptane, PFI, CR 18:1, 500 cc, single-cylinder engine with an inlet-manifold temperature of 30 °C. Design parameters vary: for lambda from 1.5 to 15, EGR from 0 to 70 % by mass, avoiding the misfiring and knock. Maximum IMEP was achieved for the lowest lambdas, where the coefficient of variation of IMEP, main combustion delay and duration, and CO emissions were most sensitive to EGR, and the NOx and HC emissions were highest. The low temperature reaction was controlled by EGR whereas the AFR controlled the duration. The start and duration of the main combustion were controlled by lambda and EGR for the higher loads.

2.5 Dual Fuel Engine Concepts

2.5.1 Gas diesel dual fuel operations

Traditionally, CI engines are operated on liquid diesel fuels. However, due to the recent rise in oil prices and the availability of cheaper gaseous fuels such as natural gas, CI engines operating on gaseous fuels have gained much interest. With relatively simple modification and conversion processes, diesel CI engines can be made to operate on gaseous fuels efficiently in what is known as "dual fuel CI engine". Unlike normal diesel operation whereby only fresh air is inducted (as explained in earlier section), in dual fuel engine a homogenous mixture of gaseous fuel and air is compressed and then ignited through the injection of a smaller amount of diesel fuel. With the overall combustion process being similar to that of diesel cycle, dual fuel CI engine tends to retain most of the positive trades of diesel operation (i.e. high thermal efficiency and power output) (Badr et al., 1999). Papagiannakis et al. (2008) suggested two operating modes, (i) conventional dual fuel operation and (ii) pilot ignited dual fuel operation.

Under conventional dual fuel operation, at a given engine speed, enough amount of liquid diesel is provided to achieve the certain percentage of the required engine power output. The rest percentage of engine power output required is then achieved by supplying gaseous fuel into the system. As such, only small amounts of gaseous fuel is used and this operating mode is suitable for low engine load operations (Abd Alla et al., 2000). For pilot ignited dual fuel operation, a constant quantity of diesel fuel (pilot injection) is used mainly as the ignition source for the gaseous fuel. In this case, the small quantity pilot diesel injected (i.e. between 10% and 20% of the operation on diesel alone) covers approximately the mechanical losses of the engine and the remaining required engine power output is achieved using the gaseous fuel supplied. This operating mode allows for high substitution level of liquid diesel but suffers from low thermal efficiency and high unburned hydrocarbon (UHC) emissions at low engine load (Bedoya et al., 2009).

2.5.2 Dual fuel combustion

In dual fuel engines, the combustion process is dependent on the spray and ignition characteristic of the pilot fuel used and also on the type and concentration of gaseous fuel present in the combustion chamber. Nonetheless, a typical ROHR diagram for a dual fuel engine can be considered as a process being made up of three over-lapping components (Figure 2.12) as suggested by Karim (2003). The first component (I) is mainly due to the combustion of the pilot fuel, hence resulting in the almost similar level of ROHR in Figure 2.12 (a) and (b) at both heavy and light load respectively. For the second component (II), the proportion of gaseous fuel that is in the immediate vicinity of the ignition and combustion centers of the pilot is being burnt rapidly. And lastly, the third component (III) is due to the subsequent turbulent flame propagation advancing through the remainder of the premixed gaseous fuel-air charge present in the combustion chamber (Karim G.A., 1980).

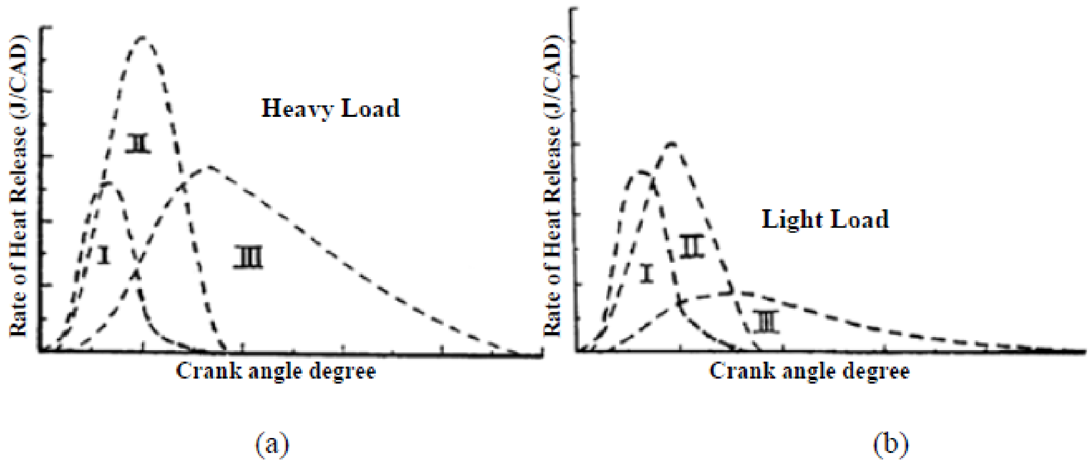

Figure 2.12. Schematic representation of the different components of the combustion.

ROHR diagram in a dual fuel engine at: (a) heavy load (b) light load (Karim, 2003). From Figure 2.12 (b), it can be seen that with very lean gaseous fuel-air mixture or at light engine load, the bulk of the energy release only comes from the ignition and subsequent rapid combustion of the small pilot zone together with part of the gaseous fuel-air mixture entrained into the pilot zone. The energy release also comes from the combustion of the immediate surrounding zones where the local temperatures are higher. This is mainly due to the absence of consistent flame propagation from ignition centre to the gaseous fuel, resulting in the low ROHR for component (III) as shown in Figure 2.12 and the high amount of UHC emission in the engine exhaust as mentioned earlier. It was suggested that by increasing the quantity of the pilot fuel, the effectively larger amount of mixtures entrained within the larger pilot combustion zone promotes partial flame propagation and consequently producing a higher amount of total energy release at engine part load operations (Karim et al., 1992). Equally important in the combustion process is the variation in ignition delay of a dual fuel engine compared to that of a diesel engine, which has a profound effect on the subsequent combustion process, engine performance and engine emissions. Karim (2003) studied the effect of introducing different types of gaseous fuel into a dual fuel engine at constant pilot quantity and found out that the ignition delay trend is significantly different from those seen in similar diesel operating conditions, as shown in Figure 2.13. It can be seen that the trend is very much dependable on types of gaseous fuel used and the ignition delay tends to increase with increasing amount of gaseous fuel up to a certain point followed by a dip before reaching the total stoichiometric ratio (based on combined gaseous and liquid fuel with the air available). Liu and Karim (1998) explained that the introduction of gaseous fuel into a diesel engine together with the air intake charge resulted in both the physical ignition delay (i.e. change in charge temperature, pressure, pre-ignition energy release and heat transfer) and the chemical ignition delay (i.e. chemical interactions between the gaseous and diesel fuel, such as the formation of radicals), depending strongly on the type of gaseous fuel used and its concentration in the combustion chamber.

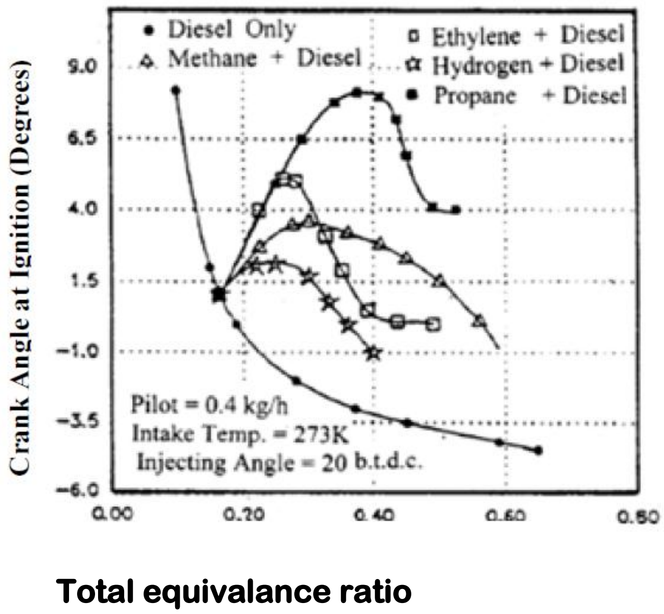

Figure 2.13. Variations of the ignition point with total equivalence ratio for gaseous fuels at a constant pilot quantity together with the corresponding diesel operation (Karim, 2003).

The main factor contributing to the physical ignition delay of a dual fuel engine is the decrease in charge temperature when gaseous fuel is introduced together with the intake air. Prakash et al. (1999) showed that the induction of gaseous fuel replaced part of the intake air, hence decreasing the oxygen partial pressure activity inside the charge during the compression stroke and subsequently reduces the charge temperature. Secondly, the use of gaseous fuel increases the overall specific heat capacity, leading to a significant drop in charge temperature at the TDC (Papagiannakis and Hountalas, 2004). Nielsen et al. (1987) too came to the same conclusion by concluding that the use of gaseous fuel with higher specific heat capacity increases ignition delay further in a dual fuel engine compared to that of a gaseous fuel with lower specific heat capacity.

In terms of chemical delay, it was shown that the homogenous gas fuel-air mixture in the vicinity of the pilot zone can undergo some chemical reactions during the compression stroke (i.e. rise in cylinder temperature), forming intermediates which competes with the pre-ignition process of diesel fuel. This is supported by Nielsen et al. (1987) whereby it was discovered that the induction of diatomic gaseous fuels (i.e. hydrogen, carbon monoxide and nitrogen) with comparable specific heats produces different ignition delay periods, suggesting that the difference in ignition delay is predominantly caused by chemical effects.

2.5.3 Dual fuel emissions

The emissions of a diesel fuelled engine remains a concern for causing environmental pollutions, in particularly the generation of PM and NOx through the combustion process. Research work investigating the emissions of dual fuel engines have shown that the application of gas-diesel dual fuel operation is capable of reducing both PM and NOx, simultaneously, hence capable of potentially breaking the PM-NOx trade off resulted from diesel combustion. Nonetheless, the downside for dual fuel operation is the increased emissions of both carbon monoxide (CO) and unburned hydrocarbons (UHC), which are almost negligible in the case of diesel fuel operation.

Nitrogen Oxides (NOx) emissions consist of nitric oxide (NO) and nitrogen dioxide (NO2) formed through the combination of dissociated oxygen with nitrogen, with NO being the dominating species (Heywood, 1988). As shown in Figure 2.14, NOx formation is affected considerably by the introduction of gaseous fuel, generally showing lower levels of formation compared to that of diesel at similar operating conditions (engine speed and load). It is commonly known that the formation of NOx is mainly determined by the cylinder charge temperature and the local oxygen access ratio (Papagiannakis et al., 2007). At low engine loads, the lower rate of premixed controlled combustion of the gaseous fuel resulted in lower charge temperature inside the combustion chamber compared to normal diesel operation, hence resulting in the lower NOx emissions (Figure 2.14). At higher engine loads, apart from the lower charge temperature effect, the low oxygen concentration in the charge due to the higher level of gaseous fuel inducted reduced NOx formation even further. Nonetheless, it was shown that too high gaseous fuel concentration at high engine loads led to an increase in the rate of energy released and consequently increased the NOx formation due to higher in-cylinder maximum temperature (Abd-Alla et al., 2000).

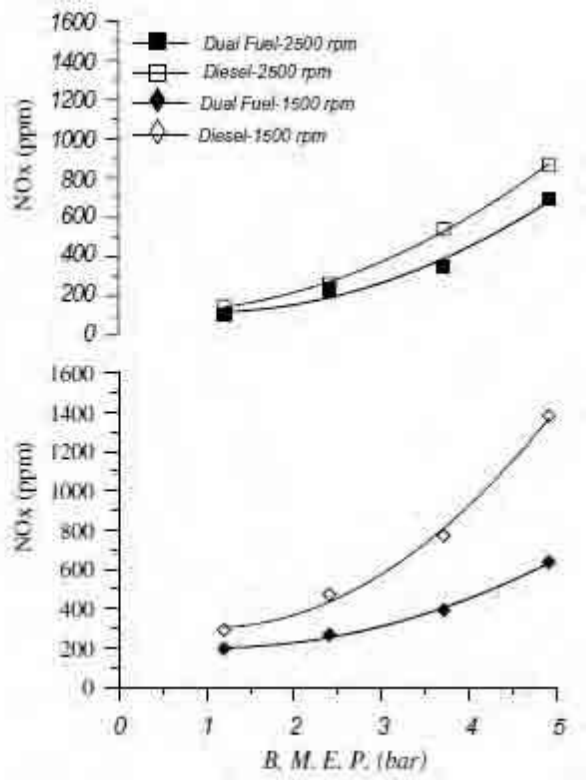

Figure 2.14. Variation of NOx emissions under diesel and pilot ignited dual fuel operation versus load at 1500 and 2500 rpm engine speed (Papagiannakis and Hountalas, 2004).

Particulate Matters (PM) emissions are formed from unburned hydrocarbon fuel which nucleates from the vapor phase to a solid phase in fuel-rich regions and at elevated temperatures. After hydrocarbons or other available molecules may condense on, or be absorbed by the particulate, depending on the surrounding conditions (Tree and Svensson, 2007). For normal diesel operation, high PM emissions are observed at high engine loads and it decreases with decreasing engine load. At high engine loads, the increasing amount of liquid diesel injected into the combustion chamber for the diffusion combustion process and the corresponding increase in total equivalence ratio promotes soot formation. Nonetheless, significant amount of reduction in PM emissions are found in dual fuel operations, with up to 70% reduction being reported (Mustafi and

Raine, 2008). As the majority of PM is formed from liquid diesel fuel, the reduction in liquid diesel fuel due to the gaseous fuel substitution simply reduces PM emissions at the same time. In addition, most of the gaseous fuel type used (e.g. methane, propane and etc.) are lower members of the paraffin with no aromatic compounds and the high hydrogen/carbon ratio decreases the PM formation tendency (Tree and Svensson, 2007). At dual fuel high engine loads, the increased charge temperature contributes to the oxidation of PM, hence further reducing its emission.

Unburned Hydrocarbons (UHC) emissions are in essence partially burned hydrocarbon fuels found in the engine exhaust. For normal diesel operation, UHC exists only in small quantities and does not have significant effect on overall diesel emissions. Despite that, UHC emissions are considerably higher in dual fuel operation, especially at low engine loads as shown in Figure 2.15. The formation of UHC emissions are influenced by the quality of engine combustion process. At low engine load, the lower charge temperature and excess air-fuel ratio (AFR) caused the suppression of turbulent flame propagation from ignition regions of pilot, allowing small quantities of gaseous fuel to escape the combustion process (Liu and Karim, 1997). In addition, the higher ignition delay for dual fuel operation also caused an increase in UHC emissions (Karim, 2003).

It was shown that an effective approach to decrease UHC emissions at low engine load would be to increase the quantity of pilot diesel injected and to decrease the gaseous fuel inducted. By doing so, the pilot ignition centre could be increased; hence more gaseous fuel that is entrained by or in the immediate vicinity of the larger ignition centre will burn (Abd Alla et al., 2000). Apart from the combustion process, there are contributions from crevice volumes whereby some gaseous fuel-air mixture is forced into during the compression process and remained unburned. In addition, valve overlapping between intake and exhaust stroke for scavenging purposes could also increase UHC emissions as unburned gaseous fuel-air mixture is blown out of the cylinder (Weaver and Turner, 1994).

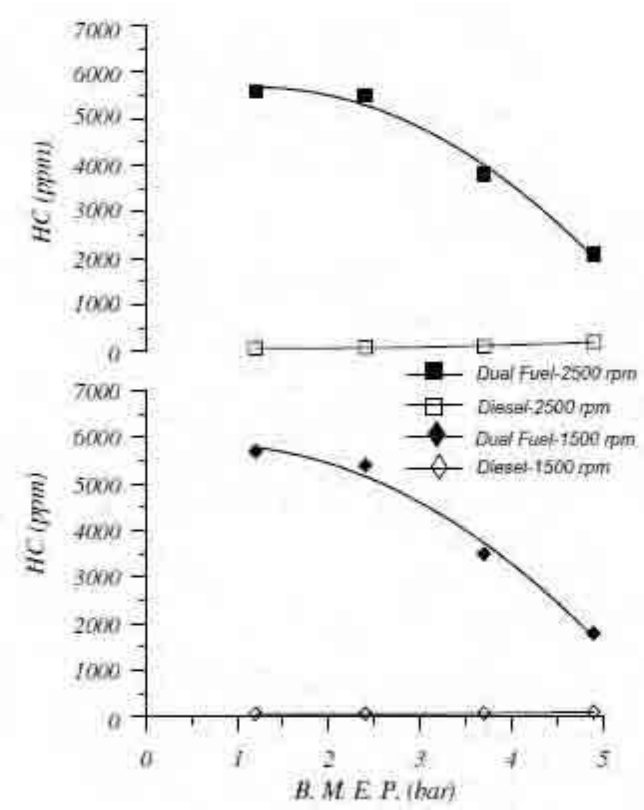

Figure 2.15. UHC emissions under normal diesel operation and duel fuel operation versus load at 1500 and 2500 rpm engine speed (Papagiannakis and Hountalas, 2004).

Carbon Monoxide (CO) emissions are a result of incomplete combustion of fuel due to insufficient oxygen concentration. Therefore, its formation is controlled primarily by the total equivalence ratio (Heywood, 1988). Much of the CO produced is formed at the early stage of combustion process and most of it is oxidized further to CO2, thus the low CO emissions level for normal diesel operation. In dual fuel operation, CO emissions are significantly higher (Papagiannakis and Hountalas, 2004) and its formation is thought to be resulted from the partial oxidation of gaseous fuel in regions within and adjacent to the burning pilot zone (Bittner and Aboujaoude, 1992). It was shown that at similar equivalence ratio test condition, increasing pilot quantity increases the size of the burning zone, hence resulting in higher CO emission for dual fuel operation (Karim, 2003).

The UHC – CO Emissions Trend was suggested by Badr et al. (1999) to summarize the relation between the two main emission constituents for dual fuel operation. At constant pilot quantity, the UHC-CO trend is affected by the total equivalence ratio and it can be represented as four different operating regions (Figure 2.16). For Region I, at extremely low equivalence ratio (i.e. low gaseous fuel admission), there was low level of CO formation produced mainly from the incomplete combustion of pilot diesel. However, due to the limiting combustion of surrounding gaseous fuel, UHC emissions are high in this region. In Region II, the consumption of gaseous fuel (i.e. decreasing UHC) and formation of CO continues with increasing amount of inducted gaseous fuel. The start of Region III signifies the beginning of flame initiation through the gaseous fuel surrounding the pilot zone. It can be seen from Figure 2.16 that further increasing the equivalence ratio into Region III allows some limited flame propagation through the gaseous fuel, hence decreasing both UHC and CO emissions simultaneously. In Region IV, the flame spread limit (FSL) is reached and flame propagation now extends to all parts of gaseous fuel in the combustion chamber, producing high rates of heat release with the smallest value of UHC and CO emissions. In general, it can be said that limiting values of equivalence ratio at Φ1, Φ2 and Φ3 (Figure 2.16) may signify the start of local partial oxidation, flame initiation and the successful spread of flame propagation through the gaseous fuel-air mixture respectively.

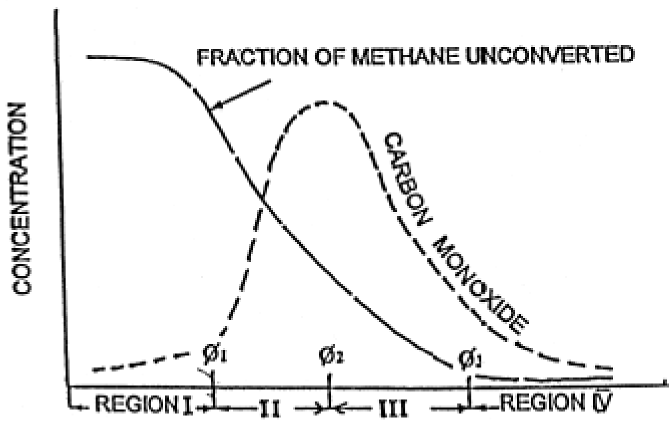

Figure 2.16. Schematic variations of UHC and CO emissions with total equivalence ratio, showing various operating regions (Badr et al., 1999).

2.5.4 Biogas–Diesel dual fuel operations

The engine performance and emission characteristics for gas-diesel dual fuel operations are largely dependent on the types of gaseous fuel used, as shown earlier in Figure 2.16.

In the past, compressed natural gas (CNG, which comprised mainly of methane) and liquefied propane gas (LPG) have shown greatest potential to be applied as gaseous fuels for dual fuel operation. Due to their high octane rating; those fuels are not susceptible to the knocking phenomenon which is common in CI engines with high compression ratio. Table 2.6 shows the comparison of fuel properties between various alternative gaseous fuels suitable for dual fuel operation and liquid diesel fuel. Nevertheless, both CNG and LPG are categorized as non-renewable sources of energy; hence their usage contributes to the emission of GHG into the atmosphere.

Biogas, as mentioned earlier in Chapter 1 is a type of clean and renewable gaseous fuel derived from the anaerobic digestion of organic mass. Table 2.7 shows the various properties of biogas. In biogas, the main constituent contributing to the fuel heating value is methane and therefore the performance of biogas usage in dual fuel operation is largely determined by the amount of diluents (mainly carbon dioxide) present in it (Bedoya et al., 2009). Tests were carried out by Bari (1996) to investigate the effect of carbon dioxide on the biogas-diesel dual fuel engine performance by introducing pure carbon dioxide at various substitution levels together with methane gas at a constant engine speed and load. It was shown that when the percentage induction of carbon dioxide increases, the biogas supply needed to provide the same engine power output also increases, hence resulting in a higher brake specific fuel consumption (BSFC).

Table 2.6. Various properties for alternative gaseous fuels and diesel (Owen and Coley, 1995).

Fuels	**Hydrogen**	**CNG**	**LPG**	**Diesel**
Chemical Formula	H_2	CH_4	C_3H_8	$\sim C_{15}H_{29.13}$
Molecular Weight	2.016	~17.06	44	~170
Density @ 15°C (kg/m^3)	0.082	0.46	0.5	~835
LHV (MJ/kg)	120.0	50.01	92	42.9
Stoich Air/Fuel	34.3	17.19	15.6	14.5
(RON+MON)/2	-	124.5	102.5	~0
CN	-	-	-	52-60
Flammability (Upper)	75.0	15	9.5	7.5
Limits (%vol.) (Lower)	4.0	5	2.1	0.6

Henham and Makkar (1998) also reported that the overall efficiency of the dual fuel operation decreases with the addition of carbon dioxide and this effect is even more pronounced at high engine speed. Duc and Wattanavichien (2007) studied the effect of using biogas produced from a pig farm in an indirect injection (IDI) diesel engine at different engine load conditions and showed that at high engine load, the engine thermal efficiency for the biogas-diesel dual fuel system is comparable to that of normal diesel operation. Nonetheless, the engine thermal efficiency deteriorates greatly at low and medium engine load when biogas is used.

Table 2.7. Properties of biogas (Yoon and Lee, 2011).

Properties	**Data**
Methane (%, by vol.)	30-73
Carbon dioxide (%, by vol.)	20-40
Nitrogen (%, by vol.)	5-40
Hydrogen (%, by vol.)	1-3
Oxygen (%, by vol.)	0-5
Boiling point (°C)	(-) 126-162
Density (kg/m3)	0.65-0.91
Octane number	130
Auto-ignition temperature (°C)	632-813
A/F ratio (by vol.)	17.2
Lower heating value (MJ/kg)	26.17

To understand the emissions characteristics resulted from biogas-diesel operation, Mustafi and Raine (2008) investigated the effect of using three biogas composition, (i) BG1: 80% methane, 20% carbon dioxide (ii) BG2: 70% methane, 30% carbon dioxide and (iii) BG3: 60% methane, 40% carbon dioxide on the emissions of dual fuel operation compared to that of using pure methane at high engine load conditions. It was concluded that while increasing carbon dioxide present in biogas does not affect the formation of CO emissions, there was a minor increase in the emission of UHC when biogas is used and the emission is increased with increasing amount of carbon dioxide present. On the contrary, as shown in Figure 2.17, both NOx and PM emissions were reduced tremendously when biogas is used. The experiment conducted by Yoon and Lee (2011) also showed that at low engine load, both NOx and soot emissions decreased with the use of biogas compared to normal diesel operation. Nonetheless, they also concluded that there is a significant increase in CO and UHC emissions at low engine loads for biogas-diesel dual fuel operation.

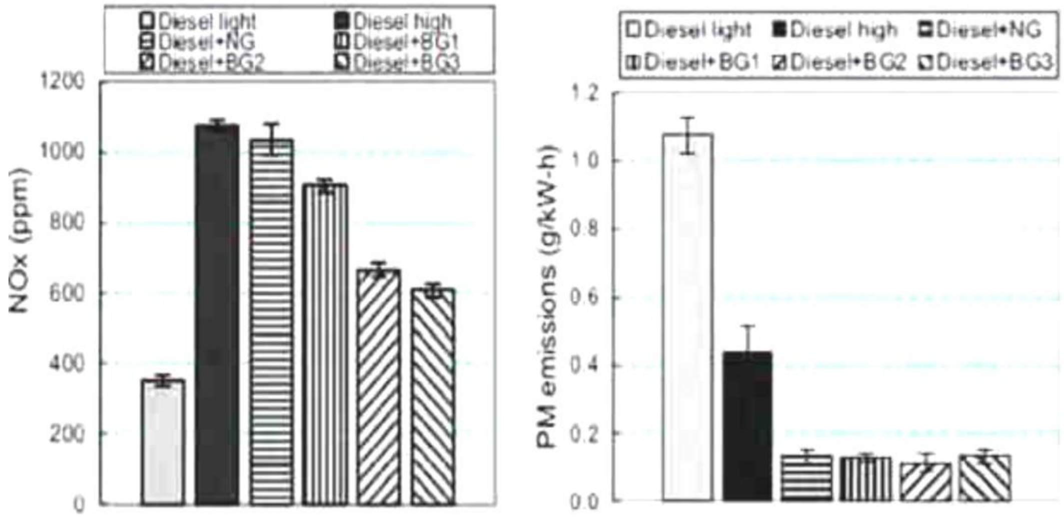

Figure 2.17. NOx concentration and PM mass emission for diesel and dual fuelling (engine speed: 1750 rpm; torque: 3 Nm (light load) and 28 Nm for others), (Mustafi and Raine, 2008).

It was explained that the reduced engine power output in biogas-diesel dual fuel operation is mainly due to the higher biogas induction (due to the low energy content) compared to other gaseous fuels such as CNG, which resulted in a higher fresh air substitution level (Henham and Makkar, 1998). Hence, there is a drop in the engine volumetric efficiency and less power is being generated. In addition, it was also shown that the presence of diluents (carbon dioxide) in biogas further increases the heat capacity of the cylinder charge per unit mass of fuel, reducing the flame temperature and inhibiting flame propagation at the same time (Abd-Alla, 2002). The reduction in charge temperature contributes to the prolonged ignition delay for biogas-diesel dual fuel operation, which in turn is beneficial in reducing the NOx and PM emissions simultaneously. A thorough investigation was done by Kobayashi et al (2007) to understand the characteristics of methane-air mixture turbulent premixed flames diluted with carbon dioxide. The study concluded that with the presence of carbon dioxide, the local turbulent burning velocity was reduced and the combustion oscillation of the premixed gaseous fuel-air mixture was restrained, hence resulting in less gaseous fuel being burnt.

2.5.5 Hydrogen for enhancing Biogas – Diesel dual fuel operation

It was clear that even though the use of biogas for the gas-diesel dual fuel operation provides better NOx and PM emissions, it resulted in lower engine thermal efficiency together with higher CO and UHC emissions at low and medium engine load operating conditions. Bedoya et al. (2009) suggested that gaseous fuels with high burning rates could be used to improve the combustion process of the biogas-diesel dual fuel engine, especially at part load operations. Hydrogen, as shown in Table 2.6 has very high mass lower heating values and its wide flammability limits allow a wide range of engine power output at various mixture equivalence ratios, rendering it superior to other gaseous fuels. It was shown that the minimum ignition energy of hydrogen-air mixture is an order magnitude lower than that of methane-air mixture at atmospheric condition (Ono et al., 2007).

An experimental study was done by Roy et al. (2011) to investigate the effect of adding hydrogen at various substitution levels into low quality producer gas for combustion at constant pilot injection pressure and quantity. The result shows that the average values of maximum engine thermal efficiency increases with increasing hydrogen substitution level and concluded that it was contributed by the higher ratio of specific heats and flame speed of hydrogen. In addition, lower UHC and CO emissions were reported with increased hydrogen substitution level. Nonetheless, it was shown that there was an increase in NOx emissions when more hydrogen was being introduced into the dual fuel system. Gomes Antunes et al. (2009), on the other hand reported an approximately 20% drop in NOx levels with the use of direct injected hydrogen into a diesel engine, stating that the presence of hydrogen reduces high-temperature zones inside the combustion chamber, which acts as the main factor for NOx formation. A detailed experimental study on the combustion of natural gas and hydrogen mixture by Tinaut et al (2011) also reported that the addition of hydrogen increases burning velocity of the gaseous fuel-air mixture, which in effect reduces the overall combustion duration.

It is clear there are many research work investigating the potential of using gas-diesel dual fuel operation for better CI engine emissions and energy security purposes based on the literature review presented in this section. Although both NOx and PM are widely reduced in dual fuel engine applications, the indispensable releases of both UHC and CO in the engine exhaust emissions and low engine performance, particularly at low engine load operating conditions is a concern.

Clean and renewable CBG fuel has shown tremendous benefits to be used as an energy sources. Also, the digestate waste produced could be recycled back into the carbon chain as fertilizers for farming purposes from the anaerobic digestion process, potentially making production and usage of CBG carbon neutral. However, CBG-diesel dual fuel operation suffers from low engine thermal efficiency without optimization engine parameters and high UHC emissions at low load engine operating conditions, due to the high amount of diluents gas. Moreover, Hydrogen content of CBG is a highly efficient and low polluting effect on the engine exhaust emissions. The entrance of H2 into the biogas-diesel dual fuel operation is able to improve the engine thermal efficiency and exhaust emissions concurrently according to literature review. Nevertheless, utilizing pure hydrogen for engine applications still proves to be impractical with the known problems related to the production and storage of hydrogen. In the following chapters of this thesis, diesel single fuel and CBG-diesel dual fuel cases to obtain higher engine performance and lower emission results for a CI engine operation will be presented.

A multi-dimensional modeling, multi-objective optimization and experimental investigation were employed to find out the effects of CBG-diesel dual fuel combustion characteristics on the combustion performance and exhaust emissions of a CI engine. Experimental studies were performed in Marmara University Engine Lab. with Yilmaz T., I., still in progress for coating of low heat loss engine. Both diesel fuel as a single fuel and CBG-diesel dual fuel combustion were modeled in multi-dimensional framework by using CFD code, optimized by coupling multi-objective optimization code with CFD solver and tested in experimental setup. In CFD study, complete intake, compression, power and exhaust strokes were modeled as a full geometry including intake port, exhaust port, intake and exhaust valves. Both naturally aspirated and turbo charged modes were analyzed at different engine loads. In addition, cold flow, fuel spray, single and dual fuel combustion phenomena are modeled incrementally. Each fuels CBG and diesel (Dodecane) are defined as leading reactants in dual fuel combustion operations by using user defined code. During the optimization study, CFD solver and multi-objective optimization code have been coupled by using user defined code and about 20000 cases are analyzed depending upon the input variables. In multi-objective optimization code, start of pilot diesel fuel injection, engine speed, intake and exhaust valve timing, compression ratio and fuel rates both CBG and pilot diesel fuel are defined as input variables to obtain the proper operating conditions of dual fuel CBG engine.

In this study, in order to investigate the combustion performance and exhaust emissions of single fuel real diesel test engine and modified CBG- diesel dual fuel CI engine, in-cylinder combustion pressure, ROHR and in-cylinder temperature were evaluated at different operating conditions. Moreover, to define the optimum operating conditions new designed CBG-diesel dual fuel engine, flow structure for cold flow simulations, fuel consumption, combustion efficiency, in-cylinder temperatures and NOx, CO, CO2, unburned HC emissions were evaluated under various engine operating conditions by comparing single fuel diesel engine and dual fuel CBG-diesel engine numerically and experimentally. In the course of experimental research intake port system of the test engine was modified to convert into CBG-diesel dual fuel diesel engine to perform the dual fuel combustion operations. CBG fuel was injected throughout the intake stroke by electronic gas injectors which were fixed in the intake port system.

In multidimensional study, beside the pilot diesel injector at top of the cylinder geometry, another injector was defined on the intake port system by using cylindrical coordinate system. CBG fuel was defined as a second leading reactant by adding user defined code to the CFD solver. Additionally, CBG fuel was added as a second leading reactant which it is injected from the secondary injector to the intake port beside diesel dodecane fuel.

Obtained results show that in-cylinder combustion characteristics of multi-dimensional modeling and experimental study for single fuel combustion operations indicated similar patterns at various engine conditions (Yoon and Lee, 2011).

Using gaseous fuel such as CBG and CNG in diesel engines that use the dual fuel combustion process has many economically and environmentally advantageous because of these emission improvements. CBG–biodiesel dual-fuel combustion is an encouraging regime to the clean diesel combustion for automotive industry that offers potential for important reductions in both NOx and PM emissions, without any effect on efficiency of the diesel engine. CBG gaseous fuel induced during the intake stroke and then mixed with fresh air before the premixed mixture enters the cylinder combustion chamber. In combustion chamber, the compressed mixture doesn't self-ignite for the high auto-ignition temperature, until after the compression stroke when it is ignited through the injection of liquid-fuel (pilot fuel) in to the combustion chamber (Yoon and Lee, 2011). Therefore, this allows diluted mixtures and very lean combustion of involving low combustion temperatures, providing a reduced NOx emission. Many scientific studies have studied the combustion and emission characteristics with the dual-fuel engines fueled with gaseous liquid-fuels. Mustafi et al. experimentally investigated the exhaust emission characteristics of a direct injection (DI) diesel engine operated with gas main or gas-diesel dual-fuels (Mustafi, N. 2008). Their study showed that stable engine operation may be possible with natural gas (NG) and biogas fueling without any modifications to either the engine or its operation, and that the PM (about 70% by mass) and NOx emissions (more 37% by mass) of duel-fueling tend to be small compared to the ones from diesel fueling operating under the same operation. Maji et al. investigated the use of compressed natural gas (CNG) in lessening the noise level, specific fuel consumption, and NOx emissions, however, the UHC increased inside the dual-fuel mode having a substitution of CNG for 75% of the diesel fuel (Maji S., 2008). Shen et al. investigated the influence in the CNG ratio, the advance of the pilot injection for diesel fuel and also the intake temperature around the combustion process, emissions, and engine performance of a dual-fueled engine (Jie, S., 2003).

These outcomes demonstrated that the gas flow rate, pilot injection timing, engine speed and intake temperature play active roles in the formation of pollutant emissions along with the performance associated with an engine fueled with dual-fuels. It's important to analyze in depth the reduction characteristics of exhaust emissions along with the combustion performance of the CBG-diesel dual-fuel engine as a substitute fuel, in spite of there are researches about the combustion and emission characteristics of biofuels and petroleum fuels with all dual-fuel concept experimentally and numerically.

In 1D and multi-objective optimization study, initial and boundary conditions are defined and about 20000 cases employed coupling with multi-objective optimization code. In 3D CFD study, selected proper cases modeled using full geometry of diesel engine in different engine loads. Fine grids were tested with 1,700,000 hexahedral cells.

In this paper, fine grid results are evaluated. Typical execution time for 742 ^{o}CA with fine mesh takes about 15 hours on a workstation with 32 processors running in parallel. Detailed specifications of engine are given in Table 3.2. Lastly, proper cases which have acquired operating conditions using 1D and 3D simulations are investigated. In this study diesel (Dodecane) is used as a pilot injection fuel. Because of diesel has comparatively high cetane number as a pilot injection fuel, it has good tendency to be ignited in engine. For the dual-fuel system, injectors are defined on the intake port of the dual-fueled combustion engine to model biogas which is injected during the intake process. In this study, it is investigated that the influence of dual fuel combustion characteristics to decrease in exhaust emissions along with the combustion performance in the diesel engine fueled with biogas-diesel dual-fuel. That’s why, with this work, the combustion pressure and the rate of heat release (ROHR) are evaluated such as Yoon and Lee, 2011’s study under changed operating conditions and different engine loads and analyzed the combustion characteristics of the CI engine for single-fuel (Dodecane) and dual-fuel (CBG-diesel) combustions. Moreover, combustion pressure or indicated mean effective pressure (IMEP), exhaust gas temperature, and also the concentrations of soot, NOx, HC, CO and CO2 exhaust emissions are also investigated under various engine operating conditions to compare the engine performance and exhaust emission characteristics of single-fuel and dual-fuel modes. The results confirmed that, the ignition delay for single fuel indicated shortened trends compared to CBG–diesel dual-fueling due to the higher cetane number (CN) of diesel. The results showed that, in dual-fuel combustion mode, the peak pressure and heat release for CBG–diesel are slightly lower compared to diesel modes. The results are in agreement qualitatively with the previous experimental studies in the literature.

CBG fuel which produced by the anaerobic fermentation of organic materials such as cellulose biomass is a very clean fuel for internal combustion engines especially for NOx emissions. Besides the clean fuel since fuel shortage situations, it may act as a promising alternative fuel, by substituting for a considerable amount of fossil bio-fuels particularly for diesel engines. Diesel engines can be easily modified to gas-diesel dual fuel engines without any interference to the combustion chamber. This way is the most practical and proper method to utilize high spontaneous ignition temperature alternative fuels such as CBG fuel. In the fumigated dual fuel method, CBG mixes with air before this mixture enters the cylinder, and at the end of the compression stroke, an amount of the pilot diesel injection fuel is injected to ignite air-CBG fuel mixture. This new method has the advantage of the ability to switch back to diesel combustion in case of a shortfall in CBG fuel supply during an important operation. Because of these benefits, dual fuelling of diesel and CBG fuel, alongside producer gas, LPG, NG or hydrogen, have been studied widely worldwide for some past decades. Karim G.A. et al. have worked on dual fuel operation with different gaseous fuels (hydrogen, LNG, propane, CNG, LPG) according to engine performance, combustion characteristics, exhaust gas emissions and factors influencing them (Phan, M., 2007). These factors contain the engine loads, diesel substitution, injection timing, intake air temperature and EGR. They resulted that the prolonged ignition delay caused by the existence of gaseous fuel in the compression process, the reduction of oxygen concentration in the charge and the increase in the polytropic index of the charge leads to important changes in engine combustion characteristics, exhaust gas emission, engine performance and fuel consumption. In addition these researches, many studies were confirmed by other researchers in this field. In past decade years, a considerable number of studies concentrated on engine performance, exhaust emissions and fuel consumption. During those revealed decreases in engine output, others resulted unchanged or even increased output. A loss in thermal efficiency had been concluded by some authors, whereas others reported comparable or higher efficiencies or loss at low to medium engine loads but increases at high to full loads. Solutions to develop dual fuel part load have been investigated and proposed, like throttling the intake air charge, increased intake air pressure, temperature, controlled fuel amount and time of pilot diesel injection or analyzed EGR flow and temperature (Phan, M., 2007). While more information of the composition of gaseous fuel and kind of fuel used were provided, less detailed information about engine geometry and optimization study on engine parameters was mentioned. These parameters make it more difficult to evaluate the reported results since the engine performance, thermal efficiency, diesel substitution and exhaust gas emissions depend not only on the physical and chemical properties of the gaseous fuels but also on the engine geometry used. Moreover, almost all past studies were conducted with engines on test setup at which engine cooling water and lube oil temperatures had been controlled to provide not exceeding a predefining value. These situations prevent the real operational conditions at which the temperatures may increase to high values. The mentioned information about long reaching use with dual fuelling has also not been reported clearly and these type of researches dramatically increased. Also, investigations resulted that dual fuel operation for IDI engines has less efficient than for DI engines because of too high surface to volume ratio of the cylinder combustion chamber. Moreover, optimization results showed that the change in combustion chamber geometry of this type would have an effect on the dual fuel combustion characteristic. In this study, a comparative investigation between straight diesel and CBG premixed charge diesel dual fuel CI which called DDF was conducted to obtain clear information. Single fuel and dual fuel engine performance, diesel substitution, energy consumption and the effect of long term use also were concerned as following aspects.

3 EXPERIMENTAL SETUP AND CFD TECHNIQUE

3.1 Problem Description

In this chapter the experimental facilities and CFD technique used for this research are mainly describes. The test setup and data or sample acquisitions performed in this thesis for both the engine experimental tests and CFD simulations are described.

A combustion phenomenon is the most important event of an IC engine that affects directly the engine performance and exhaust emissions. In this study, single fuel and CBG-diesel dual fuel combustion operations of a real diesel engine are studied by optimizing SOI, fuel rates, CR, RPM and valve timing. In order to optimize the dual fuel engine parameters, SOI, fuel rates, CR, RPM and valve timing are iterated to reach the proper engine performance and exhaust emissions by using multi-objective optimization code. Since the 1.5 lt light duty diesel engine is used on a vehicle, the emission values must obey the Euro-6 standards which are valid as from the September of 2015 as shown in Table 3.1. As it is mentioned before, CO, CO2, NOx, and PM are the most important ecological engine parameters for emission standards of European Council. Particularly, formation of NOx can be named as the hardest controlled phenomena for IC engines. The main goal is to keep the nitrogen oxides values under the Euro VI restrictions. Test engine properties used in experimental and CFD study is given in Table 3.2.

Table 3.1. European emission standards for light commercial vehicles (Commission Regulation, 2013).

Tier	Date	CO	THC	NMHC	NOx	HC+NOx	PM	P
Diesel								
Euro 1	October 1994	5.17	-	-	-	1.4	0.19	-
Euro 2	January 1998	1.25	-	-	-	1.0	0.12	-
Euro 3	January 2001	0.80	-	-	0.65	0.72	0.07	-
Euro 4	January 2006	0.63	-	-	0.33	0.39	0.04	-
Euro 5	September 2010	0.630	-	-	0.235	0.295	0.005	-
Euro 6	September 2015	0.630	-	-	0.105	0.195	0.005	-

3.2 Experimental Setup

The aim of this chapter is to present the experimental test facilities and data acquisition systems used in this research work. The engine utilized for this research is based on a four-cylinder, turbocharged compression ignition (CI) engine with a single overhead cam (SOHC). It possesses a bore of 76 mm, a stroke of 80.5 mm, a displacement volume of 1461 cm^3 and a compression ratio of 18.25. The rated maximum power along with the maximum torque was 48 kW at 4000 rpm and 160 Nm at 2000 rpm with the boost pressure of 0.03 MPa, respectively. The detailed specifications and measurements of engine were summarized in Table 3.2. The experimental apparatus for the dual-fuel engine consisted of test engine, fuel tanks for biogas, and the dynamometer which used for the engine performance tests, control systems, the combustion analyzer, the exhaust emission analyzer, and the gas fuel injection system as shown in Fig. 3.1. The engine load and speed are controlled utilizing an eddy current (EC) dynamometer system (Cussons – 1200 – 8000 rpm) has a maximum braking power 165 kW. The in-cylinder pressure was measured with a piezo-electric pressure transducer (Kistler) coupled with a charge amplifier (5044, Kistler). In every test case, the combustion pressure data is measured over 1000 cycles and purchased with a DAQ board with a sampling interval of 0.1° crank angle (CA) to make certain accurate ignition timing and phasing of heat release. The obtained in-cylinder pressure data is averaged on the crank angle to get rid of the effect of cycle-to-cycle variations and after that calculated on the rate of warmth release (ROHR) for the analysis of combustion characteristics each test fuel. The exhaust emission measurements without catalytic treatment systems are conducted using a NOx analyzer (Bosch-combo), a soot analyzer (Bosch-combo / BAE-460), along with a HC-CO analyzer (Bosch-combo). Detailed test equipments are given in Table 3.4. The measurements from the exhaust gas components are recorded following this test engine operation had sufficiently stabilized to steady state engine conditions. The temperature of the intake-air, exhaust gas, and coolant, along with the flow rate of the intake-air are monitored from the data acquisition system. Two K-type thermocouples (Omega, KMTSS-020 G-12) are placed in the intake port and consequently with the exhaust port to determine intake-air and exhaust temperatures within ±1 °C, as well as a digital thermometer (Omega, 2168A) is applied to measure the temperatures. The diesel fuel is pressurized with the common rail injection system and the flow rate of the diesel fuel is measured by the fuel flow meter system. The intake system with the test engine is modified for a dual-fuel combustion engine. CBG fuel is injected in the intake process by gas injectors which are positioned in the intake pipe as soon as the outlet from the turbocharger. Gas fuel injector is electrically controlled by valve. The flow rate of gas fuel is digitally controlled by an electric control system and program with the use of pulse signal. Injection mass is controlled in accordance with engine speeds and loads at constant injection timing. Gas fuel is held in a top pressure with 3.2 MPa of fuel pressure.

Table 3.2. Test engine specifications.

Engine parameters	Value
Type	4 Cylinder-four stroke
Bore × Stroke	76×80.5 mm
Connecting rod length	131.2 mm
Displacement	1461 cm3
Compression ratio	18.25:1
Max. Lift (exhaust)	10,1 mm
Max. Lift (intake)	9,7 mm
Operating speed	2000 rpm
Maximum power	48 kW at 4000 rpm
Maximum torque	160 Nm at 2000 rpm

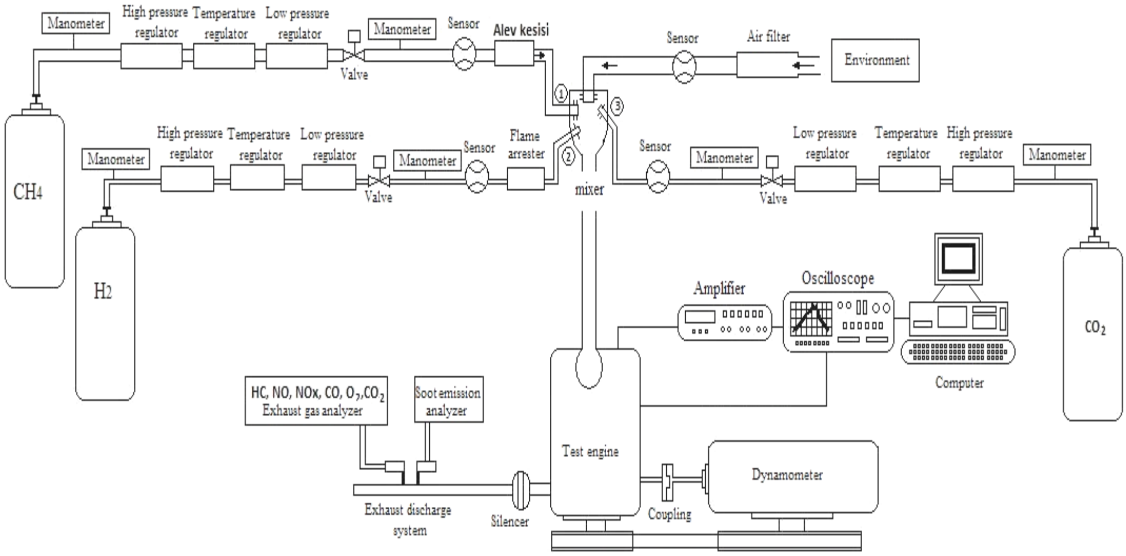

Figure 3.1. Experimental setup.

Table 3.3. Properties of diesel fuel.

Properties	Value
Chemical formula	$C_{12}H_{26}$
Density	786 kg/m^3
Boiling point	214-218 ^oC
Cetane number	52-53
Self-ignition temperature	205-210 ^oC
Lower heating value	43Mj/kg
F/A ratio	0.0714
Vapor point	40 Pa at 20 ^oC

Table 3.4. Test equipments.

Name	Brand / Model
Engine dynamometer for multiple cylinder engines	Cussons / E038EC38TA / 165kW / 1200-8000 RPM
Amplifier	Kistler / 5044
Thermal bulk methane flow meter	Sierra / 7805-FMN2-E2-P2-V4-DD-9-Pulse
Thermal bulk hydrogen flow meter	Sierra / 7805-FMN2-E2-P2-V4-DD-7-Pulse
Fuel pump testing device for diesel engine	Merlin / MM8-7.5
Injector test device	Merlin
Exhaust emission measurement device (CO_2, CO, HC, NO_X, O_2)	Bosch-combo
Soot emission measurement device	Bosch-combo / BAE-460
Carbon dioxide regulator	Voltran-Vogas / V-SGI System
Methane regulator	Voltran-Vogas / V-SGI System
Hydrogen regulator	Voltran-Vogas / V-SGI System
Flash reducer	Solar Gas Keys
The storage tanks for methane, carbon dioxide and hydrogen gases	HATGAZ / 50lt / Steel tube

3.3 Experimental conditions and procedure

All engine tests are performed in a constant speed of 2000 rpm employing a dynamometer in a constant engine speed mode, and the coolant and oil temperatures are maintained at 68 ± 1 °C to lessen the variation inside the test results. The experimental investigation was conducted in two combustion modes within a steady state condition with some other engine loads. Different engine loads were 20%, 40%, 60%, 80% and 100%, and also the brake torque corresponding to each driving condition is measured on the control system with the dynamometer. Within the single-fuel combustion mode, a diesel pilot fuel is respectively fueled without the additives, and therefore the combustion and exhaust emission characteristics of diesel fuel are compared at various test conditions. The injection timing from the pilot fuel was constant at 12° bTDC as well as the injection pressure is maintained at 160 MPa. In the case of dual-fuel combustion, the engine is dual-fueled with a mix of biogas-diesel. Inside the dual-fuel combustion mode, biogas is injected to the intake port with the injection pressure of 0.3 MPa. The amount of biogas is fixed, as well as the mass with the pilot fuel is controlled based on the engine load. The detailed experimental test conditions for this study are given in Table 3.6.

Table 3.5. Properties of CBG fuel.

Properties	Value
Chemical formula	Mixture
CH_4	65-70 % by volume
CO_2	25-35 % by volume
H_2	1-2 % by volume
Self-ignition temperature	630-810 ^oC
Lower heating value	26 Mj/kg
F/A ratio	0.058
Octane number	135
Density	0.79 kg/m^3

Table 3.6. Operating conditions.

RPM	2000 rev/min
Test fuels	Diesel and CBG
Single fuel	Diesel
Dual fuel	Diesel + CBG
Engine loads	1-2 % by volume
Gas injection pressure	0.3 MPa
Gas injection type	Port injection
Injected gas mass	30 mg/cycle
Pilot diesel injection pressure	13 MPa
Start of injection	12^0, 18 ^{0}CA bTDC

3.3.1 Test bench engine

The test engine used in this research work is the real engine, which is a turbo-charged and water-cooled four-cylinder direct injected diesel engine as shown in Figure 3.10. An externally CBG injector system was also implemented in this engine. For fuel injection parameters, the fuel injector has an opening pressure of 160 MPa and the injection timing is set by the manufacturer at 12^{o} CA before TDC. The detailed engine specifications for test engine are given in Table 3.6.

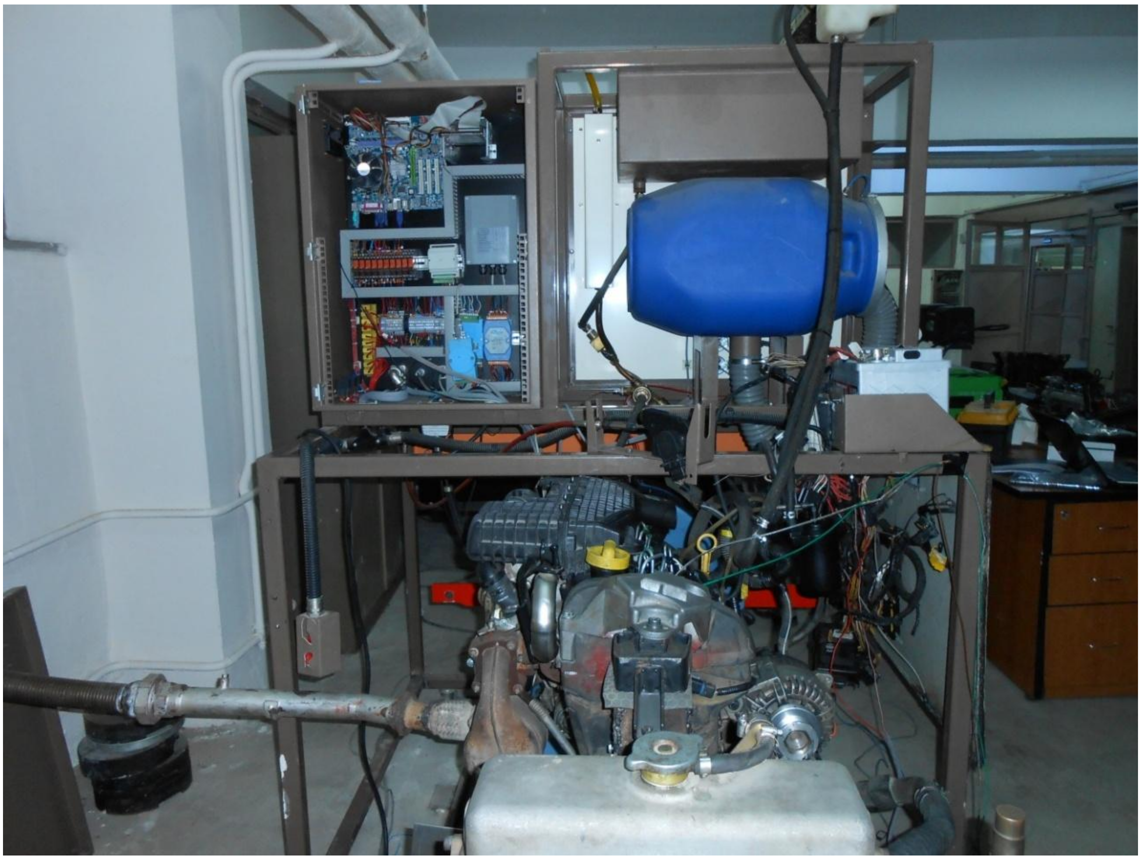

Figure 3.2. Dynamometer and common rail DI diesel test engine.

The equipment used throughout this research work is described in this chapter. This includes the details of the four cylinder test hardware and instrumentation with the emissions equipment. Control methodology of the engine, data collection process and analysis software which used in experimental study are all described by turns. The test facility was upgraded for CBG-diesel dual fuel engine operations.

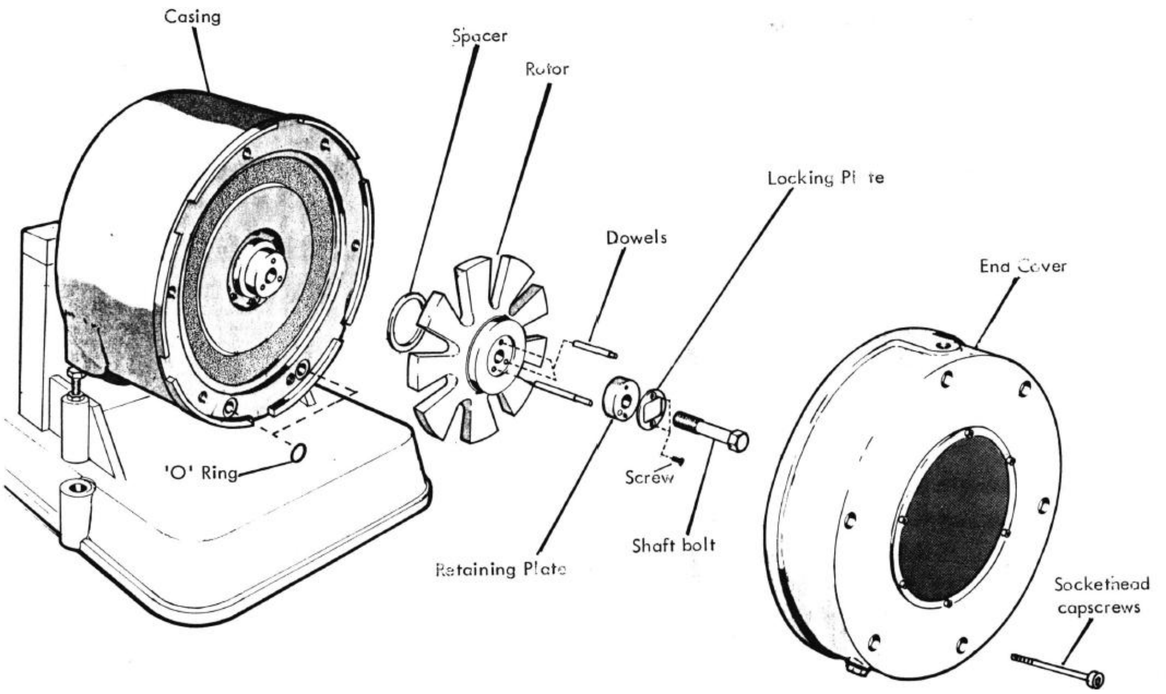

Figure 3.3. Exploded view of items in rotor compartment (p8602 multi-cylinder engine test bed)

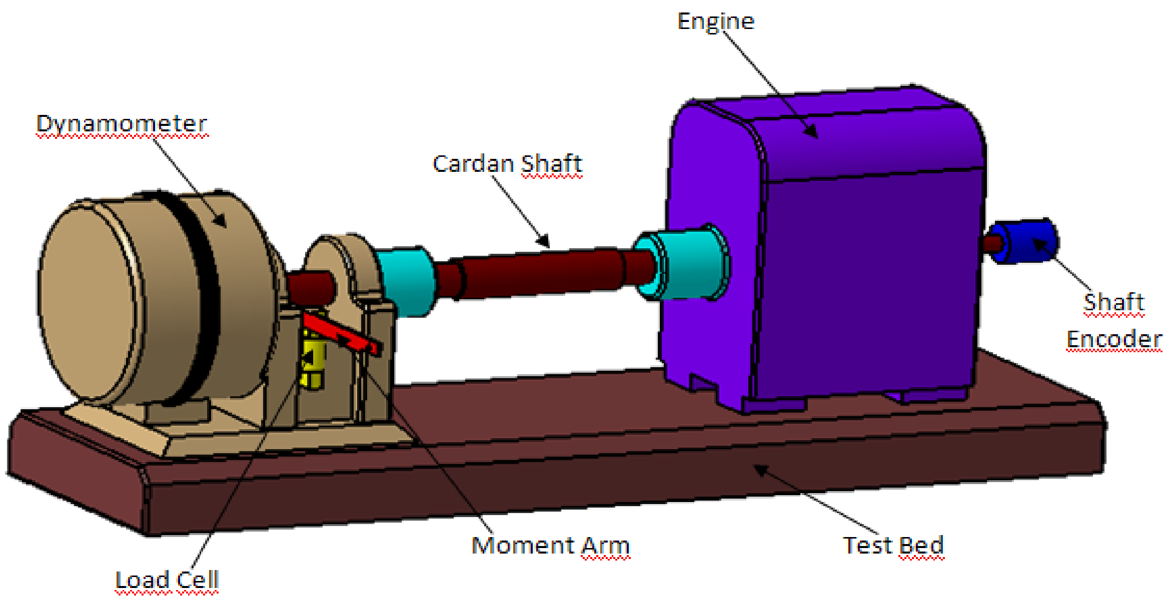

Figure 3.4. Dynamometer and test bed schematic diagram.

3.3.2 Control System

The engine timing control system (ETCS) controls the SOI injection and injection pulse width, together with the ignition timing and coil charge time. The ETCS software is written using LABVIEW (NI card 6602) and was originally developed by the ICE Group but was then modified by a previous researcher at this institution (Luszcz, 2009). Each ETCS parameter can be changed in real-time, whilst the engine is running. Two injections per cycle (independent pulse widths) are allowed with either PFI or DI. This is sometimes referred to as double pulse injection, but is herein termed split-injection. When operating the engine in dual-injection mode, the PFI and DI injectors can be run simultaneously. This is achieved by changing the terminal connections on the control panel and the use of an external DI injector controller. When running in this mode, split-injection is disabled.

The control of air flow whilst at constant engine speed was achieved through the adjustment of a butterfly throttle valve. The mixture strength was then controlled by adjusting the injector pulse width using the ETCS software (Daniel, L., 2012).

3.3.3 Dynamometer

In this study, test engine is loaded to obtain the engine performance characteristics such as indicated pressure, power, torque and specific fuel consumption. In this way, engine torque on the output shaft is measured depending on the engine speed on the test bench as shown in Fig. 3.2. Load systems are called as a dynamometer and force which performed on the engine output shaft is called as a load. Engine power and torque can be obtained by measuring the dynamometer torque which equaled test engine torque. Engine speed and load conditions must be controlled to obtain the engine performance and emission characteristics truly. These conditions can be controlled via dynamometer as shown in Figure 3.5. Break moment occurs in the torque arm which is connected to the dynamometer. This force is transmitted to the load cell by torque arm. Engine torque is calculated by determining in load cell. 165kW and 8000 rpm maximum test ranges can be measured in this dynamometer. Obtained power from the test engine was transmitted to the dynamometer. Engine torque was measured by torque arm and load cells. In this test system, CI engine is fastened and connected to the dynamometer to measure combustion performance. Kistler piezo-electric pressure transducer was used to get pressure date inside combustion chamber.

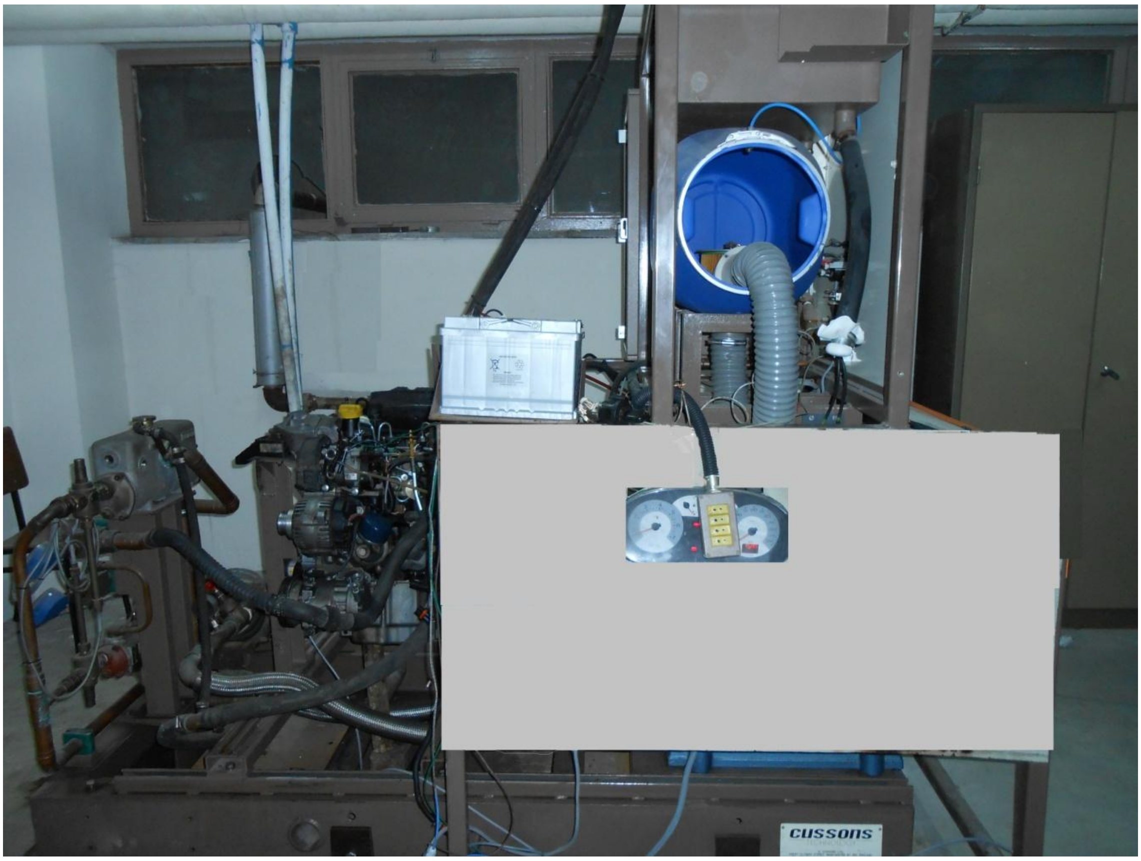

Figure 3.5. Experimental setup.

3.3.4 Gas flow measurement

This device biogas fuel is measured utilizing a gas flow-meter system that features a % 0–250 L/min flow range, accuracy of ±1.0%, and repeatability of ±0.5% using a given pressure. The principles of operation are the following: metered gases are divided into two laminar flow paths, one through the primary flow conduit, and also the other through a capillary sensor tube. When gas flow occurs, the resultant temperature differential between two precision temperatures is linearly proportional towards the instantaneous rate of flow. Prior to each experiment, the combustion transducers and emission analyzers are calibrated to be sure consistency across the measured datum. Moreover, the injection pressure (0.3 MPa) and the temperature in the biogas fuel are adjusted and maintained with the pressure regulator and the heat exchanger with coolant water, respectively.

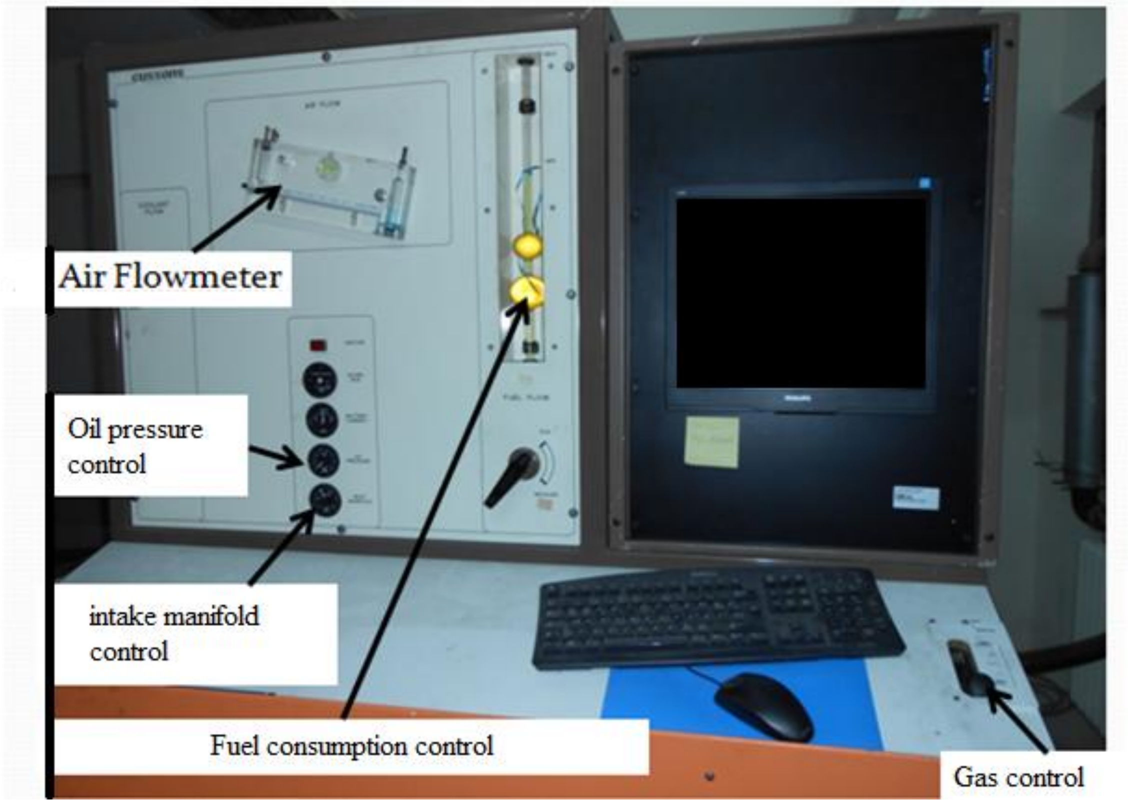

Figure 3.6. Control system.

The breaking force is measured corresponding to the moment and multiplied the moment arm length because of the breaking moment is not measured directly as seen in the Figure 3.7. (Turkcan A., 2006).

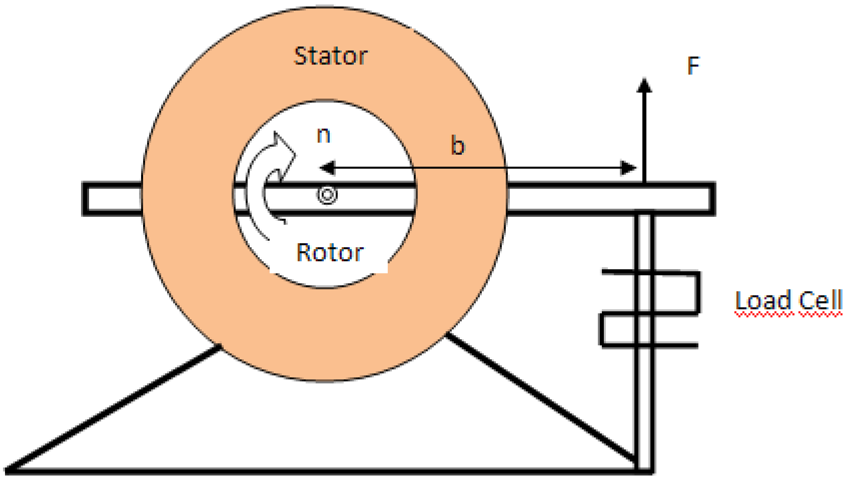

Figure 3.7. Breaking torque measuring principle.

3.3.5 In- cylinder pressure sensor

In this study, the optrand brand pressure sensor was used to measuring of the in-cylinder pressure. The sensing element is coupled via an optical fiber to an enclosure. The enclosure has four or five color-coded leads (depending upon system grounding requirements) for terminating to a power source and data acquisition system. In 3.7 detailed specifications of sensor were given sensor. (AutoPSI Pressure Sensor)

Table 3.7. Sensor characteristics

Model	Optrand Auto PSI pressure sensor
Diaphragm Resonant Frequency	120 kHz min.
Frequency Range	1.0 Hz to 25 kHz
Fiber optic Cable Min.Bending Radius	5mm (3/16")
Sensor Type	Sealed Gauge
Interface Unit	Integrated with Sensor
Pressure Output Signal	**9-18V DC input**: 0.5 – 4.5 V
(Analog) **5V DC input**	0.5 - 4.5 V
Diagnostic Output Signal	**9-18V DC input**: 0.5 – 2.5 V
(Analog) **5V DC input**	0.5 – 2.5 V
Input voltage	9-18V DC
Output voltage	0.5-4.5V DC
Current Draw	85 mA Max, 50 mA Typical
Interface Temperature Range	**AutoPSI-S,A,TC:**-20°C to 60°C
Sensor Housing Temperature Range	-40°C to 380°C
Cable Operating Temperature	-40°C to 200°C
Sensitivity	1.32mV/psi @ 200^{o} C
Pressure range	0-3000 psi

The sensor has either four or five wires extending out of the electronic enclosure tube. The purposes of each wire were given in Table 3.8:

Table 3.8. In-cylinder pressure sensor wires.

White Wire	Sensor Output Signal
Blue or Green Wire	Diagnostic, Static Calibration
Red Wire	Power
Black Wire	Ground (Power and Signal)
Bare Wire	Case (if present, otherwise case is connected to Ground)

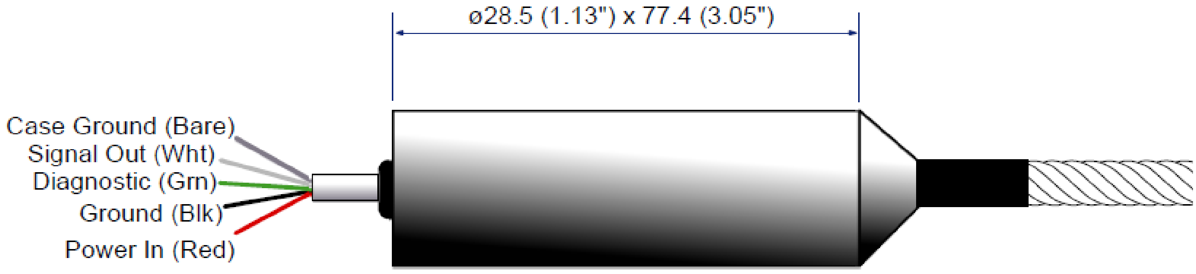

Figure 3.8. Detail of sensor cable autopsi pressure sensor.

3.3.5.1 Sensor output signal:

Connect between the White and Black wires. The output signal is analog, 0.5 – 4.5 Volts for all sensors. The analog signal and Sensor Sensitivity Value must be used to calculate the correct pressure. (AutoPSI Pressure Sensor)

3.3.5.2 Diagnostic output signal:

Connect between the Blue or Green wire and the Black wire. The diagnostics output signal is a DC Voltage, proportional to the LED current level, and indicates when the sensor is in or out of calibration. This voltage is typically in the 1.0 – 2.0 Volts range for all sensors and can vary from sensor to sensor. (AutoPSI Pressure Sensor)

3.3.5.3 Static pressure calibration

The AutoPSI sensor can measure static pressure when the diagnostic (blue or green) wire is used as input instead of an output. If the diagnostic wire is connected to a DC power source (0-2.5 volt) or a potentiometer to ground the sensor will measure static pressure. This mode is useful for calibrating the sensor with a dead weight tester or other static pressure calibration technique. (AutoPSI Pressure Sensor)

3.3.6 Fuel line pressure sensor

In this study, the Kistler type piezoresistive high pressure sensor with amplifier was used to measuring fuel-line pressure. The pressure to be measured acts through a rugged diaphragm on an arrangement of piezoresistive ”rods”. The pressure changes the values of the resistances diffused into the rods. These resistances are arranged in a Wheatstone bridge. The pressure sensor itself is not temperature compensated. The amplifier Type 4618A... provides temperature compensation, linearization of the pressure signal and contains a stabilized power supply. For this reason, the sensor must always be operated with the amplifier adjusted to it. In the table 3.9, there are some characteristics about this type sensor (Kistler, 2012).

Table 3.9. Sensor characteristics.

Model	Kistler
Range	0-3000 bar
Sensitivity	3.333 mv/bar
Output impedance	10Ω
Supply (Amplifier)	18-30V DC
Thermal sensitivity shift	< ±1%
Tightening torque	15 N.m
Acceleration error	<10 mbar/g
Natural frequency	>200 kHz

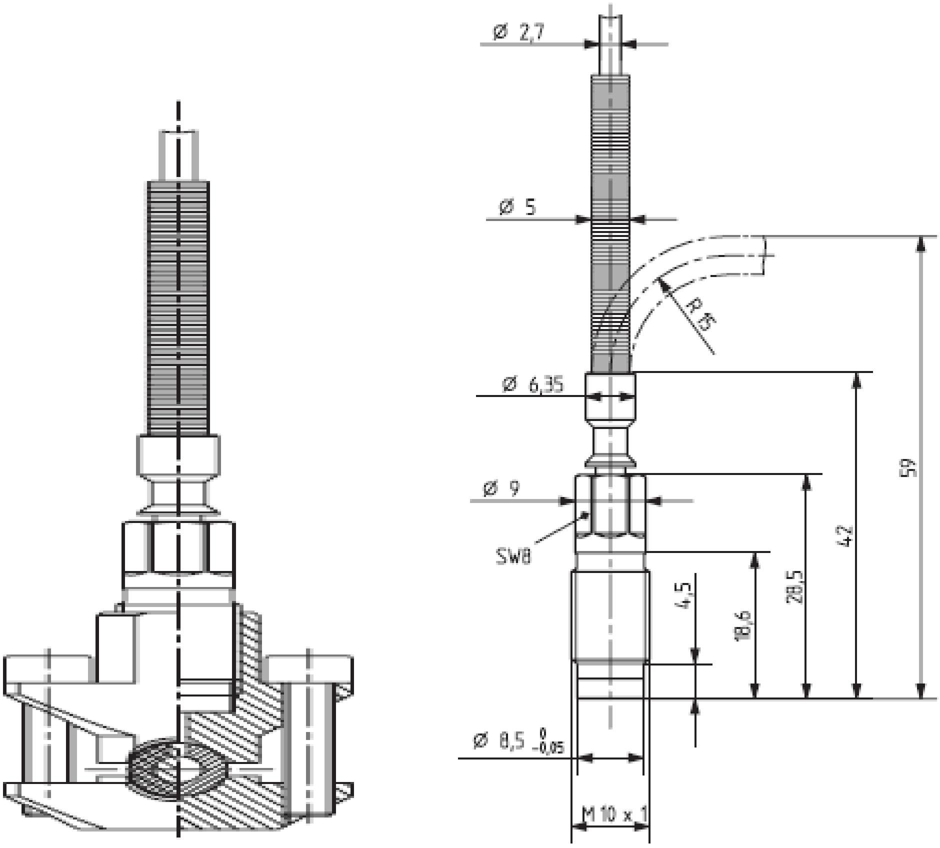

Figure 3.9. Dimensions (Kistler) and mounting in clamp adapter (Kistler).

Figure 3.10. Fuel line and ın-pressure sensors.

3.4 Software

In this study, MOTEST was used as the programme which controls the dynamometer, engine and all devices including engine test room. MOTEST is developed by the TUZEKS. This system has completely user-specify test screen and the test procedures are designed by user.

In figure 3.11, It computes an excel creation which are made of tests results in the desired extent in order. In the report menu, clicking on the previously defined report gives the results depending on time and type of test condition which are determined by user. We see that in the figure 3.11, automated test record takes the average of data which has the same functionality of automated tests. The manual test takes average of the results in the same minutes (Motest10).

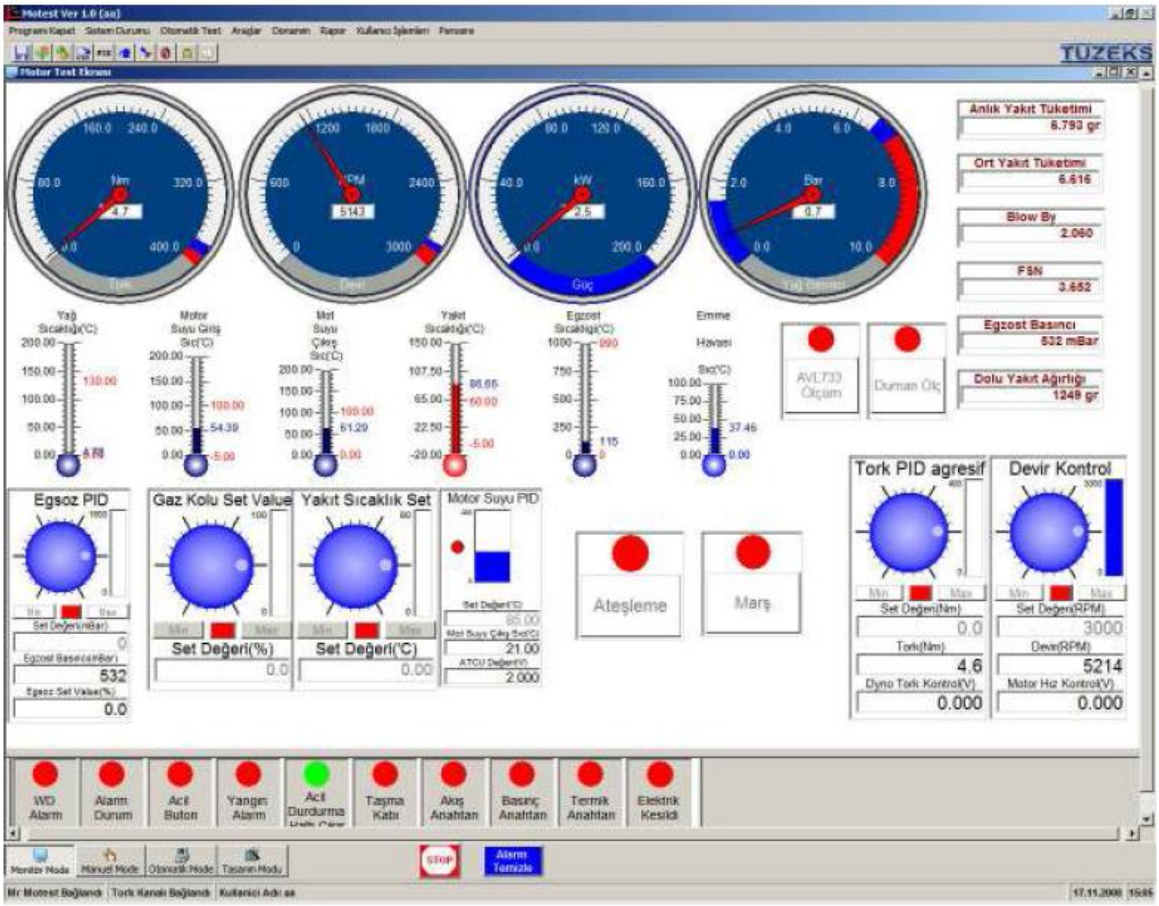

Figure 3.11. View of software interface.

Calibration is operated for the defined analog channels. These are reel analog input and output channels. The calibration button which is located under the tools menu is pressed down and the calibration window appears on the screen. Channel and calibration list are listed as defined under the analogue channels (Motest10).

3.5 Encoder

A rotary encoder, also called a shaft encoder, is an electro-mechanical device that converts the angular position or motion of a shaft or axle to an analog or digital code. There are two main types: absolute and incremental (relative). The output of absolute encoders indicates the current position of the shaft, making them angle transducers. The output of incremental encoders provides information about the motion of the shaft, which is typically further processed elsewhere into information such as speed, distance, and position. Rotary encoders are used in many applications that require precise shaft unlimited rotation including industrial controls, robotics, special purpose photographic lenses, computer input devices and rotating radar platforms (Mitchell Electronics, 2014).

In this study, the kübler standard optical incremental encoder was used for the rotational speed, angular displacement, acceleration and rotational motion. An optical encoder is a complex system which converts a mechanical rotary motion (angular position or speed) into a usable electrical signal. Each encoder optimizes the operating characteristics of three systems (mechanics, optics, and electronics). Encoder specifications were given in Table 3.10 (Kubler, 2010).

Table 3.10. Encoder characteristics.

Model	Kubler optical incremental encoder 5000
Working temperature range	-40^{o}C……+80^o C
Shaft material	Stainless steel
Power supply	5…30V DC
Pulse frequency	max. 300 kHz
Shock resistance	2500m/s^2
Vibration resistance	100m/s^2

The optical encoder's disc is made of glass or plastic with transparent and opaque areas. A light source and photo detector array reads the optical pattern that result from the disc's position at any one time. This code can be read by a controlling device, such as a microprocessor or microcontroller to determine the angle of the shaft. The absolute analog type produces a unique dual analog code that can be translated into an absolute angle of the shaft.

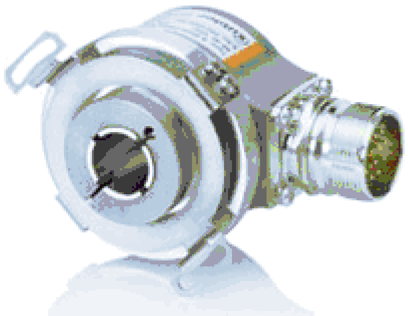

Type 5000/5020

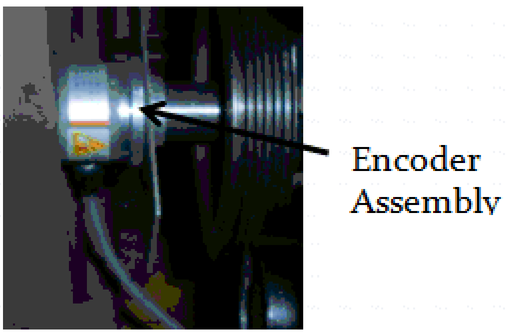

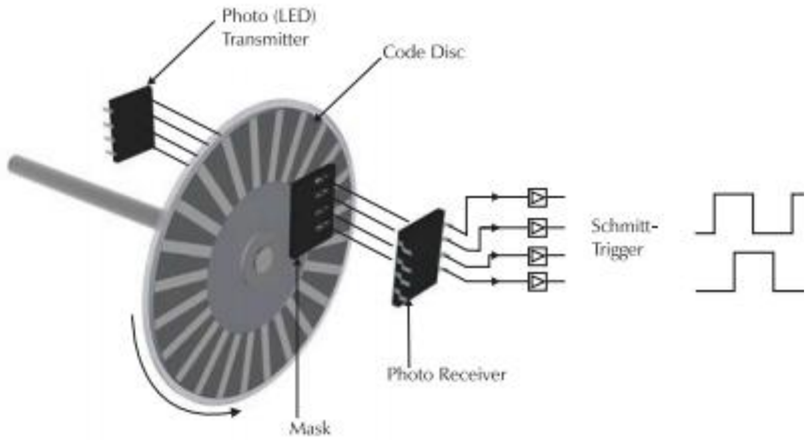

Figure 3.12. An encoder assembly and a photoelectric emitter receiver pair looking through a slotted disk.

Light from the LED passes through the disc, the mask and into the photo transistors. The photo transistor outputs a sine wave which corresponds to the flashing light pulses from the LED.

3.6 Thermocouple

The thermocouple is a simple, widely used component for measuring temperature. A thermocouple, shown in Figure 3.13, consists of two wires of dissimilar metals joined together at one end, called the measurement ("hot") junction. The other end, where the wires are not joined, is connected to the signal conditioning circuitry traces, typically made of copper. This junction between the thermocouple metals and the copper traces is called the reference ("cold") junction.

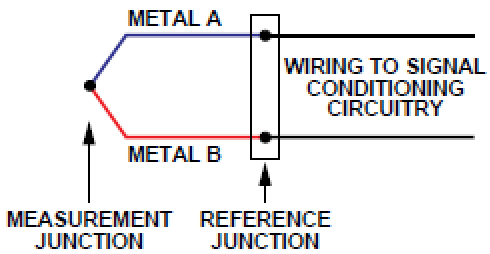

Figure 3.13. Thermocouple (Reotemp manual).

3.7 Emission Measurement

NOx analyzer (Bosch-combo), a soot analyzer (Bosch-combo / BAE-460), along with a HC-CO analyzer (Bosch-combo) exhaust emission measurements without catalytic treatment systems were used. Test equipments were given in Table 3.4. The measurements from the exhaust gas components were recorded following this test engine operation had sufficiently stabilized to steady state engine test conditions.

3.7.1 Data processing

Experimental data were transferred to engine analyze software to compare and evaluate. Indicated pressure, temperature, engine speed, engine load and fuel mass flow were obtained by this software.

3.7.2 Fuel properties

The fuels injected in the combustion chamber (pilot fuel), which acts as the cause of ignition, is a conventional diesel fuel. The diesel utilized in this study is dodecane that chemical formula is $C_{12}H_{26}$. Diesel which satisfies the standard specification for diesel fuel is used as the reference fuel. Table 3.3 shows the detailed properties of the liquid test fuel used in this experiment. In comparison to conventional diesel fuel, the physical properties of undiluted diesel fuels are somewhat different in the literature. In this study the dodecane has higher density, viscosity, and cetane number and normal C-H ratio and LHV as a diesel fuel. These specificities possess a significant influence on the fuel atomization and evaporation characteristics inside the combustion chamber; because of this a new combustion and exhaust emission characteristics are obtained from study. Biogas is often a gaseous fuel produced by the anaerobic fermentation of organic waste biomass and possesses vastly different fuel characteristics from that relating to liquid fuels, including biodiesel or diesel fuels. The purified biogas used in this research is comprised of methane (CH_4), CO_2, H_2S, N_2, H_2, and O_2, coupled with a high octane number (Yoon and Lee, 2011). It has high potential to deal with the knock phenomenon when compared with conventional diesel fuel thereby is a very suitable fuel for dual-fuel combustion in diesel engines. The detailed properties of biogas are given in Table 3.5.

3.8 Uncertainty Analysis

The method is based on a careful specification of the uncertainties in the various primary experimental measurements. If a very careful calibration of an instrument has been performed recently, with standards of very high precision, then the experimentalist will be justified in assigning a much lower uncertainty to measurements than if they were performed with a gage or instrument of unknown calibration history (J.P Holman, 1988). Uncertainty analysis was used to find out the error rates of experimental results. Effects of variables on the error rates and variables that cause on the biggest error are defined by this method. According to uncertainty analysis, rate of in-cylinder pressure error was obtained in regard of below principles.

Analysis of the data on common sense basis has many forms. One rule of thumb that could be used is that the error in the result is equal to maximum error in any parameter used to calculate the result. Another commonsense analysis would combine all the errors in the most detrimental way in order to determine the maximum error in the final result (J.P Holman, 1988).

A set of measurements is made and the uncertainty in each measurement may be expressed with the same odds. These measurements are then used to calculate some desired result of the experiments. To estimate the uncertainty in the calculated result on the basis of uncertainties uncertainty analysis was used in the primary measurements. The result R is a given function of the independent variables x_(1,) x_(2,) x_3……..,x_n Thus,

$$R = R(x_{1,} x_{2,} x_3 \ldots \ldots .., x_n) \tag{4.3}$$

Let w_R be the uncertainty in the result and $w_1, w_2, \ldots \ldots w_n$ be the uncertainties in the dependent variables. If the uncertainties in the dependent variables are all given with same odds, then the uncertainty in the result having these odds,

$$w_R = \left[\left(\frac{\partial R}{\partial x_1} w_1\right)^2 + \left(\frac{\partial R}{\partial x_2} w_2\right)^2 \ldots \ldots + \left(\frac{\partial R}{\partial x_n} w_n\right)^2\right]^{1/2} \tag{4.4}$$

3.8.1 Uncertainty analysis with using of empirical equations

In-cylinder pressure error analysis and ignition delay error analysis;

$$\tau = A\lambda^k P^{-n} exp(E/RT) \tag{4.5}$$

Depending on the upward equation $\tau = \tau(\lambda, P, T)$ and according to uncertainty analysis, ignition delay error ratio is (Gümüş, M. 2005);

$$w_R = \left[\left(\frac{1}{z}\sum_{i=1}^{z}\left(\frac{\partial\tau}{\partial\lambda}\right)_i w_{\lambda i}\right)^2 + \left(\frac{1}{z}\sum_{i=1}^{z}\left(\frac{\partial\tau}{\partial P}\right)_i w_{pi}\right)^2 + \left(\frac{1}{z}\left(\frac{\partial\tau}{\partial T}\right)_i w_{Ti}\right)^2\right]^{\frac{1}{2}} \tag{4.6}$$

In this equation;

w_λ= Excess Air Coefficient Measurement Error Ratio,

w_p= Pressure Determination Error Ratio,

w_T=Temperature Determination Error Ratio.

According to equation (4.5) ;

$$\frac{\partial\tau}{\partial\lambda} = kA\lambda^k P^{-n} exp(E/RT) \tag{4.7}$$

$$\frac{\partial\tau}{\partial P} = -nA\lambda^k P^{-n-1} exp(E/RT) \tag{4.8}$$

$$\frac{\partial\tau}{\partial T} = -\frac{E}{RT}\ln(A\lambda^k P^{-n})A\lambda^k P^{-n} exp(E/RT) \tag{4.9}$$

are determined.

Cylinder Pressure Level Error Analysis; (Gümüş, M. 2005)

$$L = l + pP + t\tau \tag{4.10}$$

Depending on the upward equation, $L = L(P, \tau)$ according to the uncertainty analysis, cylinder pressure level error ratio;

$$w_L = \left[\left(\frac{1}{z}\sum_{i=1}^{z}\frac{\partial L}{\partial P}w_p\right)^2 + \left(\frac{1}{z}\sum_{i=1}^{z}\frac{\partial L}{\partial\tau}w_\tau\right)^2 + \right]^{\frac{1}{2}} \tag{4.11}$$

In this equation;

w_p=Pressure Determination Error Ratio,

w_τ= Ignition Delay Error Ratio.

According the equation (4.10),

$$\frac{\partial L}{\partial P} = P \tag{4.12}$$

$$\frac{\partial L}{\partial \tau} = k \tag{4.13}$$

are determined.

The Percentages Deviation;

$$\sigma_i = \frac{y_{gi} - y_i}{y_{gi}} \times 100 \tag{4.14}$$

The Percentage Mean Deviation;

$$\sigma = \frac{1}{z} \sum_{i=1}^{z} \sigma_i \tag{4.15}$$

The Correlation Coefficient;

$$R = \left(1 - \frac{(z-1) \sum_{i=1}^{z} \left(y_{gi} - y_i\right)^2}{(z-F) \sum_{i=1}^{z} \left(y_{gi} - y_i\right)^2}\right)^{1/2} \tag{4.16}$$

z= Number of Experiment,

y_{gi}= Experimental Value,

y_i= Theoretical Value,

$y_i = \frac{1}{z} \sum_{i=1}^{z} y_{gi}$

F= y dependent variables is dependent on the variable number

For the P pressure value, percentage mean deviation is calculated as 0,87.

3.9 CFD Analysis

3.9.1 Zero-dimensional modeling

1D engine code is used to represent the flow and heat transfer in the components of the engine model by using 1D gas dynamics. The program works with a pre-processor, in this environment the model is built. The solver calculates the mass and energy flow through the different components and the results of the calculations are shown in a pre-processor.

Engine performance can be studied by analyzing the mass and energy flows between individual engine components and the heat and work transfers within each component.

Simulation of 1D flow involves the solution of the conservation equations; mass-, energy-and momentum, in the direction of the mean flow (Gamma Inc., 2004). Mass conservation is defined as the rate of change in mass within a subsystem which is equal to the sum of   and from the system dm/dt :

$$\dot{m}_{sub} = \sum_i \dot{m}_i - \sum_e \dot{m}_e \tag{3.1}$$

In 1D flow the mass flow rate, $\dot{m}_i$, is defined by:

$$\dot{m} = \rho AU \tag{3.2}$$

where ρ is the density, A the cross-sectional flow area and U the fluid velocity.

Energy conservation, the rate of change of energy in a subsystem is equal to the sum of the energy transfer of the system. The energy conservation can be written in the following from:

$$\frac{DE}{Dt} = \frac{DW}{Dt} + \frac{DQ}{Dt} \tag{3.3}$$

Energy conservation results :

$$\frac{d(me)}{dt} = p\frac{dv}{dt} + \sum_i \dot{m}_i H - \sum_e \dot{m}_e H - h_g A(T_{gas} - T_{wall}) \tag{3.4}$$

Where *e* is the internal energy, H the total enthalpy, h_g the heat transfer coefficient (Möller, C.,2006), T_{gas} and T_{wall} the temperature of the gas and wall respectively. The heat transfer from the internal fluids to the pipe and flow split walls is dependent on the heat transfer coefficient, the predicted fluid temperature and the internal wall temperature. The heat transfer coefficient, which is calculated every time step, is a function of fluid velocity, thermo physical properties and the wall surface roughness. The internal wall temperature is defined by the user.

$$h_g = \frac{1}{2} + C_f \rho U_{eff} Cp \Pr^{-\frac{2}{3}} \qquad (3.5)$$

In equation 3.5 C_f is the friction coefficient, U_{eff} the effective speed outside boundary layer, C_p the specific heat and Pr the Prandtl number.

The friction coefficient is related to the Reynolds number as follows (Gamma Inc., 2004)

$$\mathrm{Re} = \frac{\rho U_c L_c}{\eta} \qquad (3.6)$$

Where ρ is the density, U_c the characteristic speed, L the characteristic length and η the dynamic viscosity.

The friction coefficient for smooth walls is given by:

$$C_f = \frac{16}{Re_D} \qquad (3.7)$$

$$C_f = \frac{0.08}{Re_D{}^{0.25}} \qquad (3.8)$$

Where equation 3.7 is used in the region where $Re_D < 2000$ and equation 3.8 is used in de region where $Re_D > 4000$ with a linear transitional region in between. The Prandtl number is:

$$\Pr = \frac{\eta C_p}{\lambda} = \frac{\nu}{a} \qquad (3.9)$$

Where η is the dynamic viscosity, C_p the specific heat, λ the heat conduction coefficient, ν the kinematic viscosity and a the thermal diffusivity

In case that the wall surface is rough and the flow is not laminar, the value of the friction coefficient above is given by Nikuradse’s formula (J.Nikuradse, 1937):

$$C_{f\,(rough)} = \frac{0.25}{(2\log_{10}(\frac{1}{2}\frac{D}{h}) + 1.74)^2} \qquad (3.10)$$

Where D is the pipe diameter and h the roughness height. If necessary, the friction attribute in pipes and flow splits can be used to scale the calculated friction.

Momentum conservation, the net pressure forces and wall shear forces acting on a sub system are equal to the rate of change of momentum in the system (Gamma Inc., 2004):

$$\frac{\dot{m}}{dt} = \frac{dpA + \sum_{i} \dot{m}_i u + \sum_{e} \dot{m}_e u - 4C_f \frac{\rho u^2}{2} \frac{dxA}{D} - C_p \frac{1}{2} \rho u^2 A}{dx} \tag{3.11}$$

Where u is fluid velocity, C_f the friction loss coefficient, D the equivalent diameter, Cp the pressure loss coefficient and dx the element length. In order to obtain the correct pressure and friction loss coefficient the software uses empirical correlations to account for pipe curvature and surface roughness (Gamma Inc., 2004).

The pressure loss coefficient is defined by (Gamma Inc., 2004):

$$C_{pressure} = \frac{p_1 - p_2}{\frac{1}{2} \rho V_1^2} \tag{3.12}$$

Where p_1 is the inlet pressure, p_2 is the outlet pressure, ρ the density and V_1 the inlet velocity.

3.9.2 Time discretization

The entire sub-system is discredited into smaller volumes, where a flow split is represented by a single volume and pipes are divided into several volumes (Möller, C., 2006). Scalar properties, such as temperature, pressure, density etc. are assumed to be uniform for each volume. Accuracy improvements can be considered by choosing a finer discretization length. However, the discretization length is limited by the size of the time step. The time integration of the governing equations is explicit. An explicit method calculates the state of a system the following time step from the state of the system at the current time. If we put Y (t) in the current system state and Y (t +Δt) in the state at the later time (Δt is a small time step), then the explicit method is:

$$\mathrm{Y}(\mathrm{t} + \Delta\mathrm{t}) = \mathrm{F}(\mathrm{Y}(\mathrm{t})) \tag{3.13}$$

The time step during this integration is limited by the Courant condition (Courant et al., 1928.), which restricts the time step to be less than 0.8 of the time required for the pressure and flow to propagate across any discredited volume:

$$\frac{\Delta t}{\Delta x}(u + c) \leq 0.8 \tag{3.14}$$

Δx where Δt is the time step, Δx the discretized length, u the fluid velocity and c the speed of sound. Due to the link between discretization length and time step, a small discretization length will generally result in slow execution of the software. In the system a pipe is divided into many volumes depending on the choice of discretization length while a flow split is only represented by one single volume, the volumes are connected to others by boundaries. The equation for continuity, momentum and energy are solved simultaneously one dimensionally, therefore all the values across an area of the flow direction are averaged values. The scalar quantities (density, pressure, and energy) are calculated at the subsystem center. The vector quantities (mass flux and mass flux fractions) are calculated at the subsystem faces (boundaries). Using small time steps, the flow is reached by explicit time integration of the equations for continuity, momentum and energy (Gamma Inc., 2004).

3.9.3 Multidimensional modeling

In this study, multidimensional modeling refers to flow spray and combustion modeling in 3D, also known as Computational Fluid Dynamics (CFD).

The most general methodology to solve fluid flow is based on modeling of the Navier-Stokes equations. This methodology includes that the continuity equation, Navier-Stokes equations of momentum and the energy equation are discretized to solve a specific fluid problem limited in space and divided in a large number of computational cells (Strålin, P., 2007).

Spray injection and mixture formation modeling using CFD in IC engines is a multi-component multiphase problem that contains liquid fuel and the various species that participate in mixture formation. Commonly, the gas phase is treated in an Eulerian fashion, which means that the property of a fluid φ is computed in each cell, i.e. φ(x,y,z,t). The liquid phase is treated in a Lagrangian fashion, which means that an individual particle is traced and the property of this particle is calculated as it moves through the domain as a φ(t). The interaction between the phases is accounted for by source terms in the Eulerian gas phase. If an Eulerian perspective is considered for the liquid phase, the cell sizes in the computational domain need to have the same size as the injector orifice diameter due to the orifice is several orders of magnitude smaller than the dimensions of the cylinder. An Eulerian perspective would consequently be very computationally demanding.

3.9.3.1 Mathematical modeling

The equations of motion for the fluid phase can be solved turbulent flow. The equation for conservation of species mass fraction Yα is given in the following equation.

$$\frac{\partial}{\partial t}(\rho Y_\alpha)+\frac{\partial}{\partial x_i}(\rho Y_\alpha U_i)=\frac{\partial}{\partial x_j}\left(D\frac{Y_\alpha}{\partial x_j}\right)+\rho\dot{r}_\alpha+\dot{\rho}_s \tag{3.15}$$

The first term on the right hand side represents mass molecular diffusion, where D is the mass diffusion coefficient. The second term is the chemical mass source term and represents the net mass formation rate per unit volume through reaction of species α. Finally, the third term represents mass source evaporated from the liquid (Strålin, P., 2007).

Newton's second law states that the rate of change of momentum is equal to the sum of the forces acting on a fluid particle. These forces are divided into surface forces and body forces. The surface forces consist of pressure and viscous forces, whereas the body forces contain gravity, centrifugal, coriolis and electromagnetic forces. The momentum equation for the fluid mixture is:

$$\frac{\partial}{\partial t}(\rho U_i)+\frac{\partial}{\partial x_j}\left(\rho U_i U_j\right)=-\frac{\partial p}{\partial x_i}+\frac{\partial}{\partial x_j}\left\{\mu\left[\frac{\partial U_i}{\partial x_j}+\frac{\partial U_j}{\partial x_i}-\frac{2}{3}\frac{\partial U_k}{\partial x_k}\delta_{ij}\right]\right\} \tag{3.16}$$

On the right hand side, the first term represents the pressure gradient. The expression in the bracket in the second term is the molecular stress tensor, where δij is the unit tensor (i.e. if i=j then δij=1, if i≠j then δij=0). The third term indicates body force per volume unit. The last term represents rate of momentum gain or loss per unit volume due to the spray.

The internal energy equation can be formulated in many ways. In the equation that follows, it is expressed as the specific total energy (E), which is the sum of the specific internal energy and the specific kinetic energy.

$$\frac{\partial}{\partial t}(\rho E)+\frac{\partial}{\partial x_j}\left(\rho E U_j\right)=\frac{\partial p}{\partial t}+\frac{\partial}{\partial x_j}\left(\sigma_{ij} U_j\right)+\frac{\partial}{\partial x_j}\left(\lambda\frac{\partial T}{\partial x_j}\right)+\rho\dot{q}_g+\dot{Q}_s \quad (3.17)$$

The first term on the right hand side represents the temporal change of pressure. It is of importance where large pressure changes occur, such as internal combustion engines (8). The second term is work due to external forces, where σij is the stress tensor. The third term represents the heat influx through conduction. The fourth term is work due to body forces. The last term is a source term due to spray interaction.

The ideal gas relationships are used for the equation of state to relate internal energy to temperature:

$$p=R_0 T\sum_{\alpha}\frac{\rho_\alpha}{M_\alpha} \quad (3.18)$$

$$E(T)=\sum_{\alpha}\frac{\rho_\alpha}{\rho}E_\alpha(T) \quad (3.19)$$

$$E_\alpha(T)=h_\alpha(T)\frac{R_0}{M_\alpha}T \quad (3.20)$$

where R_0 is the universal gas constant, M_α is the molecular weight of species α, $E_\alpha(T)$ is the specific internal energy of species k at temperature T, and $h_\alpha(T)$ is the specific enthalpy of species k, taken from the JANAF thermodynamic tables (Strålin, P., 2007).

3.9.3.2 Turbulence models

Turbulent flow is present in most realistic flow situations. The flow is irregular, random and chaotic. In spite of the stochastic behavior of turbulence, the governing equations describe the fluid motion as long as the fluid can be considered as a continuum. However, the energy cascade process occurs over a wide length scale spectrum, which implies that the grid has to be extremely fine to resolve the smallest Kolmogorov eddies. Following the hypotheses of Kolmogorov, the energy spectrum contains three distinct ranges, namely the:

- Energy containing integral scales
- Inertial sub-range (cascade, energy transfer from the large to the small eddies)
- Dissipation at the small scales, namely in the viscous sub-range

A very fine resolution in time is also needed, since turbulent flow is always unsteady. Considering the complex and reactive flow that occurs in internal combustion engines, an exact solution of the flow within realistic timeframes is beyond the capacity of the largest computer today.

Reynolds averaging:

When turbulent flow is considered, it is advisable to express the instantaneous velocity by a mean and a fluctuating part. For instance, the velocity can then be expressed as follows

$$U_i = \langle U_i \rangle + u_i \quad (3.21)$$

The mean component <Ui> can be calculated in three different ways: time average ($\overline{U_i}$), density average ($\overline{U_i}$) and ensemble average ($\hat{U_i}$) according to the following equations.

$$\overline{U_i} = \lim_{\tau \to \infty} \frac{1}{\tau} \int_0^{\tau} U_i(x_i, t)dt \quad (3.22)$$

$$\rho\overline{U_i} = \lim_{\tau \to \infty} \frac{1}{\tau} \int_0^{\tau} \rho U_i(x_i, t)dt \quad (3.23)$$

$$\hat{U}_i = \lim_{n_e \to \infty} \frac{1}{n_e} \sum_{i=1}^{n_e} U_i(x_i, t) \quad (3.24)$$

The density average is preferable to use in reacting flows (8). The density averaged mean and fluctuating value are used in the governing equations, and the governing equations are averaged to filter out small scale fluctuations in order to obtain equations which describe behavior of the mean field variables. Averaging of the non-linear terms generates additional statistical correlations and there are more unknown variables than available equations. This is known as the closure problem. One of the unknown terms in the governing equations is the Reynold stress tensor.

$$\tau_{ij} = -\rho \overline{u_i u_j} \tag{3.25}$$

The closure problem could be approached by solving the Reynold stress tensor. Reynold Stress Models (RSM) refers to models which consist of transport equations to solve the Reynold stress tensor. A more widely used approach to handle the closure problem is the application of the Boussinesq assumption. This hypothesis states that the Reynold stresses are linked to mean rates of deformation by introducing a turbulent viscosity (μt).

$$\tau_{ij} = -\rho \overline{u_i u_j} = \mu_t \left(\frac{\partial \tilde{U}_i}{\partial x_j} + \frac{\partial \tilde{U}_j}{\partial x_i}\right) \tag{3.26}$$

The turbulent viscosity can, on basis of dimensional analysis, be expressed as the product of the characteristic turbulent length scale (L) and velocity scale (U).

$$\nu_t = \frac{\mu_t}{\rho} \propto L \cdot U \tag{3.27}$$

The velocity scale is obtained from the expression for turbulent intensity.

$$U = k^{1/2} = \sqrt{\frac{1}{2}(\overline{u_1^2} + \overline{u_2^2} + \overline{u_3^2})} \tag{3.28}$$

The remaining part of solving the turbulent viscosity is determination of the length scale, which depends on the turbulence model that is used.

Two equation models are the most wide-spread models used in averaged Navies-Stokes simulation. By avoiding the problem inherent to the former models, namely requiring the specification of a flow-dependent length scale, they provide both a length and a time-scale by solving an additional equation.

The simplest one is the standard k-ε model, which Launder and Spalding propose. It is widely used in turbulence simulations because of its general applicability, robustness and economy. The two transport equations for the kinetic energy and dissipation rate are solved to form a characteristic scale for both turbulent velocity and length. These scales represent the turbulent viscosity.

The RNG k-ε turbulence model is derived from the Navier-Stokes equations using a mathematical technique called "renormalization group" (RNG) methods. The analytical derivation results in a model with different constants than those in the standard k-ε model. In addition, additional terms and functions will appear in the transport equations for the kinetic energy and the dissipation that will be discussed in the see Appendix A.

The last turbulence model that will be discussed is the k-ω model. This model is based on the Wilcox k-ω model (Wilcox, 1993). It incorporates modifications for low-Reynolds number effects, compressibility and shear flow spreading. The Wilcox model predicts free shear flow spreading rates that are in close agreement with measurements for far wakes, mixing layers and different types of jets (Star-CD, 2006).

3.9.3.3 Spray modeling

There are numerous additional models for spray injection, spray breakup, droplet collision, evaporation, wall impingement, ignition, combustion etc. CFD code used contains built-in capabilities for modeling the behavior of special-purpose atomizers (nozzles) used in fuel-injected internal combustion engines. The injection process being modeled includes the flow in the nozzle hole (most importantly its exit velocity) and atomization. The latter gives rise to a fuel droplet spray represented by a set of computational parcels, each containing a number of droplets with the same properties (velocity, size, temperature, density, etc.). These properties are calculated on the basis of various atomization models whose characteristics and assumptions are given below. The histories of the computational parcels are obtained from the Lagrangian conservation equations of mass, momentum, and energy in the normal way.

Interaction of the fuel with air was modeled by using Lagrangian approach in the simulations. The entrained particle phase is modeled using the following set of ordinary differential equations for mass, momentum and energy that characterize the change in particle properties along particle trajectory as it moves through the gas continuum (Yilmaz, M, 2012):

Continuity Equation:

$$\frac{dm_d}{dt} = -A_s F_m \quad (3.29)$$

where is A_s the droplet surface area and F_m is mass transfer rate per unit surface area.

Conservation of Momentum:

$$m_d \frac{du_d}{dt} = F_{dr} + F_p + F_{am} + F_b \quad (3.30)$$

Here, F_{dr} is drag force which depends on Reynolds number and cross-sectional area of the droplet; F_p is pressure force; F_{am} is virtual mass force; and F_b implies body forces (gravity, magnetic forces, etc.).

Conservation of Energy:

$$m_d c_{p,d} \frac{dT_d}{dt} = -A_s \dot{q}_d'' + h_{fg} \frac{dm_d}{dt} \quad (3.31)$$

$\dot{q}''$ shows the heat transfer rate per unit surface area of the droplet and h_{fg} is the latent heat of phase change.

Atomization Model:

Huh’s (see Appendix B) model was used as an atomization model in the simulations. This model is based on the premise that the two most important phenomenas in spray atomization are the gas inertia and the internal turbulence stresses generated in the nozzle. This situation can be introduced in two steps:

First one is the turbulence generated in the nozzle hole produces initial perturbations on the jet surface when it exits the hole.

The second is the perturbations have reached a certain level; they grow exponentially due to the pressure forces induced through interaction with the surrounding gas, until these perturbations become separated from the jet surface as droplets.

The model presumes the initial perturbations from an analysis of the flow through the hole and then uses established wave growth theory, coupled with other hypotheses, to represent the atomization process.

The average turbulent kinetic energy, k_a and its dissipation rate at the hole exit can be shown as follows, according to Huh's atomization model:

$$k_a = \frac{U^2}{8\frac{L}{D}}\left(\frac{1}{{c_d}^2} - K_c - 1\right)$$
$$\varepsilon_a = \frac{K_\varepsilon U^3}{2L}\left(\frac{1}{{c_d}^2} - K_c - 1\right) \tag{3.32}$$

where U is the average injection velocity over the time period of injection, L and K_c are the hole length and form loss coefficient, K_ε is an empirical coefficient and c_d is the nozzle's discharge coefficient.

The initial values of the turbulence length and time scales can be shown as:

$$\left[L_t^0 = C_\mu^{0.75}\frac{{k_a}^{1.5}}{\varepsilon_a}; \tau_t^0 = C_\mu^{0.75}\frac{k_a}{\varepsilon_a}\right] \tag{3.33}$$

where C_μ is the coefficient of $k-\varepsilon$ model. The time dependent values of the turbulence length and time scales can be shown in following relations:

$$L_t(t) = L_t^0\left(1 + C_{a1}\frac{t}{\tau_t^0}\right)^{C_{a2}}$$
$$\tau_t(t) = \tau_t^0\left(1 + C_{a1}\frac{t}{\tau_t^0}\right) \tag{3.34}$$

where C_{a1} and C_{a2} are the model coefficients.

The second step of the atomization model, so-called "surface wave growth", is the interaction between discrete and continuous phases. Wave growth rate $\mathrm{Re}(\omega)$ increases the amplitude of the perturbation, until the perturbations becomes detached from the surface of the liquid jet. These detached perturbations create the secondary droplets.

Droplet Break-up Model:

The fuel particles may become unstable due to the interfacial forces acting on their surfaces during the relative motion according to the continuous phase. This problem was solved by using the break-up model of Reitz and Diwakar.

Droplet break-up due to aerodynamic forces exists in two modes in Reitz and Diwakar model. First one is 'Bag break-up', in which the non-uniform pressure field around the droplet causes it to expand in the low-pressure wake region and eventually disintegrate when surface tension forces are overcome. The other one is 'Stripping break-up', which is a process in which liquid is sheared or stripped from the droplet surface.

In each case, theoretical studies have provided a criterion for the onset of break-up and concurrently an estimate of the stable droplet diameter, $D_{d,stable}$, and the characteristic time scale of the break-up process. This allows the break-up rate to be calculated from the following equation:

$$\frac{dD_d}{dt} = -\frac{D_d - D_{d,stable}}{\tau_b} \qquad (3.35)$$

where D_d is the instantaneous droplet diameter. The criteria and time scales are as follows:

Bag break-up:

Here, instability is determined by a critical value of the Weber number, We, thus:

$$We = \frac{\rho\left|u - u_d\right|}{2\sigma_d} \geq C_{b1} \qquad (3.36)$$

where σ_d is the surface tension coefficient and C_{b1} is an empirical coefficient which gets a value between 3.6 and 8.4. The droplets must satisfy the equation above to have a stable condition according to the Bag Break-up Model of Reitz and Diwakar (Yilmaz, M., 2012).

Stripping break-up:

The criterion of this regime is as follows:

$$\frac{We}{\sqrt{\mathrm{Re}_d}} \geq C_{s1} = 0.5 \quad (3.37)$$

Collision Model:

The collision model of O'Rourke was used for inter-droplet collisions in the computations. And also it was improved with a speed-up algorithm of Schmidt and Rutland. Moreover, this model includes a coalescence timescale highlighted by Aamir and Watkins. The constraints noted by Nordin, and a cell clustering mechanism that allows parcels in neighboring cells to collide.

Evaporating Model:

This model provides to explain the effects of the change on discrete phase, when the droplet temperature reaches the boiling or critical temperature. The following conditions are considered:

1. $T_d \geq T_c$

Here, Tc is the critical temperature, i.e. the temperature at which

$$\left(\frac{\partial \rho}{\partial V}\right)_{T_c} = 0 \quad (3.38)$$

2. $T_d \geq T_b(p_t)$

Here, Tb is the boiling temperature at the ambient pressure. The boiling temperature is defined by the temperature at which the pressure of saturation, p_s, balances the gas pressure.

For the first condition, the droplet evaporates suddenly. Moreover, if the second condition satisfied, then mass transfer rate can be introduced as follows:

$$\frac{dm_d}{dt} = \frac{-2\pi k D_d}{c_p}(1 + 0.23\,\mathrm{Re}^{0.5})\ln\left[1 + \frac{c_p(T - T_d)}{h_{fg}}\right] \quad (3.39)$$

where k is the conductivity and c_p the specific heat of the mixture. During the boiling droplet temperature is constant. Thence, the rate of the heat transfer from droplet to the continuous phase can be introduced as follows:

$$\dot{q}_g = -h_{fg} \frac{dm_d}{dt} \tag{3.40}$$

Spray Impingement Model:

Bai's Spray impingement model was used in the simulations as a wall-interaction model for discrete phase. This model was formulated within the framework of the Lagrangian model, which is based on literature findings and mass, momentum and energy conservation constraints. A random procedure is customized to determine some of the droplet post-impingement quantities to explain the chaotic structure of the impingement process. This allows secondary droplets which are developed from a primary droplet splash to have a distribution of sizes and velocities. The complete model formulation distinguished between dry and wetted wall impingement and is applicable to wall temperatures that are less than the liquid boiling or critical temperature.

In this research work, besides the diesel liquid fuel injector, another CBG fuel injector which represents the experimental CBG injector is defined on the intake port system by using cylindrical coordinate system.

3.9.3.4 Combustion and emission modeling

Wiebe function for 1D approximation and Extended Coherent Flame Model (ECFM) for 3D CFD solution are used to carry out Combustion modeling.

The Wiebe function can be expressed follows.

$$x_b = 1 - \exp(-a(\frac{\theta - \theta_0}{\Delta\theta})^{m+1}) \tag{3.41}$$

Where xb is the mass fraction burned, θ is the crank angle, θ0 , which fixes the timing is the crank angle at the start of combustion, a and Δθ are adjustable constants that determine the combustion duration and m is an adjustable parameter that fixes the shape of the combustion progress curve.

ECFM (Duclos et. al., 1999) and the 3-Zone ECFM (ECFM-3Z) broadly belong to the Coherent Flame Model (CFM) family, but are extended to non-homogeneous turbulent premixed and unpremixed (diffusion) combustion.

In the ECFM3Z combustion model, the state of the gases mixture is defined in the 2D space. It is simultaneously described in terms of mixing and progress of reaction as schematically represented in Fig. 3.14 (Colin and Benkenida, 2004).

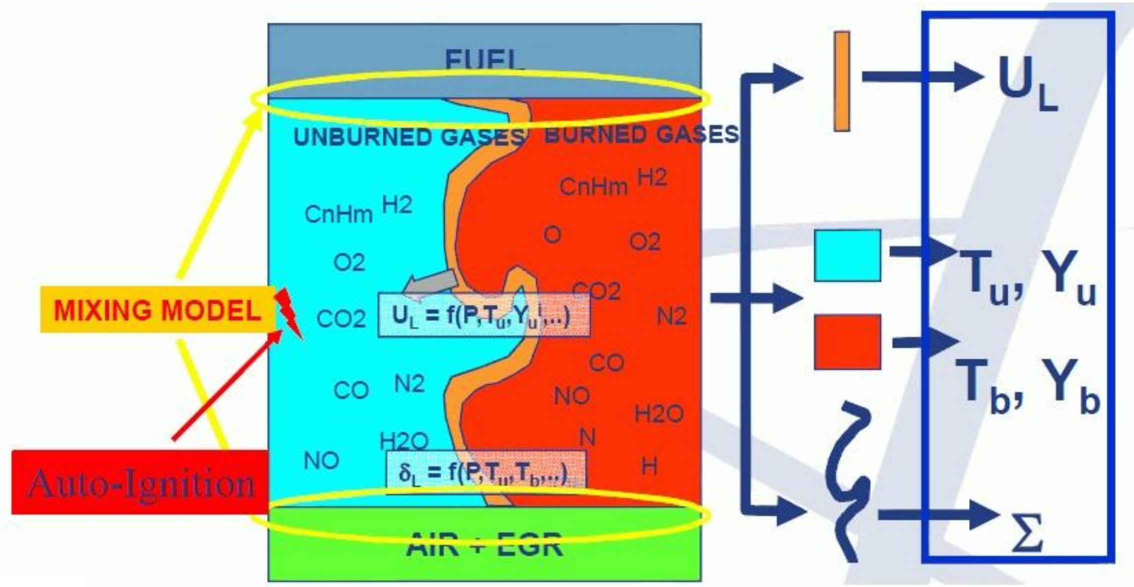

Figure 3.14. Schematic of the ECFM3Z model computational cell (Star Methodology).

The differential equations are formulated in a density-weighted ensemble-averaged frame to facilitate the use of mathematical models of the turbulent transport and combustion processes.

There are two recommended models for Diesel combustion, the Magnussen model and a laminar-and-turbulent characteristic-time model.

Magnussen et al. (Star-CD, 2006) presented a model, based on the eddy break-up (EBU) concept, which relates the rate of combustion to the rate of dissipation of eddies and expresses the rate of reaction by the mean mass fraction of a reacting species, the turbulence kinetic energy and the rate of dissipation of this energy (see previous section).

Abraham et al. (Star-CD, 2006) presented a laminar-and-turbulent characteristic-time combustion model for spark ignition engines. Patterson et al. (Star-CD, 2006) extended this concept to model Diesel engines. In Diesel engines, a significant portion of the combustion is thought to be mixing controlled, so Magnussen's model presented earlier should be able to describe the rate of combustion. However, it is recognized (Star-CD, 2006) that the initiation of combustion relies on laminar chemistry. Turbulence starts to have an influence only after combustion events have already been observed. Eventually, combustion will be dominated by turbulent mixing effects in the regions of $\Delta l << \Delta t$; where Δl is the laminar (or chemical) time scale and Δt is the turbulence (or mixing) time scale.

The laminar time scale, however, is not negligible near the injector regions (where the high injection velocity makes the turbulence time scale very small), in shear layers generated by the fuel sprays and in near-wall regions. For this reason, the model described below has been made available.

According to Magnussen et al.

$$R_f = \frac{\rho A}{\tau_t} \min\left(Y_f, \frac{Y_{O_2}}{r_f}, \frac{BY_p}{1+r_f} \right) \quad (\text{kg m}^{-3}\ \text{s}^{-1}) \tag{3.42}$$

where $\tau_t = k/\varepsilon$, the turbulence time scale.

As mentioned in the previous section, Patterson et al. (Star-CD, 2006) recognised that the laminar time scale cannot be assumed to be negligible in a number of important regions of the Diesel engine combustion chamber. It is for this reason that the turbulence time scale in Equation (3-1) is now replaced by a characteristic time τ_c to give:

$$R_f = \frac{\rho A}{\tau_c} \min\left(Y_f, \frac{Y_{O_2}}{r_f}, \frac{BY_p}{1+r_f} \right) \tag{3.43}$$

where

$$\tau_c = \tau_l + f \tau_t \tag{3.44}$$

A CFD simulation of an internal combustion engine should give, as far as possible, a comprehensive insight into the wide-ranging physics of the device, such as turbulent mixing between fuel and air, the ignition and combustion chemistry, knock occurrence, formation and destruction of pollutants like NOx and soot, the influence of exhaust gas recirculation (EGR) on the emissions, and the power output and efficiency. CFD codes offer a set of models to simulate the above processes.

The Extended Coherent Flame Model (ECFM) and the 3-Zone ECFM (ECFM-3Z) (Star-CD, 2006) broadly belong to the Coherent Flame Model (CFM) family, details of which are given in "The CFM-ITNFS model" (Star-CD, 2006), but are extended to non-homogeneous turbulent premixed and unpremixed (diffusion) combustion.

Generally speaking, ECFM-3Z can be used for all types of combustion regime whereas ECFM, being a subset of ECFM-3Z, is mostly suitable for non-homogeneous turbulent premixed combustion with spark ignition. As part of these models, two options are provided for modeling spark ignition:

A spark ignition model employing a correlation to account for the delay between spark and flame kernel appearance.

A more complex model (AKTIM) where the physics of the spark are modeled in more detail (StarCD Methodology, 2009).

On the subject of auto ignition, two options are also provided, a simple model and a double-delay model for more accurate predictions, especially with engine simulations.

For emission simulation, the 3-step Zeldovich model is available for NOx and three options are provided for soot (Star-CD, 2006).

The Mauss model based on a pre-computed soot source-term library and the PSDF model of moments, where the soot particle size distribution are transported. The moment source terms are calculated using the soot flamelet library.

3.9.3.5 Boundary conditions

Commercial CFD code offers a number of options for boundary conditions. In addition to inflow, outflow, and pressure boundaries, there are also impermeable wall and baffle surfaces, non-reflecting pressure and stagnation conditions, slip surface, symmetry plane, cyclic boundaries, transmissive free stream, transient transmissive, Riemann, prescribed temperature/mass fraction, prescribed flux, prescribed surface reaction. There are, by turn, several types of rigid walls depending on velocity and temperature boundary conditions. The velocity boundary conditions on rigid walls can be free slip, no slip, or turbulent law-of-the-wall. Temperature boundary condition options are adiabatic walls and fixed temperature walls. In engine calculations, one ordinarily uses turbulent law-of-the-wall velocity conditions with fixed temperature walls. Under this boundary condition, the normal gas velocity is set equal to the normal wall velocity, while the tangential components are determined by matching to a logarithmic profile. The heat flux to the walls is calculated using a modified Reynolds analogy formula.

3.9.3.6 Numerical scheme

Commercial CFD code discretizes the governing equations listed in the previous section both in space and time. The discretization is made possible through finite volume.

In temporal differencing, computational cells move along with the fluid in a Lagrangian fashion. Then the flow is frozen and rezoned, or remapped onto a new computational mesh. The interior vertices are then re-distributed to form a valid mesh that matches the desired geometry. The spatial differencing is based on the Arbitrary Lagrangian Eulerian (ALE) method that can accommodate a wide range of moving-boundary problems, such as the flow in a reciprocating-engine combustion chamber with moving piston and valves.

The spatial region of interest is divided into small cells. These cells make up the computational mesh, with respect to which spatial differences are formed. In addition to the regular cells, auxiliary cells, named momentum cells, are used for differencing the momentum equations. In the ALE method, no interpolation is required when determining vertex motion in the Lagrangian phase of calculation. In the finite volume approximations of commercial CFD code, velocities are located at the cell vertices, whereas thermodynamic properties are located at the cell centers. Quantities needed at points where they are not fundamentally located are obtained by averaging neighboring values.

Spatial differences are performed by integrating over the volume of a cell. Volume integrals of gradient or divergence terms are usually converted to surface are integrals using the divergence theorem. During the phase where the computational cells move along with the fluid, the solution procedure is patterned after the PISO method, with the individual equations solved using the conjugate gradient method.

For the solution of the flow field, the broadly established CFD solver is employed. Used CFD code is a finite volume solver for hexa and tetrahedral cells, offering a choice of RANS and LES turbulence models and which is capable of treating two-phase flow physics with atomization and combustion. A number of user coding interfacing options allow replacement of sub-models and hence coupling of CFD solver with other codes. Integration of the flow field by CFD code uses a time-step of the order of 1.0E-6 s, which also denotes how often the aerodynamics (i.e. velocities, diffusivity, mixture fraction field, scalar dissipation rate, pressure, and pressure rate of change). The exact values for the time-steps are dependent on the set-up and will be discussed further in the results.

Turbulence is modeled using the RNG k-ε model with standard model constants. Concerning spray modeling and depending on the set-up, both the Huh and the Reitz-Diwakar atomization model have been used. For the secondary break-up, the Reitz-Diwakar model is employed with default model constants in all cases; droplets impinging on solid walls are modeled with a splashing model (Yilmaz, M., 2009).

Thermo-physical properties of the droplets are defined as functions of temperature by a user-supplied subroutine. Enthalpy is solved in the form of the total enthalpy; hence, no transport equations for the mean species mass fractions are required in the flow-field solver.

3.9.4 Simulation of gas exchange processes

The simulation of the gas exchanges processes is performed using commercial CFD code. Commercial CFD code is used to simulate the exhaust, intake, compression and expansion processes. The calculation starts a few CAD before Intake Valve Opening (IVO).

3.9.4.1 Computational grid

The engine that is modeled is a commercial four-cylinder 1.5lt light-duty diesel real engine. The geometrical specifications of the engine, as well as the engine's original valve timings are summarized before chapter. The computational grid is shown in Fig. 3.15. It consists of about 700,000 cells at TDC. As it can be seen, the grid resolution is not adequate to capture the details of the boundary layer and the top-land crevice of the piston. This prevents the prediction of the low temperature regions in the cylinder, which can account for 5-10% of the total mass in the cylinder and are the main contributors to reduced combustion efficiency and increased unburned hydrocarbon emissions. This problem could be overcome by increasing the grid size; however this would increase dramatically the computational time. A finer grid could include the top-land crevice. In addition, a crevice model could be introduced in commercial CFD software, in order to simulate flow in the crevices and blowby. Nevertheless, even though the low temperature regions are not captured well commercial CFD software, can still provide reasonable predictions for the bulk temperature in the cylinder and the overall temperature and composition distributions.

All the calculations are performed by means of the CFD code. The moving mesh (i.e. piston and intake valves regions) is provided be CFD code's tool designed to facilitate transient analyses of internal combustion engines. CFD solver pre-processor creates the fixed mesh (intake ports). The computational grid is made up of cells of mainly hexahedral shape, whose number ranges from approximately 700.000 at TDC up to over 1.700.000 at BDC for fine mesh.

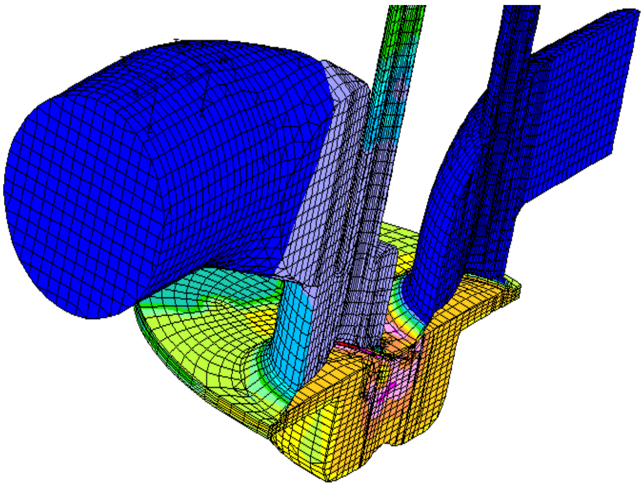

Figure 3.15. Example of volume mesh.

3.9.4.2 Initial conditions

In order to initialize the run, the pressure and the temperature in the cylinder at the start of the calculation need to be estimated. The latter is assumed to be uniform and the gas in the cylinder consists of complete combustion products. The temperatures of the two ports are also assumed to be uniform. The initial pressure, temperature and composition in the intake port are specified according to the prescribed intake conditions. The pressure in the exhaust port is prescribed as well, while the temperature is an estimation of the average exhaust gas temperature. Finally the composition of the gas in the exhaust port is the same as that in the cylinder (complete combustion products). Having homogeneous initial conditions, although not realistic, is not a significant problem, since there is enough time to form a more complex and realistic flow field in the cylinder near the end of compression, when the information about the detailed temperature and composition distributions will be used in the chemistry calculations.

3.9.4.3 Boundary conditions

All the walls are treated with the turbulent law-of-the-wall. The heat fluxes to the walls are calculated assuming constant wall temperatures. The prescribed boundary condition at the inlet of the intake port is that of "pressure inflow", while that at the outlet of the exhaust port is "pressure outflow".

3.9.5 Overall cycle simulation

The modeled engine is supposed to have 4 valves per cylinder (2 intake valves and 2 exhaust ones). This system is assumed to have no limits due to design problems (there is no check if valve can crash with piston, etc.). The maximum valve lift remains constant.

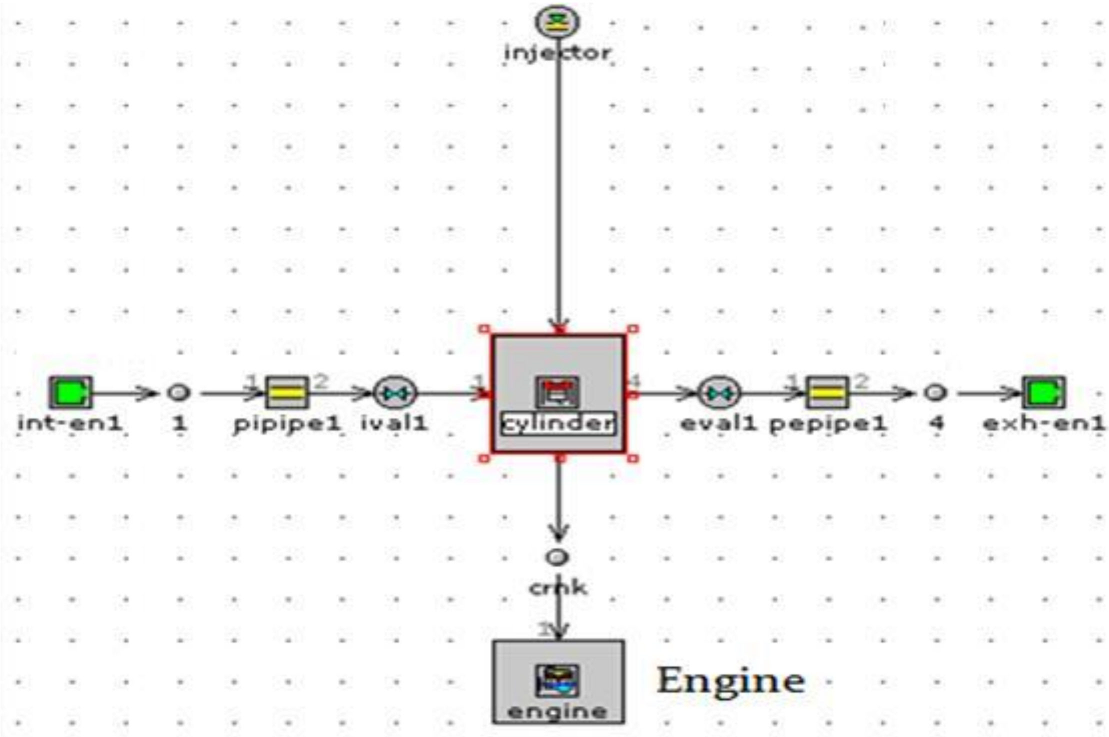

Figure 3.16. Base engine model in 1D simulation.

Configuration and lengths of both intake and exhaust manifold are based on a real engine, no additional pressure losses due to wall roughness were used (pressure losses were computed using dependency on Reynolds number only). Valve discharged coefficients and valve lifts (for both valves) were provided by IC engine producer. No in-cylinder pressure indication data were available that is why rate-of-heat release and wall temperatures were estimated using experience with similar engines. The same applies to the model of mechanical losses. No knocking was taken into account and for each engine speed. Dependency of combustion start and duration on engine speed only is used.

Table 3.11. 1D simulation inputs.

Bore (mm)	76.0
Stroke (mm)	80.5
Connecting Rod Length (mm)	131.2
Piston Pin Offset (mm)	0.00
Displacement/Cylinder (cc)	365.25
Total Displacement (liter)	1.461
Number of Cylinders	1
Compression Ratio	18.25
Bore/Stroke	0.894

3.9.6 Cold flow simulation

This present work describes a detailed three-dimensional cold flow study is conducted on piston engine geometry with a mesh density of 0.65 million cells to simulate the engine cold flow condition. CFD simulation is conducted over two complete motoring cycles involving intake, compression and expansion and exhaust processes on bowl in-piston engine geometry at compression ratio (CR), 18.25. Data on the turbulence parameters and reverse squish velocities (referred as the reverse squish period at the beginning of the expansion process) derived from the above study have been used as input in the zero dimensional modeling.

3.9.7 Spray simulation

Spray penetration, droplet number, and particle size are some of the key parameters for the fuel atomization and mixing process. ‘All the atomization models in CFD code utilize physical atomizer parameters, such as orifice diameter and mass flow rate, to calculate initial droplet size, velocity, and position. The atomizer model use stochastic trajectory selection and staggering to attain a random distribution (Star-CD, 2006).

The calculations are performed using CFD code, a general-purpose finite volume CFD code that uses the PISO algorithm (a multi-corrector variant of SIMPLE). CFD code incorporates a variety of physical models for sprays, turbulence, and combustion chemistry. Sprays are treated via a Lagrangian approach with sub-models for break-up, turbulent dispersion, and collision. In the analyses to be presented, initial spray distributions are formulated to match available experimental data, although CFD code also incorporates semi-empirical models to create distributions from available injector geometry information. The standard k-ϵ model with wall functions is used to describe turbulence. The mesh generation process, including the description of the piston and valve motion, was automated using ICE.

When modeling a multi-component fuel with CFD code, two areas of the analysis need modification, sprays and combustion. The spray module of CFD code is already capable of handling multi-component fuels to a certain degree. As a standard feature, droplets can be composed of up to ten components, each with different specific heat, heat of vaporization, and vapor pressure characteristics and each capable of vaporizing to a different gas phase species. Other liquid parameters (density, surface tension, and viscosity) remain properties of the droplet (Yilmaz, M., 2009).

Concerning spray modeling, Huh-Gosman (Huh and Gosman, 1991) atomization model is used to represent the fuel jet primary break-up at the nozzle exit; the model is based on the assumption that atomization is governed by two main mechanisms: the gas inertia and the internal turbulent stresses generated within the nozzle. The model estimates the initial perturbations from the analysis of the flow through the hole and then uses established wave growth theory to evaluate the atomization process.

As far as secondary break-up is concerned, Reitz- Diwakar model (Reitz and Diwakar, 1986, 1987) is adopted. The model is based on the assumption that droplets may become unstable under the action of the interfacial forces generated by their motion relative to the continuous phase. According to the model, droplets break-up under the effect of aerodynamic forces, can be subdivided in “bag breakup” and “stripping break-up”. The first depends on the non-uniform pressure surrounding the droplets, while the latter is a process in which liquid is stripped from the droplet surface by the continuous phase. These breakup regimes change according to the Weber number. Additional sub-models are used for the spray simulation, accounting for both droplet-droplet interaction and droplets-wall impingement. The former characterizes droplets history by three kind of events: coalescence, separation and bouncing, and is based on the model proposed by O’Rourke (1981); the latter, based on the model proposed by Bai and Gosman (1995), recognizes different regimes (stick, spread, rebound and splash) according to: incident droplet velocity relative to the wall, incidence angle, droplet size and properties as well as wall temperature, surface roughness, film thickness and near-wall gas conditions. Turbulent dispersion and condensation are activated, while collision is deactivated.

3.9.8 Combustion & emissions simulation

3.9.8.1 Single fuel combustion

Combustion models can be categorized into two main groups based on the assumptions on the reaction kinetics. Reactions can either be assumed as infinitely fast compared to e.g. species mixing, or the time scale of the mixing process. The simple approach is to assume infinitely fast chemistry. Species mixing is the oldest approach, and it is still in wide use today.

The Eddy Break - Up model (EBU) was developed by Spalding (1971) and is based on the assumption that the chemistry is much faster than the mixing and, thus the rate controlling phenomena is the turbulent mixing.

The Eddy Dissipation Model (EDM) is a variant of the EBU model developed for non-premixed combustion by Magnussen and Hjertager (1977). The mean chemical source term is computed in a similar manner to EBU, except for the fact that the reaction rate is limited by a deficient species (i.e., fuel, oxidizer or combustion products) (Veynante and Vervisch, 2002). The model has been employed in turbulent combustion simulations with some degree of success (Byggstoy and Magnussen, 1988). EDM assume that reaction rates are controlled by turbulence thereby avoiding the use of computationally expensive Arrhenius kinetic calculations. In non-premixed or diffusion flames, turbulence slowly convects and mixes fuel with oxidizer into the reaction zones where they burnt up quickly.

The Probability Density Function (PDF) transport equation model is based on the derivation of a joint PDF transport equation for the velocity and the reactive scalars as well as, in some approaches, their gradients or other quantities considered of interest. To the date, several models in this category have been proposed: Pope (1990) proposed a joint PDF of velocity; viscous dissipation and reactive species, Dopazo (1994) used a joint pdf of velocity, velocity gradient, reactive scalars and their gradients. The method has the advantage that is valid for both premixed and non-premixed combustion but its accuracy is strongly dependent on the models employed for the remaining unclosed terms.

Coherent flame models (CFM) were originally developed for premixed combustion and view the flame front as a thin interface, separating the fresh mixture from the burnt gases. Based on the assumption, that the combustion occurs in premixed mode, even for very lean or rich mixtures, the model was investigated for highly stratified combustion regimes in und subsequently successfully applied to a direct injected (DI) spark ignited (SI) engine (Duclos et. al., 1999). Modifications originally proposed by Duclos, and Zolver (1998), included a formulation for the mean reaction progress variable tailored to include the effects of stratification. For stratified charges, as encountered in DI engines, transported conserved scalar markers were introduced for the unburned gas and the partially/fully burnt mixture (Hélie and Trouvé, 2000). The ECFM-3Z model, described in detail by Colin and Benkenida (2004), extends this approach further to non-premixed combustion regimes by introducing a three zone concept based on conditioning with the mixture fraction.

The soot formation reaction model uses an Arrhenius rate. The soot oxidation assumes two different reactive sites and the resulting oxidation rate is a function of soot properties (ρ_s: density, D_s: average diameter) and other kinetic parameters. The predicted soot emission is a result of the competition between formation and oxidation reactions.

Net soot mass = Soot mass formed – Soot mass oxidized

$$= A_{sf} MP^{0.5} \exp\left(-\frac{E}{RT}\right) - \frac{6MW}{\rho_s D_s} M_s R_{total} \tag{3.42}$$

The NOx model uses the extended Zeldovich NO mechanism where, basically, there are no adjustable model constants. However, a scaling factor is provided for model calibration that accounts for differences in the computed NOx and measured NOx level based on different experimental techniques. Note that the predicted NOx is strongly related to the in-cylinder thermal field.

Net NO x mass = Predicted NOx mass x Scaling factor

3.9.8.2 Dual fuel combustion modeling

ECFM-3Z combustion model developed for all combustion regimes and it is used in CBG-diesel dual fuel modeling as for single fuel combustion analysis.

The ECFM-3Z model (StarCD methodology, 2009) is a general-purpose combustion model capable of simulating the complex mechanisms of turbulent mixing, flame propagation, diffusion combustion and pollutant emission that characterize modern internal combustion engines. It can also be used for in-cylinder analysis in a multi-injection environment and for multi-cycle simulations. The model's structure, illustrated in Figure 3.14, consists of four major components:

1. Mixing model

2. Flame propagation model

3. Post-flame and emissions model

4. Spark ignition and auto ignition/knock models.

In dual fuel combustion modeling, main fuel CBG and pilot fuel diesel were defined as a leading reactant. To define the leading reactants, user defined code were written to activate ECFM-3Z dual fuel library. In dual fuel combustion cases, CBG fuel has lower heating value as a 26170kj/kg with respect to diesel fuel 42500kj/kg.

Diesel and CBG fuels which used in single and dual fuel combustions were given in Eq. 3.43.

$$\begin{aligned} &C12H26 + 18.5O2 => 12CO2 + 13H2O \\ &0.65CH4 + 0.3CO2 + 0.05H2 + 1.325O2 => 0.95CO2 + 1.35H2O \end{aligned} \tag{3.43}$$

4 RESULTS AND DISCUSSIONS

4.1 Real Engine Results

CBG-Diesel dual fuel experimental studies on 1.5 CI engine were given below figures.

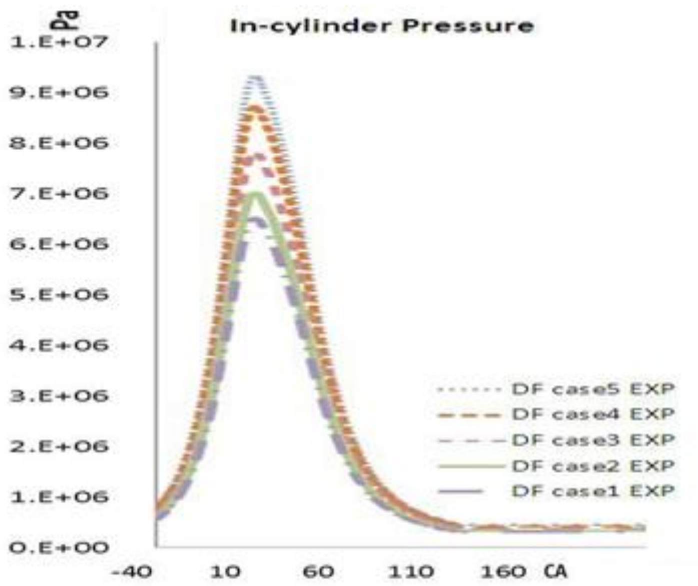

Figure 4.1. Experimental in-cylinder pressure at different engine loads.

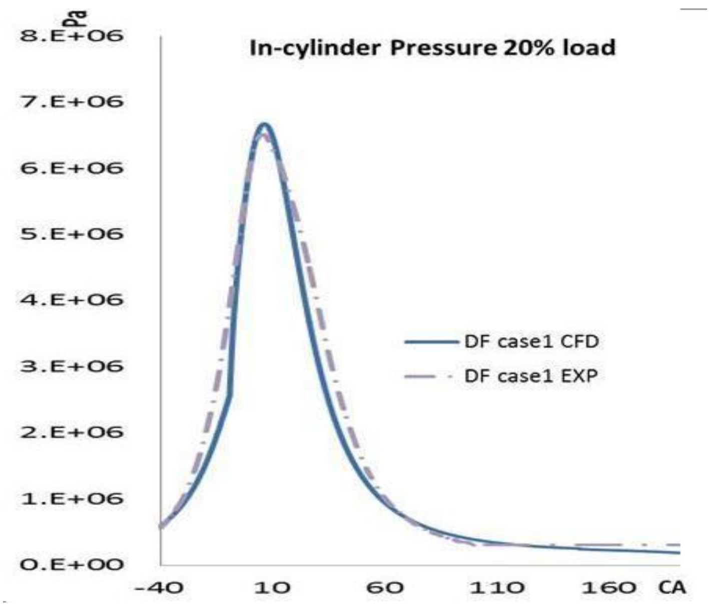

Figure 4.2. CFD and experimental pressure value at 20% engine load.

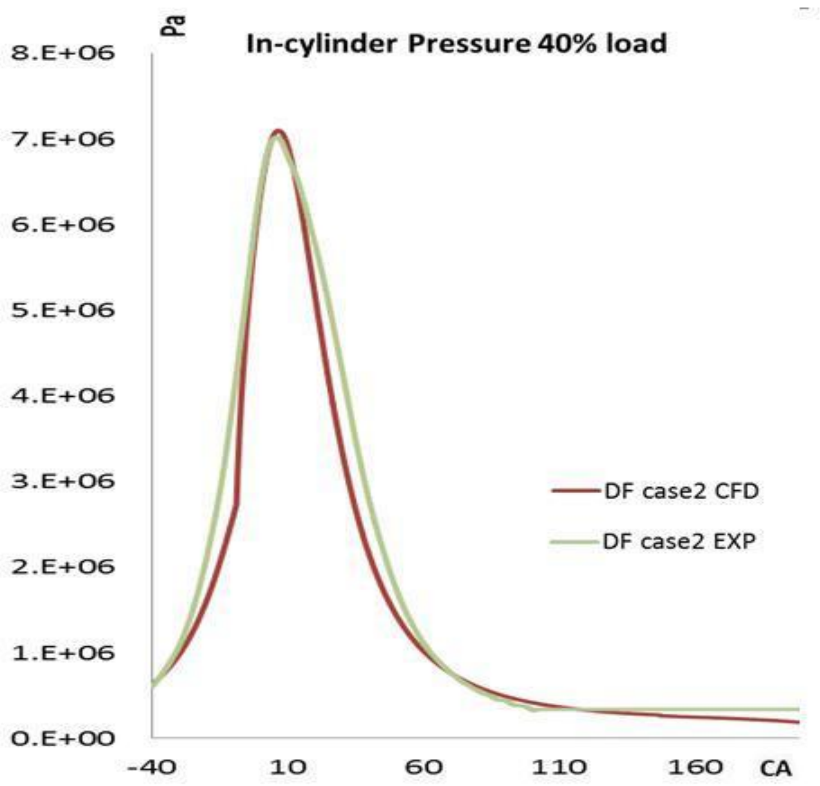

Figure 4.3. CFD and experimental pressure value at 40% engine load.

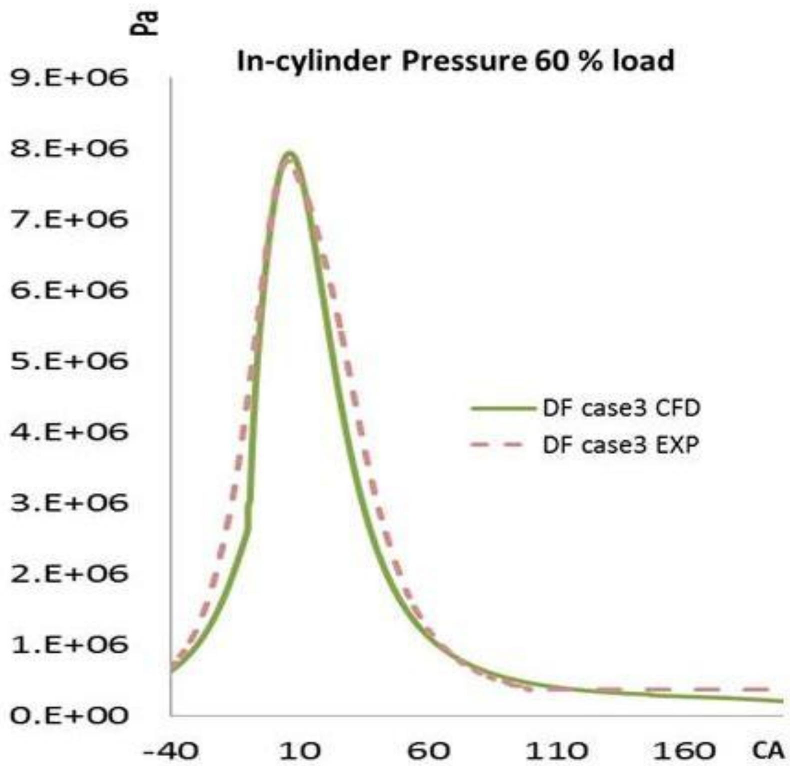

Figure 4.4. CFD and experimental pressure value at 60% engine load.

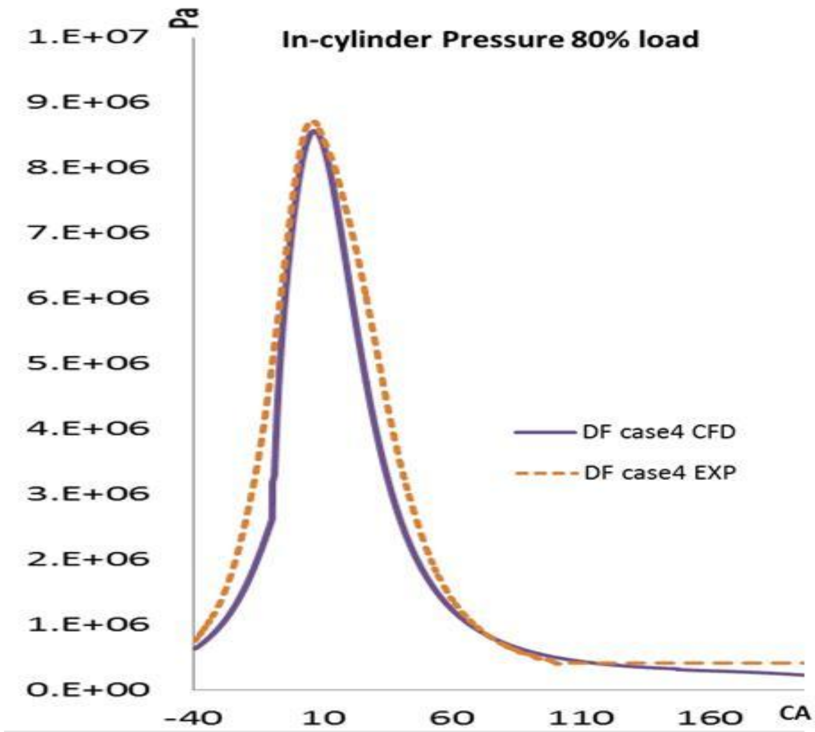

Figure 4.5. CFD and experimental pressure value at 80% engine load.

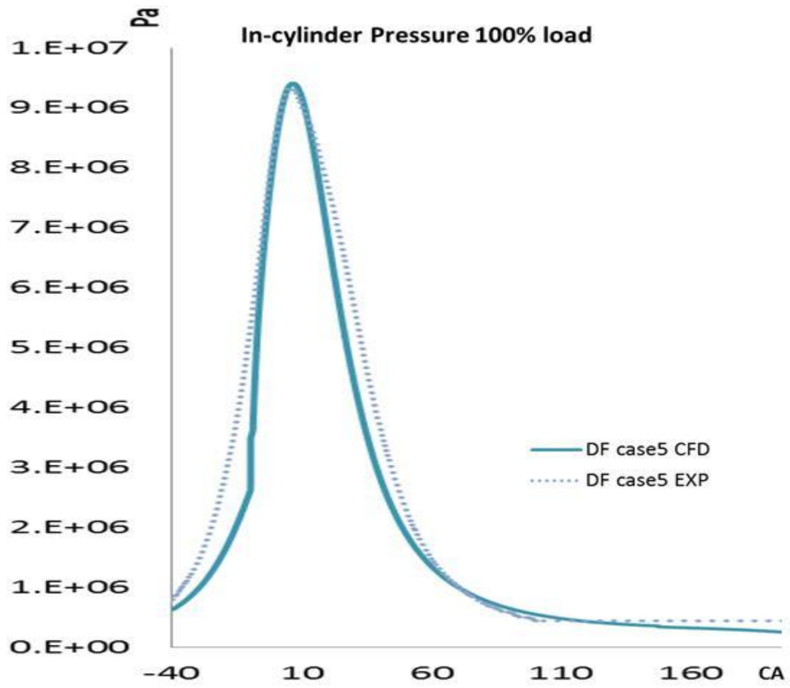

Figure 4.6. CFD and experimental pressure value at 100% engine load.

4.2 1D Engine Simulation

1D engine code was used to simulate engine performance and exhaust emissions such as CO and NOx gases. The combustion pressure and in-cylinder temperature were evaluated under real engine geometry conditions in order to verify 3D and experimental results. Wiebe function for 1D approximation and Extended Coherent Flame Model (ECFM) for 3D CFD solution were used to carry out combustion modeling. 3D engine code was used to find out flow structure in-cylinder and behavior of the mixture combustion. Also, 1D engine code was employed to validate 3D results as shown in Figure 4.7. ECFM and the 3-Zone ECFM (ECFM-3Z) broadly belong to the Coherent Flame Model (CFM) family, but are extended to non-homogeneous turbulent premixed and unpremixed (diffusion) combustion. In the ECFM-3Z combustion model, the state of the gases mixture was defined in the 3D space.

In-cylinder 1D pressure value is slightly bigger than 3D engine simulation and experimental results as shown in Figure 4.7. 1D, 3D pressure value reached maximum value near 4^o CA aTDC however, experimental analysis reached a few degree crank angle later than engine codes, (near 6^o CA aTDC, Figure 4.7). At the same time, 3D temperature results reached maximum value near 3^o CA aTDC and 1D analysis yields a maximum about 20^o CA aTDC (Figure 4.8). It is shown that a few difference between 1D, 3D CFD and experimental results possibly due to the injection parameters used in CFD calculation (i.e. maximum droplet and parcel number).

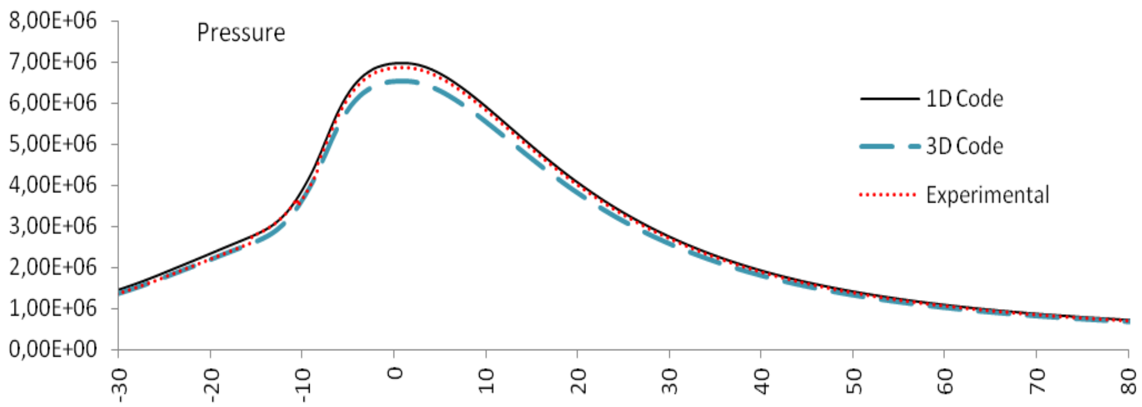

Figure 4.7. 1D, 3D and experimental in-cylinder pressure results.

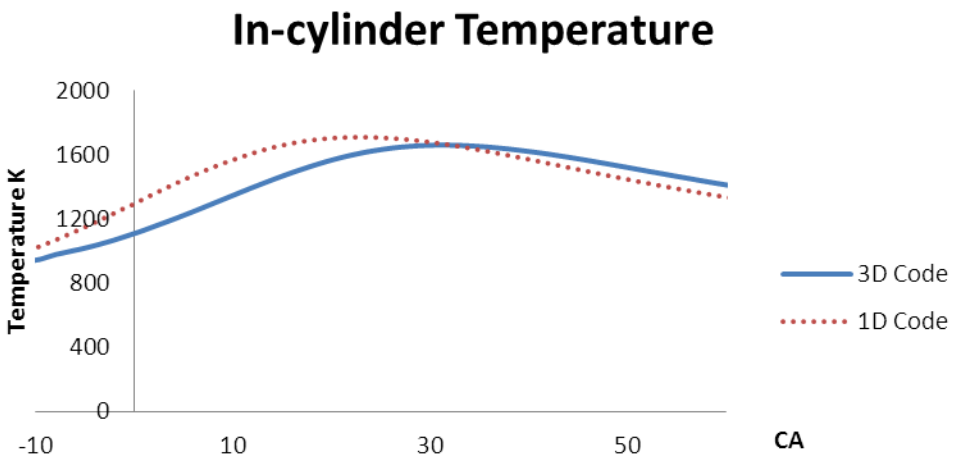

Figure 4.8. 1D and 3D in-cylinder temperature results.

Turbulence is very important factor in-cylinder combustion phenomenon. 1D and 3D analyzes results showed that turbulence is driven by combustion effect as seen Fig. 4.8. 1D and 3D results have little difference due to the intake port effect. Swirl and tumble which are a result of intake port also squish flow motion inside the combustion chamber affected 3D results. In addition, fuel injection at high inlet pressure was another main parameter on turbulence level and 3D results. Turbulence kinetic energy value during the intake, compression, combustion and exhaust stroke was shown in Figure 4.9.

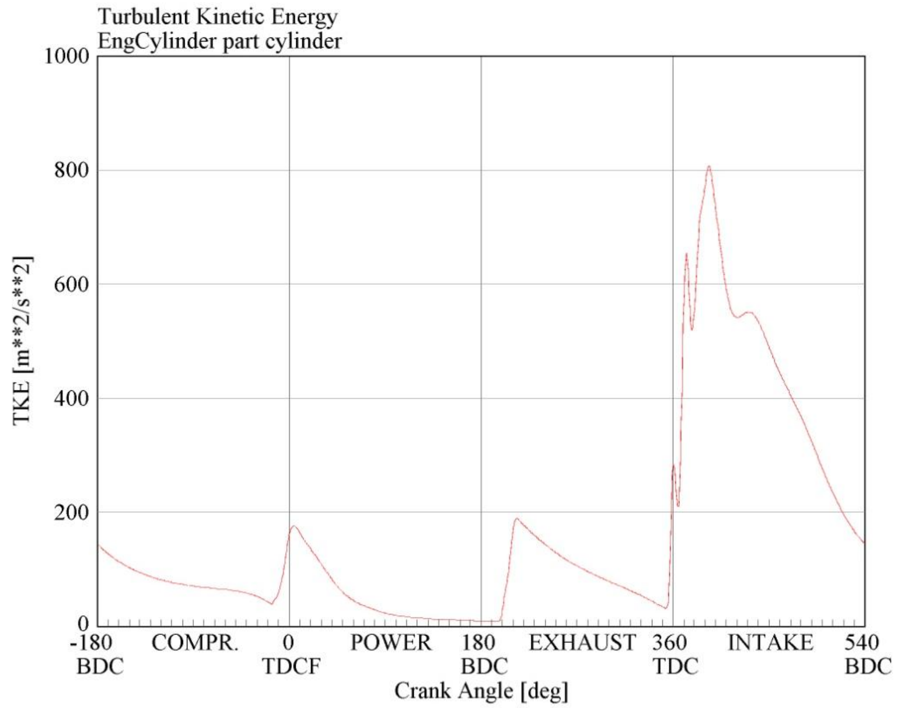

Figure 4.9. In-cylinder Turbulent Kinetic Energy result for 1D analysis.

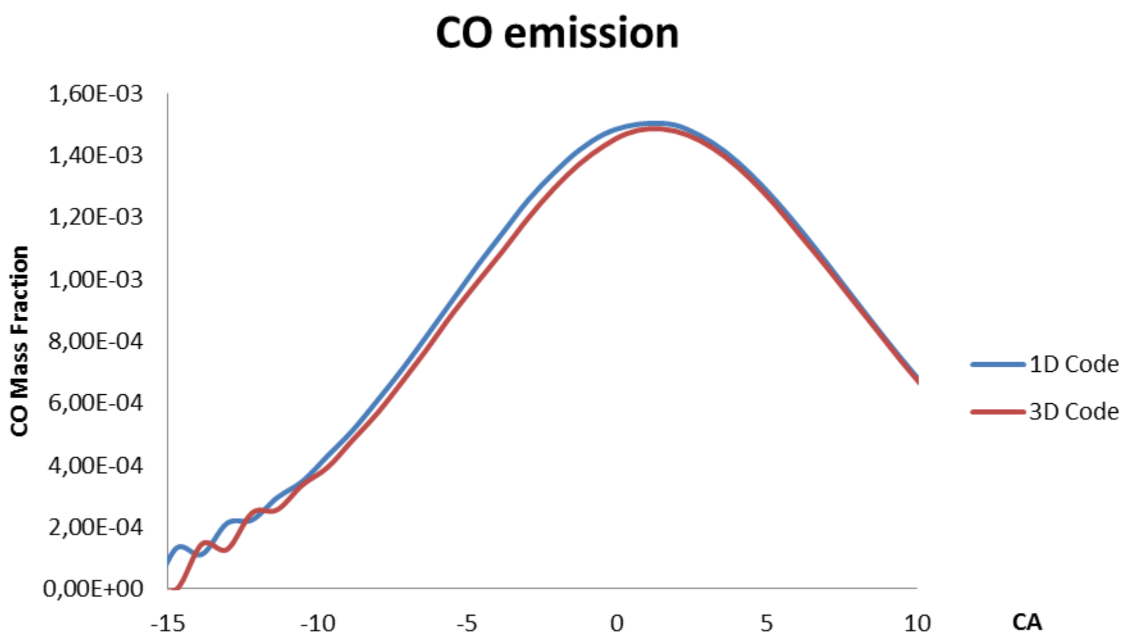

a) CO Mass fraction results

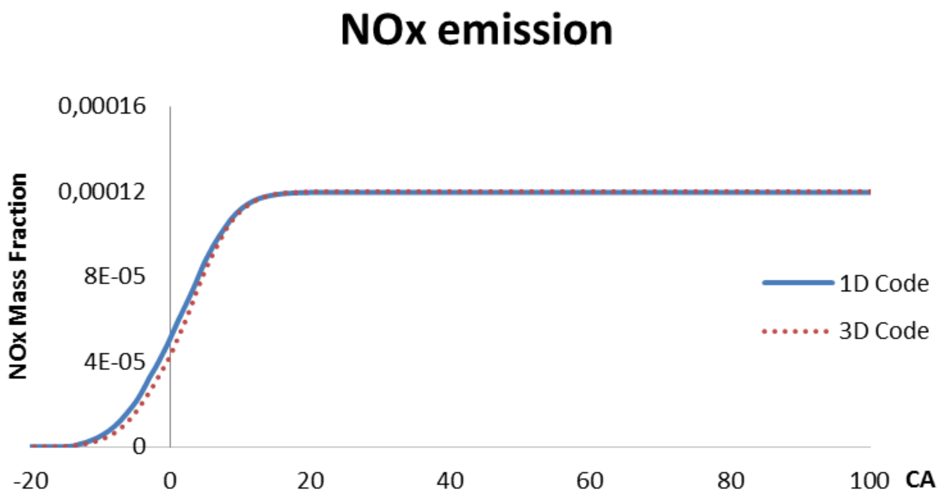

b) NOx Mass fraction results

Figure 4.10. In-cylinder mass fraction results.

4.3 Cold Flow Simulation

In cold flow study, moving mesh feature was used to analyze the flow structure inside the combustion chamber. Cold flow simulation in 3D was investigated as intake and compression strokes. Both intake and compression strokes were simulated including full geometry, intake port, exhaust port, intake valve, exhaust valve and combustion chamber in transient condition. Single fuel cases contained air flow through ports and cylinder. In dual fuel cases, also CBG fuel spray simulation was modeled and analyzed beside air flow.

To depict flow vector field and contour map inside the engine, slays were taken from the cylinder in different crank angle. While cross sections selected, four different crank angles were chosen, namely 406, 460, 450 and 540 (BDC) degrees crank angle and start of the combustion stroke was assumed 0 CAD. Selected slays were shown in Figure 4.11.

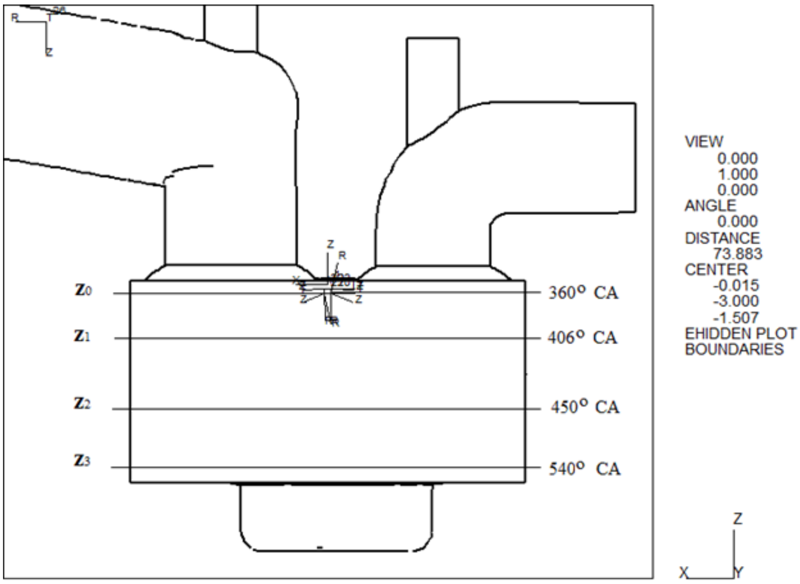

Figure 4.11. Horizontal lines represent measuring levels in-cylinder for different crank angle.

Parallel planes to the cylinder were taken in different crank angle to show detailed velocity vector fields and contour map and indicated in Fig. 4.12. Parallel planes cut both centers of the inlet and exhaust valves. When the jet air flows made through the intake valve, is clearly visible at 406 ^{o}CA. The vortex increased in size due to the shape of the inlet runners during the induction stroke. The jet flow started to decrease and intake valve was nearby closure as shown in Fig. 4.13 (d). In addition, increase and decrease of the jet flow on the intake valves are showed.

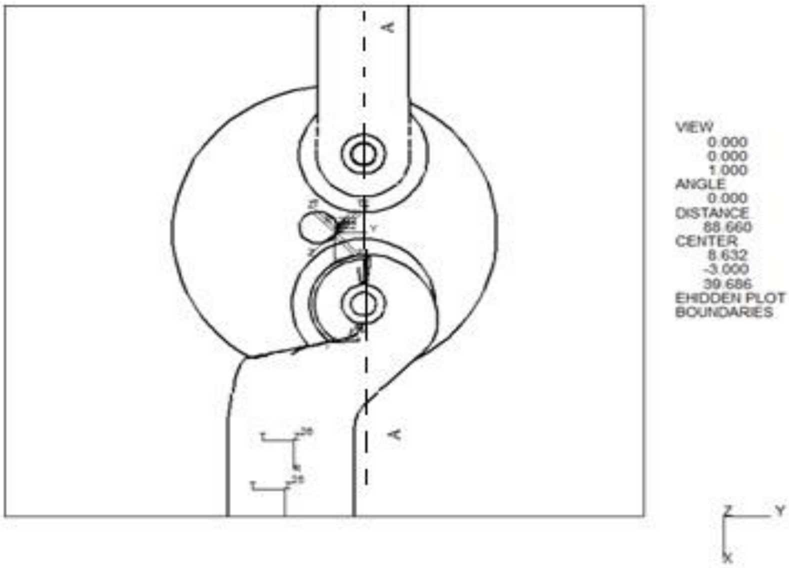

Figure 4.12. Dashed line represents section position inside combustion chamber.

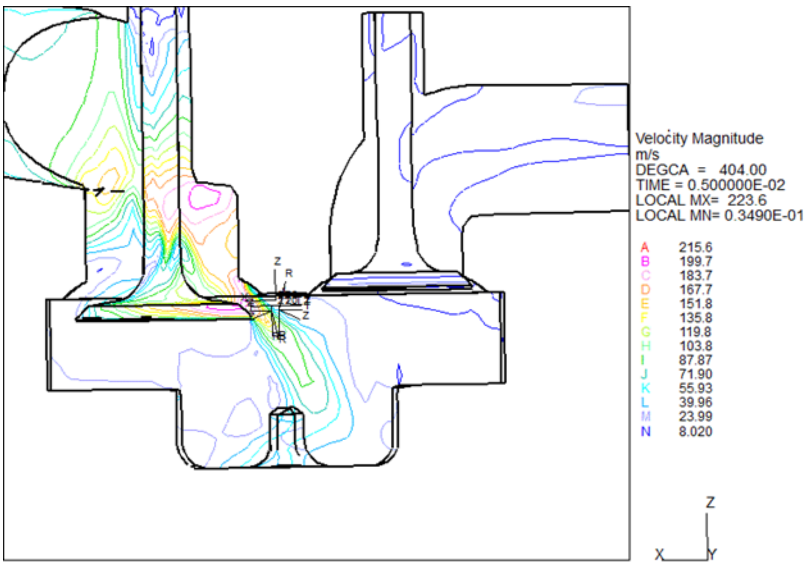

a) Velocity magnitude @ 46^{o} CA aTDC.

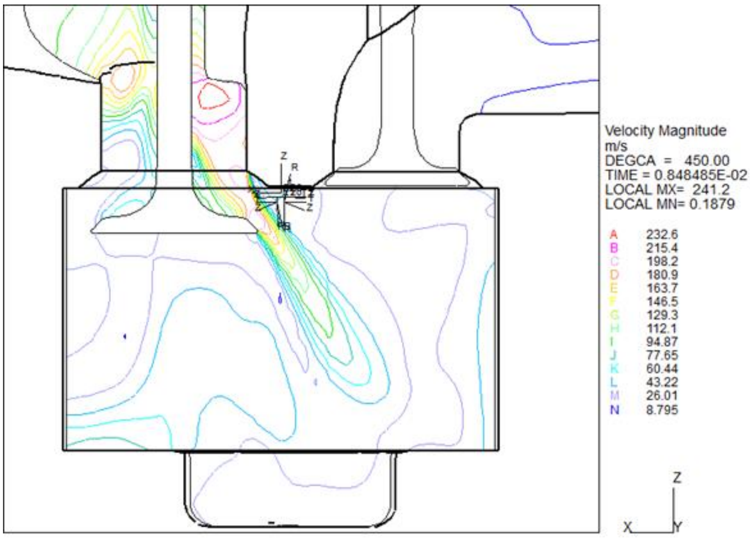

b) Velocity magnitude @ 90^{o} CA aTDC.

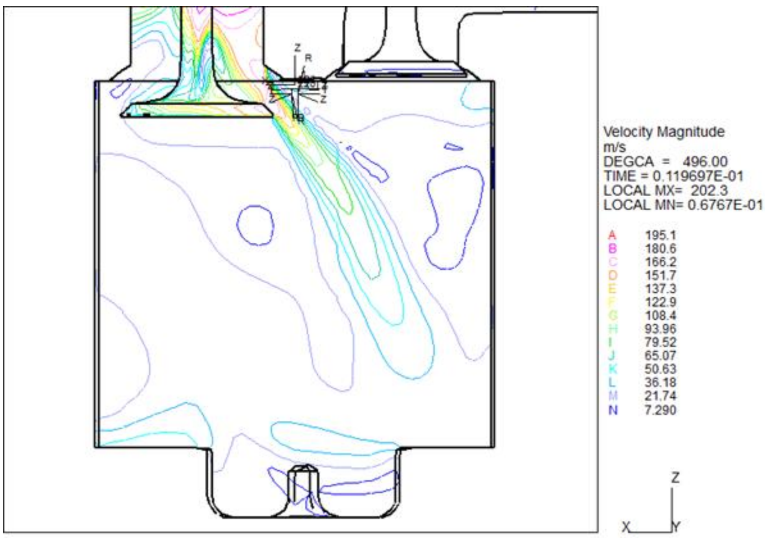

c) Velocity magnitude @ 136^{o} CA aTDC.

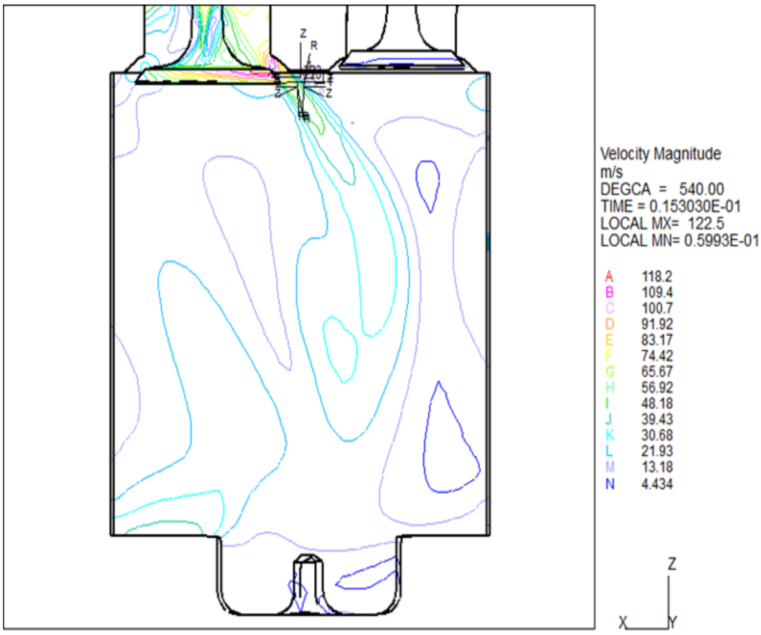

d) Velocity magnitude @ BDC.

Figure 4.13. Contours of velocity magnitudes at different crank angles during the intake stroke.

Different flow structures can be easily distinguished inside the cylinder at 406 CAD. The vector field shows less large structures and larger vortices can be seen at 450 CAD in Fig. 4.13 (b). As shown in Fig. 4.13 (c), in a larger distance from the cylinder head, these vortices start to become small structure. At 496 CAD during the intake stroke, air flow field under the valves has disordered structure. Smaller vortices and smaller vortex flow structures can be seen inside the combustion chamber in Fig. 4.13 (e). The change on the flow structure is easily recognizable as Fig. 4.13 (c) and 4.14 (e) are compared. In addition, vortex structure in the upper left side in Fig. 4.13 (c) is more intense and it slips to the center in Fig. 4.14 (e). At 450 CAD, the vortex in-cylinder pressed to the cylinder center and affected other flow lines. A vortex which has large clockwise rotation appears at the bottom of the combustion chamber in Fig. 4.14 (f). At 540 CAD the intake valve are still open which clearly has seen at the vector field in the left part of the combustion chamber in Fig. 4.14 (g).

Swirl flow structures can be also seen and the magnitude of the velocity vectors decreased compared to the previous vector fields. Moreover, at the bottom of the cylinder, higher velocity vectors can be seen in a clockwise swirl structure.

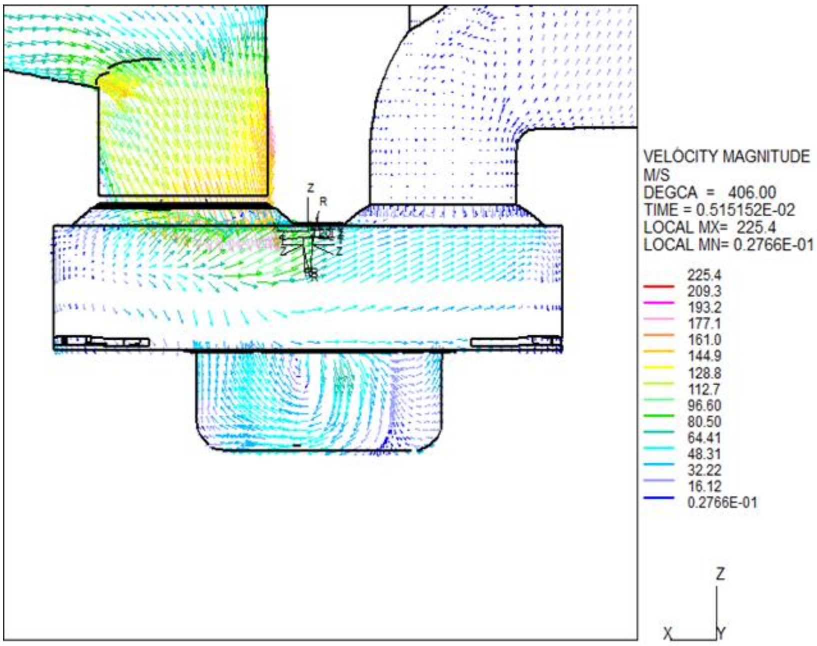

a) Velocity vectors @ 46^{o} CA aTDC

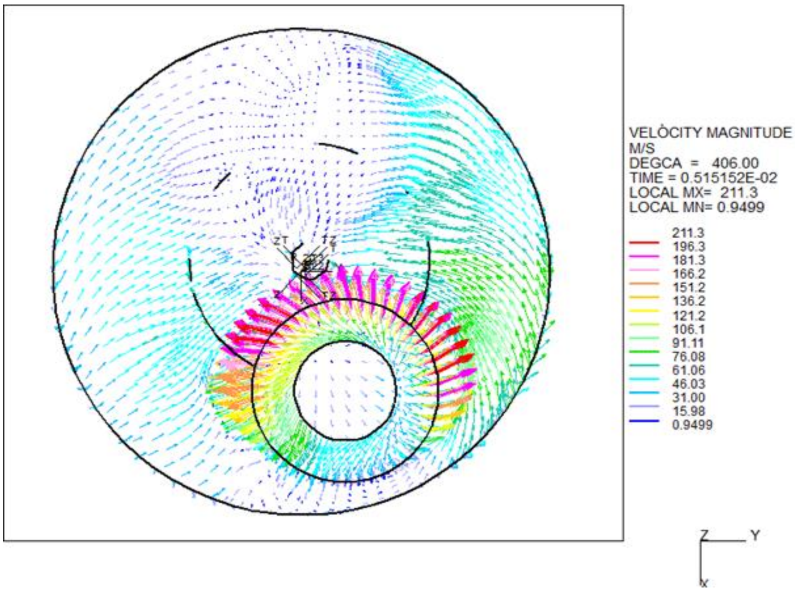

b) 450 CAD 90^{o} aTDC at z1

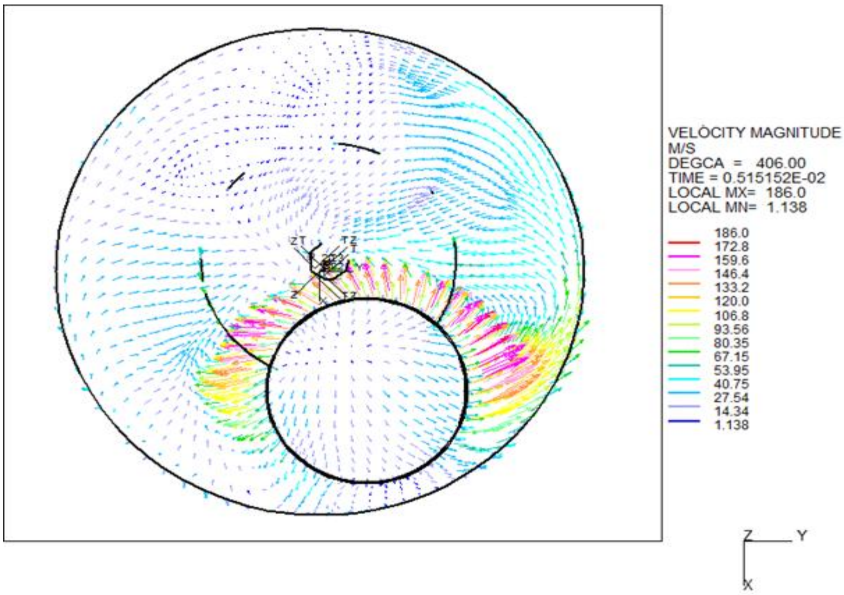

c) 450 CAD 90^o aTDC at z2

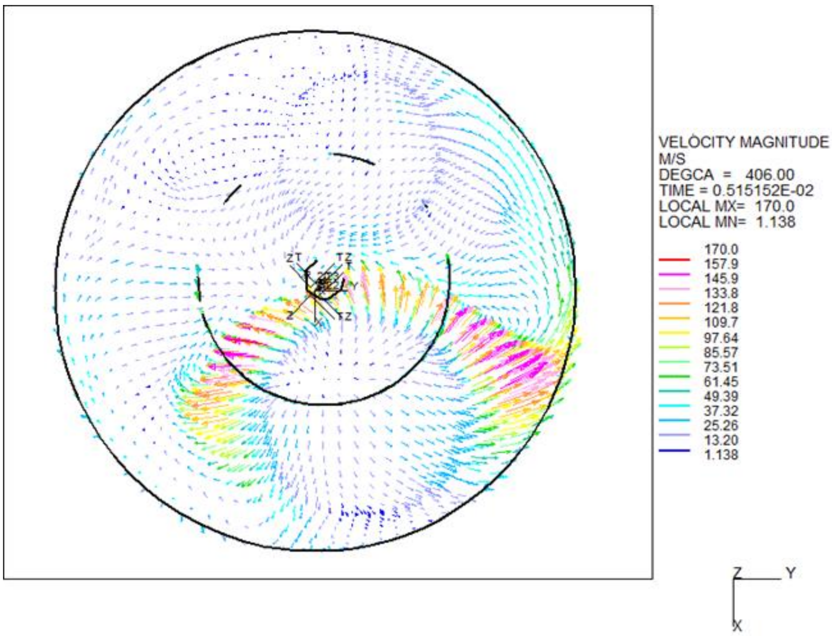

d) 495 CAD 135^o aTDC at z1

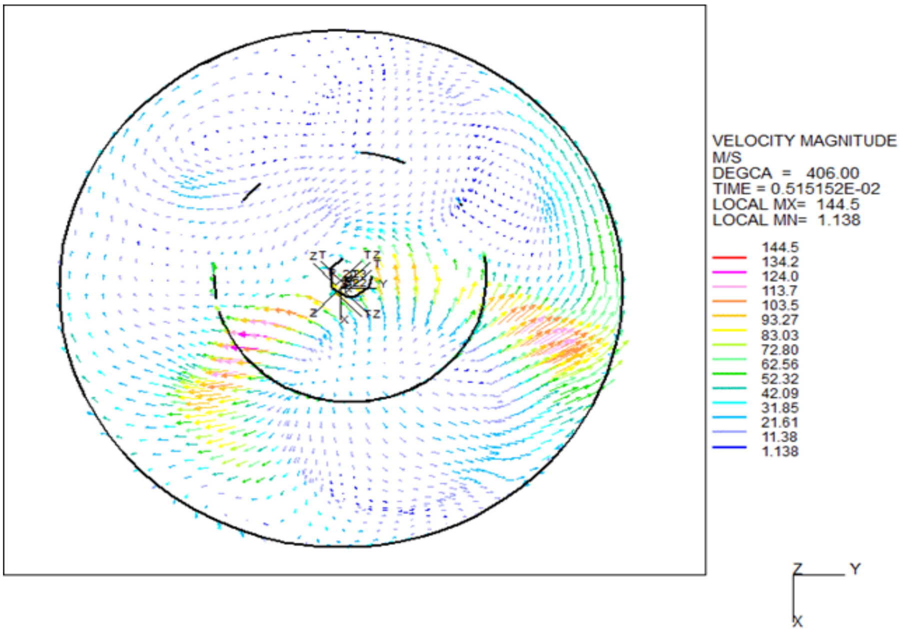

e) 495 CAD 135° aTDC at z2

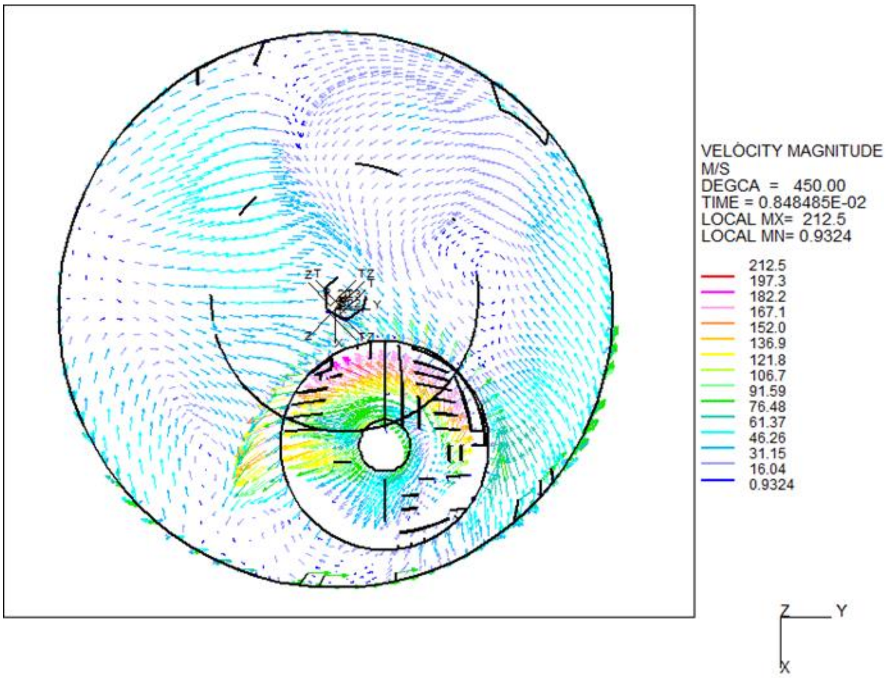

f) 495 CAD 135° aTDC at z3

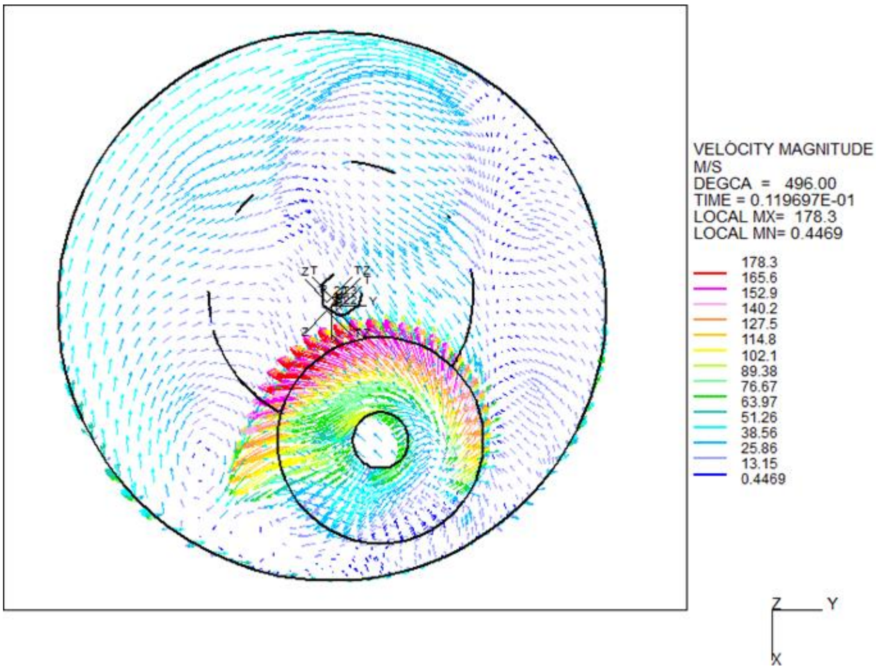

g) 540 CAD 180^o aTDC at z1.

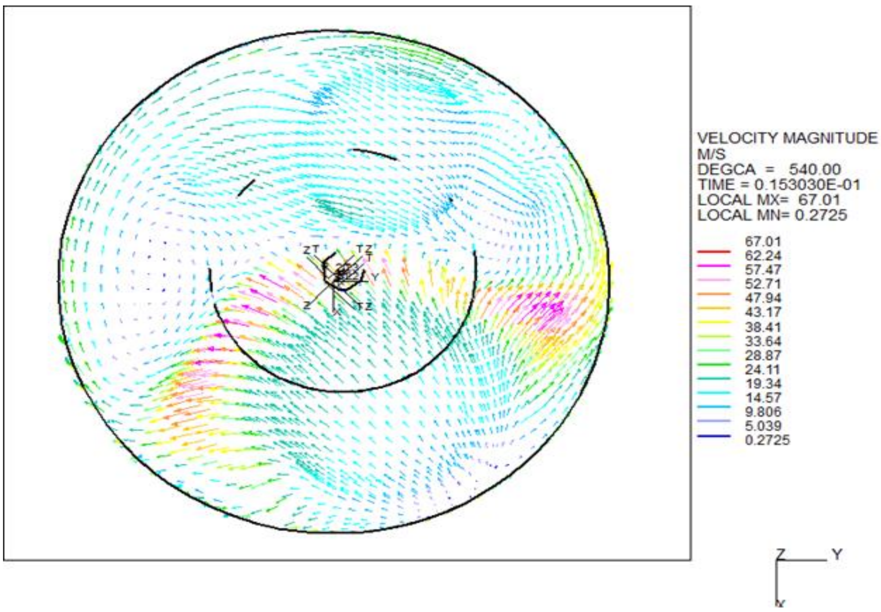

h) 540 CAD 180^o aTDC at z0.

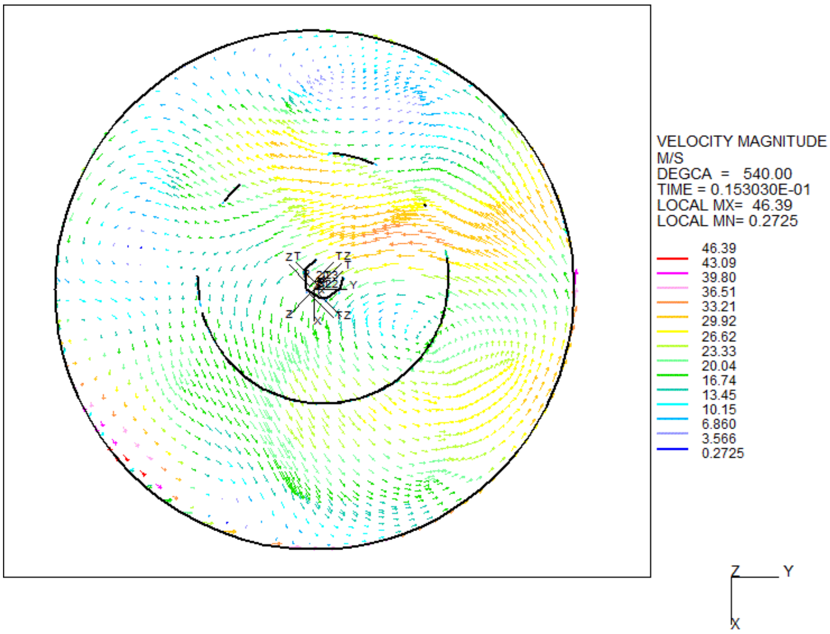

i) 540 CAD 180^{o} aTDC.

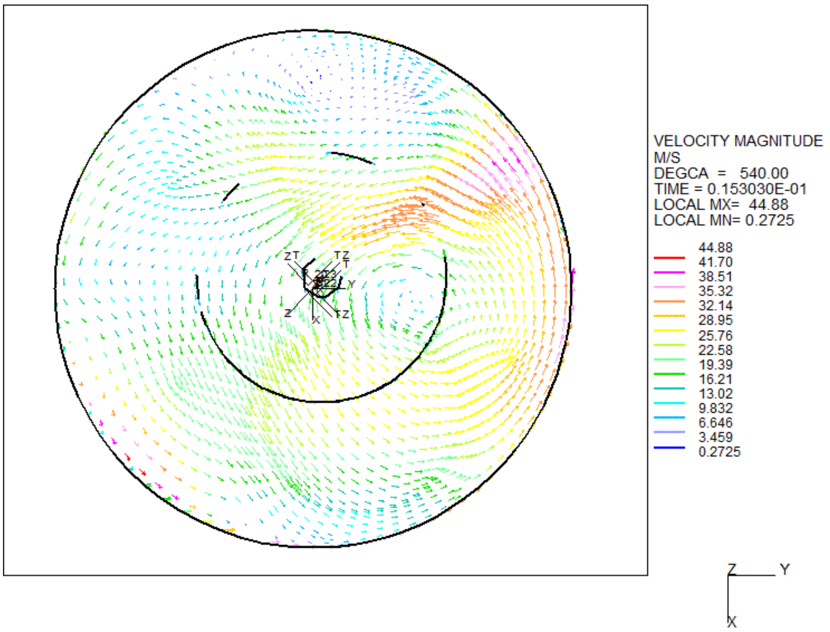

j) 540 CAD 180^{o} aTDC at z2

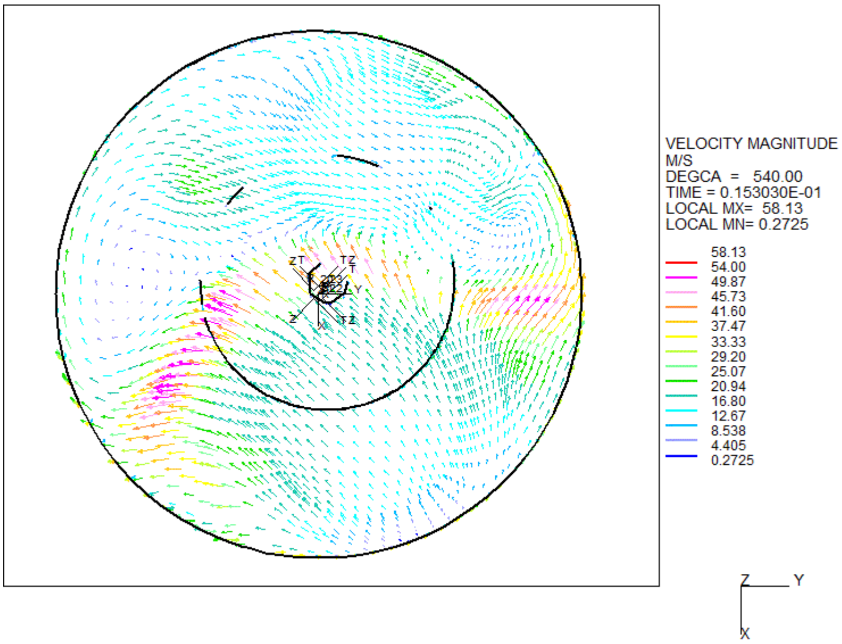

k) 540 CAD 180^o aTDC.

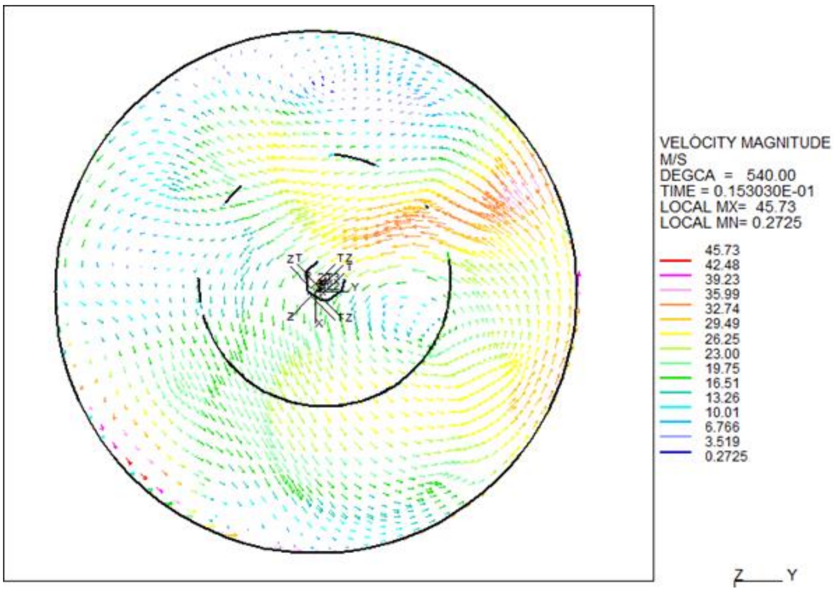

l) 540 CAD 180^o aTDC at z3

Figure 4.14. Vector fields at different crank angles during the intake stroke at positions indicated Fig. 4.11.

Single fuel compression stroke:

The induction stroke of the previous section is followed by the compression stroke. In case of compression stroke, not only the velocity fields but also the kinetic energy fields were evaluated. The kinetic energy is directly depended on turbulence phenomenon and air fuel mixture will be occurred just after the end of the compression stroke. The vector fields at different crank angles are indicated in Fig. 4.14.

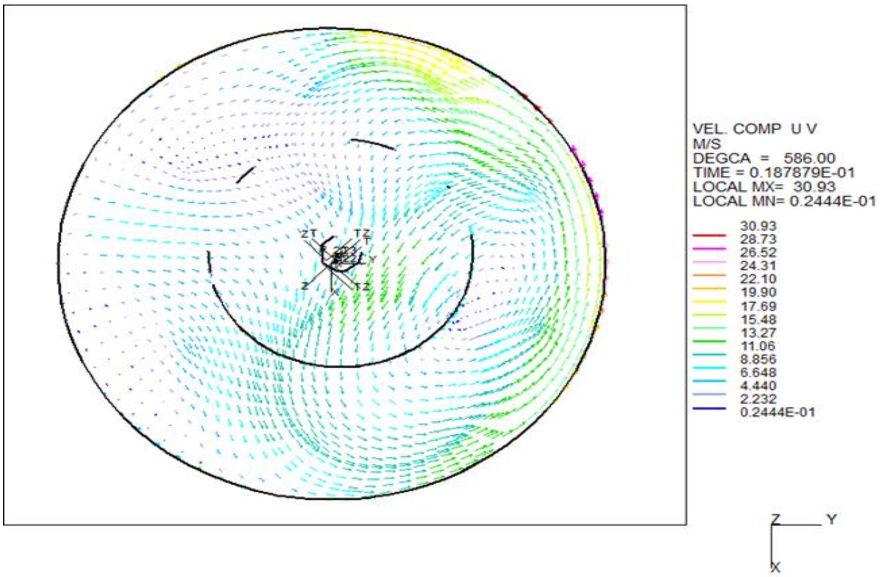

a) 585 CAD 45^o aBDC at z1.

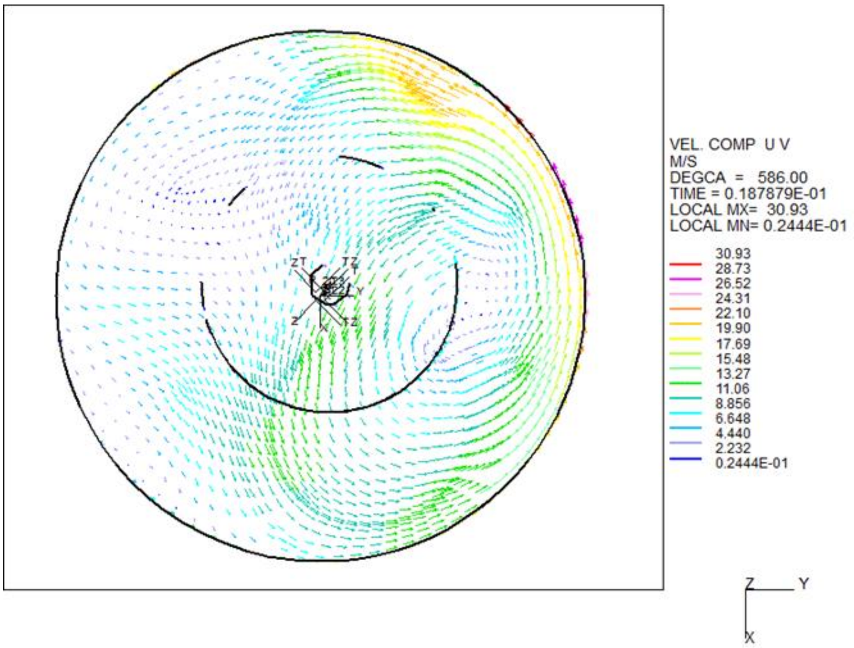

b) 585 CAD 45^o aBDC at z2.

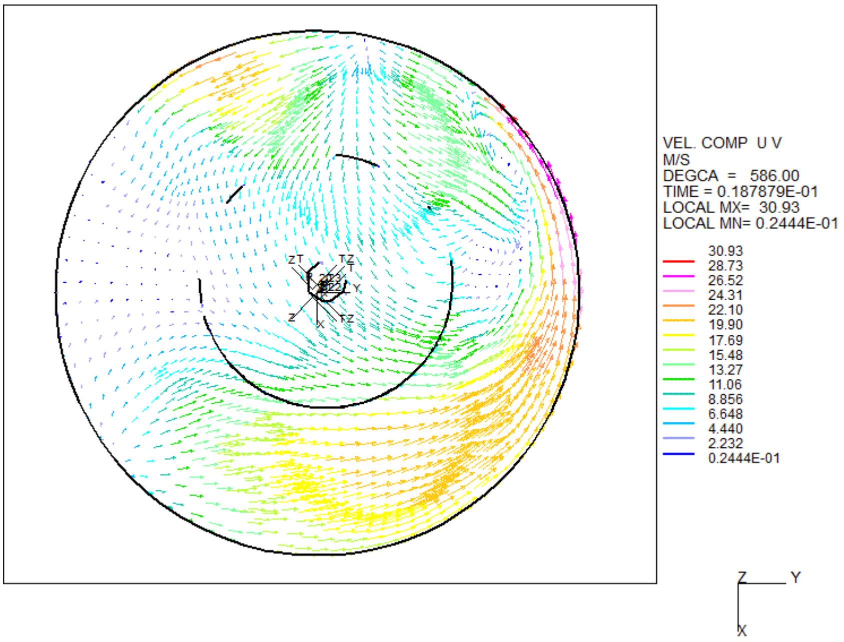

c) 585 CAD 45^{o} aBDC at z3.

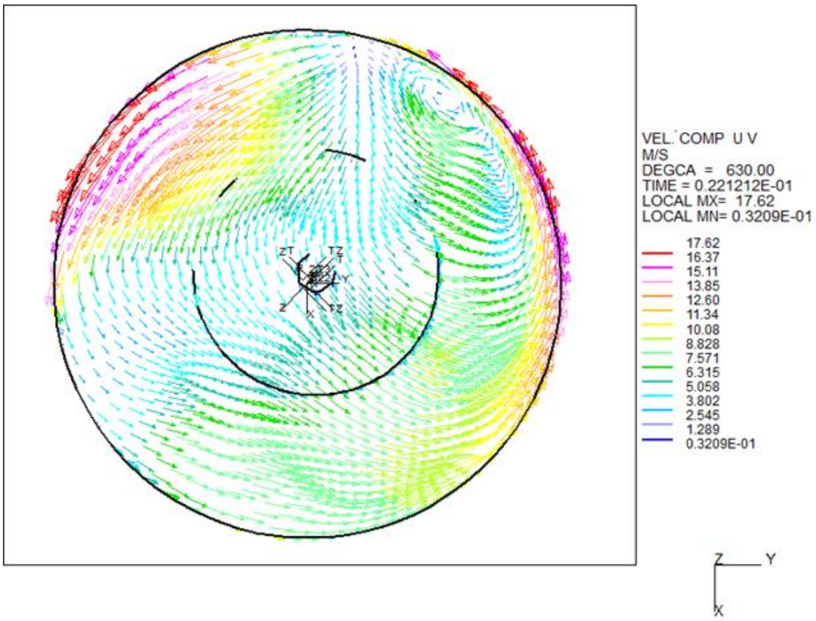

d) 630 CAD 90^{o} aBDC at z1

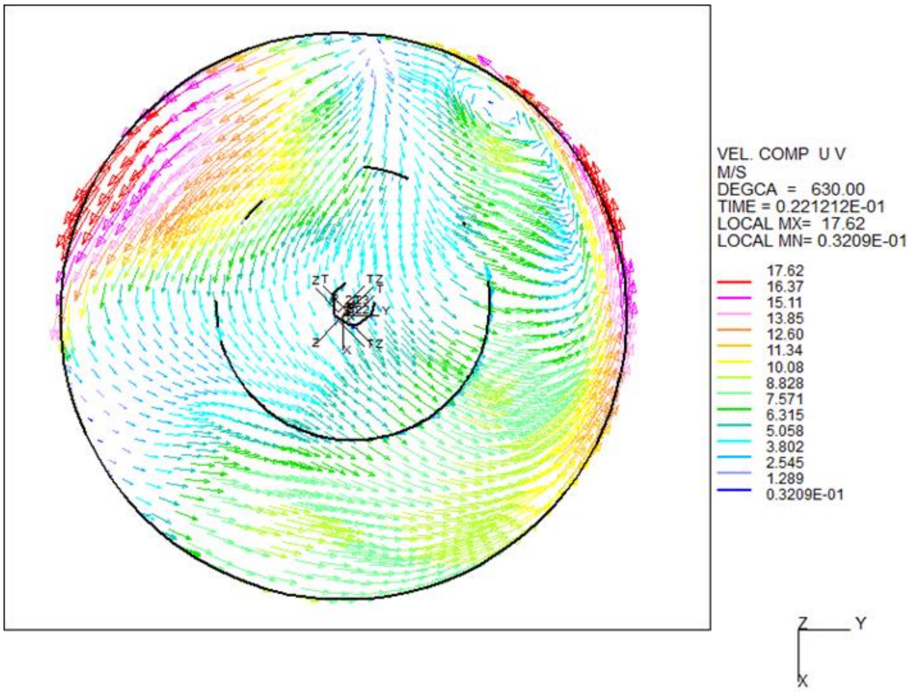

e) 630 CAD 90^{o} aBDC at z2

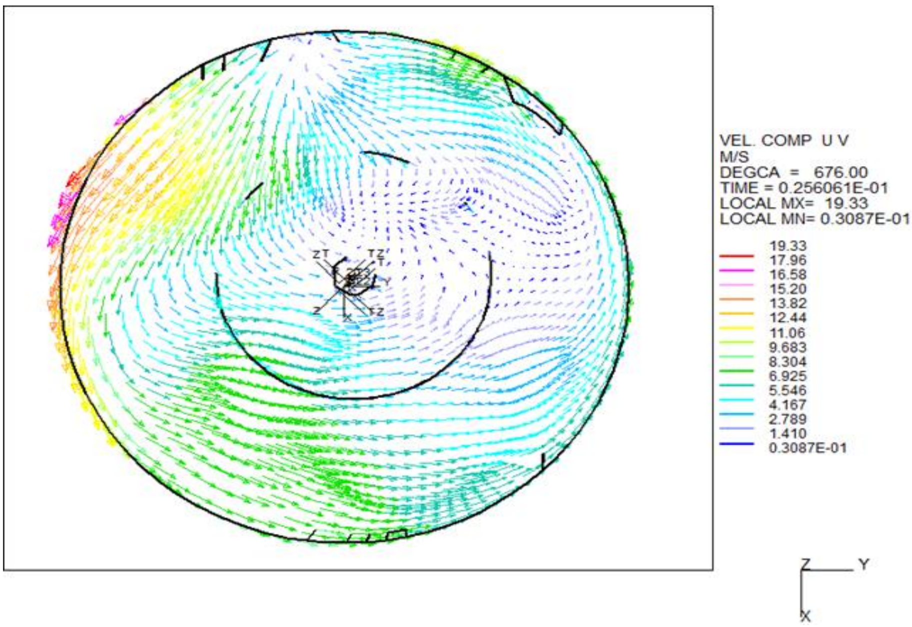

f) 675 CAD 135^{o} aBDC at z0

Figure 4.15. Vector fields at different crank angles during the compression stroke at positions indicated Fig. 4.11.

Through the compression stroke vector fields have more homogeneous structure when compared to the intake stroke. As shown in figures there are some vortices which have less intensity. At the beginning of the compression stroke in Fig. 4.15 (c), large clockwise swirl structures exist. When piston goes from BDC to TDC, magnitude of the swirl structure decreases during the compression stroke. In Fig. 4.15 (f) piston at TDC, the magnitude of the velocity has been decreased. The velocity magnitude during the compression stroke decreases due to friction causes less intensity on the flow structure.

Velocity vectors are evaluated in all direction In Fig. 4.14 and 4.15, at the specific crank angle. The maximum air flow velocity was obtained around the maximum valve lift. After maximum valve lift, velocity vectors gradually decrease during the intake stroke and compression stroke. Turbulence and air velocities generated purely during the compression stroke are much smaller than those generated during the intake stroke and can therefore be neglected (Song et al., 2000). During the compression stroke velocity vectors start to decrease due to the friction as shown in figures. During the compression stroke, turbulence dissipates due to the decrease of kinematic viscosity and increase of temperature and pressure. This is also visible in Fig. 4.17 where velocity contours were obtained at different crank angles. At the beginning of the compression stroke, higher velocity levels are necessary to have high turbulence intensity for a good air fuel mixture at the end of the compression stroke.

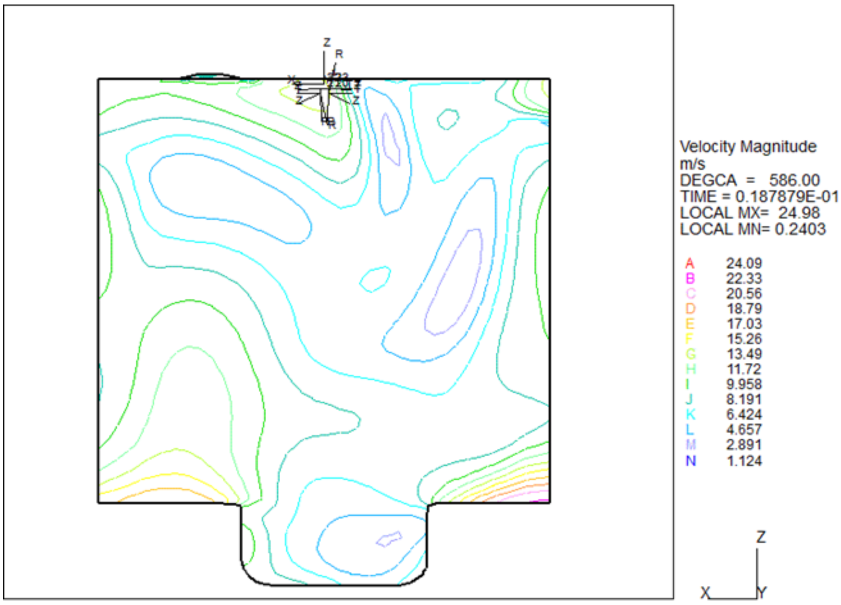

a) 585 CAD 45^{o} aBDC

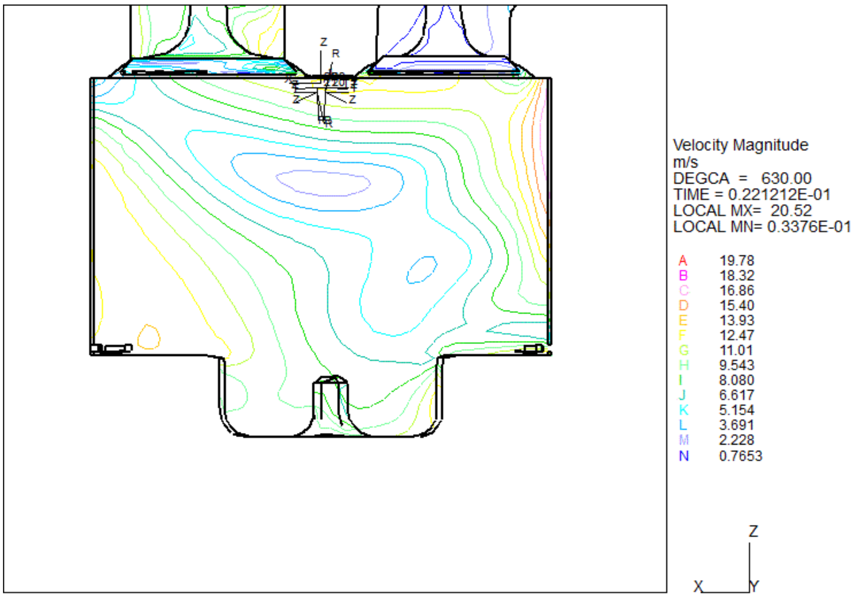

b) 630 CAD 90^o aBDC

Figure 4.16. Z-contours of velocity at different crank angles during the compression stroke at positions indicated in Fig. 4.15.

Contours of the z-velocity were depicted in Fig. 4.17 to analyze parallel flow to the cylinder axis. Air flow was still influenced by the flow features of the induction stroke at 586 ^{o}CA. Air flow is largely driven by the piston movement half of the compression stroke because of there is no extra energy entrance by the compression and z-velocity contours are flattened.

Turbulence level is very effective on the combustion process turbulence and thus inextricably connected to the turbulent kinetic energy k. In Fig. 4.17 the contours for the velocity magnitudes are depicted at different crank angles at positions indicated in Fig. 4.11.

The kinetic energy is directly related to the velocity magnitudes. It is therefore not surprising that the kinetic energy, as well as the velocity, decreases with increase of crank angle. This decrease of kinetic energy starts rapidly. At TDC in Fig. 4.16 (i) when looked at to velocity magnitudes about half of the maximum kinetic energy is increased compared to the BDC Fig. 4.17 (c). Peak velocity magnitude inside the cylinder was shown in Fig. 4.16 (b). This also will provide high kinetic energy levels.

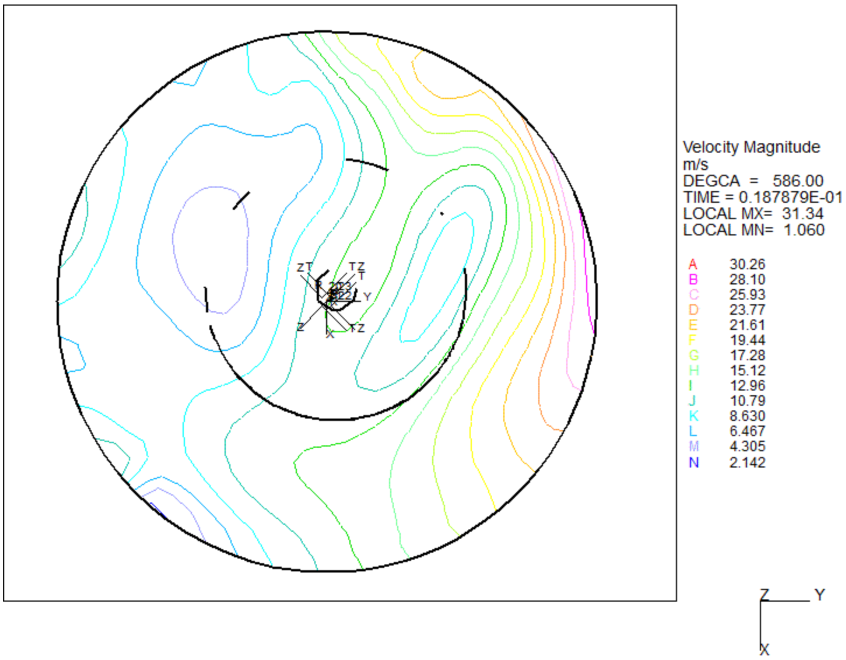

a) 540 CAD @ BDC at z1.

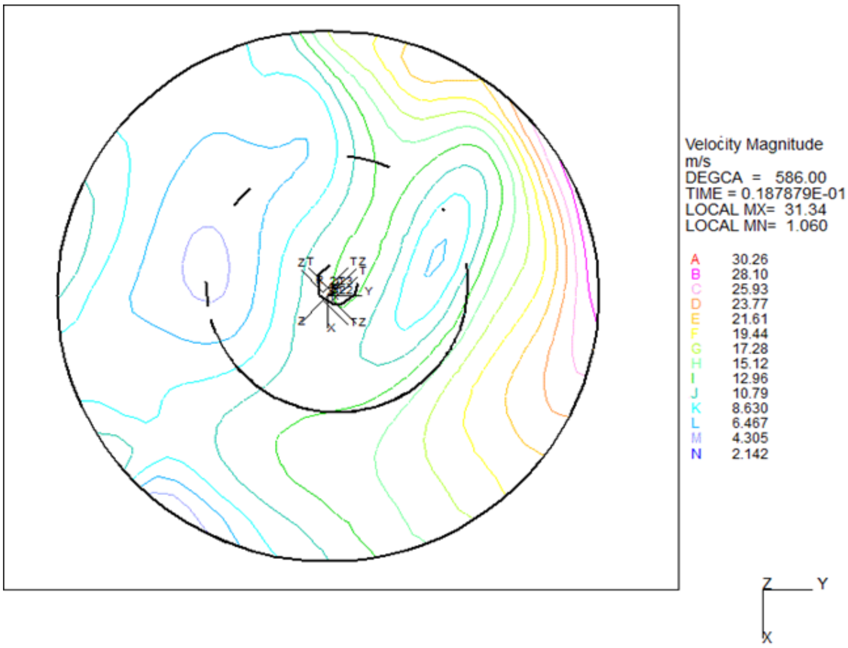

b) 540 CAD @ BDC at z2.

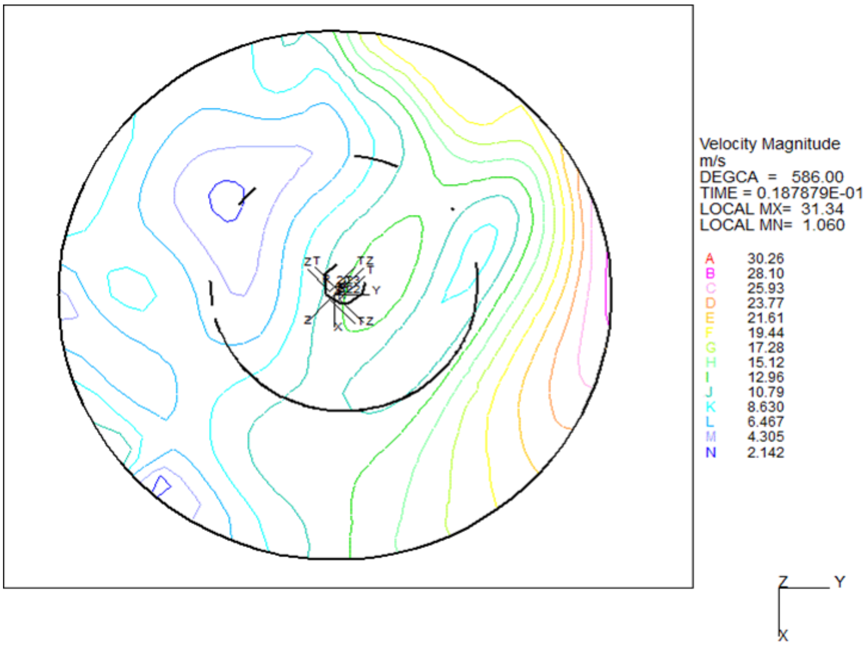

c) 540 CAD @ BDC at z3

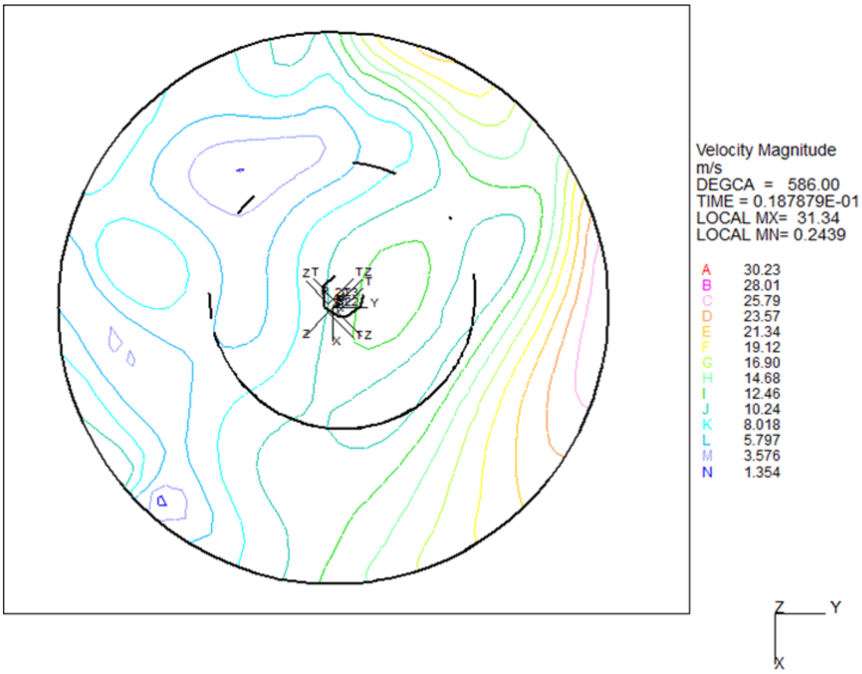

d) 585 CAD 45^{o} aBDC at z1

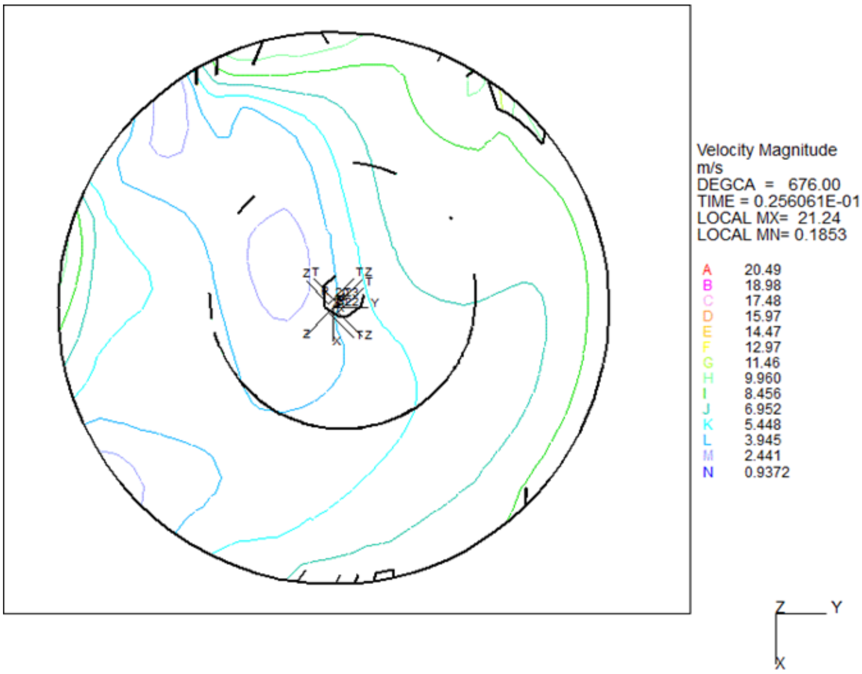

e) 585 CAD 45^{o} aBDC at z2

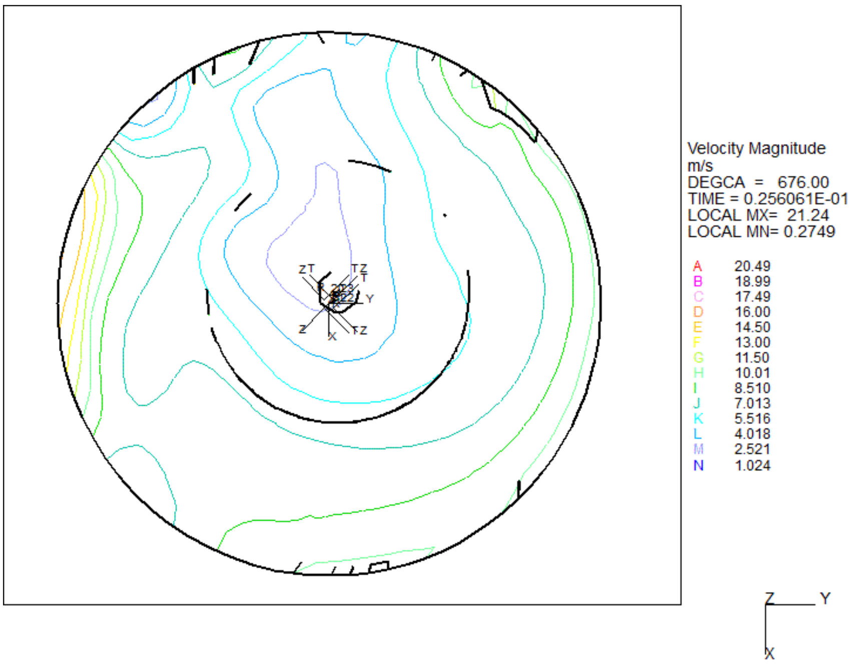

f) 585 CAD 45^{o} aBDC at z3

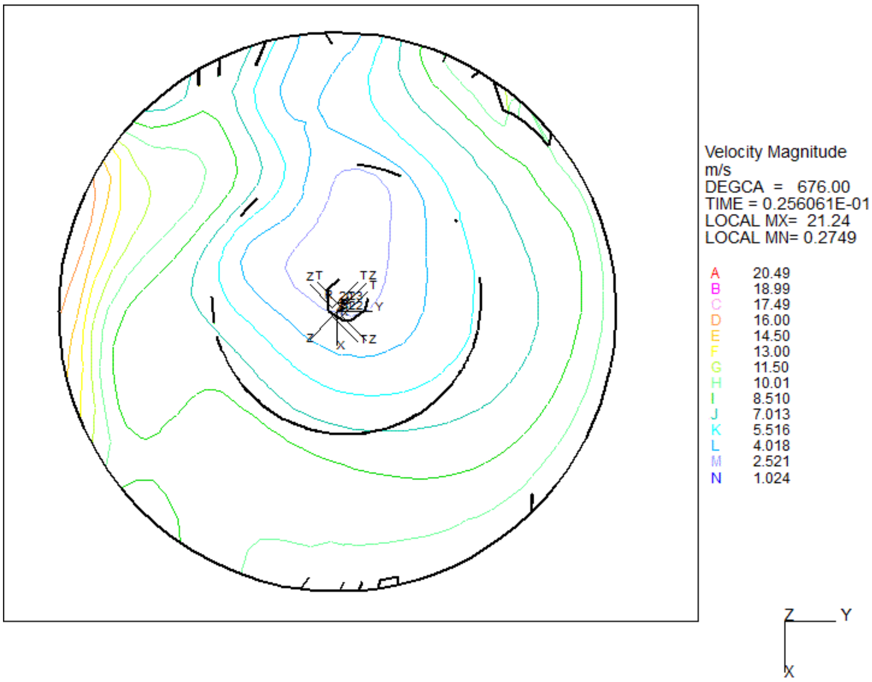

g) 630 CAD 90^o aBDC at z1

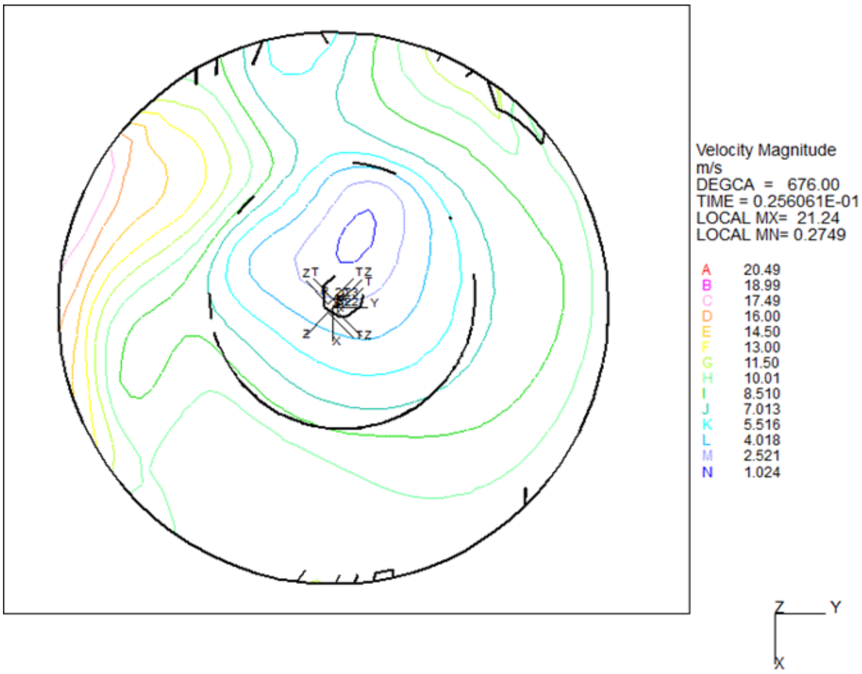

h) 630 CAD 90^o aBDC at z2

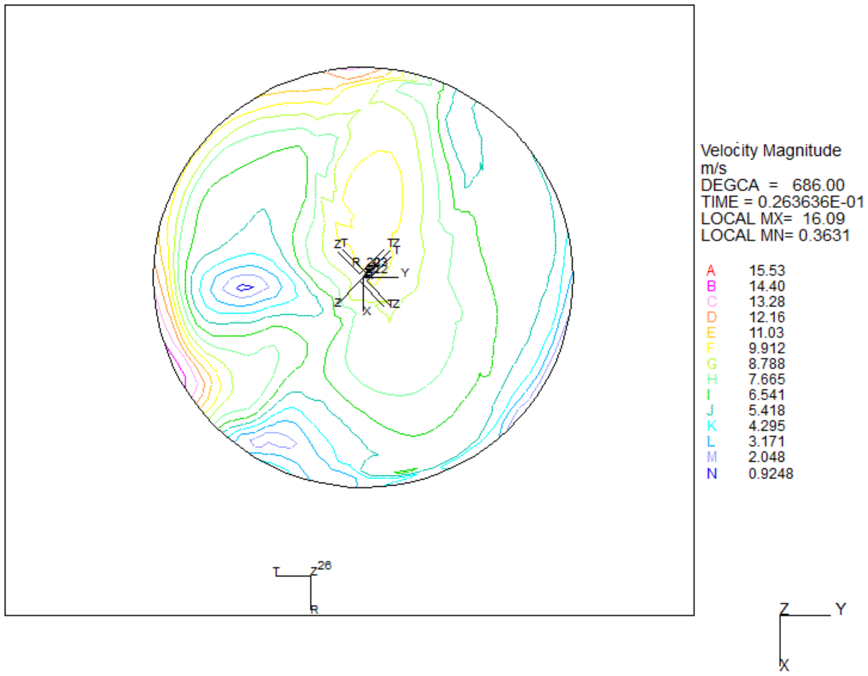

i) 685 CAD 145^{o} aBDC at z1

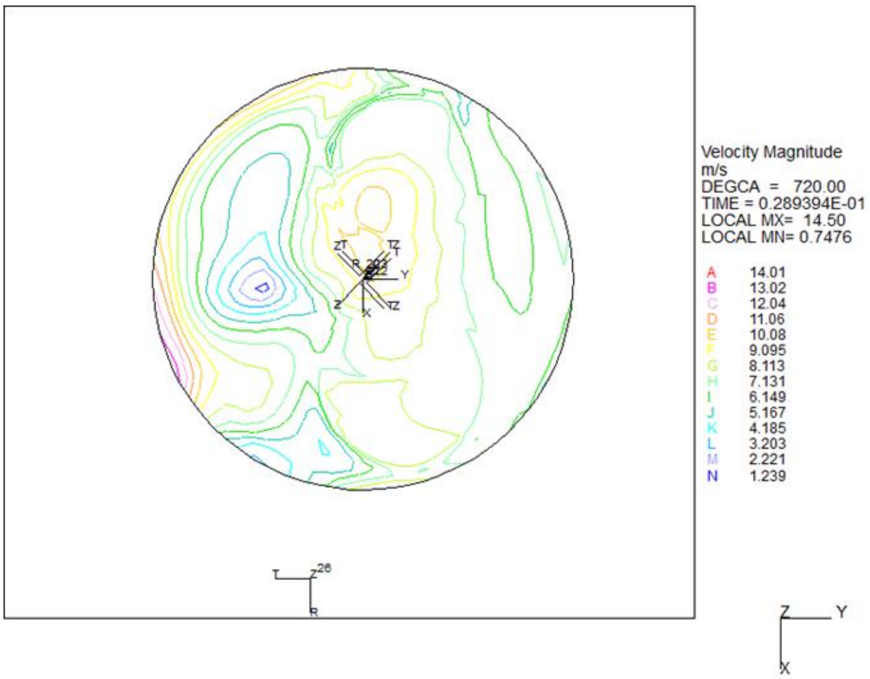

j) 720 CAD @ TDC at z0

Figure 4.17. Contours of velocity at different crank angles during the compression stroke at positions indicated Fig. 4.11.

Several calculation of the flow in the engine cylinders have been previously carried out and established on the literature. Zur Loye et al. (1989) and Kone et al. (1999)

performed calculations of the compression stroke. In particular, Kono et al. presented the analysis of the swirl intensity effects on spray formation and obtained reasonable agreement with experimental data. However, since the intake process was not included in Kono's calculation, the initial swirl was entered as a parameter. In this study, intake and exhaust strokes were added in the calculation and swirl intensity effects on spray formation in simulation at different crank angles.

4.4 Spray Modeling

4.4.1 Single fuel spray modeling

In single fuel cases, diesel fuel injector was defined at the center of cylinder. 3D calculations showed spray structure inside the combustion chamber. As can be seen in Fig. 4.18 in the fuel injection is injected directly to the combustion chamber. If the fuel spray velocity is high enough, fuel air mixture generates an additional flow vortex in the fuel spray direction and therefore some fresh air is driven to the piston bowl dome, replacing the fuel/air mixture, allowing the second and more injection to take place in a 'fresh' air area and hence leading to improved bulk air utilization (Yilmaz M., 2009). In addition, the combustion process in true spray injection process allows better control of maximum heat release leading to less combustion noise and NOx emissions. Also, early injection timing occurs at the pre-heat release by low temperature oxygen reactions before combustion.

Several injection strategies were introduced as a concept of ignition-enhancing to solve the problem in wall wetting (Akagawa, et al., 1999). According to literature review, injection strategies are very effective on exact combustion and exhaust emission. In 1D and 3D spray simulation, real engine injector data were used. Injection strategy was modeled by injecting of fuel near TDC, diesel fuel was injected at 12^o bTDC. 1D, 3D and real engine experimental results were obtained and good agreement each other. In CFD calculation, injector which has four holes was defined using cylindrical coordinate system. Start of injection, spray duration defined using CAD, cone angle and hole diameter were defined in millimeter.

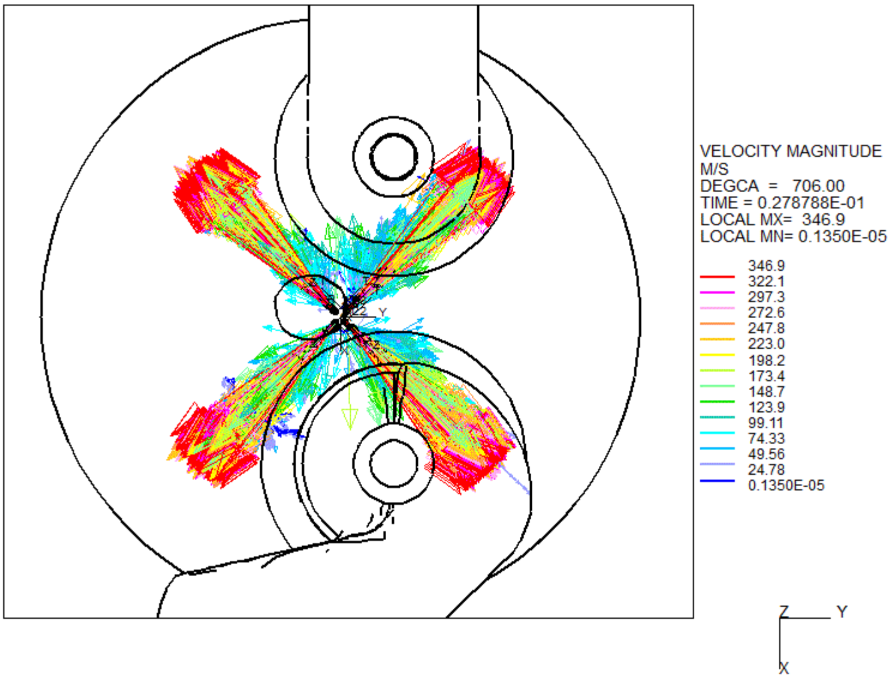

a) Velocity vectors for single fuel spray simulation.

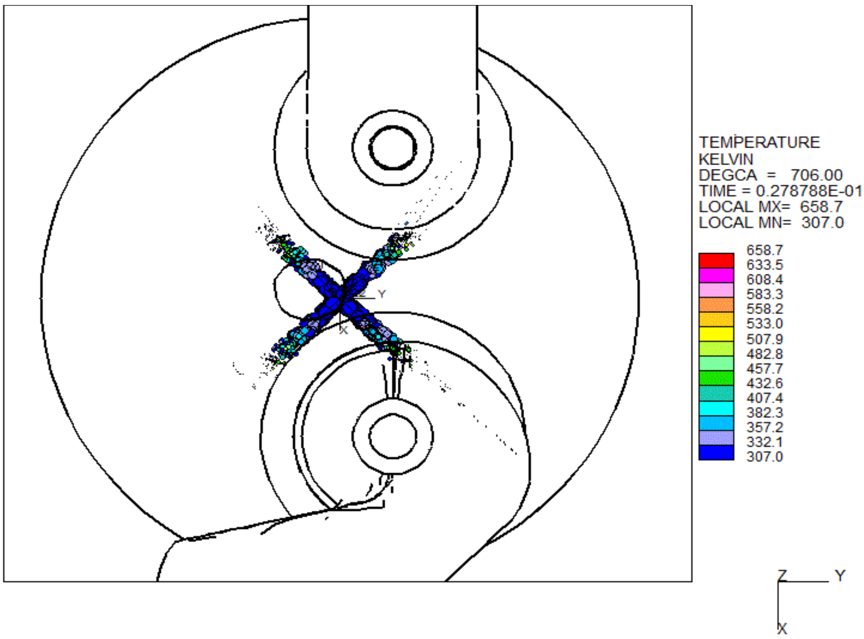

b) Droplet particles at 706 CAD.

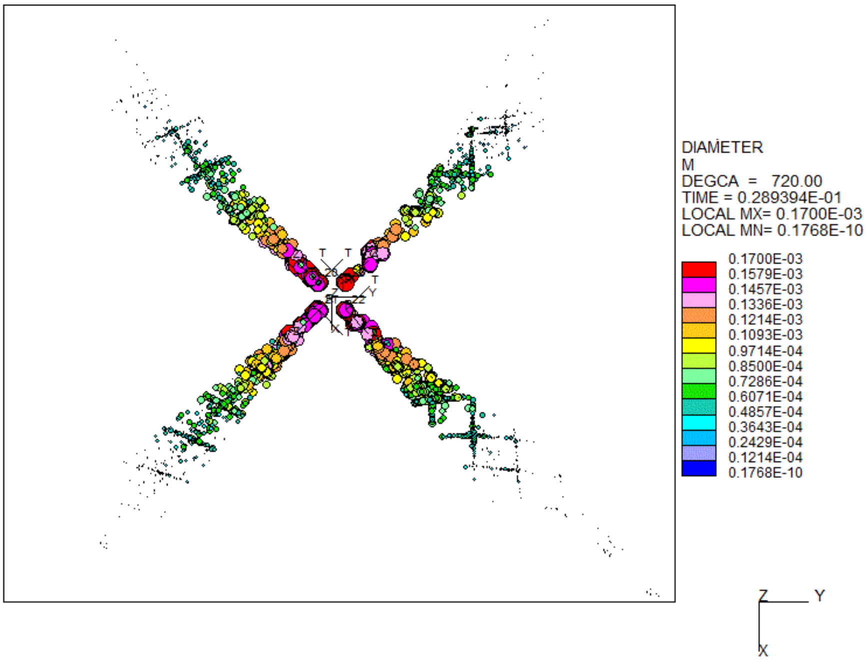

c) Droplet diameter at TDC.

Figure 4.18. Spray simulation for single fuel cases taken from cylinder head.

4.4.2 Dual fuel engine spray modeling

Real engine geometry was re-modeled to find out dual fuel flow structure inside the combustion chamber. In dual fuel engine cases, air and CBG fuel mixture was ingested into the combustion chamber and it was ignited with pilot diesel fuel at the end of compression stroke. First injector was located on the intake port as a main fuel CBG using cylindrical coordinate system as shown in Fig. 4.19. Second injector for pilot diesel fuel was retained on the cylinder head. Injector hole diameter, cone angle, hole number, start of CBG fuel injection and duration were entered to CFD code.

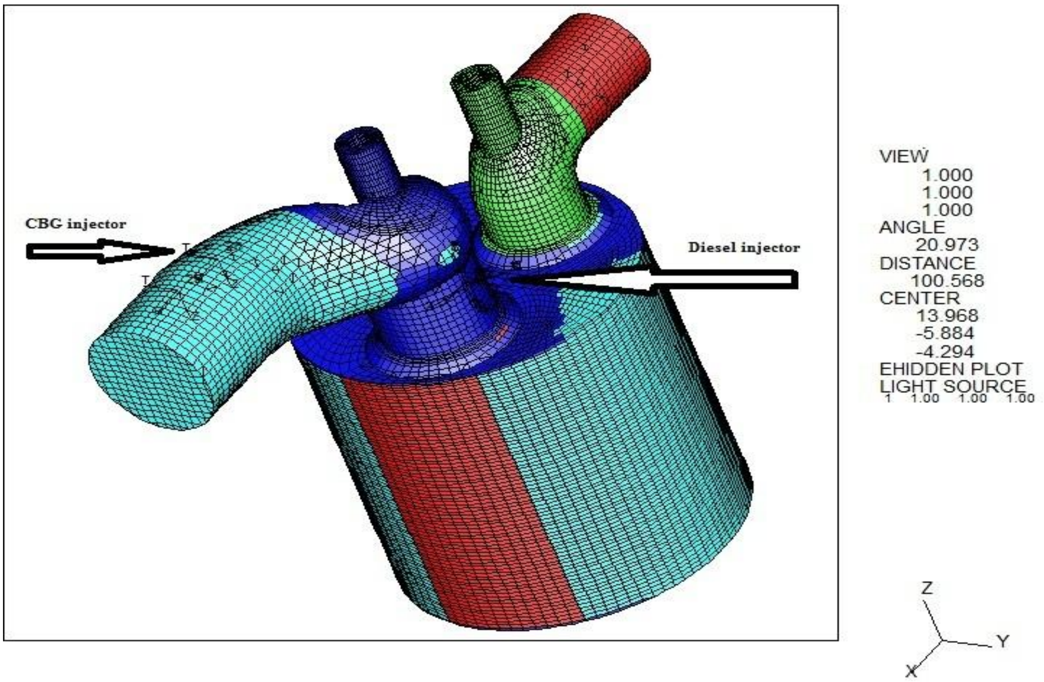

Figure 4.19. CBG and Diesel fuel injectors.

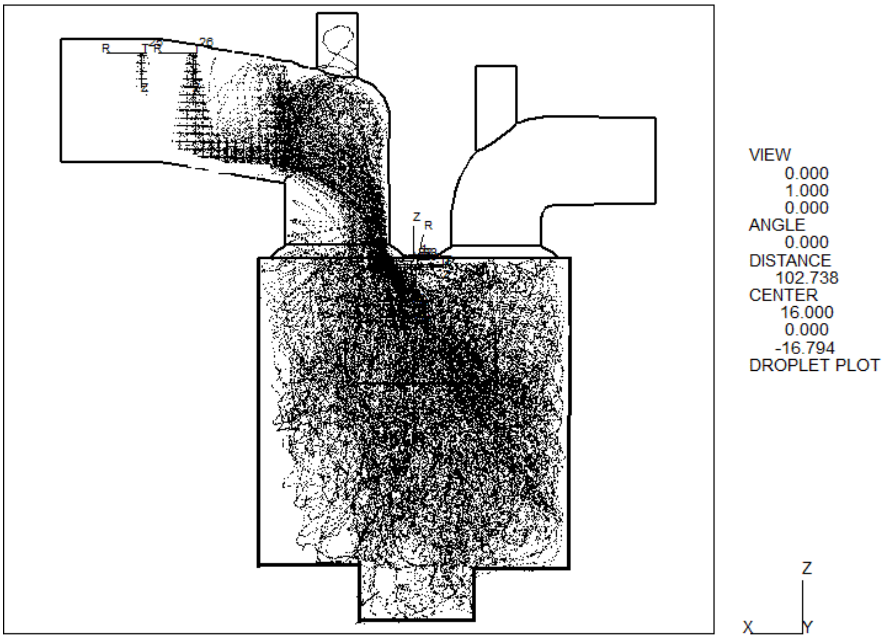

a) Droplet streaks view on the Y direction

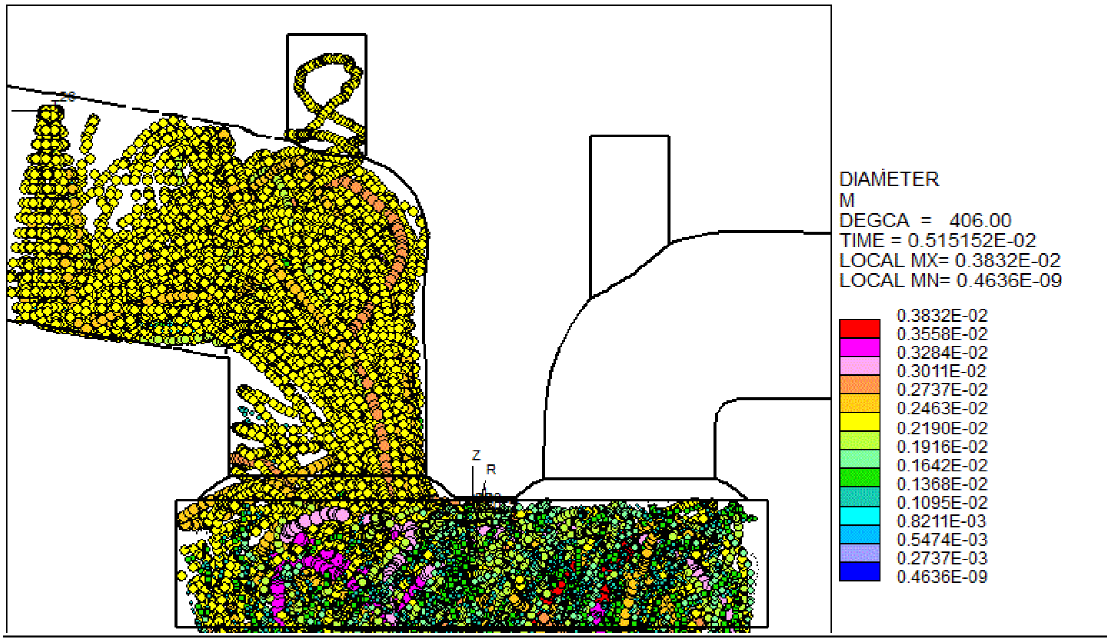

b) CBG fuel droplet diameters during intake stroke.

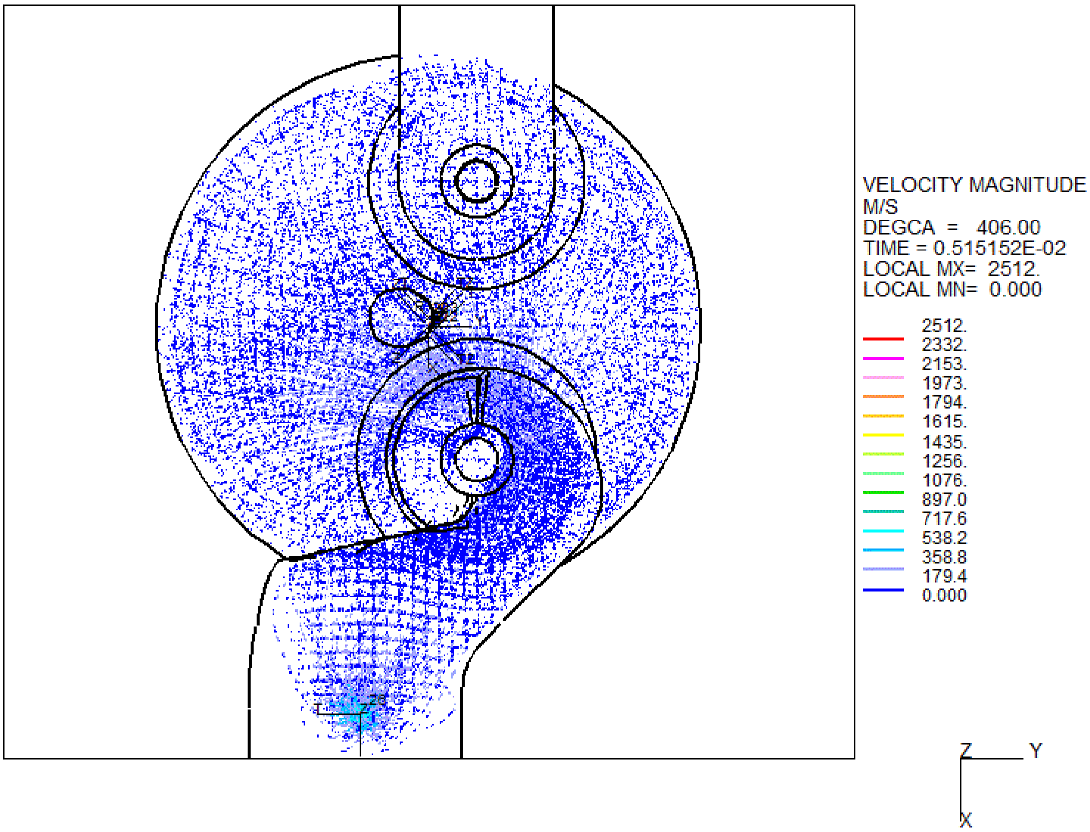

c) CBG fuel velocity magnitudes on the positive Z direction.

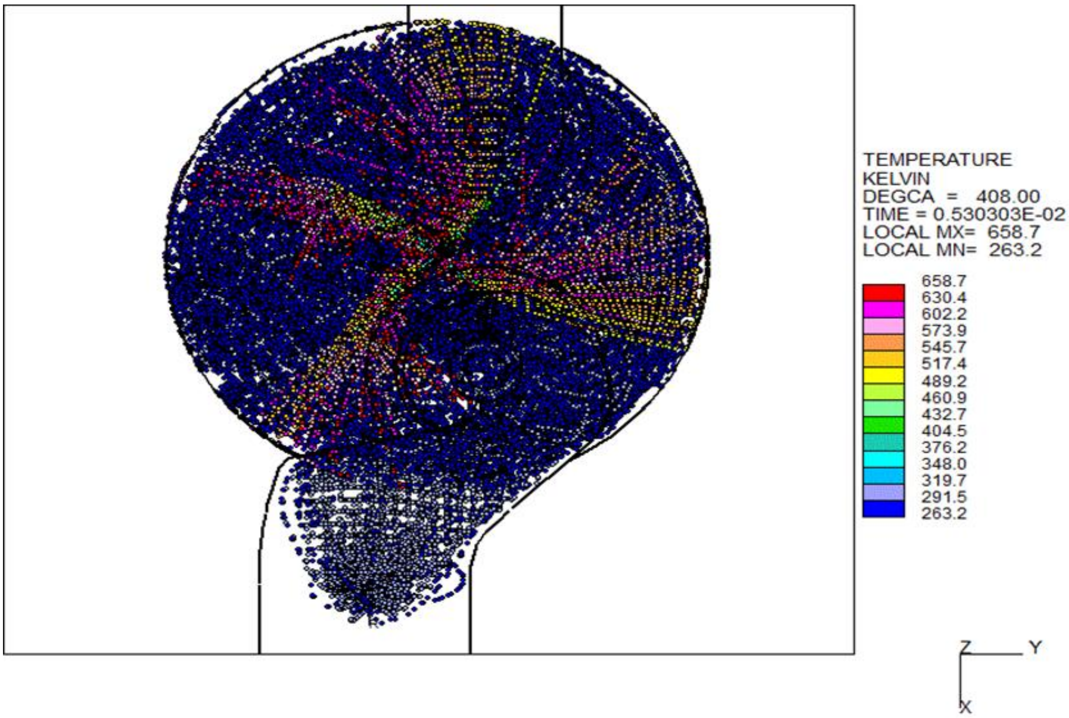

d) CBG fuel droplet temperature on the positive Z direction.

Figure 4.20. CBG fuel spray as a main fuel through intake port.

Pilot diesel fuel injector and main fuel CBG injector nozzles were defined with different spray cone angles to get exact combustion inside the combustion chamber. As can be seen from Fig. 4.20, spray and combustion simulation were performed by choosing proper parameters for single and dual fuel operations. Mass flow rate of pilot diesel fuel and main fuel CBG were separately calculated using multi-objective optimization code. Single fuel and dual fuel cases carried out in different engine loads. During the optimization process, mass flow rate of pilot diesel fuel was minimized with respect to engine load. Obtained mass flow rates for single and dual fuel cases were re-modeled and analyzed in CFD solver. Minimum mass flow rate for pilot diesel fuel was obtained in full engine load as seen in Fig. 4.21.

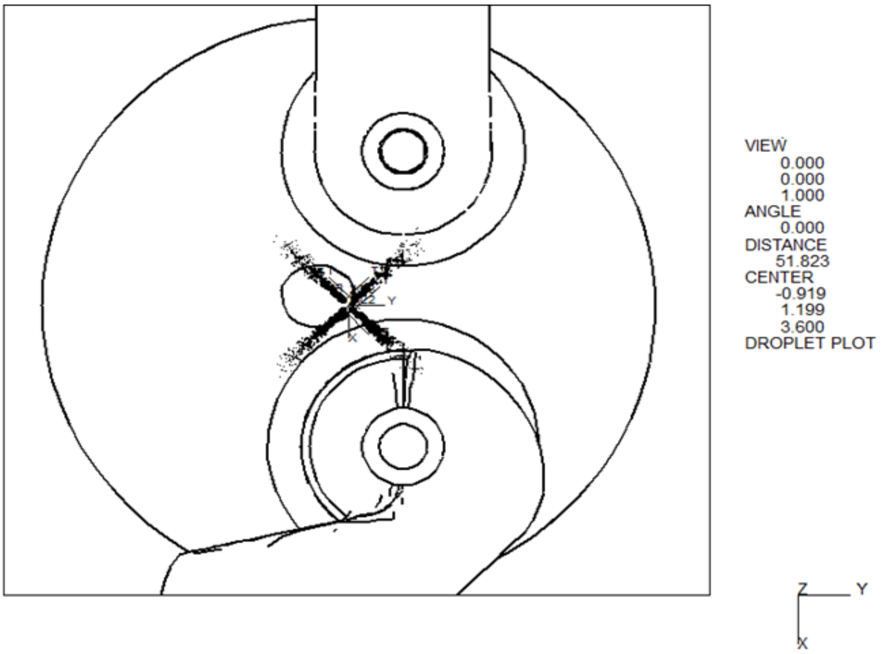

(a) Pilot diesel fuel at 20% engine load.

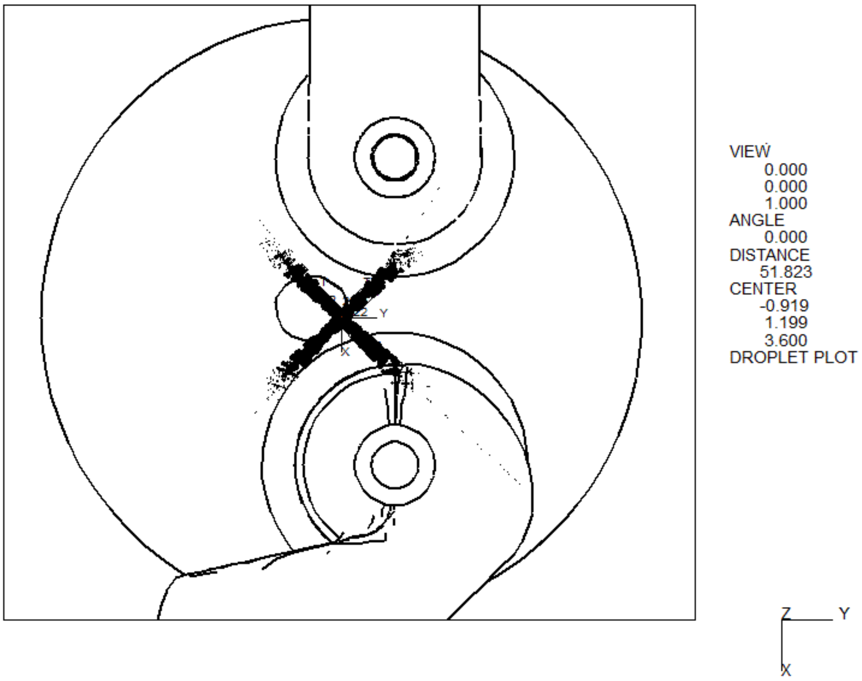

b) Pilot diesel fuel at 40% engine load.

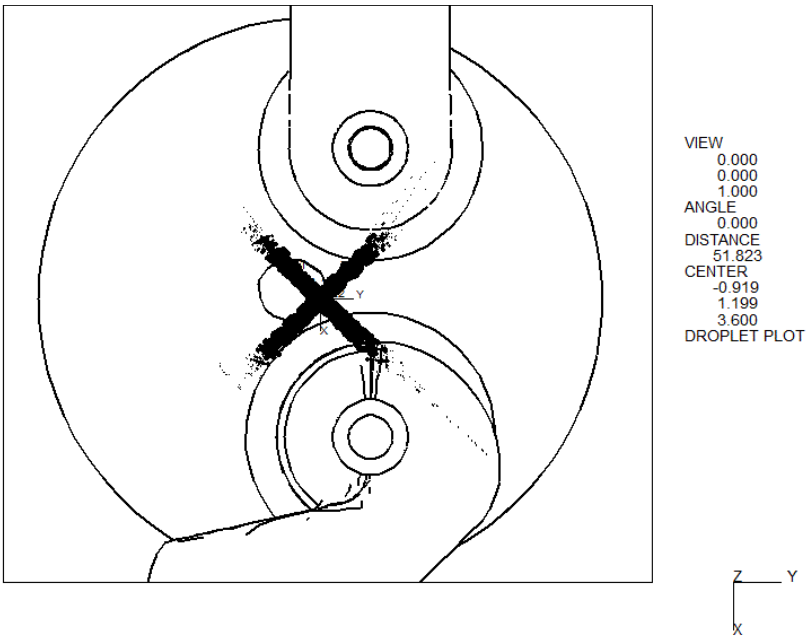

c) Pilot diesel fuel at 80% engine load.

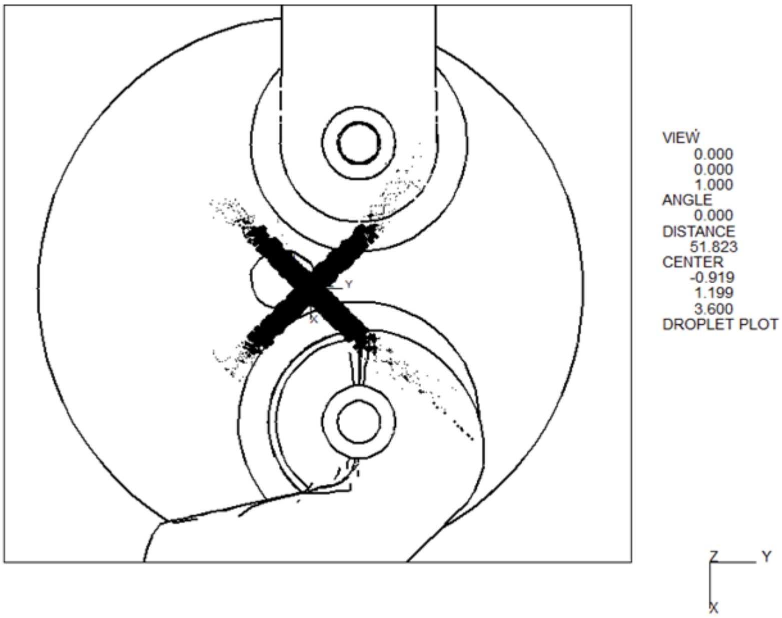

d) Pilot diesel fuel at 100% engine load.

Figure 4.21. Pilot diesel fuel in different engine loads.

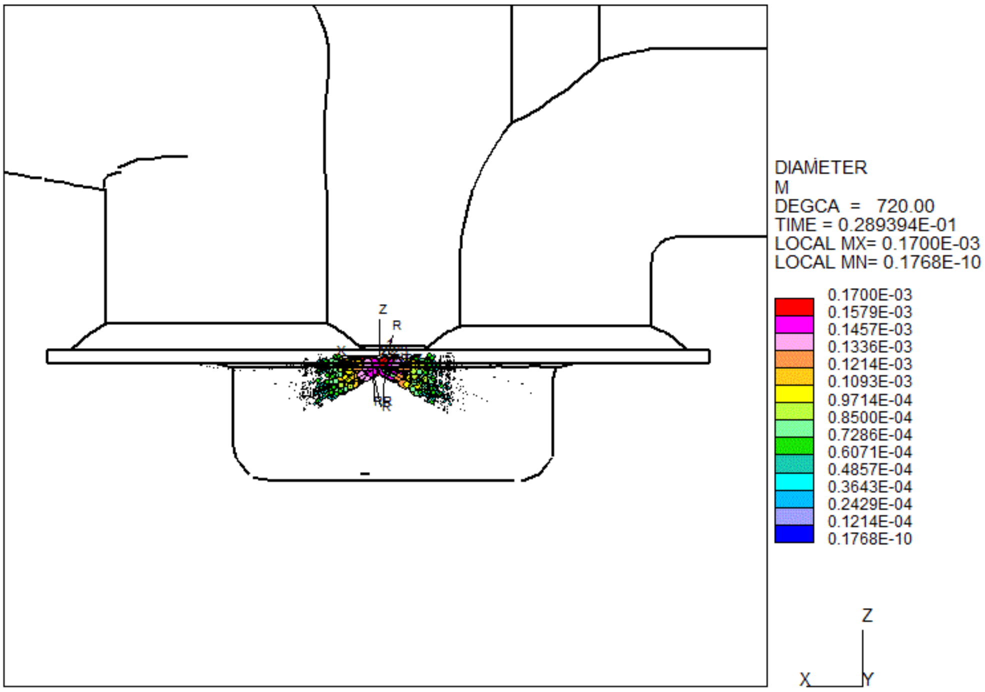

a) Pilot diesel fuel droplet diameters at 80% engine load in X direction.

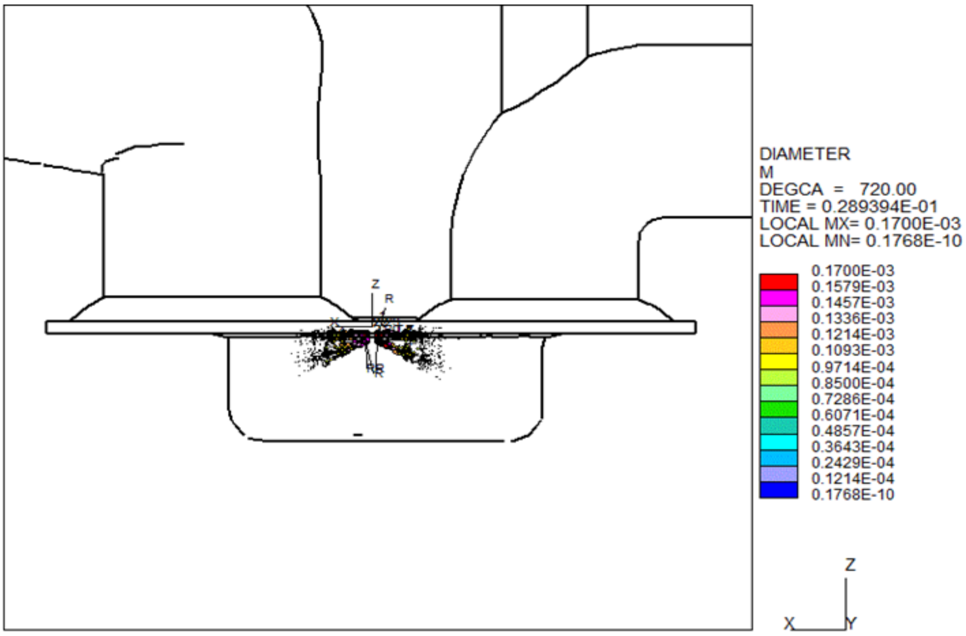

b) Pilot diesel fuel droplet diameters at 40% engine load in Y direction

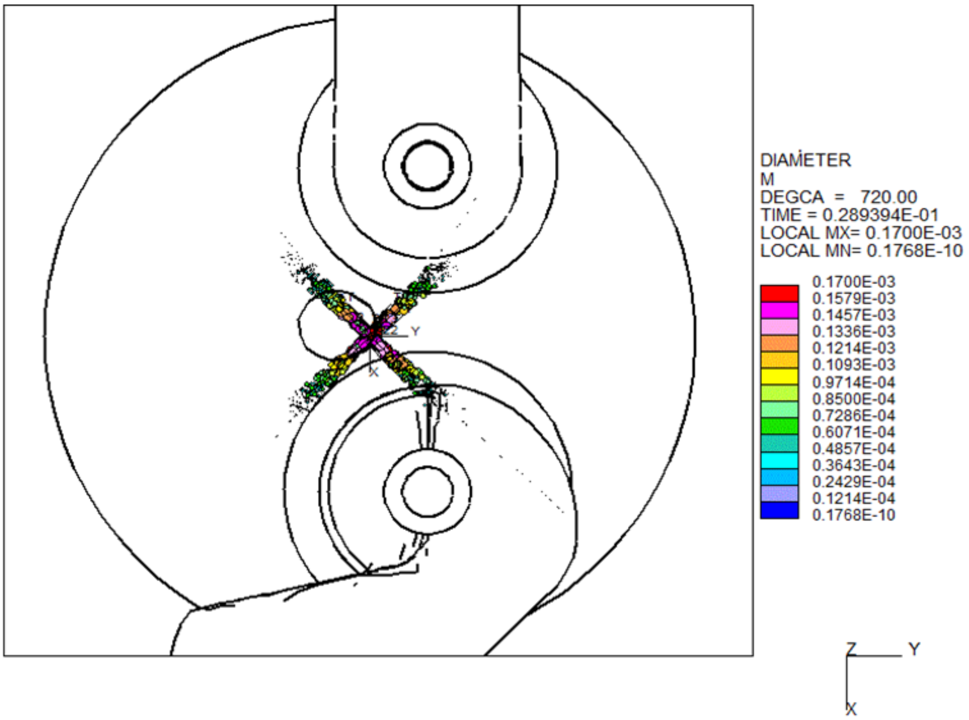

c) Pilot diesel fuel droplet diameters at 60% engine load in Z direction

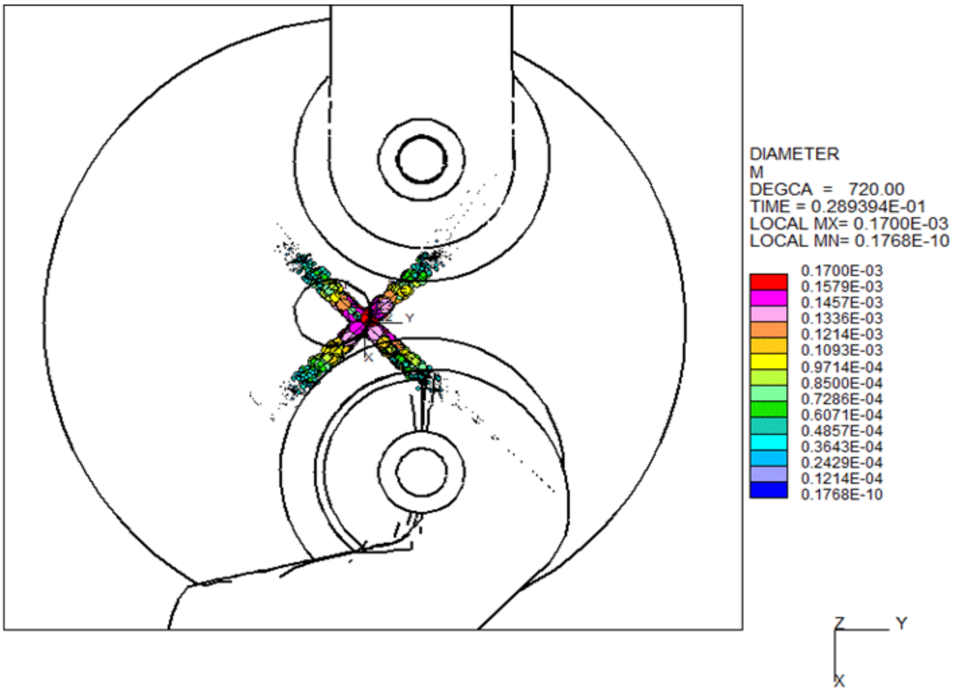

d) Pilot diesel fuel droplet diameters at 80% engine load in Z direction

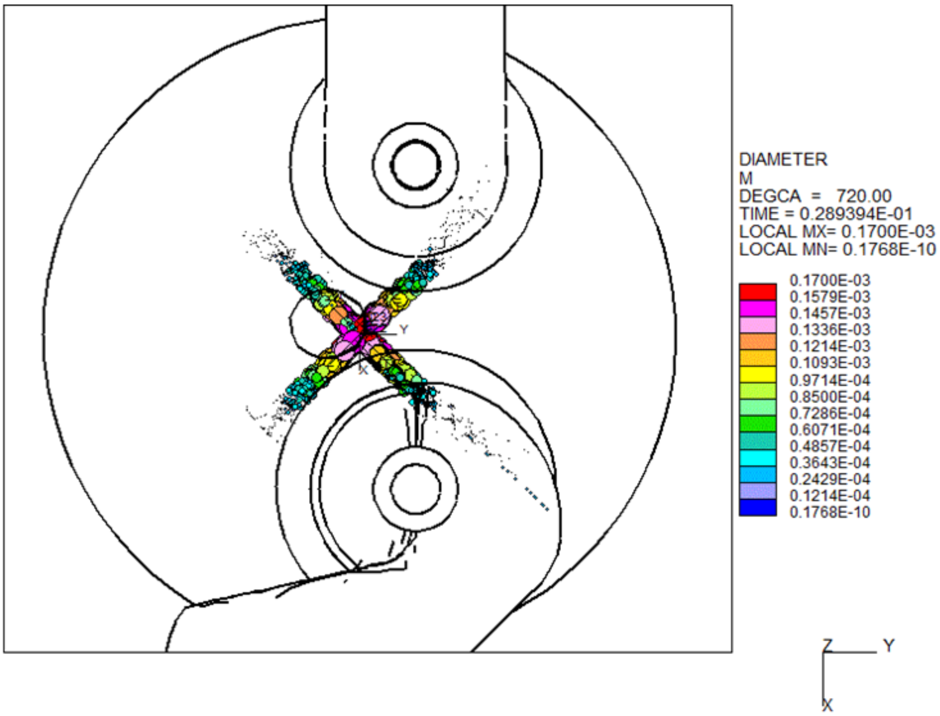

e) Pilot diesel fuel droplet diameters at 100% engine load in Z direction

Figure 4.22. Contours of droplet diameters for pilot diesel fuel in different engine load.

Fig. 4.21 shows the result of spray simulation in real engine geometry with four injection points on the injector. Fuel particles follow mainly the bowl shape and recirculation motion generated inside the bowl as can be seen in these figures. On the other hand Fig. 4.22 shows that the horizontal cross-section spray simulation was affected from the flow structure. In addition fuel consumption of diesel fuel was decreased especially in high engine load compared to the conventional single fuel diesel combustion. Detailed pilot diesel fuel spray simulations were given in Fig. 4.21 with different engine loads.

4.5 Combustion and Emission Results

In this study, both single diesel fuel combustion and dual fuel CBG-diesel combustion phenomenons were modeled via ECFM-3Z combustion model. CFD solver fully supports both binary mixtures of fuels such as gasoline-ethanol and dual fuel engine operation such as gas engine with diesel pilot using ECFM-3Z combustion model (Köten H., 2009).

In order to investigate the effect of CBG rate and dual fuel injection on the engine combustion performance and exhaust emissions, this work was carried out under the computational conditions listed in Table 3.12. Combustion performance and average gas temperature were calculated by using the heat release model based on the ideal gas equation. The result data presented in section were obtained from a single cylinder DI diesel engine with a displacement volume of 1461 cm^3. The engine was equipped with a common-rail fuel injection system turbo charger. The basic specifications are listed in Table 4.1.

Table 4.1. Engine specifications.

Bore [mm]	76.0
Stroke [mm]	80.5
Displacement volume [cc]	365,25
Number of Cylinders	4
Compression Ratio	18.25
Air intake	Turbo charged

Results reported in this section were investigated at the engine operating conditions of 2000 rpm and single fuel injection rate between 12 kg/hr. The detailed operating conditions are listed in Table 4.2. The 3D results of the SF case1 at the level of TDC were shown in Fig. 4.23 with a section that passes through the cylinder center.

Table 4.2. Operating conditions.

Engine speed	2000 rpm
Mass of fuel injection	12 kg/hr
Intake pressure	1.3 bar
Intake temperature	312 K

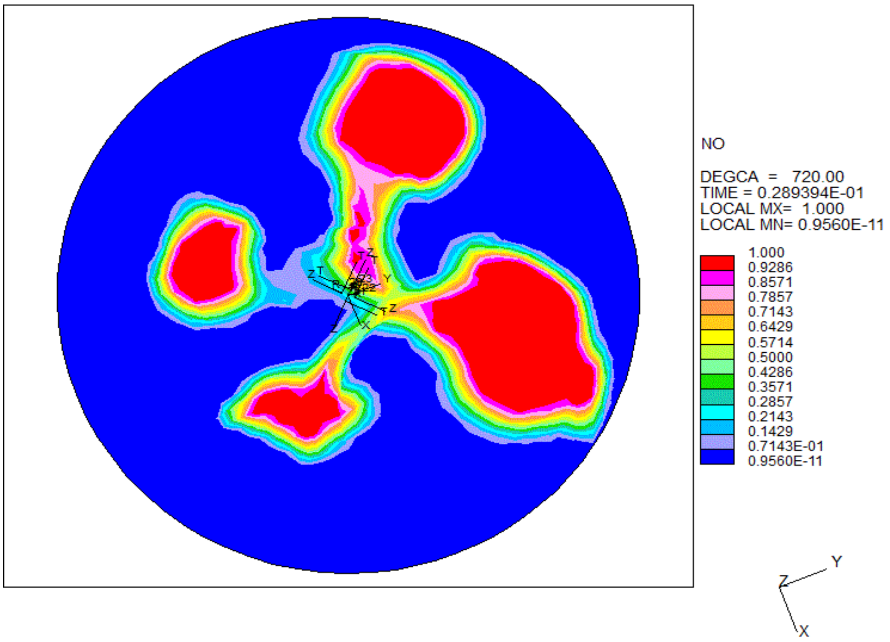

Figure 4.23. 3D NOx emission contours for SF case3 at TDC.

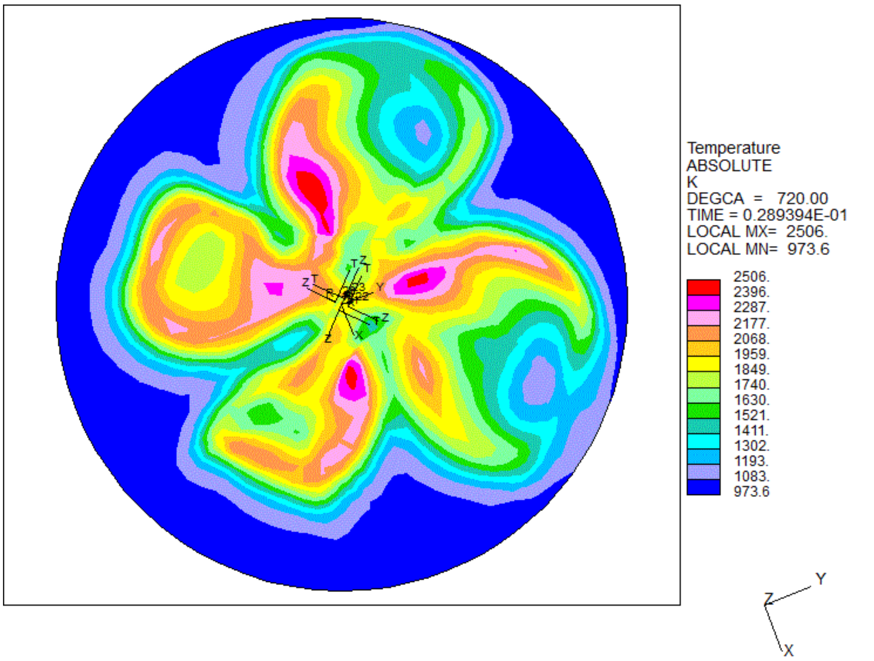

Figure 4.24. 3D Temperature contours for SF case3 at TDC in +Z direction.

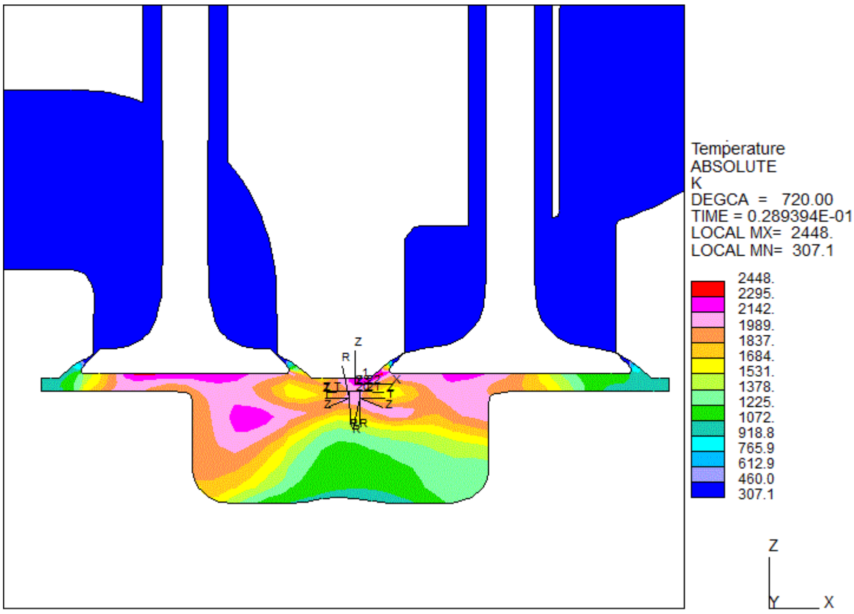

Figure 4.25. 3D NOx emission contours for SF case3 at TDC in +Y direction.

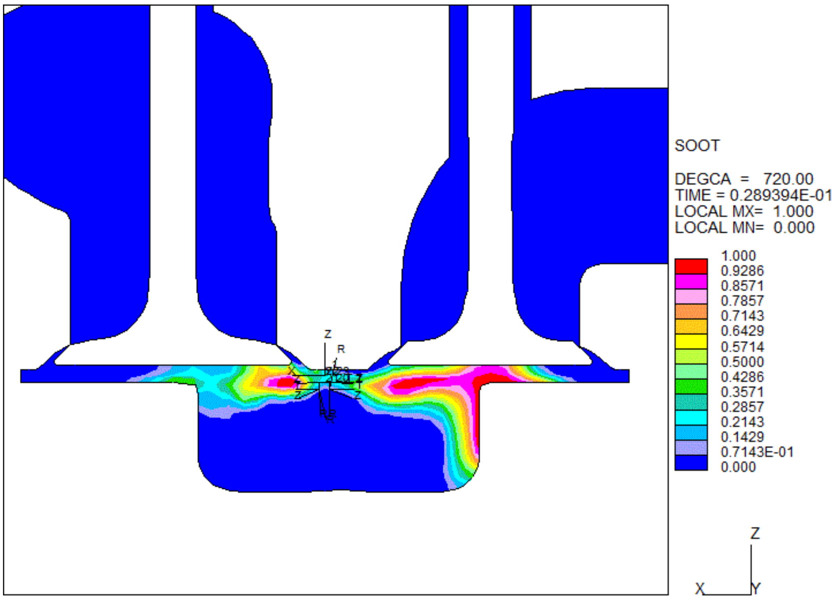

Figure 4.26. Soot emission contours for SF case3 at TDC.

Because of the shifting of combustion event to earlier side, this causes the increase of negative operating conditions for a conventional diesel engine. These trends are regarded as typical problems of injection strategies and injection rates that lower the thermal efficiency and increase the incomplete combustion products such as the HC and CO emissions ((Helmantel and Denbratt, 2004), (Lechner et al. 2005), (Kook and Bas, 2004), (Walter B, Gatellier, 2003), Shimazaki et al. 2003), (Mueller et al. 2004), Kim et al. 2004, 2005), (Neely et al. 2004), (Pekalski et al. 2002), (Shibata et al. 2005)).

Table 4.3. Case studies.

Case #	CBG rate kg/hr	Diesel fuel kg/hr	Engine load %	SOI CA
SF Case1	-	2,12	20	-12
SF Case2	-	3,13	40	-12
SF Case3	-	5,22	60	-12
SF Case4	-	8,54	80	-12
SF Case5	-	11,44	100	-12
DF Case1	2,27	1,62	20	-12
DF Case2	2,33	2,63	40	-12
DF Case3	2,61	4,37	60	-12
DF Case4	2,76	6,48	80	-12
DF Case5	3,25	7,88	100	-12

The effects of the engine load and dual fuel combustion mode on the NOx emissions with different engine configurations were shown in Fig. 4.25. NOx emissions showed a strong dependence on the type of combustion at constant injection timing. The peaks of the NOx emissions occurred on the single fuel cases as typical of the operating conditions of a conventional diesel engine. As the CBG rate was increased, the magnitude of the NOx emissions fell near to nearly undetectable levels. At these early dual fuel cases, it was shown that the ignition delays were greatly prolonged and an adequately premixed fuel/air mixture was formed before ignition. Therefore, a lean mixture was burned at a high temperature in single fuel combustion. As a result, low NOx emissions were achieved in the dual fuel combustion processes. The case studies as listed in the Table 4.3.

1D, 3D and multi-objective optimization codes were employed for single diesel fuel (Dodecane) and dual fuel (CBG-diesel) cases. For both single fuel and dual fuel, Case1, Case2, Case3, Case4 and Case5 were investigated at 20%, 40%, 60%, 80% and 100% engine loads, respectively. The combustion pressures and rates of heat release (ROHR) for the single-fuel mode with diesel fuel in a constant engine speed of 2000 (rev/min) were provided in Fig. 4.27 (a) and Fig. 4.27 (b). The figures showed similar patterns for combustion pressure and ROHR at different engine loads. The combustion pressures and ROHRs increased for both fuels, since engine load increased at constant engine speed. At low engine load condition (20%), the peak values of combustion pressure and also heat release were slightly lower than other cases as depicted in Fig. 4.27 (a). The lower diesel fuel consumption (Dodecane-2.14 kg/h) caused the reduction on the combustion performance. When it came to the 60% load, shown in Fig. 4.27 (a), the diesel combustion showed slightly higher peak combustion pressure (Pmax = 8.4 MPa) and peak heat release compared to CBG-diesel case (Pmax = 8.3 MPa). Simultaneously, a greater indicated mean effective pressure (IMEP) was obtained for single fuel diesel injected fuel mass reached 5.3 kg/h.

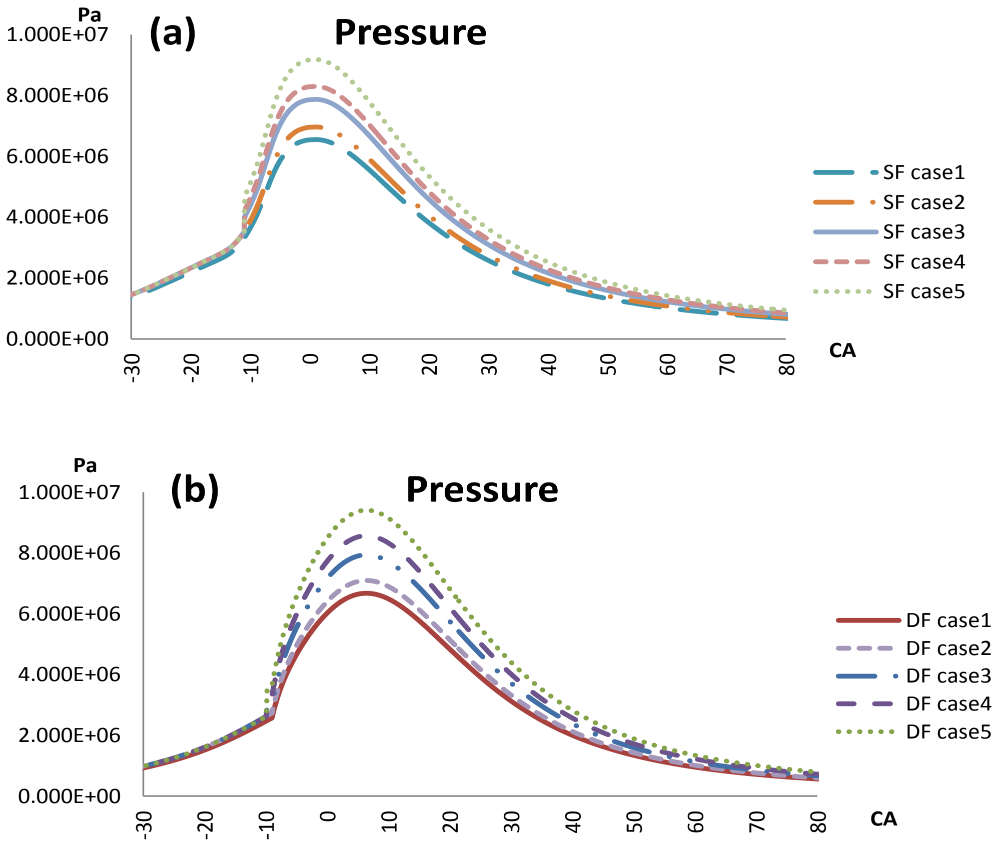

Figure 4.27. Combustion characteristics at different engine load. (a) Single fuel (Dodecane) cases. (b) Dual fuel (CBG-Dodecane) cases.

However, when compared to start of ignition ability at different engine loads, it was really observed that single fuel diesel combustion exhibited a slightly shorter ignition delay. Generally, short mixture preparation time results in shorter ignition delay. The ignition ability in a diesel engine is mainly relying on caffeine and physical fuel properties such as structure of fuel composition, density, bulk module, cetane number, oxygen content, and aromatic content of the fuel (Yoon and Lee, 2011). The high cetane number, reduced stoichiometric air requirement and the excess oxygen content of air fuel mixture play an important role in short ignition delays for diesel combustion. Effects of dual-fuel and single fuel combustion on the ROHR were shown in Fig. 4.28 at 60% engine load. In order to investigate the effect of CBG, amount of CBG fuel was changed relating to engine load. Furthermore, fuel mass for pilot fuel was optimized and SOI was adjusted with respect to engine loads in a constant speed of 2000 rpm.

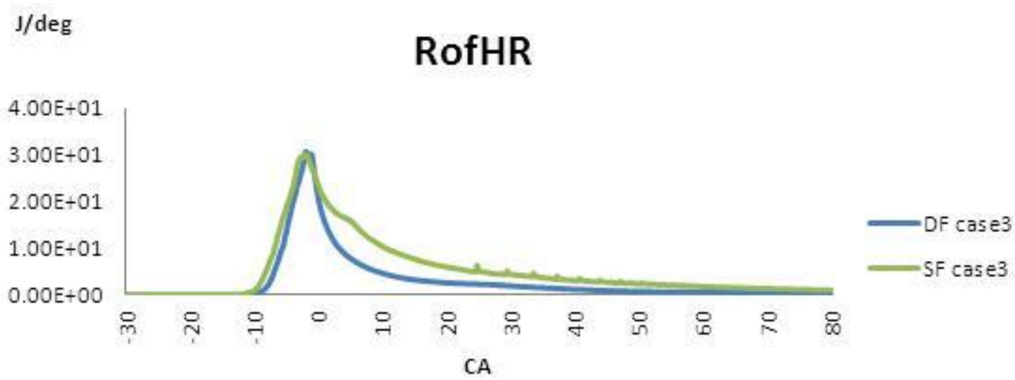

Figure 4.28. Effect of fuel types on rate of heat release inside cylinder at 60% engine load.

As shown in figures, the peak combustion pressure and heat release for CBG-diesel dual-fuel combustion are slightly lower compared to single fuel diesel combustion. In 60% engine load, diesel fuel combustion showed slightly higher peak combustion pressure (Pmax = 8.55 MPa) and ROHR. Also, ignition delay for single fuel combustion cases indicated shortened trends in comparison with CBG-diesel dual fuel cases under all engine loads. In addition, fuel properties of Dodecane which has long carbon chain played important role in short ignition delay. It is observed that dual fuel and higher CBG fuel concentration increased the ignition delay.

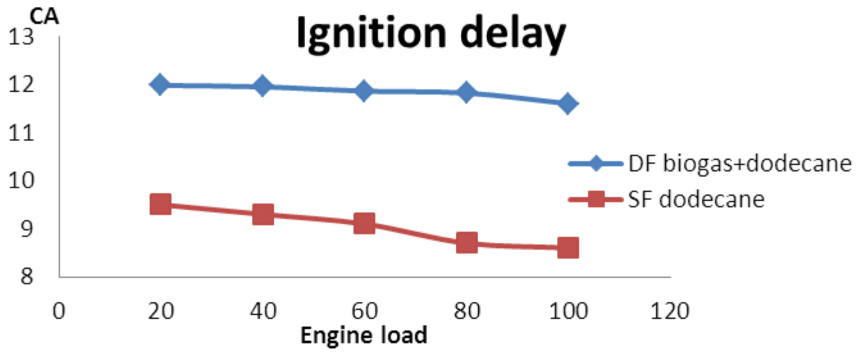

Figure 4.29. Effect of single and dual fuel combustion mode on the ignition delay.

For dual-fuel combustion, combustion durations took a long time considerably as well as the increase of pilot and CBG fuel consumption with the increase in engine load with respect to single-fuel combustion mode. These results could be explained by the reduction of oxygen concentration along with the pre-ignition with the ingestion of CBG fuel which caused the deteriorated combustion process and prolonged combustion durations. Moreover, CBG fuel caused slower burning rate, resulting in lengthened combustion durations. Especially, single diesel fuel combustion durations were relatively shorter than other fuel operations due to the difference in cetane number which actively promoted the combustion phase (Yoon and Lee, 2011).

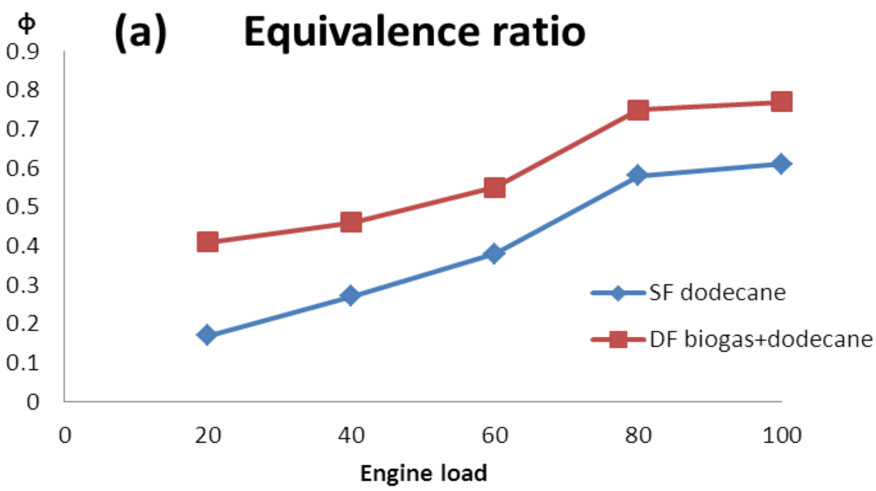

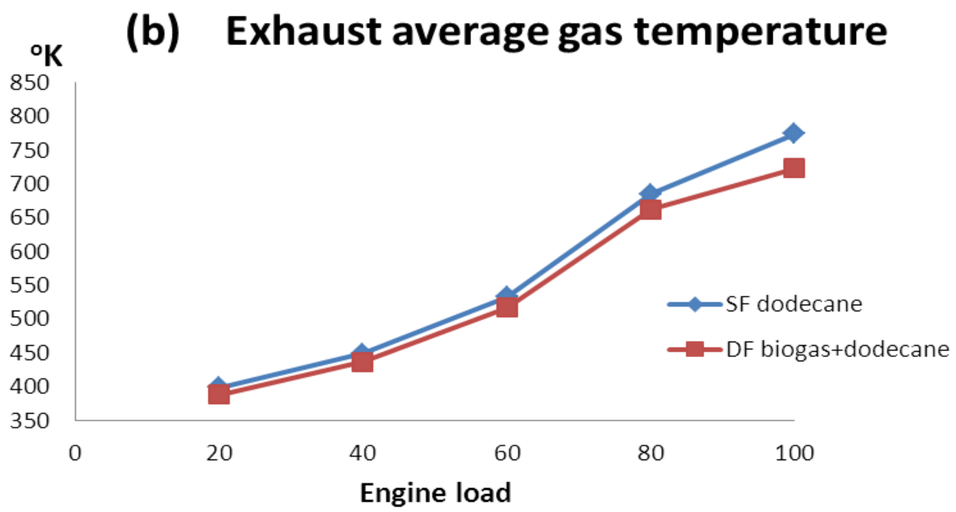

Figure 4.30. Effects of combustion on exhaust gas temperature and equivalence ratio.

Equivalence ratio and exhaust gas temperature results were shown in Fig. 4.30 (a) with the variation in engine load. Dual-fuel combustion cases had higher fuel-air equivalence ratios compared to the single-fuel cases. These results were mainly due to the supplied CBG fuel which combined and replaced with fresh air during the intake process. Furthermore, engine required more fuel to fulfill the imposed engine load-speed condition as engine load was increased and consequently more gaseous fuels need to be injected into the combustion chamber. The relationships between the variation of engine load and exhaust gas temperatures for the all fuel modes were provided in Fig. 4.30 (b). According to figures, as the engine load increased exhaust gas temperature seemed linearly increased tendency due to the increase in total energy input. In addition, the for dual-fuel combustions exhaust gas temperatures were slightly lower than single-fuel modes and these differences increased at high engine loads. The difference in exhaust gas temperature could be explained by decreasing charge temperature with CBG ingestion and the delaying combustion phase (Yoon and Lee, 2011). Combustion process shifted and retarded to the expansion stroke due to the prolonged ignition delay for dual-fuel cases. These properties caused lower exhaust gas temperature. In this project, single and dual-fuel combustion performances were also analyzed by means of fuel consumption rate. In the dual-fuel combustion mode, the gaseous fuel (CBG) flow rate and the liquid pilot fuel flow is optimized. The effects of combustion mode and engine load on fuel consumption were shown in Fig. 4.31. In dual-fuel cases, fuel consumption was illustrated for just usage of pilot fuel (Dodecane) in Fig. 4.31.

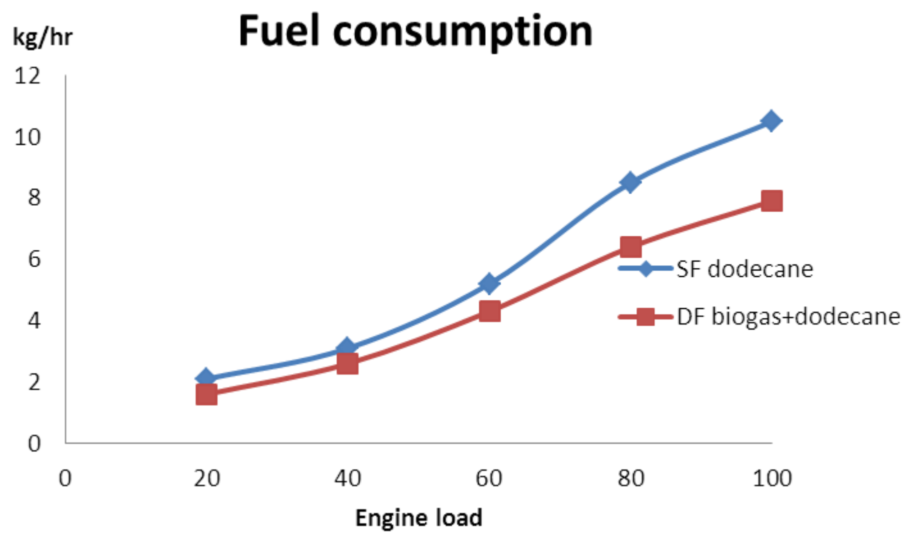

Figure 4.31. Effect of dual fuel combustion mode on fuel consumption versus engine load.

The concentrations of NOx and soot emissions for the engine operated with single and dual-fuel combustion modes were shown in Fig. 4.32 (a) and (b), respectively. In Fig. 4.32 (a), when the engine load increased, NOx concentrations of all test cases increased steeply. Significantly lower NOx emissions were emitted within the dual-fuel operations compared to the single mode at all conducted test ranges. In Fig. 4.32 (a), single fuel diesel combustion cases resulted in higher NOx emissions at all engine loads compared to dual fuel cases. The reason behind this trend could be explained by the faster injection and early ignition characteristics of diesel which are visible in previous outcomes of combustion characteristics.

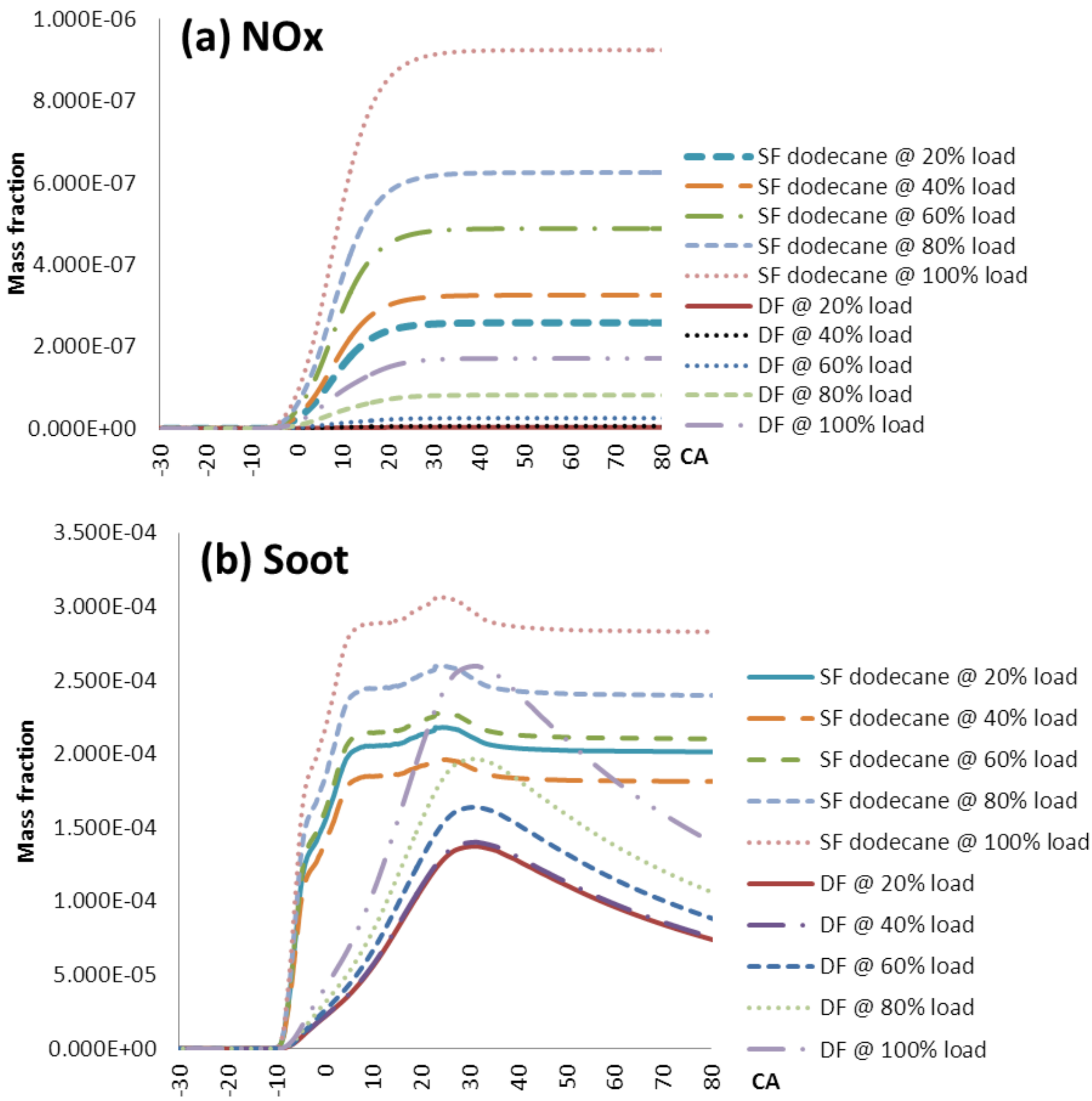

Figure 4.32. NOx and Soot emissions for single and dual fuel cases versus CA. (a) NOx emissions. (b) Soot emissions.

As shown in Fig. 4.32 (b), soot emissions for dual-fuel operations were significantly lower than single-fuel modes. CBG-diesel combustion cases exhibited superior performance in reduction of soot emissions. In soot emissions, this considerable reduction might be caused by the properties of the absence of aromatics which are precursors of soot emissions (Yoon and Lee, 2011). In addition, CBG fuel normally needs a lower stoichiometric air which allows complete combustion than Dodecane although the oxygen concentration is decreased through the ingestion of CBG. Excess oxygen in single fuel which promotes more complete combustion played active role in reduction soot formation and increase the oxidation in the soot emission throughout the combustion process. Furthermore, CBG includes no sulfur content and replaced a fraction of liquid fuel and reduced the injected fuel of Dodecane in the case of dual-fuel combustion.

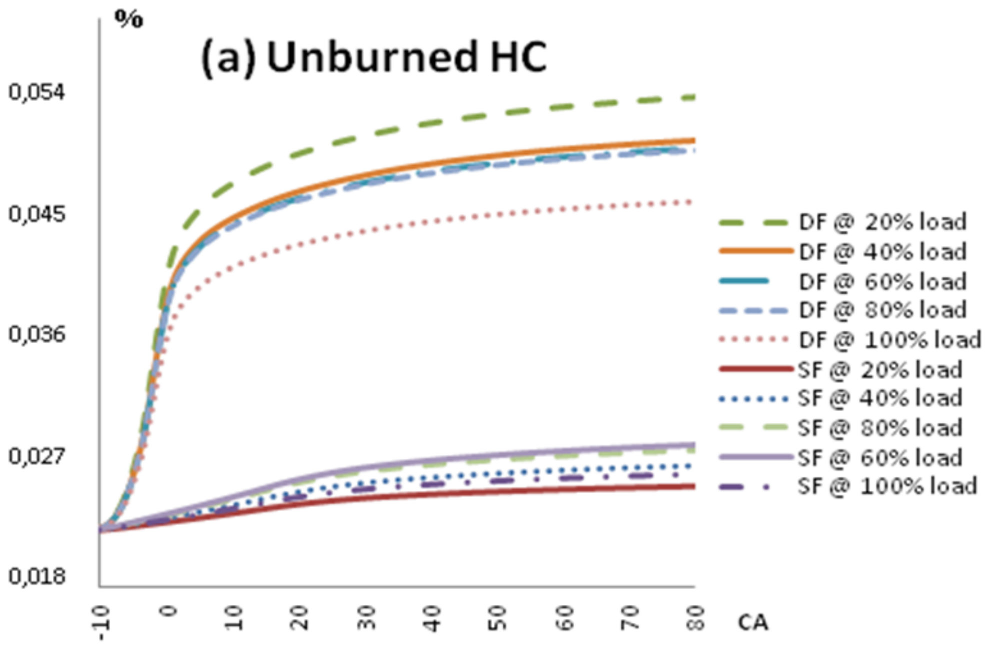

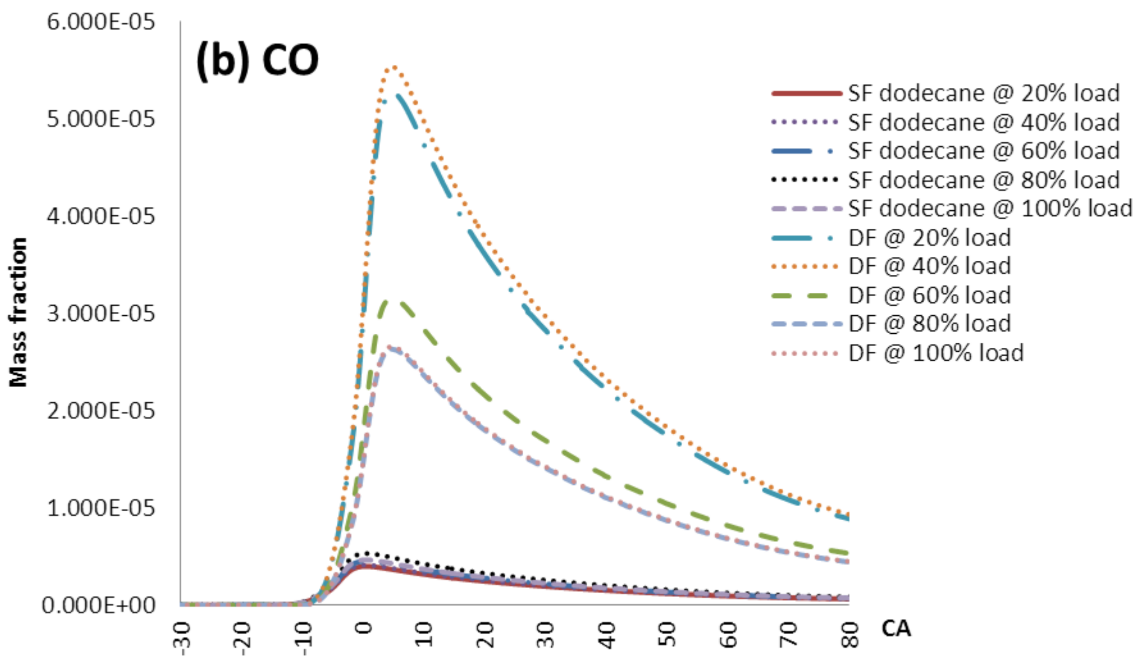

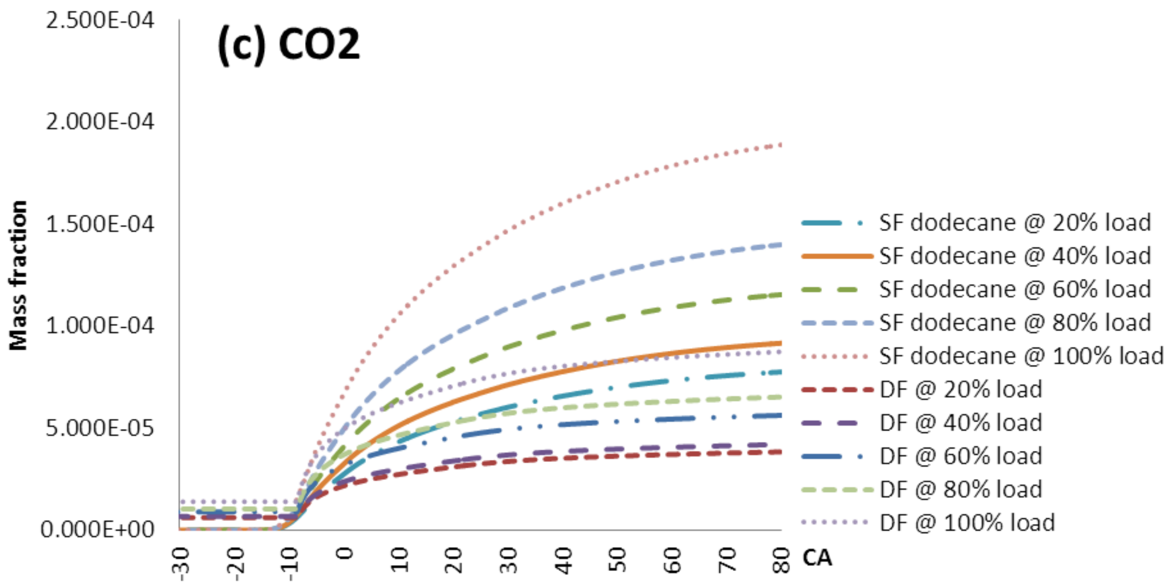

Figure 4.33. Exhaust emissions for single and dual fuel cases with different engine loads.

CO2, HC and CO concentrations were shown in Fig. 4.33 (a), (b) and (c) for single and dual fuel cases at various engine loads. As shown in these figures, the concentrations of CO2 emissions for dual fuel were obviously under those regarding single diesel combustion modes. Moreover, higher cetane number of diesel and the faster injection timing shortened the ignition delay and this reduction is related to a decrease in fuel-rich zone throughout the combustion process. When single and dual-fuel combustions were compared, the concentrations of HC and CO emissions for the single-fuel mode were considerably lower than dual-fuel mode under all test conditions. CBG-air mixture needs to reach the specific temperature value to continue the flame propagation in the combustion region. CO emissions for single fuel combustion emitted somewhat lower and roughly constant amounts of soot in comparison to dual fuel combustion.

4.6 Optimization Results

4.6.1 Final simulation

In final simulation, compression ratio of simulated engine was reduced from 18.25:1 to 17.6:1by widened engine bore diameter to keep more heat inside the cylinder due to the lower heating value of CBG fuel. According to optimization results, larger and smaller valve overlapped engines more suitable for CBG-Diesel dual fuel combustion. Because of the surface to volume ratio effect on combustion temperature, heavy duty dual fueled CI engines have better results combustion performance and unburned HC emissions than light duty dual fueled CI engines. Real engine geometry cases are low thermal efficiency due to the valve overlap characteristics of conventional diesel engines. Valve overlap process facilitates scavenging between the intake and exhaust valves. However, in dual fuel combustion, valve overlapping caused an increase in unburned HC emissions due to leaving of unburned CBG-Diesel air fuel mixture from cylinder. At the same time, low valve overlap for dual fuel CI engine caused incomplete combustion inside the combustion chamber due to the insufficient scavenging process. Valve overlap values also were optimized in final CFD simulation. Because of compression ratio effects on temperature and pressure during the compression phase, the engine compression ratio has an influence on the auto-ignition phase of the combustion: a reduction prolongs the air/fuel mixing process before combustion. In optimization study, compression ratio was limited in 19:1 due to the knock phenomenon during the compression stroke of CBG-air mixture. Higher compression ratio resulted lower power due to the auto-ignition of air fuel mixture. Different works (Gatellier et al., 2006, Ranini et al., 2002, Chauvin et al., 2006, Albrecht et al., 2006) studied on experimental single cylinder engines showed this significant advantage. Another optimization parameter is SOI for modified dual fuel engine geometry. In dual fuel modified engine geometry cases, SOI was reduced about 18^{o} CA bTDC by optimization study due to the late ignition delay of CBG-air fuel mixture. Single fuel cases have low ignition delay compared to that of the CBG-Diesel dual fuel combustion as seen in ignition delay figure. In single fuel cases diesel fuel has higher cetane number and this is allowed faster combustion than dual fuel engine cases. Optimized dual fuel engine cases resulted better combustion performance by changing SOI, compression ratio, modified engine size and valve overlap values.

Table 4.4. Specification of modified dual fuel combustion chamber.

Engine type	Single cylinder direct injection diesel engine
Engine speed	2000 RPM
Valves per cylinder	2
Bore	86 mm
Stroke	76 mm
Injection system	Common-rail
Number of nozzle holes	4
Nozzle diameter	0.170 mm
Valve overlapping	39 CAD and 19 CAD
Compression ratio	17.6
Start of injection	18 CAD bTDC

The peaks of pressure and temperature values occurred in DF case6 and DF case7 cases which have lower valve overlap, 19^{o} CA. Therefore, these two cases have indicated that the high temperature reaction (HTR) occurs at around 1200–1300 K. Calculated peak gas temperature for reduced valve overlap cases as shown in Fig. 4.34 (a) was 1790 K such as conventional single fuel diesel combustion, also these cases have lower CO formation and slightly higher NOx formation but quite under acceptable emission standards.

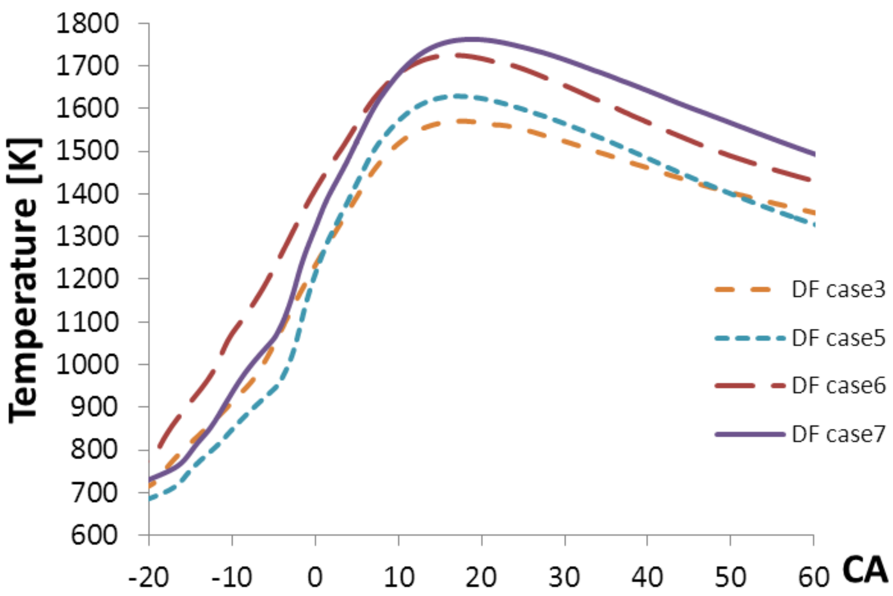

a) In-cylinder calculated temperature

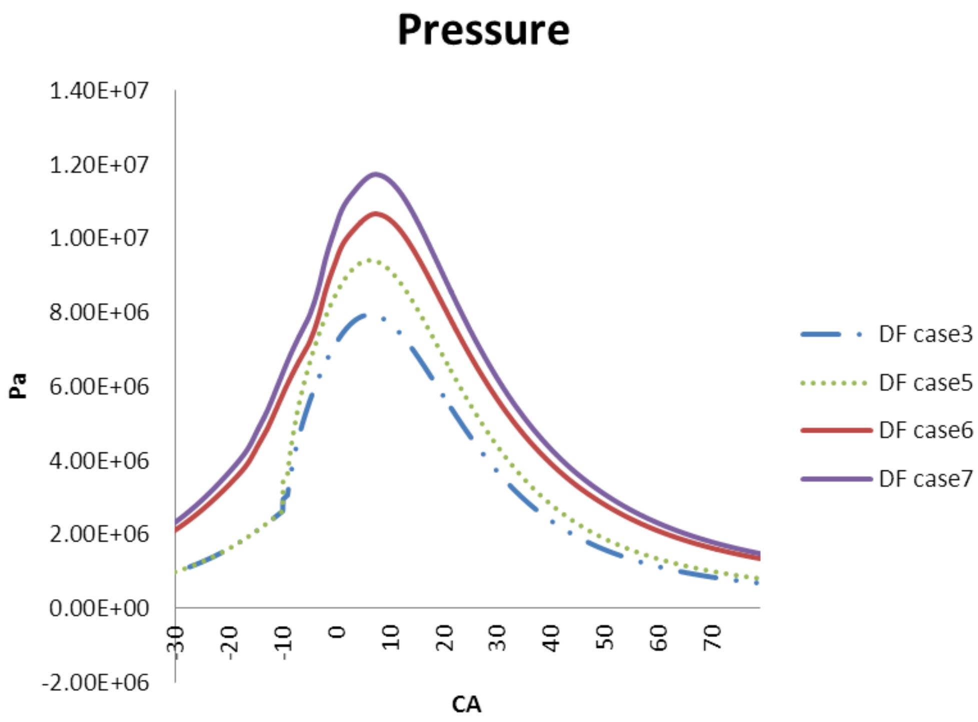

b) In-cylinder calculated pressure

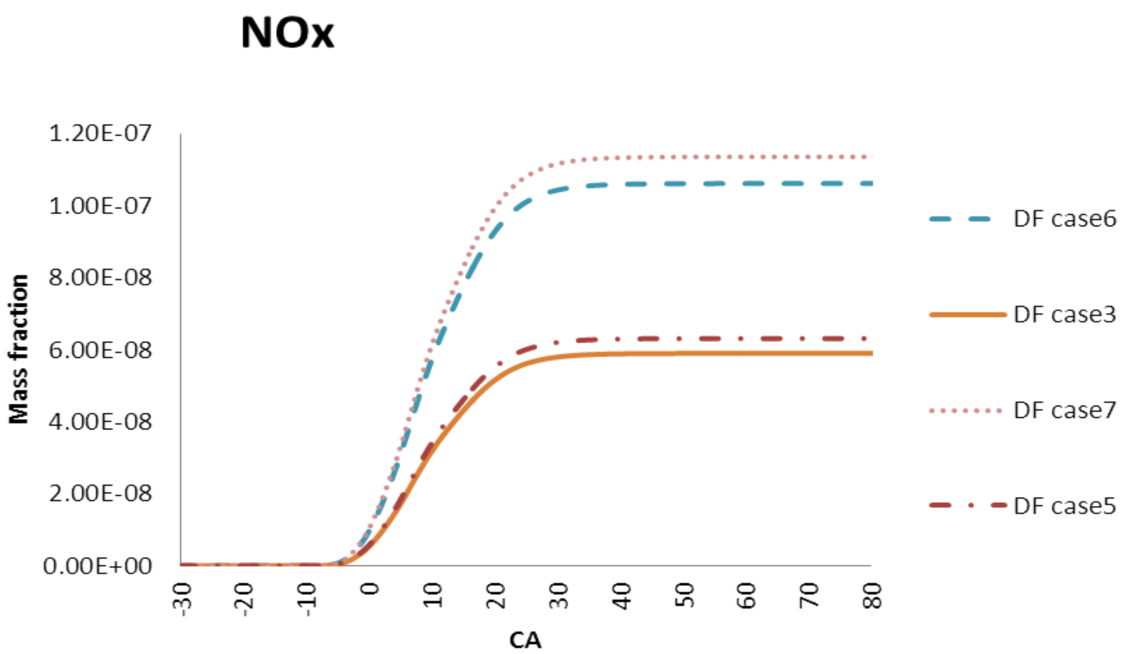

c) NOx emissions

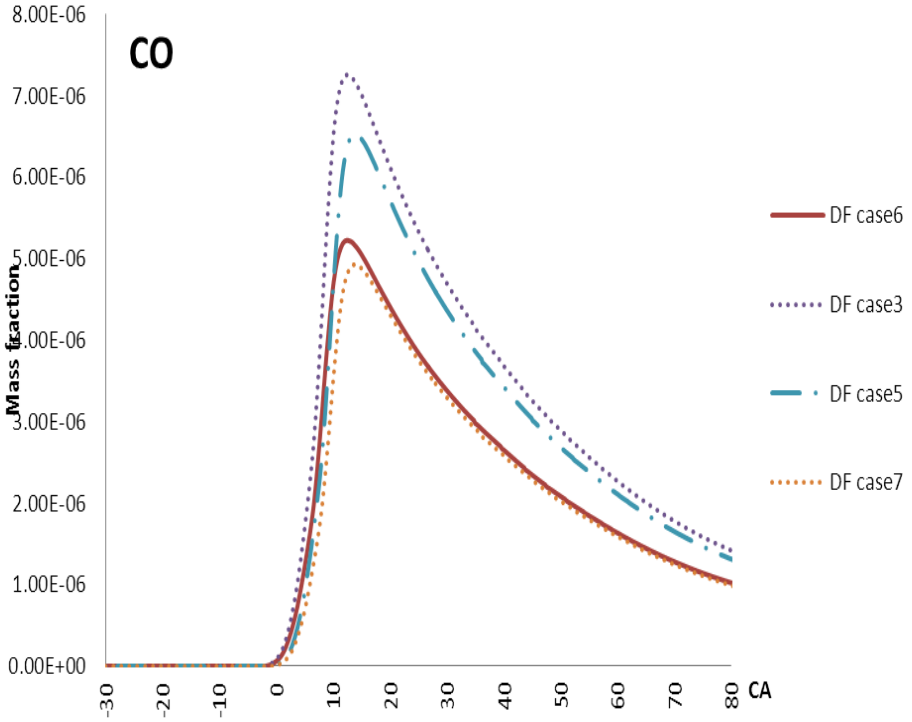

d) CO emissions

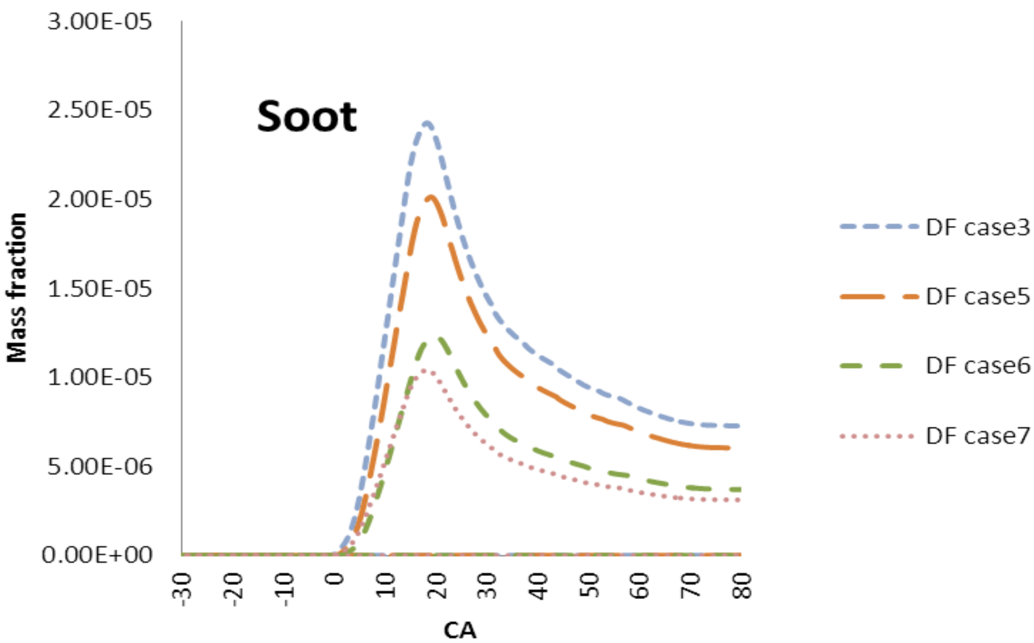

e) soot emissions

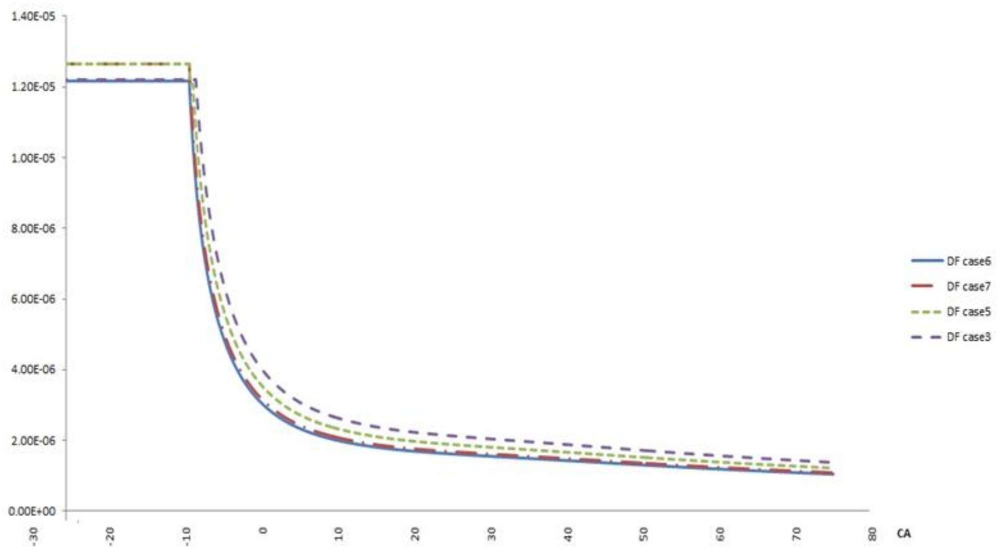

f) Total fuel mass.

Figure 4.34. Effects of valve timing on the dual fuel combustion performance.

As the valve overlap reduced, the peaks of heat release in-cylinder pressure and temperature rapidly increased and the initiating timings of the reaction were also fastened. In real engine geometry cases, the ignition delay was very long and ignition had begun very late after pilot started at 12^{o} bTDC. After SOI started at 18^{o} bTDC and valve overlap reduced to 19^{o} CA in optimization study, this led to significant development in engine performance and better combustion control during combustion for CBG-Diesel dual fuel cases. In addition to engine performance development, CO emissions were decreased very low levels by means of exact combustion. NOx emissions resulted higher for DF case6 and DF case7 than other DF cases, but these NOx emission values are very low in regard to EURO VI emission levels. Similarly, Soot emissions resulted better for optimized DF case6 and DF case7 than other DF cases and kept in a reduction trend. Furthermore, it can be said that CBG fuel was burned effectively in regard to other cases (Fig. 4.34 f) especially for DF case7 which has 19^{o} CA valve overlap value. Beside valve overlap value, optimization results showed that larger CI engines which have big surface to volume ratio have better combustion performance according to light duty CI engines. It can be concluded that, CBG-Diesel dual fuel process with these optimization parameters more proper for heavy duty CI engines.

5 CONCLUDING REMARKS AND RECOMMENDATIONS

5.1 Conclusion

The combustion performance and characteristics of exhaust emissions were investigated for a CI engine fueled with diesel fuel and CBG fuel under various operating conditions to find out the effects of the dual-fuel combustion. The combustion characteristics of diesel (Dodecane) single-fuel and CBG-diesel (Dodecane) combustion for 1D and 3D had similar combustion characteristics at various engine loads. CBG and diesel fuels were defined as leading reactants by writing user defined code. In dual-fuel combustion, the peak pressure and ROHR for CBG-diesel dual-fuel were slightly under that relating to Dodecane diesel fuel combustion. CBG-diesel dual fuel combustion showed slightly lower peak ROHR than single-fuel diesel combustion. Also, the ignition delay for single- fuel combustion indicated shortened trends in comparison with CBG-diesel dual fueling due to the high cetane number of diesel fuel.

The ignition delay for dual-fuel cases took a long time with respect to single-fuel cases due to the decrease in charge temperature of CBG air mixture and high overall specific heat capacity of CBG. Particularly, single-fuel combustion cases were slightly shorter compared to dual-fuel cases under all test conditions due to the short ignition delay, the high cetane number and also the excess oxygen of mixture. In dual fuel combustion cases, exhaust gas temperatures were slightly lower compared to single-fuel cases. Low gas temperature was obtained as a result of the delayed combustion process and decreased charge temperature with CBG fuel ingestion during the intake process. At high engine loads (case4 and case5), the increase of CBG conversion into work generated a large improvement of the total BSFC. At low engine loads (case1 and case2), the absolute fuel consumption for dual-fuel combustion were obtained considerably higher than the single-fuel combustions. Particularly, lower NOx emissions were emitted under the dual-fuel cases compared to the single-fuel mode under all test conditions. In addition, CBG–diesel cases exhibited superior performance in decrease of soot emissions due to the lack of aromatics and lower stoichiometric air requirement. Concentrations of HC and CO emissions for dual-fuel mode were considerably higher than others under all test conditions. The excess oxygen in air fuel mixture allowed more CO emissions to oxidize into CO_2 in single-fuel combustion cases and resulted higher concentrations of CO_2 emissions. When CBG was ingested to the cylinder, the CO_2 content in the gas mixture was caused to increase of unburned fuel in dual-fuel combustion cases.

5.2 Recommendations For Future Work

Recently alternative energy sources have been more interested due to the lack of petroleum sources and energy crises. In this study, CBG fuel which is one of the alternative and renewable energy sources in the world was used. CBG fuel is produced in many countries including Turkey but it hasn't been used in commercial vehicles just used for electrical power generation. This awarded study from economy ministry aimed to get proper boundary conditions for CBG fueled CI engines using multi-objective optimization, 1D, 3D CFD and experimental studies. This full geometry including intake, exhaust ports, valves and combustion chamber 3D dual fuel CFD models were performed first time.

In this study, four-stroke, four cylinder, 1.5 liter, turbo charged diesel engine with common rail injection system investigated and analyzed experimentally also 1D, 3D and multi-objective optimization study were performed for the same real engine geometry. In addition, CBG-Diesel dual fuel engine operations were investigated and engine parameters conditions were optimized. In dual fuel engine operations, CBG fuel was ingested from the intake pipe and air-fuel mixture was ignited by pilot diesel fuel. Experimental and numerical studies were dwelled on port injection system for dual fuel cases due to unwillingness on engine modification and rapid use on commercial vehicles easily. However, studies in direct injection CBG-diesel dual fuel operations showed that double way direct injection systems are more efficient than port injection system due to the increase of volumetric efficiency. Under obtained these results can be recommended below suggestions:

- PIV and LIF experimental studies should be performed for detailed investigation in-cylinder due to the chaotic features of combustion phenomenon.
- Purification of CBG fuel should be made because of this study showed that when methane rate increased inside CBG, combustion efficiency increased. However

this process is very expensive and higher methane rate inside CBG causes very peak combustion temperature in-cylinder. Therefore this type of engine needs coating on the surface of piston and combustion chamber.

- Detailed experimental studies need to be performed using optical engine with high speed camera and optical study of swirl during combustion with different SOI, compression ratio and injection pressures.

- This optimization study showed that some modeled dual fuel cases which have different cam timing gave better combustion performance and exhaust emission gasses. These studies also can be investigated in real engine which has VVT.

- In dual fuel experimental works, common-rail injection pressure needs to increase for shorter ignition delay by penetrating pilot fuel into CBG-air mixture.

- Also it is seen that in CFD studies, valve locations affected exhaust emissions. These studies can be tested in experimental setup.

- Lastly, due to the surface volume ratio effect on combustion, CFD studies showed that larger bore engine are more proper for CBG fuel. Using larger bore engines in experimental studies will be more effective on the combustion process.

REFERENCES

A. Upatnieks, C.J. Muller, Clean, controlled DI diesel combustion using dilute, cool charge gas and a short-ignition-delay, oxyenated fuel, SAE 2005-01-0363, 2005.

Aamir,M.A., and Watkins, A.P. 1999. ‘Dense propane spray analysis with a modified collision model’, ILASS-Europe’99, Toulouse, France, 5-7 July 1999.

Aceves S. M., Flowers D. L., J. Martinez-Frias, F. Espinosa-Loza, Christensen M., Johansson B., R. P. Hessel, “Analysis of the Effect of Geometry Generated Turbulence on HCCI Combustion by Multi-Zone Modeling”, SAE Brazil Fuels & Lubricants Meeting & Exhibition, Rio de Janeiro, Brazil, December 15, (2004).

Aceves, S. M., Flowers D. L., Joel Martinez-Frias, Francisco Espinosa- Loza, and Robert Dibble, “Detailed Analysis and Control Issues of Homogenous Charge Compression Ignition (HCCI)”, 8th Diesel Engine Emissions Reduction (DEER) Workshop 2002, San Diego, (2002).

Aceves, S. M., Flowers, D. L., Westbrook, C. K., Smith, J. R., Pitz, W., Dibble, R. Christensen, M., and Johansson, B., "A Multi-Zone Model for Prediction of HCCI Combustion and Emissions," SAE Paper 2000-01-0327, (2000).

Akagawa, H., Miyamoto, T., Harada, A., Sasaki, S., Shimazaki, N., Hashizume, T., Tsujimura, K. “Approaches to Solve Problems of the Premixed Lean Diesel Combustion”, SAE Paper 1999-01-0183, (1999).

Akihama K, Takatori Y, Inagaki K, Sasaki S, Dean A (2001), ‘Mechanism of the smokeless rich Diesel combustion by reducing temperature’, SAE International, SAE no. 2001- 01-0655.

Albrecht, A., Grondin, O., Le Berr, F. and Le Solliec, G., ‘Towards a stronger simulation support for engine control design: a methodological point of view’, Les Rencontres Scientifiques de l’IFP – New Trends in Engine Control, Simulation and Modelling; 2006.

Aoyama, T., Hattori, Y., Mizuta, J., Sato, Y. “An Experimental Study on Premixed-Charge Compression Ignition Gasoline Engine”, SAE Paper 960081, (1996).

Araki, M., Umino, T., Obokata, T., Ishima, T., Shiga, S., Nakamura, H., Long, W.-Q., Murakami, A. “Effects of Compression Ratio on Characteristics of PCCI Diesel Combustion with Hollow Cone Spray”, SAE Paper 2005-01-2130, (2005).

Asian Development Bank web page, (2008) http://www.adb.org/documents/guidelines/Vehicle_Emissions/im_ch07.pdf

B.B. Sahoo, N. Sahoo, U.K. Saha, “Effect of engine parameters and type of gaseous fuel on the performance of dual-fuel gas diesel engines-A critical review”, Renewable and Sustainable Energy Reviews 13 (2009) 1151–1184.

Babajimopoulos A., D. N. Assanis1, D. L. Flowers, S. M. Aceves and R. P. Hessel, “A Fully Integrated CFD and Multi-zone Model with Detailed Chemical Kinetics for the Simulation of PCCI Engines”, 15th International Multidimensional Engine Modeling User’s Group Meeting, Detroit, MI, April (2005).

Badami, M., Mallamo, F., Millo, F., Rossi, E., E. “Influence of Multiple Injection Strategies on Emissions, Combustion Noise and BSFC of a DI Common Rail Diesel Engine”, SAE Paper 2002-01-0503, (2002).

Badr O, Karim GA, Liu B. An examination of the flame spread limits in a dual fuel engine. Appl Therm Eng;19:1071–80, 1999.

Bae, C. H., Kang, J. “Diesel Spray Characteristics of Common-Rail VCO Nozzle Injector”, Proceedings of Thiesel 2000, Thermofluidynamic Processes in Diesel Engines, 2000, 57-66, (2000)..

Bae, C., Yu, J., Kang, J., Kong, J., Cuenca, R., Lee, K., O. “The Influence of Injector Parameters on Diesel Spray”, Proceedings of Thiesel 2002, Thermo-and Fluid Dynamic Processes in Diesel Engines, 2002, 55-66, (2002).

Bai, C., and Gosman, A.D. ‘Development of methodology for spray impingement simulation’, SAE Technical Paper Series 950283, 1995.

Bari, S. 1996. Effect of Carbon Dioxide on the Performance of Biogas/Diesel Dual-Fuel Engine. Renewable Energy, 9, 1007-1010.

Beatrice, C., Belardini, P., Bertoli, C., Lisbona, M., G., Rossi Sebastiano, G., M. “Diesel Combustion Control in Common Rail Engines by New Injection Strategies”, International Journal of Engine Research, (2002a), Volume 3, Number 1, 23-36.

Beatrice, C., Bertoli, C., Migliaccio, M. “Basic Concepts of the homogeneous Charge Compression Ignition Engines”, (2002b), ATA, Volume 55, Issue 7/8, . 226-234

Bedoya, I. D., Arrieta, A. A., Cadavid, F. J. 2009. Effects of Mixing System and Pilot Fuel Quality on Diesel-Biogas Dual Fuel Engine Performance. Bioresource Technology, 100, 6624-6629.

Bedoya, I. D., Arrieta, A. A., Cadavid, F. J. 2009. Effects of Mixing System and Pilot Fuel Quality on Diesel-Biogas Dual Fuel Engine Performance. Bioresource Technology, 100, 6624-6629.

Bittner, R. W., Aboujaoude, F. W. 1992. Catalytic Control of NOx, CO, and NMHC Emissions From Stationary Diesel and Dual-Fuel Engines. Journal of Engineering for Gas Turbines and Power, 114, 597-601.

Blessing, M., Köenig, G., Krüger, C., Michels, U., Schwarz, V. “Analysis of Flow and Cavitation Phenomena in Diesel Injection Nozzles and its Effects on Spray and Mixture Formation”, Proceedings of Fuel Injection Systems Conference, (2002), number 3.

Börjesson, P., L. Tufvesson & M. Lantz “Report 70 Livscykelanalys av svenska biodrivmedel” Department for Environment and Energy Lund University, 2010.

Brooks, T., D., Pugh, G., J., Gambrill, R., Shayler, P., J. “Investigating the Effects of Split Main Fuel Injection Parameters on NOx, Soot, HC and CO Emissions from a Light Duty Diesel Engine”, Proceedings of Internal Combustion Engine Performance and Emissions Conference, (2004), 1-12.

Browne, K., R., Partridge, I., M., Greeves, G. “Fuel Property Effects on Fuel/Air Mixing in an Experimental Diesel Engine”, (1986), SAE Paper 860223.

Byggstoyl, S. and Magnussen, B. F., Model for flame extinction in turbulent flow. Turbulent Shear Flows, 4:381-395, 1988.

C. Rahmouni, M. Tazerout, O. Le Corre, A method to determine biogas composition for combustion control, SAE 2002-01-1708, 2002.

C. Tricase, M. Lombardi, State of the art and prospects of Italian biogas production from animal sewage: technical-economic considerations, Renewable Energy 34 (2009) 477–485.

C.S. Weaver, S.H. Turner, Dual fuel natural gas/diesel engines: technology, performance, and emissions, SAE 940548, 1994.

Chauvin, J., Corde , G., Petit, N. and Rouchon, P., 'Experimental air path control of a Diesel engine', Les Rencontres Scientifiques de l'IFP – New Trends in Engine Control, Simulation and Modelling, 2006.

Chen, Y.S., and Kim, S.W. 'Computation of turbulent flows using an extended k-ε turbulence closure model', NASA CR-179204, 1987.

Chi, Y., Cheong, J., Kim, C., Choi, K. "Effects of VGT and Injection Parameters on Performance of HSDI Diesel Engine with Common Rail FIE System", SAE Paper 2002-01-0504, (2002).

Chia Sheng, L. "Biogas upgrade through exhaust gas reforming process for use in ci engines", PhD thesis, University of Birmingham, 2012.

Chmela, F., Riediger, H. "Analysis Methods for the Effects of Injection Rate Control in Direct Injection Diesel Engines", Proceedings of Thiesel 2000, Thermofluidynamic Processes in Diesel Engines, (2000), 333-344.

Christensen M. and Johansson B., 'Supercharged Homogeneous Charge Compression Ignition (HCCI) with Exhaust Gas Recirculation and Pilot Fuel' SAE Paper 2000- 01-1835, (2000).

Christensen, M., Hultqvist A. and Johansson, B. Demonstrating the Multi Fuel Capability of a Homogeneous Charge Compression Ignition Engine with Variable Compression Ratio, SAE Technical Paper 1999-01-3679, 1999

Christensen, M., Johansson, B. "The Effect of In-Cylinder Flow and Turbulence on HCCI Operation", SAE Paper 2002-01-2864, (2000).

Colin, O. & Benkenida, A. (2004): "The 3-Zones Extended Coherent Flame Model (ECFM3Z) for Computing Premixed/Diffusion Combustion", Oil & Gas Sci. and Tech. 59, 593-609

Colin, O., Benkenida, A. & Angelberger, C. (2003) "3D Modeling of Mixing, Ignition and Combustion Phenomena in Highly Stratified Gasoline Engines", Oil & Gas Sci. and Tech. 58, 47-62

Commission Regulation (EU) No 582/2011 (Euro VI), date is for new registrations". Retrieved 2013.

Courant R. K. Lewy F. H.. "Uber die partiellen Differenzengleichungen der mathematischen Physik", volume 1. (1928).

Daniel, L., "Combustion and emissions performance of oxygenated fuels in a modern spark ignition engine" PhD thesis, University of Birmingham, 2012.

Dec JE, Kelly-Zion PL. The effect of injection timing and diluent addition late-combustion soot burnout in a DI diesel engine based on simultaneous 2-D imaging of OH and soot. SAE Paper 2000; 2000¬01-0238.

Dec JE. A computational study of the effect of low fuel loading and EGR on heat release rates and combustion limits in HCCI engines. SAE Paper 2002; 2002-01-1309.

Dec JE. A conceptual model of DI diesel combustion based on laser-sheet imaging. SAE Paper 1997; 970873.

Dopazo, C., Recent developments in pdf methods. Turbulent Reactive Flows, pages 375-474, 1994.

Duc, P. M., Wattanavichien, K. 2007. Study on Biogas Premixed Charge Diesel Dual Fuelled Engine. Energy Conversion and Management, 48, 2286-2308.

Duclos, J.-M. & Zolver, M. (1998): "3D Modeling of Intake, Injection and Combustion in a DI-SI Engine under Homogeneous and Stratified Operating Conditions", COMODIA 4.

Duclos, J.-M., Zolver, M. & Baritaud, T. (1999): "3D Modeling of Combustion for DI-SI Engines", Oil & Gas Sci. and Tech. 54, 259-264.

Duclos, J.M., Zolver, M., Baritaud, T. "3D modelling of combustion for DI-SI engines." Oil & Gas Science and Technology, Vol.54 (1999).

Duret P, Gatellier B, Monteiro L, Miche M, Zima P, Maroteaux D, Guezet J, Blundell D, Spinnler F, Zhao H, Perotti M, Araneo L (2004), 'Progress in Diesel HCCI combustion within the European space light project', SAE International, SAE no. 2004-01-1904.

EU Emission Standards for Heavy-Duty Diesel and Gas Engines: Transient Testing https://www.dieselnet.com/standards/eu/hd.php

Fang T., Coverdill R. E., Lee C. F. and White R. A. Smokeless Combustion within a Small-Bore HSDI Diesel Engine Using a Narrow Angle Injector. . 2007 World Congress Detroit, Michigan April 16-19, 2007.

G. A. Karim, The dual fuel engine of the compression ignition type-prospects, problems and solutions-a review, SAE 831073, 1983.

G. H. Abd Alla, H. A. Soliman, O. A. Badr, and M. F. Abd Rabbo, "Effect of injection timing on the performance of a dual fuel engine", Energy Conversion and Management, vol. 43, 2002.

G. Prakash, A. Ramesh, A.B. Shaik, An approach for estimation of ignition delay in a dual fuel engine, SAE 1999-01-0232, 1999.

Gamma Inc. Users Maunual, volume 61. Gamma Technologies, (2004).

Garrett T.K., K. Newton, W. Steeds, "The Motor Vehicle", 13 th Edition Butterworth-heinemann (2001), 516-549.

Gartner, U., Hohenberg, G., Daudel, H., Oelschlegel, H. "Development and Application of a Semi-Empirical NOx Model to Various HD Diesel Engines", Proceedings of Thiesel 2002, Thermo-and Fluid Dynamic Processes in Diesel Engines, (2002), 487-506.

Gatellier, B., Ranini, A. and Castagné, M., 'New development of the NADITM Concept to improve operating range, exhaust emissions and noise. Combustion'. Oil and Gas Science and Technology, Vol. 61 (2006), No 1, pp. 7–23.

Gatellier, B., Walter, B. "Development of the High Power NADITM Concept Using Dual Mode Diesel Combustion to Achieve Zero NOx and Particulate Emissions", Proceedings of Thiesel 2002, Thermo-and Fluid Dynamic Processes in Diesel Engines, . 131-143 and SAE Paper 2002-01-1744, (2002).

Gill, D., Chmela, F., Jager, P. “The Emissions and Performance Potential of a Pressure Modulated Common Rail Injection System on a Heavy Duty Diesel Engine”, Proceedings of Fuel Injection Systems Conference, (2002), number 10.

Gomes Antunes, J. M., Mikalsen, R., Roskilly, A. P. 2009. An Experimental Study of a Direct Injection Compression Ignition Hydrogen Engine. International Journal of Hydrogen Energy, 34, 6516-6522.

Gray, A. W. and Ryan III, T. W. Homogeneous Charge Compression Ignition (HCCI) of Diesel Fuel, SAE Technical Paper 971676, 1997

Groenendijk, A., Müller, E. “Mixture Formation and Combustion Control for Low Emission DI Diesel Combustion with HCCI-Characteristics”, Proceedings of Thiesel 2002, Thermo-and Fluid Dynamic Processes in Diesel Engines, (2002), 145-157.

Hasegawa R, Sakata I, Yanagihara H, Hildingsson L, Johansson B, Collin R, Nygre J, Richter M (2004), ‘Analysis on homogeneity effects in HCCI combustion using simultaneous OH and formaldehyde LIF measurements’, Aachener Kolloquium Fahrzeug- und Motorentechnik, Vol. 13.

Hasegawa, R., Yanagihara, H. “HCCI Combustion in DI Diesel Engine”, SAE Paper (2003)-01-0745.

Hashizume, T., Miyamoto, T., Akagawa, H. and Tsujimura, K., Combustion and Emission Characteristics of Multiple Stage Diesel Combustion, SAE paper No. 980505 (1998).

Hélie, J. &Trouvé, A. “A modified coherent flame model to describe turbulent flame propagation in mixtures with variable composition”, Proc. Combust. Inst. 28, 193-20, 2000.

Helmantel A, Denbratt I. HCCI Operation of a passenger car common rail DI diesel engine with early injection of conventional diesel fuel. SAE Paper 2004; 2004-01-0935.

Henein, N., A., Lai, M.-C., Singh, I., Wang, D., Liu, L. “Emissions Trade-Off and Combustion Characteristics of a High-Speed Direct Injection Diesel Engine”, SAE Paper (2001)-01-0197

Henein, N., A., Singh, I., P., Zhong, L., Lai, M.-C., Bryzik, W. “New Integrated “O.P.E.R.A.S.” Strategies for Low Emissions in HSDI Diesel Engines”, SAE Paper (2003)-01-0261

Henham, A., Makkar, M. K. 1998. Combustion of Simulated Biogas in a Dual-Fuel Diesel Engine. Energy Conversion and Management, 39, 2001-2009.

Heywood, J.B., ”Internal Combustion Engine Fundamentals”, International edition, McGraw-Hill, New York, 1988.

Hildingsson L, Persson H, Johansson B, Collin R, Nygren J, Richter M, Alden M, Hasegawa R, Ranagihara H , ‘Optical diagnostics of HCCI and UNIBUS using 2-D PLIF of OH and formaldehyde’, SAE International, SAE no. 2005-01-0175, 2005.

Hotta H, Inayoshi M, Nakakita K (2002), ‘Achieving lower exhaust emissions and better performance in a HSDI Diesel engine with multiple injection’, R&D review of Toyota Central R&D Labs, Vol: 37 no. 3, 9–16.

Huh, K.Y., and Gosman, A.D. : ‘A henomenological model of Diesel spray atomisation’, Proc. Int. Conf. on Multiphase Flows (ICMF ’91), Tsukuba, 24-27 September, (1991).

Hultqvist, A. – Engdar, U., Johansson, B., Klingmann, J. “Reacting Boundary Layers in a Homogeneous Charge Compression Ignition (HCCI) Engine”, SAE Paper (2001)-01-1032.

I. Saanum, M. Bysveen, J.E. Hustad, Study of particulate matter-, NOx- and hydrocarbon emissions from a diesel engine fueled with diesel oil and biodiesel with fumigation of hydrogen, methane and propane, SAE 2008-01-1809, 2008.

Iwabuchi, Y., Kawai, K., Shoji, T., Takeda, Y. “Trial of New Concept Diesel Combustion System – Premixed Compression-Ignited Combustion”, SAE Paper -01-0185, 1999.

J. P. Holman, “Experimental Methods for Engineers,” McGraw-Hill Book Company, 4th Edition, pp. 50, 1988.

Jackson, N., S. “The High Speed Direct Injection Diesel Engine – Future Potential”, Proceedings of Thiesel 2000, Thermofluidynamic Processes in Diesel Engines, 33-42, (2000).

James P. Szybist, Stephen R. Kirby, Andre L. Boehman, NOx emissions of alternative diesel fuels: a comparative analysis of biodiesel and FT diesel, Energy and Fuels 19 (2005) 1484-1492.

Jie, S., Q. Jun, Y. Mingfa, Turbocharged diesel/CNG dual-fuel engines with intercooler: combustion, emissions and performance, SAE 2003-01-3082, 2003.

Kaiadi, M. “Diluted Operation of a Heavy-duty Natural Gas Engine”, Thesis (PhD), University of Lund, Dept. of Mechanical Engineering, 2011.

Kaneko, M., Morikawa, K., Itoh, J., Saishu, Y. “Study on Homogeneous Charge Compression Ignition Gasoline Engine”, Proceedings of COMODIA 2001, Fifth International Symposium on Diagnostics and Modeling of Combustion in Internal Combustion Engines, 457-462, (2001).

Karim G.A., A review of combustion processes in the dual fuel engine—the gas diesel engine, Progress in Energy and Combustion Science 6 277–285, 1980.

Karim, G. A., Wierzba, I.. Methane-Carbon Dioxide Mixtures as a Fuel. SAE Paper, 21557, 1992.

Kawamoto, K., Araki, T., Shinzawa, M., Kimura, S., Koide, S., Shibuya, M. “Combination of Combustion Concept and Fuel Property for Ultra-Clean DI Diesel”, SAE Paper (2004)-01-1868.

Kawano, D., Suzuki, H., Ishii, H., Goto, Y., Odaka, M., Murata, Y., Kusaka, J., Daisho, Y. “Ignition and Combustion Control of Diesel HCCI”, SAE Paper (2005)-01-2132.

Kawashima, J.-I., Ogawa, H., Tsuru, Y. “Research on a Variable Swirl Intake Port for 4-Valve High-Speed DI Diesel Engines”, SAE Paper 982680, (1998).

Kennaird, D., Crua, C., Lacoste, J., Heikal, M., Gold, M., Jackson, N. “In-cylinder Penetration and Break-up of Diesel Sprays Using a Common-rail Injection System”, SAE Paper (2002)-01-1626.

Kidoguchi, Y., Miwa, K., Goda, E. "Effect of Stratified Rich and High Turbulence Combustion on the Reduction of NOx and Particulate Emissions from a DI Diesel Engine", Proceedings of Thiesel 2002, Thermo-and Fluid Dynamic Processes in Diesel Engines, 227-235, (2002).

Kim DS, Kim MY, Lee CS. "Combustion and emission characteristics of partial homogeneous charge compression ignition engine" Combust Sci Technol 2005; 177:107–25.

Kim DS, Kim MY, Lee CS. Effect of premixed gasoline fuel on the combustion characteristics of compression ignition engine. Energ Fuel 2004; 18(4), p. 1213–9, American Chemical Society.

Kim M. Y. and Lee C. S. Effect of a narrow fuel spray angle and a dual injection configuration on the improvement of exhaust emissions in a HCCI diesel engine. Fuel, Volume 86, Issues 17-18, December 2007, Pages 2871-2880

Kimura, S., Aoki, O., Kitahara, Y., Aiyoshizawa, E. "Ultra-clean Combustion Technology Combining a Low-Temperature and Premixed Combustion Concept for Meeting Future Emission Standards", SAE Paper (2001)-01-0200.

Kimura, S., Aoki, O., Ogawa, H., Muranaka, S., Enomoto, Y. "New Combustion Concept for Ultra-Clean and High-Efficiency Small DI Diesel Engines", SAE Paper (1999)-01-3681

Kistler indicating pressure test systems, Febris v1.0 User manual NEL presto,2012.

Knecht, W. "European Emission Legislation of Heavy Duty Diesel Engines and Strategies for Compliance", Proceedings of Thiesel 2000, Thermofluidynamic Processes in Diesel Engines, (2000), 289-302.

Kong S-C., Reitz R. D."Application Of Detailed Chemistry And CFD for Predicting Direct Injection HCCI Engine Combustion and Emissions", Proceedings of the Combustion Institute, (2002), Volume 29, 663–669.

Kong, S.-C., Marriott, C., D., Reitz, R., D. -Christensen, M. "Modeling and Experiments of HCCI Engine Combustion Using Detailed Chemical Kinetics with Multidimensional CFD", SAE Paper (2001)-01-1026.

Königsson, F. “Advancing the Limits of Dual Fuel Combustion”, Thesis Department of Machine Design, Royal Institute of Technology, 2012.

Kono, S., Terashita, T. T. and Kudo, H., “Study of the swirl effects on spray formation in DI engines by 3D numerical calculations”, 1999, SAE Paper 910264.

Kook, S., Bae, C., Combustion control using two-stage diesel fuel injection in a single-cylinder PCCI engine. SAE Paper 2004; 2004-01¬0938.

Köten, H., Yilmaz, M., Gül M.Z. and Soyhan H., “Comparison of Turbulence Models for a Heavy Duty CI Engine”, ISCSE, 2011.

Köten H., “Comparison of various combustion models within a multidimensional framework applied to heavy duty CI engine” MSc. Thesis, 2009.

Kubler for Turck works incremental and absolute encoder manual, 2010.

Laguitton, O., Gold, M., Kennaird, D., Crua, C., Lacoste, J., Heikal, M. “Spray Development and Combustion Characteristics for Common Rail Diesel Injection Systems”, Proceedings of Fuel Injection Systems Conference, (2002a), number 6.

Laguitton, O., Streater, S., R., Gordon, R., L. (2002) “Realising the Benefits of Supervisory Control – An Essential Approach for Hybrid Drivetrains”, Proceedings of Total Vehicle Technology, I.Mech.E. Paper T002/003/(2002b), 29-45.

Launder, B.E., and Spalding, D.B. 1974. ‘The numerical computation of turbulent flows’, Comp. Meth. in Appl. Mech. and Eng., 3, pp. 269-289.

Lechner, G. A, Jacobs, T. J., Chryssakis, C. A., Assanis, D. N., Siewert, R. M., Evaluation of a narrow spray cone angle, advanced injection timing strategy to partially premixed compression ignition combustion in a diesel engine. SAE Paper 2005; 2005-01-0167.

Lejeune, M., Lortet, D., Michon, S. “Combustion Development for Euro 4”, Proceedings of Thiesel 2002, Thermo-and Fluid Dynamic Processes in Diesel Engines, (2002), 277-292.

Lejeune, M., Michon, S., Hedna, M. “Combustion Process Optimisation for Euro 3”, Proceedings of Thiesel 2000, Thermofluidynamic Processes in Diesel Engines, (2000), 347-367.

Liu, Z., Karim, G. A. 1997. Simulation of Combustion Processes in Gas-Fuelled Diesel Engines. Proceedings of the Institution of Mechanical Engineers, Part A: Journal of Power and Energy, 211, 159-169.

Luszcz, P. M. 2009. Combustion Diagnostics in Homogeneous Charge Compression Ignition Optical and Thermal Single Cylinder Engines. PhD Thesis, University of Birmingham.

M. Yilmaz, H. Koten, M.Z. Gul, (2012) "Effects of the injection parameters of a heavy duty diesel engine", IJVD vol.59 p.164-181.

M.D. Phan, W. Kanit, Study on biogas premixed charge diesel dual fuelled engine, Energy Conversion and Management 48 (2007) 2286–2308.

M.Y. Kim, S.H. Yoon, C.S. Lee, Impact of split injection strategy on the exhaust emissions and soot particulates from a compression ignition engine fueled with neat biodiesel, Energy and Fuels 22 (2008) 1260–1265.

M.Y. Kim, S.H. Yoon, J.W. Hwang, C.S. Lee, Characteristics of particulate emissions of compression ignition engine fueled with biodiesel derived from soybean, Journal of Engineering for Gas Turbine and Power 130 (5) (2008) 052805-1–052805-7.

M.Z. Gül, "Prediction of In-Cylinder Flow By Use of a Multiple Time Scale Turbulence Models", Thesis (PhD), University of Manchester, Dept. of Mechanical Engineering, 1994.

Magnussen, B. F. and Hjertager, B. H., On mathematical models of turbulent combustion with with special emphasis on soot formation and combustion. Sixteenth Symposium (International) on Combustion, pages 719-729, 1977.

Mahr, B. "Future and Potential of Diesel Injection Systems", Proceedings of Thiesel 2002, Thermo-and Fluid Dynamic Processes in Diesel Engines, (2002), 5-17.

Maji S., Amit Pal, B.B. Arora, Use of CNG and diesel in CI engines in dual fuel mode,

Matsuda, Y. (2005), 'Toyota's environmental challenge: Prius lobbying kit', Presentation at SAE Fuel & lubricant meeting 2005, Rio de Janeiro, Brazil.

Mitchell Electronics, TI-5000EX Serial/Incremental Encoder Test System User Manual, Inc., 2014.

Möller, C., “1-D Simulation of Turbocharged SI Engines - Focusing on a New Gas Exchange System and Knock Prediction” Royal Institute of Technology, 2006.

Monaghan, M., L. “The Design and Development of the High Speed Direct Injection Diesel”, Proceedings of Koex 95, Seoul Motor Show Seminar, Korea SAE, Paper 5, (1995).

Morel, T. and Mansour, N. N., "Modeling of Turbulence in Internal Combustion Engines," SAE Technical Paper Series, 820040, International Congress and Exposition, Detroit, Mich., February 22-26, 1982.

Morimoto, S., S., Kawabata, Y., Sakurai, T., Amano, T. “Operating Characteristics of a Natural Gas-Fired Homogeneous Charge Compression Ignition Engine (Performance Improvement Using EGR)”, SAE Paper (2001)-01-1034

Morita, A., Iwashiro, Y., Aoyagi, Y., Hashizume, T. “Observation of the Diesel Combustion Process in Multiple Stage Injection”, Proceedings of Thiesel 2000 Thermofluidynamic Processes in Diesel Engines, (2000), 447-452.

Mototest user guide, 2010.

Mueller CJ, Martin GC, Briggs TE, Duffy KP. An experimental investigation of in-cylinder processes under dual-injection conditions in a DI diesel engine. SAE Paper 2004; 2004-01-1843.

Mustafi, N.N., Raine, R.R., A study of the emissions of a dual fuel engine operating with alternative gaseous fuels, SAE 2008-01-1394, 2008.

N. Bahman, P. Vahab, N. Gholamhassan, Y. Talal, G. Barat, Experimental investigation of performance and emission parameters of a small diesel engine using CNG and biodiesel, SAE 2007-32-0075, 2007.

N.N. Mustafi, R.R. Raine, A study of the emissions of a dual fuel engine operating with alternative gaseous fuels, SAE 2008-01-1394, 2008.

Najt, P., Foster, D., E. “Compression-Ignited Homogeneous Charge Combustion”, SAE Paper 830264, (1983).

Nakayama, S., Fukuma, T., Matsunaga, A., Miyake, T., Wakimoto, T. “A New Dynamic Combustion Control Method Based on Charge Oxygen Concentration for Diesel Engines”, SAE Paper (2003)-01-318.

Nakayama, S., Fukuma, T., Matsunaga, A., Miyake, T., Wakimoto, T. “A New Dynamic Combustion Control Method Based on Charge Oxygen Concentration for Diesel Engines”, SAE Paper 2003.

Neely GD, Sasaki S, Leet JA. Experimental investigation of PCCI-DI combustion on emissions in a light-duty diesel engine. SAE-Paper 2004; 2004-01-0121.

Nielsen, O. B., Qvale, B., Sorenson, S.. Ignition Delay in the Dual Fuel Engine. SAE Paper, 870589, 1987.

Nishijima, Y., Asaumi, Y., Aoyagi, Y. “Impingement Spray System with Direct water Injection for Premixed Lean Diesel Combustion Control”, SAE Paper (2002)-01-0109 -.

Noda, T., Foster, D. E. “A Numerical Study to Control Combustion Duration of Hydrogen-fueled HCCI by Using Multi-zone Chemical Kinetics Simulation”, SAE Paper (2001)-01-0250.

O’Rourke, P.J. “Collective Drop Effects on Vaporising Liquid Sprays”. PhD Thesis, University of Princeton, 1981.

Oakley, A., Zhao, H., Ladommatos, N. -Ma, T. “Experimental Studies on Controlled Auto-ignition (CAI) Combustion of Gasoline in a 4-Stroke Engine”, SAE Paper -01-1030, 2001.

Olsson, J.-O., Tunestal, P., Johansson, B. “Closed-Loop Control of an HCCI Engine”, SAE Paper (2001)-01-1031.

Onishi, S., Jo, S., H., Shoda, K., Jo, P., D., Kato, S. “Active Thermo-Atmosphere Combustion (ATAC) – A New Combustion Process for Internal Combustion Engines”, SAE Paper 790501, (1979).

Ono, R., Nifuku, M., Fujiwara, S., Horiguchi, S., Oda, T. 2007. Minimum Ignition Energy of Hydrogen–Air Mixture: Effects of Humidity and Spark Duration. Journal of Electrostatics, 65, 87-93.

Owen, K., Coley, T. 1995. Automotive fuels reference book, Warrendale, PA. USA, Society of Automotive Engineers, Inc.

Papagiannakis R G; Hountalas D T. Combustion and exhaust emission characteristics of a dual-fuel compression ignition engine operated with pilot diesel fuel and natural gas. Energy Conversion & Management, 45, 2971–2987, 2004.

Papagiannakis, R. G., Hountalas, D. T., Rakopoulos, C. D. 2007. Theoretical Study of the Effects of Pilot Fuel Quantity and its Injection Timing on the Performance and Emissions of a Dual Fuel Diesel Engine. Energy Conversion and Management, 48, 2951-2961, 2007

Payri, F., Benajes, J., Molina, S., Manuel Rieso, J. “Combustion and Exhaust Emissions in a Heavy-Duty Diesel Engine with Increased Premixed Combustion Phase by Means of Injection Retarding”, Oil & Gas Science and Technology – Rev. IFP, Vol. 61 (2006), No. 2, pp. 247-258.

Payri, F., Benajes, J., Molina, S., Manuel Rieso, J. “Reduction of Pollutant Emissions in a HD Diesel Engine by Adjustment of Injection Parameters, Boost Pressure and EGR”, SAE Paper (2003)-01-0343.

Pekalski AA, Zevenbergen JF, Pasman HJ, Lemkowitz SM, Dahoe AE, Scarlett B. The relation of cool flame and auto-ignition phenomena to process safety at elevated pressure and temperature. J Hazard Mater 2002; 93:93–105.

Peng, Z., Zhao, H., Ladommatos, N. “Effects of Air/Fuel Ratios and EGR Rates on HCCI Combustion of n-heptane, a Diesel Type Fuel”, SAE Paper (2003)-01-0747.

Phan, M., “Study on biogas premixed charge diesel dual fuelled engine” Energy Conversion and Management 48 (2007) 2286–2308, 2007.

PSIauto pressure sensor operating instructions and pressure sensor user manual optrand incorporated, 2012.

Pucher G. R., Gardiner D. P., Bardon M. F. and Battista V.. ‘Alternative Combustion Systems for Piston Engines Involving Homogeneous Charge Compression Ignition Concepts – A review of Studies Using Methanol, Gasoline and Diesel Fuel’. SAE Paper 962063 (1996).

R.L. McCormic, C.J. Tennant, R.R. Hayes, S. Black, Sharp, Regulated Emissions from Biodiesel Tested in Heavy Duty Engines Meeting 2004 Emission Standards, SAE 2005-01-2200, 2005.

Rahmouni, C., Tazerout, M., O. Le Corre, A method to determine biogas composition for combustion control, SAE 2002-01-1708, 2002.

Ranini, A., Potteau, S., Gatellier, B. "New Developments of the NADITM Concept to Improve Operating Range, Exhaust Emissions and Noise", Proceedings of Thiesel 2004, Thermo-and Fluid Dynamic Processes in Diesel Engines, (2004), 469-482.

Reitz, R.D., and Diwakar, R. 'Effect of drop breakup on fuel sprays', SAE Technical Paper Series 860469, 1986.

Reitz, R.D., and Diwakar, R.: 'Structure of High-Pressure Fuel Spray', SAE Technical Paper Series 870598, 1987.

Revaille B, Miche M, Jay S, Heinriot S (2004), 'Contribution of 3D CFD tools to the development and understanding of Diesel engines: improving today's engines and designing tomorrow's power units', Congrès Le Diesel: aujourd'hui et demain, Société des ingénieurs d'automobile, Lyon, France.

Ricaud, J.-C., Lavoisier, F. "Optimizing the Multiple Injection Settings on an HSDI Diesel Engine", Proceedings of Thiesel 2002, Thermo-and Fluid Dynamic Processes in Diesel Engines, (2002), 251-276.

Rounce, P. "Engine performance and particulate matter speciation for compression ignition engines powered by a range of fossil and biofuels" PhD thesis, University of Birmingham, 2011.

Ryan III, T., W. "Fuels for Compression Ignition Engines", Proceedings of Thiesel 2000, Thermofluidynamic Processes in Diesel Engines, (2000), 233-248.

Ryan III, T., W., Matheaus, A. "Fuel Requirements for HCCI Engine Operation", Proceedings of Thiesel 2002, Thermo-and Fluid Dynamic Processes in Diesel Engines, , 362-375, 2002.

S. B. Pope. Computations of turbulent combustion: Progress and challenges. Twenty-Third Symposium (International) on Combustion, pages 591-612, 1990.

S. Jie, Q. Jun, Y. Mingfa, Turbocharged diesel/CNG dual-fuel engines with intercooler: combustion, emissions and performance, SAE 2003-01-3082, 2003.

S. Maji, Amit Pal, B.B. Arora, Use of CNG and diesel in CI engines in dual fuel mode, SAE 2008-28-0072, 2008.

S.H. Park, S.H. Yoon, C.S. Lee, Effect of the temperature variation on properties of biodiesel and biodiesel–ethanol blends fuels, Oil & Gas Science and Technology 63 (6) (2008) 737–745.

S.H. Yoon, H.K. Suh, C.S. Lee, Effect of spray and EGR rate on the combustion and emission characteristics of biodiesel fuel in a compression ignition engine, Energy and Fuels 23 (2009) 1486–1493.

S.H. Yoon, S.H. Park, C.S. Lee, Experimental investigation on the fuel properties of biodiesel and its blends at various temperatures, Energy and Fuels 22 (2008) 652–656.

SAE 2008-28-0072, 2008.

Sahoo, B.B., N. Sahoo, U.K. Saha, "Effect of engine parameters and type of gaseous fuel on the performance of dual-fuel gas diesel engines-A critical review", Renewable and Sustainable Energy Reviews 13 1151–1184, 2009.

Schmidt, D.P., and Rutland, C.J. 'A new droplet collision algorithm', J. Comput. Phys., 164, pp. 62-80, 2000.

Shenghua, L., Ou, C., J., Won, H., J. "Development of New Swirl System and its Effect on DI Diesel Engine Economy", SAE Paper (1999)-01-2889.

Shi L., Cui Y., Deng K., Peng H., Chen Y. Study of low emission homogeneous charge compression ignition (HCCI) engine using combined internal and external exhaust gas recirculation (EGR), Energy, 2006, vol.31, pp.2665-2676.

Shibata G, Oyama K, Urushihara T, Nakano T. Correlation of low temperature heat release with fuel composition and HCCI engine combustion. SAE Paper 2005; 2005-01-0138.

Shimazaki, N., Akagawa, H., Tsujimura, K. "An Experimental Study of Premixed Lean Diesel Combustion", SAE Paper (1999)-01-0181.

Shimazaki, N., Tsurushima, T., Nishimura, T. “Dual Mode Combustion Concept with Premixed Diesel Combustion by Direct Injection near Top Dead Center”, SAE Paper (2003)-01-0742.

Shudo, T., Ono, Y. “HCCI Combustion of Hydrogen, Carbon Monoxide and Dimethyl Ether”, SAE Paper (2002)-01-0112.

Simescu, S., Fiveland, S., B., Dodge, L., G. “An Experimental Investigation of PCCI-DI Combustion and Emissions in a Heavy-Duty Diesel Engine”, SAE Paper (2003)-01-0345.

Song, Y.S., Hong, J.W. and Lee, J.T.. “The turbulence measurement during the intake and compression process for high-turbulence generation around spark timing”, Proceedings of the Institution of Mechanical Engineers, Part D: Journal of Automobile Engineering, 2000, vol. 215, 493-501.

Soyhan H., et al., “Double-Wiebe function: An approach for single-zone HCCI engine modeling” Applied Thermal Engineering , volume 28, 1284-1290, 2008

Spalding, D. B., Mixing and chemical reaction in steady con¯ned turbulent °ames. Thirteenth Symposium (International) on Combustion, pages 649-657, 1971.

Speziale, C. G.. ‘On nonlinear k-l and k-ε models of turbulence’, J. Fluid Mech., 178, pp. 459-475, 1987.

Stanglmaier R. H. and Roberts, C. E. Homogeneous Charge Compression Ignition (HCCI): Benefits, Compromises, and Future Engine Applications, SAE Technical Paper 1999-01-3682, 1999.

StarCD Manual “Fuel spray and atomization models” page 223-225, 2010.

Star-CD Methodology Manual, CD-adapco Inc., (2009).

Strålin, P., “Lagrangian CFD Modeling of Impinging Diesel Sprays for DI HCCI” Royal Institute of Technology, 2007.

Su, W., Lin, T., Pei, Y. “A Compound Technology for HCCI Combustion in a DI Diesel Engine Based on the Multi-Pulse Injection and the BUMP Combustion Chamber”, SAE Paper (2003)-01-0741.

Suzuki, H., Koike, N., Ishii, H., Odaka, M. “Exhaust Purification of Diesel Engines by Homogeneous Charge with Compression Ignition Part 1: Experimental Investigation of Combustion and Exhaust Emission Behavior Under Pre-Mixed Homogeneous Charge Compression Ignition Method”, SAE Paper 970313, 1997.

Takeda, Y., Keiichi, Na., Keiichi, Ni. “Emission Characteristics of Premixed Lean Diesel Combustion with Extremely Early Staged Fuel Injection”, SAE Paper 961163, 1996.

Takeuchi, K., Toyao, T. “Development of 2nd Generation Common Rail System”, Proceedings of Fuel Injection Systems Conference, 2002.

Tanaka, K., Endo, H., Imamichi, A., Oda, Y. – Takeda, Y., Shimada, T. “Study of Homogeneous Charge Compression Ignition Using a Rapid Compression Machine”, SAE Paper (2001)-01-1033.

Taylor, C., F. “The Internal Combustion Engine in Theory and in Practise – Combustion, Fuels, Materials, Design”, Volume 2, Revised Edition, pp. 103-104, 1984.

Tinaut, F. V., Melgar, A., Giménez, B., Reyes, M. 2011. Prediction of performance and emissions of an engine fuelled with natural gas/hydrogen blends. International Journal of Hydrogen Energy, 36, 947-956.

Tree, D. R., Svensson, K. I. 2007. Soot Processes in Compression Ignition Engines. Progress in Energy and Combustion Science, 33, 272-309.

Tricase C., M. Lombardi, State of the art and prospects of Italian biogas production from animal sewage: technical-economic considerations, Renewable Energy 34 477–485, 2009.

Trueba, A., Barbeau, B., Pajot, O., Mokaddem, K. (2002) “Pilot Injection Timing Effect on the Main Injection Development and Combustion in a DI Diesel Engine”, SAE Paper 2002-01-0501

Turkcan A., “Eexperimental determination of a diesel-engines performance parameters” MSc thesis, 2006.

Veynante, D. and Vervisch, L., Turbulent combustion modeling. Progress in Energy and Combustion Science, 28:247, 2002.

Walter B, Gatellier B. Near zero NOx emissions and high fuel efficiency diesel combustion: the NADITM concept using dual mode combustion. Oil Gas Sci Technol 2003, 58(1):101–14.

Walter B, Monteiro L, Miche M, Gatellier B (2004), ‘Improvement of exhaust and noise emissions of the NADI concept using pre-mixed type combustion with multiple stages injection’, Congrès Le Diesel: aujourd’hui et demain, Société des ingénieurs d’automobile, Lyon, France.

Walter, B. and Gaterllier, B. Development of the High Power NADITM Concept Using Dual Mode Diesel Combustion to Achieve Zero NOx and Particulate Emissions, SAE Technical Paper 2002-01-1744, 2002.

Weissback, M., Csato, J., Glensvig, M., Sams, T., Herzog, P. (2003) “Alternative Combustion – An approach for Future HSDI Diesel Engines”, MTZ Worldwide, Volume 64, Issue 9/2003, pp. 17-20

Whelan, S. (2001) “Down-Sizing Diesel Powertrain for Use in Fuel Efficient Mild Hybrid Vehicles”, JSAE Paper 20015343

Wilcox, D.C. “Turbulence Modeling for CFD”. 2nd edition, DCW Industries, Inc, 1998.

Wilcox, D.C. “Turbulence modeling for CFD”. Griffin Printing, Glendale, (1993)

Wuensche, P., Moser, F., X., Dreisbach, R., Sams, T. (2003) “Can the Technology for Heavy Duty Diesel Engines be Common for Future Emission Regulations in USA, Japan and Europe?”, SAE Paper 2003-01-0344

Y. Zhang, A.L. Boehman, Impact of biodiesel on NOx emissions in s common rail direct injection diesel engine, Energy and Fuels 21 (2007) 2003–2012.

Yakhot, V., Orszag, S.A., Thangam, S., Gatski, T.B., and Speziale, C.G. 1992. ‘Development of turbulence models for shear flows by a double expansion technique’, Phys. Fluids, A4(7), pp. 1510–1520.

Yanagihara, H. “A Study on Combustion Structure of Premixed Compression Ignition Diesel Engines”, Proceedings of Thiesel 2002, Thermo- and Fluid Dynamic Processes in Diesel Engines, pp. 111-129, 2002.

Yanagihara, H. “Ignition Timing Control at Toyota “UNIBUS” Combustion System”, Proceedings of the IFP International Congress, A New Generation of Engine Combustion Processes for the Future, pp. 35-42, 2001.

Yanagihara, H., Sato, Y., Mizuta, J. (1997) “A Study of DI Diesel Combustion Under Uniform Higher-Dispersed Mixture Formation”, JSAE Review, July 1997, pp.247-254.

Yilmaz T., I. “Investigation of the Combustion Characteristic and Exhaust Emissions of a Dual Fuel (Biogas-Diesel) Low Heat Rejection Diesel Engine” PhD thesis, In Progress.

Yilmaz, M., “Effect Of CDC Concept On The Design Parameters Of A Heavy Duty Ppci Engine By Use Of Multidimensional Modeling”, PhD thesis, 2009.

Yokota, H., Kudo, Y., Nakajima, H., Kakegawa, T., Suzuki, T. (1997) “A New Concept for Low Emission Diesel Combustion”, SAE Paper 970891.

Zhao, H., ‘HCCI and CAI Engines for the Automotive Industry’ Woodhead Publishing, (2007).

Zheng J, Yang W, Miller DL, Cernansky NP. Prediction of pre-ignition reactivity and ignition delay for HCCI using a reduced chemical kinetic model. SAE Technical Paper, No. 2001; 2001-01-1025.

Zur Loye, S. O., Siebers D. L., Mckinley T. L., Ng H. K. and Primus R. J., “Cycle-resolved LDV measurements in a motored Diesel engine and comparison with k-epsilon model predictions, 1989, SAE Paper 890618.

CURRICULUM VITAE

HASAN KÖTEN

Research assistant at Marmara University

E-mail: hkoten@gmail.com

EDUCATION

PhD	Marmara University, Department of Mechanical Engineering Marmara University, Department of Mechanical Engineering
Master of Science 2007-2009	*Comparison of Various Combustion Models Within A Multidimensional Framework Applied to Heavy Duty CI Engine* Advisor: Prof.Dr. Zafer Gul
Bachelor of Science 2003-2007	Sakarya University, Department of Mechanical Engineering with honor of degree, first degree.
Bachelor of Science 2003-2007	Sakarya University, Department of Electrical-Electronics Engineering Double Major

AWARD: CBG Engine Design, second prize over all universities in Turkey, 2013.

This prize was given from Turkish Economy Ministry for PhD thesis study.

EXPERIENCE

2011-2012 The Ohio State University (center for automotive research)

2008-2010 TUBITAK project.

2007-2009 Ford Otosan & Marmara University Project.